Anisotropic Black Branes, Shear Viscosity and possible experimental implications

A thesis submitted to

Tata Institute of Fundamental Research, Mumbai, India

for the degree of

Doctor of Philosophy in Physics

By

Rickmoy Samanta

Department of Theoretical Physics

Tata Institute of Fundamental Research

Mumbai - 400 005, India

July 2017

Declaration

This thesis is a presentation of my original research work. Wherever contributions of others are involved, every effort is made to indicate this clearly, with due reference to the literature, and acknowledgement of collaborative research and discussions.

The work was done under the guidance of Professor Sandip P Trivedi, at the Tata Institute of Fundamental Research, Mumbai.

(Rickmoy Samanta)

In my capacity as the supervisor of the candidate's thesis, I certify that the above statements are true to the best of my knowledge.

(Sandip P Trivedi)

Acknowledgments

First and foremost, I wish to express my deep gratitude and respect for my advisor, Prof. Sandip Trivedi. I have always tried my best to learn from his deep love for science, his great passion for physics and his wonderful insights in physics problems. All these years of my life in TIFR, he has been a constant source of support and encouragement. I consider myself very fortunate to see him in action in-front of the blackboard and making difficult concepts appear simple and beautiful. It was so much fun to discuss physics with him. He guided me with tremendous care and was always there for me whenever I got stuck in any problem. Even outside academics, he was a wonderful guide and a huge source of motivation and support.

I also take this opportunity to thank Prof. Rishi Sharma for his untiring efforts to help me in my projects. Along with my guide, he has always been there for me, guiding me through calculations and helping me out whenever I am stuck. He was also a huge source of inspiration for me.

My deep respect and gratitude to Prof. Monoranjan Guchait, for introducing me to the world of collider physics. Even though I was from a different department, he provided me a wonderful opportunity to learn about the exciting physics involving the LHC and sharing his experience about the experiments in progress in CERN, Geneva.

Right from the day I joined TIFR, it has been such a pleasure to learn physics from Prof. Shiraz Minwalla. I am so fortunate to have graduate courses in Classical mechanics, General Relativity and String theory from Shiraz. His enormous amount of energy and enthusiasm, his deep passion for physics always motivated me to work hard and enjoy science. Listening to him all these years, be it in the classroom, or near the sea, or during West Canteen lunch sessions, it has been a dream come true for me.

I also thank the Subject Board of Physics for providing me the opportunity to learn physics from some wonderful teachers, especially Shiraz Minwalla, Gautam Mandal, Amol Dighe, Sreerup Raychaudhuri, Sunil Mukhi, H.M Antia, Avinash Dhar and Kedar Damle. I also wish to thank Shankarnarayanan, Jaikumar Radhakrishnan and Pranab Sen for some nice courses in mathematics and computer science. Needless to say, my thesis owes a lot to all the professors I interacted with in TIFR, their wonderful teaching and untiring efforts.

I am also heavily indebted to Mrs Ether Maji, who was my maths teacher during my school days . Lots of thanks to my school friends from Nava Nalanda, Tamoghna Biswas and Shubhayu Chatterjee, for their constant support and inspiration and motivating me to choose basic science research as a career.

I am grateful to Prof. Shamit Kachru, Prof. Prasanta Tripathy and my seniors Nilay Kundu, Karthik Inbasekar, Sachin Jain and Abhishek Iyer for wonderful collaboration and insights. I consider myself very fortunate to come across Arpan Saha, a talented project student from IIT Mumbai with whom I had endless discussions on differential geometry and physics in general. He also turned out to be a very valuable friend for the rest of my life. This thesis also owes a lot to my dear friend Joe Philip Ninan, who is always by my side right from the coursework days in TIFR till today.

It was great to find some amazing friends in DTP TIFR, who were always there not only for physics discussions, but also made my life interesting in many ways- Debjyoti, Mangesh, Nilakash, Ishan, Amit, Harshant, Prathyush, Geet, Shubhajit, Ritam, Ronak, Pranjal, Yogesh, Ashish, Vishal, Lavneet, Anurag, Disha, Sarbojaya, Sarath, Sounak, Ahana, Tousik and others in the DTP students room. I am also indebted to my friends outside DTP, specially Atreyee, Nairit, Soureek, Sanmay, Neha, Randhir, Krishnendu, Nihit, Vineeth, Sagnik, Devika, Shalini, Arideep, Sayani, Charanya, Shuddhodan, Sreedhar, Lovy, Divyum and many others. I am also very thankful to come across some wonderful students of IIT Mumbai, specially Sarthak, Suryateja, Gowri, Soorya, Karthik, Srinath, Meera, Bodhi, Shruti, Sankeerth and Prateek.

My deep gratitude to Kapil for computer support and Mr. Raju, Mr. Pawar, Mr. Girish and others in DTP office for their constant support regarding official matters during my PhD. A big thank you to the staff at the Journal Section Library, West, East Canteens and Jagdish. Thanks to Ruchi Gandhi for the weekend visits to some wonderful locations in Mumbai.

Finally, I wish to thank my parents, my uncles and aunts, my brothers and sisters for their unconditional love and support. I have no words to express how deeply indebted I am to my dear mother, her endless sacrifices and constant fight against all odds, so that I receive good education and one day serve my country. It is in her endless sacrifice and love that I discover again and again the greatness of my nation. This thesis is thus dedicated to my mother, with love, respect and admiration.

Collaborators

This thesis is based on work done in collaboration with several people.

- The work presented in chapter 2 was done in collaboration with Shamit Kachru, Nilay Kundu, Arpan Saha and Sandip P. Trivedi and is based on the publication that appeared in print as JHEP 1403 (2014) 074.
- The work presented in chapter 3 was done in collaboration with Karthik Inbasekar and is based on the publication that appeared in print as JHEP 1408 (2014) 055.
- The work presented in chapter 4 was done in collaboration with Sachin Jain and Sandip P. Trivedi and is based on the publication that appeared in print as JHEP 1510 (2015) 028.
- The work presented in chapter 5 was done in collaboration with Sandip P. Trivedi and Rishi Sharma and is published in Phys. Rev. A 96, 053601 (2017).
- The work presented in chapter 6 was done in collaboration with Monoranjan Guchait and Abhishek Iyer and is based on the publication that appeared in print as Phys.Rev.D, vol.93, p.015018 (2016).
- Thanks to D. D. Ofengeim and in particular D. G. Yakovlev for sharing their notes on the calculation of the various components of viscosities in the presence of the magnetic field.

To

My mother India, with love and admiration

Synopsis

Introduction

The lessons from string theory, in particular the AdS/CFT correspondence suggest that interesting connections exist between the study of gravity and the study of strongly coupled field theories. Motivated by the large number of interesting phases seen in nature, new brane solutions have been discovered in gravity. The earliest works mostly focused on horizons with translational and rotational symmetry, but more recently examples of black brane horizons dual to field theories with further reduced space-time symmetries have been discussed, [1, 2, 3, 4, 5, 6, 7, 8, 9, 10, 11, 12, 13, 14, 15].
Extremal branes are particularly interesting, since they correspond to ground states of the dual field theory in the presence of a chemical potential or doping. Their near-horizon geometries often exhibit a type of attractor behavior, and as a result, are quite universal. Of particular interest for this thesis are the brane solutions in classical gravity which correspond to phases of matter which are homogeneous but not isotropic. It was shown (see [4, 5]) that in $4 + 1$ dimensions, such brane solutions can be classified using the Bianchi classification developed earlier for studying homogeneous cosmologies. These near-horizon solutions were given the name "Bianchi attractors".
Bianchi attractors have a non-trivial geometry along the field theory directions. It is therefore worth asking whether these attractors can arise in situations where the dual field theory lives in flat space, as opposed to the more exotic scenario where the UV field theory itself must be placed in a non-trivial geometry of the appropriate Bianchi Type. This question maps to constructing interpolating extremal black brane solutions that asymptote to Anti-De Sitter space (AdS) and asking whether the non-normalizable deformations for the metric can be asymptotically turned off near the AdS boundary which lies at the ultraviolet end.

Here, in the first half of the thesis, we take a partial step towards finding such interpolating solutions for some of the Bianchi classes. We start with a particular smoothly varying metric which interpolates between the near-horizon region and Lifshitz spacetime. The metric is chosen so that the non-normalizable deformations of the metric near the Lifshitz boundary are turned off. While we do not obtain these metrics as solutions of Einstein gravity coupled to a specific simple matter field theory, we demonstrate that if they were to arise as solutions, the required matter would satisfy the weak energy condition. In this way, we establish that there is no fundamental barrier, at least at the level of reasonable energy conditions, to having such an interpolating solution. This establishes the first main result of this thesis.

In the next part of the thesis, we turn to a study of transport properties of such anisotropic blackbranes, with a view towards strongly coupled field theories in the presence of an anisotropic driving force. The calculation of the transport properties of strongly coupled quantum theories is a challenging problem of interest to theorists working on a wide range of systems including ultra-cold Fermi gases at unitarity [16, 17], heavy ion collisions [16, 18], and neutron stars [19]. At strong coupling, perturbative expansions fail to give reliable results. Surprisingly, using AdS/CFT a large subsector of strongly interacting quantum field theories in d dimensions in some limits can be related to weakly coupled theories of gravity (called their dual) in $(d+1)$ dimensions. This correspondence [20] allows us to compute transport properties of such theories, even at strong coupling using the underlying gravity description.
The shear viscosity tensor for many interesting systems is often anisotropic. The possibility that we shall explore in detail in this thesis, is that an externally applied field can pick a particular direction and give rise to anisotropies in the shear viscosity. This possibility has been explored extensively for the case of weakly coupled theories in the presence of a background magnetic field (See Ref. [21] for a general discussion, Ref. [22] in the context of heavy ion collisions and Ref. [23] for applications to neutron stars). On the other hand, the behavior of strongly coupled theories in the presence of an external field is less well explored. With this in mind, anisotropic gravitational backgrounds have been recently studied using the AdS/CFT correspondence, see [24, 25, 26, 27, 28, 29, 30, 31] and the behavior of the viscosity in some of these anisotropic phases has also been analyzed, see [32, 33] and [6, 34, 35, 36, 37, 38].

The results of Ref. [36] and Ref. [39] indicate that one may obtain parametric violations of the KSS bound ($\eta/s \geq 1/4\pi$) in such anisotropic scenarios. This feature arises in a wide variety of examples considered and seems to be quite general. In particular, it was found that as long as one can ensure that the rotational invariance is broken by a spatially constant driving force, by increasing the value of the strength of the driving force, compared to the temperature, the ratio for appropriate components of the shear viscosity to entropy density can be made arbitrarily small; in particular violating the KSS bound. In particular, we find a general formula for the shear viscosity over the entropy density in terms of the ratio of metric components evaluated at the horizon, which in anisotropic scenarios need not be the same and thus can lead to a parametric violation of the bound proposed by Kovtun, Son and Starinets. ($\eta/s \geq \frac{1}{4\pi}$). Using techniques of Kaluza Klein reduction, we give a proof of this general formula for all situations where the force breaking isotropy is spatially constant and there is some residual Lorentz symmetry left in the boundary theory after breaking isotropy. This establishes the second important result of this thesis.

If the phenomenon of small shear viscosity components in presence of anisotropy also carries over to the unitary Fermi gases, it may be possible to measure these small viscosities in experiments with trapped ultra-cold Fermi gases. For this purpose, it is helpful to consider traps which share the essential features of the systems in Ref. [36, 39]. The goal of this part of the thesis is to give a concrete proposal for the trap geometry and parameters where this effect is likely to be seen.
We now present the main results described above in more details .

Interpolation of Bianchi attractors to Lifshitz and AdS space-times

(With Shamit Kachru, Nilay Kundu, Arpan Saha and Sandip Trivedi)
As we mentioned in the introduction, the interpolating metrics we considered in general have the form

$$ds^2 = -g_{tt}(r)dt^2 + g_{rr}(r)dr^2 + \sum_{i,j=1,2,3} g_{ij}(r, x^i)dx^i dx^j. \tag{1}$$

In the Bianchi attractor region which occurs in the deep IR, for $r \to -\infty$, the metric takes the form,

$$ds_B^2 = -e^{2\beta_t r}dt^2 + dr^2 + \sum_{i=1,2,3} e^{2\beta_i r}(\omega^i)^2, \tag{2}$$

where ω^i are one-forms invariant under the Bianchi symmetries generated by the Killing fields ξ_i, $i = 1, 2, 3$ The commutation relations of the Killing vectors

$$[\xi_i, \xi_j] = C^k_{ij}\xi_k \tag{3}$$

give rise to the corresponding Bianchi algebra.

In the far UV on the other hand, which occurs for $r \to \infty$, the metric becomes of Lifshitz form,

$$ds_L^2 = -e^{2\tilde{\beta}_t r}dt^2 + dr^2 + e^{2\tilde{\beta} r} \sum_{i=1,2,3} dx_i^2. \tag{4}$$

Here for simplicity, we only consider the case where all the spatial directions have the same scaling exponent, $\tilde{\beta}$, more generally this exponent can be different for the different spatial directions. Also, to avoid unnecessary complications we take the exponent in the time direction $\tilde{\beta}_t$ in the Lifshitz region to satisfy the condition

$$\tilde{\beta}_t = \beta_t, \tag{5}$$

where β_t is the value for the exponent in the Bianchi attractor region, eq.(2). The metric eq.(4) then becomes

$$ds_L^2 = -e^{2\beta_t r}dt^2 + dr^2 + e^{2\tilde{\beta} r}\sum_{i=1,2,3}(dx^i)^2. \tag{6}$$

The metric which interpolates between these two regions is taken to have the form

$$ds^2 = \left(\frac{1-\tanh\sigma r}{2}\right)ds_B^2 + \left(\frac{1+\tanh\sigma r}{2}\right)ds_L^2, \tag{7}$$

where ds_B^2 and ds_L^2 are defined in eq.(2) and eq.(4) respectively. σ is a positive constant which characterizes how rapid or gradual the interpolation is. One can show that as long as σ is sufficiently big the metric becomes of the Bianchi attractor form as $r \to -\infty$. Also, for sufficiently large σ the metric becomes of Lifshitz type as $r \to \infty$. More correctly, for this latter statement to be true the limit $r \to \infty$ must be taken keeping the spatial coordinates $x^i, i = 1, 2, 3$ fixed.

Classes of such smooth metrics which interpolate from such Bianchi attractor geometries (homogenous anisotropic blackbranes) of Types II, III, VI and IX in the IR to Lifshitz or $AdS_2 \times S^3$ geometries in the UV were thus constructed. It was shown that the matter sector stress-energy required to support these geometries (via the Einstein equations) does satisfy the weak and therefore also the null energy conditions. Since Lifshitz or $AdS_2 \times S^3$ geometries can in turn be connected to AdS_5 spacetime, it is thus established that there is no barrier, at least at the level of the energy conditions, for solutions to arise connecting these Bianchi attractor geometries to AdS_5 spacetime. The asymptotic AdS_5 spacetime has no non-normalizable metric deformation turned on, which suggests that furthermore, the Bianchi attractor geometries can be the IR geometries dual to field theories living in flat space, with the breaking of symmetries being either spontaneous or due to sources for other fields.

Using Raychaudhuri's equation for a family of radially outgoing null geodesics emanating from a 3-dimensional submanifold spanned by the x^i coordinates for any fixed r, t, a C-function was also found monotonically decreasing from the UV to the IR, given by

$$C = \left(\frac{\sqrt{g_{tt}}}{(\partial_r \ln A)A^{1/3}}\right)^3. \tag{8}$$

where A denotes the area element of the Bianchi hypersurface spanned by the x^i coordinates for any constant r, t, provided the matter sourcing the geometry obeys null energy conditions. For a Bianchi attractor with exponents β_t, β_i, C (Eq. 2) becomes

$$C \propto \left(\frac{e^{(\beta_t - \bar{\beta})r}}{3\bar{\beta}} \right)^3 , \tag{9}$$

where

$$\bar{\beta} = \frac{1}{3} \sum_i \beta_i. \tag{10}$$

The flows we consider include interpolations between two AdS spacetimes which at intermediate values of r can break not only Lorentz invariance but also spatial rotational invariance and translational invariance. As long as the UV and IR geometries are AdS, our results imply that the IR central charge must be smaller than the UV one. Our results therefore lead to a generalization of the holographic C-theorem for flows between conformally invariant theories which can also break boost, rotational and translational symmetries. This is in contrast to much of the discussion in the literature so far, which has considered only Lorentz invariant flows ([40]).

Bianchi attractors in Gauged Supergravity

(With Karthik Inbasekar)

In the next part of the thesis we explore the embedding of Bianchi attractors in $\mathcal{N} = 2, D = 5$ Gauged supergravity. A stable Bianchi III attractor solution was found in $\mathcal{N} = 2, d = 5$ gauged supergravity coupled to a single vector multiplet and a gauging of the $U(1)_R$ symmetry. The gravity multiplet consists of two gravitinos ψ^i_μ, $i = 1, 2$, and a graviphoton. The vector multiplet consists of a vector A_μ, a real scalar ϕ and the gaugini λ_i. The vector in the vector multiplet and the graviphoton are collectively represented by A^I_μ, $I = 0, 1$.

The scalars in the theory parametrize a very special manifold described by the cubic surface

$$N \equiv C_{IJK} h^I h^J h^k = 1 \ , \quad h^I \equiv h^I(\phi) \ . \tag{11}$$

The difference in the gauged theory is the presence of a scalar potential. The process of gauging converts some of the global symmetries of the Lagrangian into local symmetries. One of the global symmetries enjoyed by the fermions in a $\mathcal{N} = 2$ theory is the $SU(2)_R$ symmetry. We considered the gauging of the abelian $U(1)_R \subset SU(2)_R$. The R symmetry is gauged by replacing the usual Lorentz covariant derivative acting on the fermions with $U(1)_R$ gauge covariant derivative as follows

$$\nabla_\mu \lambda^i \to \nabla_\mu \lambda^i + g_R A_\mu(U(1)_R) \delta^{ij} \lambda_j \ , \nabla_\mu \psi^i_\nu \to \nabla_\mu \psi^i_\nu + g_R A_\mu(U(1)_R) \delta^{ij} \psi_{\nu j} \ .$$

g_R is the $U(1)_R$ gauge coupling constant. The $U(1)_R$ gauge field is a linear combination of the gauge fields in the theory

$$A_\mu(U(1)_R) = V_I A^I_\mu \ , \tag{12}$$

where the parameters $V_I \in R$ are free.[1]

The $U(1)_R$ covariantization breaks the supersymmetry and therefore compensating terms are added to the Lagrangian for supersymmetric closure . These terms result in the form of a potential for the scalar fields,

$$\mathcal{V}(\phi) = -2g_R^2 V_1 \left[\frac{2\sqrt{2}V_0}{\phi} + \phi^2 V_1\right] . \tag{13}$$

Generalised attractors are defined as solutions to equations of motion that reduce to algebraic equations when all the fields and Riemann tensor components are constants in tangent space

$$\phi = const \ , \quad A^I_a = const \ , \quad c_{ab}{}^c = const \ , \tag{14}$$

where $a = 0, 1, \ldots, 4$, are tangent space indices. The $c_{ab}{}^c$, referred to as anholonomy coefficients are structure constants that appear in the Lie bracket of the vielbeins

$$[e_a, e_b] = c_{ab}{}^c e_c \ , \quad e_a \equiv e^\mu_a \partial_\mu \ . \tag{15}$$

A new class of Bianchi type III attractor solution in this $U(1)_R$ gauged supergravity were constructed. The Bianchi type III solution found is as follows

$$\begin{aligned} ds^2 &= -\hat{r}^{2\beta_t} d\hat{t}^2 + \frac{d\hat{r}^2}{\hat{r}^2} + (\omega^3)^2 + (\omega^1)^2 + \hat{r}^{2\beta_2}(\omega^2)^2 \ , \\ A_3 &= \frac{\sqrt{-1+2\beta_t^2}}{\phi_c^2}, \quad \phi_c = 4\sqrt{2} g_R^2 V_0 V_1, \\ \beta_2 = \beta_t, \quad \beta_t &= \frac{1}{2}\sqrt{1 + 128 g_R^6 V_0^2 V_1^4}, \quad \beta_t^2 > \frac{7}{8} \ . \end{aligned} \tag{16}$$

where the one forms ω^i

$$\omega^1 = e^{-\hat{x}} d\hat{y} \ , \quad \omega^2 = d\hat{z} \ , \quad \omega^3 = d\hat{x} \ , \tag{17}$$

are invariant under the Bianchi type III homogeneous symmetry. The Hessian of the effective potential evaluated on this solution has a positive eigenvalue suggesting that it is a stable attractor. We next investigated the stability of the Bianchi type III solution in gauged supergravity by studying the linearized fluctuations of the gauge field, scalar field, metric about their attractor values and it was found that all the fluctuations are well behaved as one approaches the horizon. We studied the Killing spinor equations of $\mathcal{N} = 2, U(1)_R$ gauged supergravity with the background Bianchi type III solution. However, we found that the naive radial spinor which gives supersymmetric Bianchi I spaces such as AdS and

[1] When the gauging of R symmetry is accompanied by gauging of a non-abelian symmetry group K of the scalar manifold, the V_I are constrained by $f^I_{JK} V_I = 0$, where f^I_{JK} are structure constants of K.

Lifshitz fails for the Type III case. This suggests that the stable Type III solution we have constructed may be a non-supersymmetric attractor ([41])

The shear viscosity in anisotropic phases

(With Sachin Jain and Sandip Trivedi)

In the second half of the thesis, we continue studying anisotropic blackbrane solutions in a wide variety of examples where the breaking of isotropy is due to an externally applied force which is translationally invariant. We first review a simple system discussed in Ref. [36] consisting of a linearly varying massless dilaton minimally coupled to gravity via the Lagrangian

$$S = \frac{1}{16\pi G}\int d^5x\sqrt{g}\,[R + 12\Lambda - \frac{1}{2}\partial_\mu\phi\partial^\mu\phi]\ , \tag{18}$$

where G is Newton's constant in 5 dimensions and Λ is a cosmological constant. The boundary theory in the absence of anisotropy is a $3+1$ dimensional conformal field theory. The dilaton field in the background solution here has the profile

$$\phi = \rho z\ . \tag{19}$$

Clearly this choice of the background singles out the z direction, breaking isotropy. In the presence of the dilaton the conservation equations for the stress tensor get modified to be,

$$\partial_\mu T^{\mu\nu} = \langle O\rangle\partial^\nu\phi\ \ , \tag{20}$$

where O is the operator dual to the field ϕ. The right hand side arises because the varying dilaton results in a driving force on the system. We see that a linear profile results in a constant value for $\partial^\nu\phi$ and thus a constant driving force. At zero temperature the near horizon solution was found to be $AdS_4\times R$,

$$ds^2 = -\frac{4}{3}u^2dt^2 + \frac{du^2}{\frac{4}{3}u^2} + \frac{4}{3}\ u^2(dx^2+dy^2) + \frac{\rho^2}{8}dz^2. \tag{21}$$

At small temperature, $T\ll\rho$, the geometry is that of a Schwarzschild black brane in $AdS_4\times R$

$$-\frac{4}{3}u^2(1-\frac{\pi^2T^2}{u^2})dt^2 + \frac{1}{\frac{4}{3}u^2(1-\frac{T^2\pi^2}{u^2})}du^2 + \frac{4}{3}\ u^2(dx^2+dy^2) + \frac{\rho^2}{8}dz^2.$$

We see in eq.(21) that the metric component g_{zz} becomes constant due to the extra stress energy provided by the linearly varying dilaton. The $AdS_4\times R$ solution is in fact an exact solution to the equations of motion.

The behavior of shear viscosity components $\eta_{xz} = \eta_{yz} \equiv \eta_{\perp}$ (which are spin 1 w.r.t this surviving Lorentz symmetry) was studied in the example of Ref. [36] for two cases — one in the low anisotropy regime and the other in the high anisotropy regime. The results are as follows:

1. Low anisotropy regime ($\rho/T \ll 1$):

$$\frac{\eta_{\perp}}{s} = \frac{1}{4\pi} - \frac{\rho^2 \log 2}{16\pi^3 T^2} + \frac{(6 - \pi^2 + 54(\log 2)^2)\rho^4}{2304\pi^5 T^4} + \mathcal{O}\left[\left(\frac{\rho}{T}\right)^6\right] . \tag{22}$$

   We see that a small anisotropy at order $(\rho/T)^2$ already reduces this component of the viscosity and makes it smaller than the KSS bound. In the limit of zero anisotropy, we recover the KSS bound

$$\frac{\eta_{\perp}}{s} \to \frac{1}{4\pi}. \tag{23}$$

   We also note that the driving force in the conservation equation for the stress tensor (Eq. 20) is proportional to $\nabla\phi \sim \rho$ (Eq. 19) and the analogue of the mean free path is T. Thus the corrections go like $\frac{(\nabla\phi)^2}{T^2}$.

2. High anisotropy regime ($\rho/T \gg 1$):

$$\frac{\eta_{\perp}}{s} = \frac{8\pi T^2}{3\rho^2} . \tag{24}$$

   We see that in this limit the ratio can be made arbitrarily small, with $\frac{\eta_{\perp}}{s} \to 0$, as $T \to 0$ keeping ρ fixed.

In contrast the η_{xyxy} component (which couples to a spin 2 metric perturbation) was found to be unchanged from its value in the isotropic case,

$$\eta_{xyxy} = \frac{1}{4\pi} \tag{25}$$

and thus continues to meet the KSS bound.
In the work [39] we study many other examples where anisotropic phases arise and show that in all of them components of the viscosity can become parametrically small, in units of the entropy density, when the anisotropy becomes sufficiently large compared to the temperature. Depending on the example, the factor of T^2 in eq.(24) can be replaced by some other positive power of T. A common feature of all our examples is that the breaking of anisotropy is due to an externally applied force which is translationally invariant. Another common feature in our examples is that some residual Lorentz symmetry survives, at zero temperature, after incorporating the breaking of rotational invariance. Fluid mechanics then corresponds to the dynamics of the goldstone modes associated with the boost symmetries

of this Lorentz group which are broken at finite temperature.

In the work [39] we give a proof, based on a Kaluza Klein decomposition of modes, which shows quite generally that in all situations sharing these features, appropriate components of the viscosity tensor become parametrically small. For a case with a residual AdS_{d+1} factor in the metric, the basic idea behind the general analysis will be to consider a dimensionally reduced description, starting from the original $D+1$ dimensional theory and going down to the AdS_{d+1} space-time. The off diagonal components of the metric, whose perturbations carry spin 1 and which are related to the viscosity components of interest, will give rise to gauge fields in the dimensionally reduced theory. By studying the conductivity of these gauge fields, which can be related easily to the spin 1 viscosity components we derive the following general result - Let z be a spatial direction in the boundary theory along which there is anisotropy and x be a spatial direction along which the boost symmetry is left unbroken, then we show that the viscosity component η_{xz}, which couples to the h_{xz} component of the metric perturbation, satisfies the relation,

$$\frac{\eta_{xz}}{s} = \frac{1}{4\pi}\frac{g_{xx}}{g_{zz}}\Big|_{u=u_h}, \tag{26}$$

where $g_{xx}|_{u=u_h}, g_{zz}|_{u=u_h}$ refer to the components of the background metric at the horizon. Eq.(26) is one of the main results of this part of the thesis. It also agrees with the behaviour seen in all the explicit examples we consider. This result was first derived for an anisotropic axion-dilaton-gravity system in [32].

In the isotropic case the ratio $\frac{g_{xx}}{g_{zz}}\Big|_{u=u_h}$ is unity and we see that the KSS result is obtained. However, in anisotropic cases this ratio can become very different from unity and in fact much smaller, leading to the parametric violation of the KSS bound $\eta/s \geq 1/4\pi$.

The shear viscosity in an anisotropic unitary fermi gas

(With Rishi Sharma and Sandip Trivedi)

Remarkably for ultra-cold fermions at unitarity, the η/s has been measured for a wide range of temperatures and the minimum value is very close to the KSS bound. Similarly, the values measured in heavy ion collisions seem to be close to $1/(4\pi)$.

If our intuition from the study of anisotropic blackbranes in gravity also carries over to the unitary Fermi gases (the gravity duals of such systems is not yet known), it may be possible to measure these small viscosities in experiments with trapped ultra-cold Fermi gases. For this purpose, one needs to consider traps which share the essential features of the systems in [39]. The goal of this part of the thesis is to give a concrete proposal for the trap geometry and parameters where this effect is likely to be seen.

Motivated by the above results in the gravity side, we may hope to find parametrically suppressed viscosities in systems where the following basic requirements are met.

- The system is strongly interacting and in the absence of anisotropy have a viscosity close to the KSS bound.
- The equations of hydrodynamics for the system admits modes sensitive to the spin 1 viscosity components as described above and in Ref. [36, 39].
- Sufficient anisotropy needs to be introduced in the system (say in the z direction with rotational symmetry preserved along the $x-y$ plane), such that these spin 1 components of the viscosity, when measured in units of the entropy density, show an experimentally measurable decreasing tendency below the KSS bound.
- The force responsible for breaking of isotropy is approximately spatially constant.
- The velocity gradients are small enough (compared to say the inverse mean free path) ensuring that hydrodynamics is the appropriate effective theory to describe the system.

We now explain how one can meet the above conditions in a system of trapped fermions in the unitary limit. The anisotropic force is obtained by placing the system in an anisotropic trap. The trapping potential is harmonic and characterized by three angular frequencies, $\omega_x, \omega_y, \omega_z$. We consider an anisotropic situation where $\omega_z \gg \omega_x, \omega_y$, so that the trapping potential is much stronger in the z direction. For simplicity, we also take $\omega_x = \omega_y$ so that the system preserves rotational invariance in the $x-y$ plane. For some of the discussion below we can neglect the effects of the trapping potential in the x, y directions characterized by ω_x, ω_y.

On studying the equations of superfluid hydrodynamics, we identify two modes which are sensitive to the spin 1 components of the viscosity tensor. Each of these modes is characterized by the superfluid and the normal components, which we denote by $\mathbf{v}_s$ and $\mathbf{v}_n$ respectively.
The first mode, which we call **Mode a** has $\mathbf{v}_s = 0$ and $\mathbf{v}_n = \mathbf{v}$ given by

$$\mathbf{v} \; = e^{i\omega t}(\alpha_x z \; \hat{x} + \alpha_z x \; \hat{z}) \tag{27}$$

with the following relations:

$$\textbf{Mode a}: \;\; \omega = 0, \;\alpha_z = -\frac{\omega_x^2}{\omega_z^2}\alpha_x \tag{28}$$

The other mode of interest, denoted by **Mode b**, has $\mathbf{v}_s = \mathbf{v}_n = \mathbf{v}$ given by Eq. 27 with

$$\textbf{Mode b}: \;\; \omega = \sqrt{\omega_x^2 + \omega_z^2}, \;\alpha_z = \alpha_x = \lambda. \tag{29}$$

We see that in the high anisotropy limit $\omega_z \gg \omega_x$, $\alpha_z \to 0$ for **Mode a**, and hence we recover a flow profile similar to that considered in [36]; To the best of our knowledge, **Mode a** has not been studied in ultra-cold gas experiments. **Mode b** is the scissors mode which has been studied extensively (for example see Refs. [42, 43, 44]).

We next desire that the amplitude of the velocity modes be small enough that it can be described by hydrodynamics. This gives an upper limit on the amplitude of the modes given by α_x .

The energy dissipated due to viscosity is given by

$$\dot{E}_{kinetic} = -\frac{1}{2}\int d^3\mathbf{r}\,\eta_{ijij}(\mathbf{r})\left(\partial_i v_j + \partial_j v_i - \frac{2}{3}\delta_{ij}\partial_k v_k\right)^2 - \int d^3\mathbf{r}\,\zeta(\mathbf{r})\left(\partial_i v_i\right)^2 \tag{30}$$

where $\eta_{ijij} \equiv \eta_{ij}$ is the relevant component of the shear viscosity and ζ is the bulk viscosity. We note that for our chosen velocity profiles, the bulk viscosity contribution vanishes. Also in the traps we will consider, the temperature T is constant throughout the trap. Hence we also ignored contributions from thermal conductivity.

Thus,

$$\dot{E}_{kinetic} = -\frac{1}{2}\int d^3\mathbf{r}\,\eta_{xz}(\mathbf{r})\;\alpha_x^2(1 - \frac{\omega_x^2}{\omega_z^2}) \tag{31}$$

is the energy dissipation rate for **Mode a**, where we have simply written η_{xzxz} as η_{xz}.

The energy dissipated per unit cycle for the oscillatory time dependent **Mode b** is

$$\dot{E}_{kinetic} = -\int d^3\mathbf{r}\,\eta_{xz}(\mathbf{r})\;\alpha_x^2. \tag{32}$$

The evaluation of the energy loss from Eq. 31 and Eq. 32 requires the viscosity η as a function of the position $\mathbf{r}$ in the trap.

To get a first estimate of the region of the trap which gives a dominant contribution to the integral in Eq. 30, we use the local density approximation (LDA) and estimate the resulting viscosity. More specifically, we assume in this approximation that thermodynamic variables like the number density n, the entropy density s depend only on the local value of T and

μ. The viscosity is also then taken to be given by these local values of T, μ, neglecting any effects of anisotropy which could make the different components of the tensor take different values.

The effect of anisotropy on the viscosity tensor are estimated using Boltzmann transport in a weakly coupled anisotropic theory as

$$\eta_{ijkl} = \eta\frac{1}{2}[(\delta_{ik}\delta_{jl}+\delta_{il}\delta_{jk}-\frac{2}{3}\delta_{ij}\delta_{kl})+(\frac{\lambda^2(\nabla\phi(\mathbf{r}))(\nabla\phi(\mathbf{r}))}{[\mu(\mathbf{r})]^2})\sum_{\alpha=0}^{4}c_{(\alpha)}M_{\alpha\,ijkl}]+\mathcal{O}(\nabla^2\phi,(\nabla\phi)^4)\;, \tag{33}$$

where λ is a microscopic length scale of the system, $c_{(i)}$ are dimensional constants of order 1 which depend on the microscopic details of the system, and M_i are 5 orthonormal projection operators that arise in a system with one special direction (for eg. see Ref. [45]).

Our calculations show that the corrections to η for a weakly interacting, normal (unpaired) Fermi gas at low temperatures ($T < \mu$) are given by

$$\begin{aligned}
\eta_0 &= \eta(0)[1-\frac{31}{84}(\lambda k_F)^2\frac{(\nabla\phi)^2}{k_F^2\mu^2}+\mathcal{O}((\tau\nabla\phi)^4)] = \eta(0)[1-\frac{31}{84}(\lambda k_F)^2\kappa_{\mathrm{LDA}}^2+\mathcal{O}((\tau\nabla\phi)^4)]\\
\eta_1 &= \eta(0)[1-\frac{13}{28}(\lambda k_F)^2\frac{(\nabla\phi)^2}{k_F^2\mu^2}+\mathcal{O}((\tau\nabla\phi)^4)] = \eta(0)[1-\frac{13}{28}(\lambda k_F)^2\kappa_{\mathrm{LDA}}^2+\mathcal{O}((\tau\nabla\phi)^4)]\\
\eta_2 &= \eta(0)[1-\frac{11}{28}(\lambda k_F)^2\frac{(\nabla\phi)^2}{k_F^2\mu^2}+\mathcal{O}((\tau\nabla\phi)^4)] = \eta(0)[1-\frac{11}{28}(\lambda k_F)^2\kappa_{\mathrm{LDA}}^2+\mathcal{O}((\tau\nabla\phi)^4)]\\
\eta_3 &= 0,\;\; \eta_4 = 0\;.
\end{aligned} \tag{34}$$

where we have introduced the notation[2]

$$\kappa_{LDA} = \frac{(\nabla\phi)}{(\mu\;k_F)} \tag{36}$$

Let us pause here to appreciate the similarity between the weak coupling Boltzmann analysis result Eq. 34 and the results from gravity valid at strong coupling, Eq. 22.

While we cannot reliably compute the coefficients at strong coupling in the field theory, the key point of our calculations here is that they might be experimentally measured and could lie below the KSS bound as we gradually increase κ_{LDA}. We thus note that κ_{LDA} provides a good characterization of the amount of anisotropy we introduce in our system.

To get the first estimates however, we apply the LDA approximation. We start first by considering a homogeneous situation characterized by temperature T, μ and obtain the

[2] In the following discussion, we use the usual definitions

$$k_F = (3\pi^2 n)^{1/3},\; E_F = \frac{k_F^2}{2m},\; T_F = E_F/k_B,\; v_F = \frac{k_F}{m}\;. \tag{35}$$

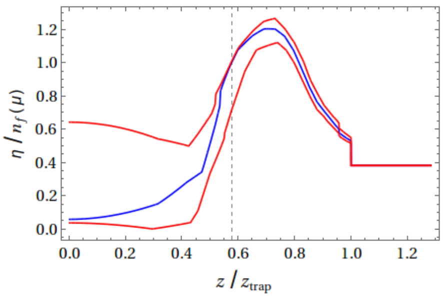

Figure 1: (Color online) Local shear viscosity at $T = \frac{2T_c}{3}$ at $\mu = 10\mu$K, $\omega_z = 2\pi \times 10^4$ rads/s. The red curves denote the error bands.

behavior of the thermodynamical parameters and the viscosity as a function of these parameters.

In the unitary Fermi gas, the chemical potential μ and the temperature T are the only energy scales in the problem. Therefore, we can express various thermodynamic quantities as a function of the dimensionless quantity $y = T/\mu$ multiplied by an appropriate dimensionless function of only one of the two variables. Following [46] we write,

$$\begin{aligned} n(\mu,\, T) =& n_f(\mu)\mathcal{F}(y), \\ s(\mu,\, T) =& \frac{2}{5} n_f(\mu)\mathcal{G}'(y)\ , \end{aligned} \tag{37}$$

where n is the number density, s is the entropy density, and $\mathcal{F}(y) = \mathcal{G}(y) - 2\ y\ \mathcal{G}'(y)/5$, $n_f(\mu) = \frac{1}{3\pi^2}(2m\mu)^{\frac{3}{2}}$ is the number density of a free Fermi gas. Therefore one can compute the desired thermodynamic quantities if the function $\mathcal{G}(y)$ is known.

At low temperatures ($\frac{T}{T_F} \lesssim 0.6$) we use the $\frac{S}{N}$ data from Fig.3b of Ref. [47] to obtain $\mathcal{G}(y)$. Having understood the thermodynamics in the absence of the trap, we now turn to incorporating the trap potential in the discussion. We first use the LDA approximation to calculate how thermodynamic quantities like s, n etc vary along the trap. In the presence of the trap μ varies in the equilibrium configuration. The effects of the trap, in this approximation, are then incorporated by using the local values for μ and T in the behavior obtained above for the homogeneous case. To evaluate η at a given μ and T we simply multiply $\frac{\eta}{n}$ of Ref. [48] with the number density that can be found using Eq. 37 (see Fig. 1).

It turns out that on starting at the center of the trap at a sufficiently low temperature, the viscosity spatial profile has a peak, z_0, close to the point where the superfluid-normal transition occurs. In turn, this leads to the viscosity and damping effects for the fluid modes of interest receiving their contribution from a region close to the peak and with a width,

δz that can be made narrow, $\delta z/z_0 < 1$, thus approximately meeting our requirement of constant driving force to break isotropy.

Furthermore, we find that the resulting energy and damping rate of this energy, from which the viscosity can be extracted, lie within the range of values which are measured by experiments currently being done on cold atom systems, in particular on Li_6 unitary fermi gas systems, Ref. [44]. For example, for trap parametrs $\mu = 10\mu$K, $\omega_z \sim 2\pi \times 77000$ rads/s, and $T = \frac{T_c}{2}$ ($T_c = 0.4\mu$) we find that the anisotropy, as measured by the parameter κ_{LDA} , Eq. 36, is of order unity and therefore significant. At these extreme values of anisotropy our theoretical calculation, strictly speaking, do not apply, but a reasonable extrapolation suggests that the total kinetic energy and damping time for the scissor mode (**Mode b**) should be of order $E \sim 10^{-18}$ joules, $\tau \sim 10^{-2}$ seconds which are within the experimental range of values currently being probed. For smaller values of anisotropy, the theoretical estimates are more reliable and suggest that the different viscosity tensor components should have a fractional difference given in terms of κ_{LDA} by Eq. 33. This tendency of the viscosity to decrease should already be measurable at more moderate values of the anisotropy.
It is worth mentioning in this context that κ_{LDA} scales as ω_z/μ while the damping time scale for the scissors mode scales as $\frac{\mu}{\omega_x^2}$. One can thus keep the damping time scale in the experimentally accessible range of about a millisecond while increasing ω_z (keeping ω_x same) and to make $\kappa_{LDA} \sim \mathcal{O}(1)$, thereby passing from a regime of low anisotropy to a regime of high anisotropy.
We hope our experimental colleagues in the cold atoms community will find our proposal interesting and we request them to carry out a careful investigation of anisotropic viscosities in trapped fermions in the unitary regime of the BEC-BCS crossover.

Lepton flavor violation in supersymmetry at the LHC

(With Monoranjan Guchait and Abhishek Iyer)
In a parallel exploration, we considered models of supersymmetry which can incorporate sizeable mixing between different generations of sfermions and performed a detailed collider analysis to devise a signal to probe the lepton flavour violating parameter in such models relevant for the LHC.([49])

Future Directions

- Although we were successful regarding the interpolation of Bianchi Types II, III, VI and IX in Sec. , the interpolating metric of Bianchi Type V failed to satisfy the null energy conditions. Our failure in this case may be due to the restricted class of functions we used to construct the interpolating metrics or perhaps it may suggest a more fundamental constraint. Another interesting question is how the anisotropic and homogeneous phases in these field theories, described by the Bianchi attractor regions, can arise in practice? It will be interesting to examine the possibility of a spontaneous breaking of rotational invariance or by turning on sources other than the metric in the field theory.

- An immediate extension of the work on shear viscosity in strongly coupled fluid in presence of anisotropy is to extend our analysis to cases where the breaking of isotropy is spontaneous or when the driving force is not spatially constant. It is also natural to consider string theory embeddings of the anisotropic systems we have studied and examining if they are stable. In principle all transport coefficients which determine the fluid mechanics can be obtained by carrying out a more systematic derivative expansion on the gravity side as discussed in the fluid gravity correspondence described in [50], [51],[52], [53]. It will be great to perform a similar analysis along those lines. Another direction is to consider transport properties in phases corresponding to Bianchi spaces which describe homogeneous but anisotropic phases in general. Some progress in this regard has been made [54] for Bianchi VII. It will be interesting to extend the analysis to all Bianchi types. It will also be interesting to see if these results are relevant for neutron stars with very high magnetic fields (known as magnetars) for breaking rotational invariance [3]. The resulting equilibrium phase could then be highly anisotropic and our results hint that suitable components of the viscosity might become small.

- An important point worth noting is that while the cold-atom system proposed here shares many features with those discussed in Ref. [36, 39], it also has some differences. First, in equilibrium the stress energy tensor is not invariant under translations even for a linear potential. Second, in addition to energy-momentum, the cold-atom system features another conserved quantity: the particle number. Consequently the system is locally characterized by two thermodynamic variables T and μ rather than just T. It will be interesting to further study the behavior of viscosity in gravitational systems which correspond to anisotropy driven strongly coupled systems with a finite chemical potential.(see [38, 55]). As a first step, we have analyzed a weakly coupled system with a linearly varying potential and we find that the anisotropic viscosity does become parametrically small in this case.

[3]A magnetic field of order 10^{16} Tesla or so is needed in order to contribute an energy density comparable to the QCD scale ~ 200 Mev.

Conclusions

To conclude, this thesis has described some computations in gravity to answer some interesting questions related to a class of strongly coupled field theories, often with reduced symmetries. Let us summarize some of the main results of this thesis :

- We investigate the interpolation of the Bianchi attractor geometries (which are dual to anisotropic phases in the field theory with generalized translational invariance) in the IR (infrared) to Lifshitz and AdS spacetimes in the UV (ultraviolet). While we do not obtain the interpolating metrics as solutions to Einstein's equations, we demonstrate that the matter required to support such geometries obey the weak and null energy conditions. These interpolating metrics do not have any non-normalizable metric deformations turned on near the boundary. This ensures that the dual field theory can indeed reside in flat space as opposed to some background of non-trivial geometry.

- We find a stable Bianchi III attractor solution in $\mathcal{N} = 2, D = 5$ gauged supergravity. We analyze the relevant Killing spinor equations and find that a radial ansatz for the spinor breaks supersymmetry. This suggests that the above solution may be a non-supersymmetric attractor.

- In the second half of the thesis we find a general formula for the shear viscosity in units of the entropy density given by the ratio of appropriate metric components evaluated at the horizon. In a situation with anisotropy, these metric components need not be the same. This can lead to a parametric violation of the bound proposed by Kovtun, Son and Starinets. ($\eta/s \geq \frac{1}{4\pi}$). Using techniques of Kaluza Klein reduction, we give a proof of this general formula for all situations where the force breaking isotropy is spatially constant and there is some residual Lorentz symmetry left in the boundary theory after breaking isotropy.

- We also propose a set-up involving trapped, ultracold fermions in the unitary regime of the BEC-BCS crossover, where the above suppression of some components of the anisotropic shear viscosity tensor may be observed experimentally. We present the relevant hydrodynamic modes and the trap parameters where this effect is likely to be seen. To the best of our knowledge, the proposal presented here is the first proposal to probe anisotropic shear viscosity in trapped fermions at low temperatures.

Bibliography

[1] S. K. Domokos and J. A. Harvey, *Baryon number-induced Chern-Simons couplings of vector and axial-vector mesons in holographic QCD*, *Phys.Rev.Lett.* **99** (2007) p. 141602, [arXiv:0704.1604]. ix

[2] S. Nakamura, H. Ooguri, and C.-S. Park, *Gravity Dual of Spatially Modulated Phase*, *Phys.Rev.* **D81** (2010) p. 044018, [arXiv:0911.0679]. ix

[3] A. Donos, J. P. Gauntlett, and C. Pantelidou, *Spatially modulated instabilities of magnetic black branes*, *JHEP* **1201** (2012) p. 061, [arXiv:1109.0471]. ix

[4] N. Iizuka, S. Kachru, N. Kundu, P. Narayan, N. Sircar, and S. P. Trivedi, *Bianchi attractors: a classification of extremal black brane geometries*, *Journal of High Energy Physics* **7** (July, 2012) p. 193, [arXiv:1201.4861]. ix

[5] N. Iizuka, S. Kachru, N. Kundu, P. Narayan, N. Sircar, *et. al.*, *Extremal Horizons with Reduced Symmetry: Hyperscaling Violation, Stripes, and a Classification for the Homogeneous Case*, *JHEP* **1303** (2013) p. 126, [arXiv:1212.1948]. ix

[6] N. Iizuka and K. Maeda, *Study of Anisotropic Black Branes in Asymptotically anti-de Sitter*, *JHEP* **1207** (2012) p. 129, [arXiv:1204.3008]. ix, x

[7] G. T. Horowitz, J. E. Santos, and D. Tong, *Optical Conductivity with Holographic Lattices*, *JHEP* **07** (2012) p. 168, [arXiv:1204.0519]. ix

[8] Y.-Y. Bu, J. Erdmenger, J. P. Shock, and M. Strydom, *Magnetic field induced lattice ground states from holography*, *JHEP* **03** (2013) p. 165, [arXiv:1210.6669]. ix

[9] M. Rozali, D. Smyth, E. Sorkin, and J. B. Stang, *Holographic Stripes*, *Phys. Rev. Lett.* **110** (2013), no. 20 p. 201603, [arXiv:1211.5600]. ix

[10] S. Cremonini and A. Sinkovics, *Spatially modulated instabilities of geometries with hyperscaling violation*, *Journal of High Energy Physics* **2014** (2014), no. 1 pp. 1–17. ix

[11] A. Donos and S. A. Hartnoll, *Interaction-driven localization in holography*, *Nature Phys.* **9** (2013) pp. 649–655, [arXiv:1212.2998]. ix

[12] D. Vegh, *Holography without translational symmetry*, arXiv:1301.0537. ix

[13] N. Bao and S. Harrison, *Crystalline scaling geometries from vortex lattices*, *Phys. Rev. D* **88** (Aug, 2013) p. 046009. ix

[14] S. Harrison, *Landau Levels, Anisotropy and Holography*, arXiv:1306.3224. ix

[15] P. Chesler, A. Lucas, and S. Sachdev, *Conformal field theories in a periodic potential: Results from holography and field theory*, *Phys. Rev. D* **89** (Jan, 2014) p. 026005. ix

[16] A. Adams, L. D. Carr, T. Schäfer, P. Steinberg, and J. E. Thomas, *Strongly Correlated Quantum Fluids: Ultracold Quantum Gases, Quantum Chromodynamic Plasmas, and Holographic Duality*, *New J. Phys.* **14** (2012) p. 115009, [arXiv:1205.5180]. x

[17] A. Bulgac, M. M. Forbes, and P. Magierski, *The Unitary Fermi Gas: From Monte Carlo to Density Functionals*, *Lect. Notes Phys.* **836** (2012) pp. 305–373, [arXiv:1008.3933]. x

[18] R. S. Bhalerao, *Transport properties of the fluid produced at RHIC*, *Pramana* **75** (2010) pp. 247–258, [arXiv:1003.3293]. x

[19] M. G. Alford, H. Nishimura, and A. Sedrakian, *Transport coefficients of two-flavor superconducting quark matter*, *Phys. Rev.* **C90** (2014), no. 5 p. 055205, [arXiv:1408.4999]. x

[20] J. Maldacena, *The large-n limit of superconformal field theories and supergravity*, *International journal of theoretical physics* **38** (1999), no. 4 pp. 1113–1133. x

[21] L. D. Landau and E. M. Lifshitz, Fluid Mechanics, Second Edition: Volume 6 (Course of Theoretical Physics), *Butterworth-Heinemann, 2 ed.* (Jan., 1987). x

[22] K. Tuchin, *On viscous flow and azimuthal anisotropy of quark-gluon plasma in strong magnetic field*, *J. Phys.* **G39** (2012) p. 025010, [arXiv:1108.4394]. x

[23] D. D. Ofengeim and D. G. Yakovlev, *Shear viscosity in magnetized neutron star crust*, *Europhys. Lett.* **112** (2015), no. 5 p. 59001, [arXiv:1512.0391]. x

[24] K. Landsteiner and J. Mas, *The Shear viscosity of the non-commutative plasma*, *JHEP* **0707** (2007) p. 088, [arXiv:0706.0411]. x

[25] T. Azeyanagi, W. Li, and T. Takayanagi, *On String Theory Duals of Lifshitz-like Fixed Points*, *JHEP* **0906** (2009) p. 084, [arXiv:0905.0688]. x

[26] M. Natsuume and M. Ohta, *The Shear viscosity of holographic superfluids*, *Prog.Theor.Phys.* **124** (2010) pp. 931–951, [arXiv:1008.4142]. x

[27] J. Erdmenger, P. Kerner, and H. Zeller, *Non-universal shear viscosity from Einstein gravity*, *Phys.Lett.* **B699** (2011) pp. 301–304, [arXiv:1011.5912]. x

[28] P. Basu and J.-H. Oh, *Analytic Approaches to Anisotropic Holographic Superfluids*, *JHEP* **1207** (2012) p. 106, [arXiv:1109.4592]. x

[29] J. Erdmenger, P. Kerner, and H. Zeller, *Transport in Anisotropic Superfluids: A Holographic Description*, *JHEP* **1201** (2012) p. 059, [arXiv:1110.0007]. x

[30] D. Mateos and D. Trancanelli, *The anisotropic N=4 super Yang-Mills plasma and its instabilities*, *Phys.Rev.Lett.* **107** (2011) p. 101601, [arXiv:1105.3472]. x

[31] D. Mateos and D. Trancanelli, *Thermodynamics and Instabilities of a Strongly Coupled Anisotropic Plasma*, *JHEP* **1107** (2011) p. 054, [arXiv:1106.1637]. x

[32] A. Rebhan and D. Steineder, *Violation of the Holographic Viscosity Bound in a Strongly Coupled Anisotropic Plasma*, *Phys.Rev.Lett.* **108** (2012) p. 021601, [arXiv:1110.6825]. x, xvii

[33] J. Polchinski and E. Silverstein, *Large-density field theory, viscosity, and '$2k_F$' singularities from string duals*, *Class.Quant.Grav.* **29** (2012) p. 194008, [arXiv:1203.1015]. x

[34] D. Giataganas, *Probing strongly coupled anisotropic plasma*, *JHEP* **07** (2012) p. 031, [arXiv:1202.4436]. x

[35] K. A. Mamo, *Holographic RG flow of the shear viscosity to entropy density ratio in strongly coupled anisotropic plasma*, *JHEP* **1210** (2012) p. 070, [arXiv:1205.1797]. x

[36] S. Jain, N. Kundu, K. Sen, A. Sinha, and S. P. Trivedi, *A Strongly Coupled Anisotropic Fluid From Dilaton Driven Holography*, *JHEP* **1501** (2015) p. 005, [arXiv:1406.4874]. x, xi, xv, xvi, xviii, xix, xxiii

[37] R. Critelli, S. Finazzo, M. Zaniboni, and J. Noronha, *Anisotropic shear viscosity of a strongly coupled non-Abelian plasma from magnetic branes*, *Phys.Rev.* **D90** (2014), no. 6 p. 066006, [arXiv:1406.6019]. x

[38] X.-H. Ge, Y. Ling, C. Niu, and S.-J. Sin, *Thermoelectric conductivities, shear viscosity, and stability in an anisotropic linear axion model*, *Phys. Rev.* **D92** (2015), no. 10 p. 106005, [arXiv:1412.8346]. x, xxiii

[39] S. Jain, R. Samanta, and S. P. Trivedi, *The Shear Viscosity in Anisotropic Phases*, *JHEP* **10** (2015) p. 028, [arXiv:1506.0189]. x, xi, xvi, xvii, xviii, xxiii

[40] S. Kachru, N. Kundu, A. Saha, R. Samanta, and S. P. Trivedi, *Interpolating from Bianchi Attractors to Lifshitz and AdS Spacetimes*, *JHEP* **1403** (2014) p. 074, [arXiv:1310.5740]. xiii

[41] K. Inbasekar and R. Samanta, *Stable Bianchi III attractor in U(1)_R gauged supergravity*, *JHEP* **08** (2014) p. 055, [arXiv:1404.1758]. xv

[42] D. Guéry-Odelin and S. Stringari, *Scissors mode and superfluidity of a trapped bose-einstein condensed gas*, *Phys. Rev. Lett.* **83** (Nov, 1999) pp. 4452–4455. xix

[43] O. M. Maragò, S. A. Hopkins, J. Arlt, E. Hodby, G. Hechenblaikner, and C. J. Foot, *Observation of the scissors mode and evidence for superfluidity of a trapped bose-einstein condensed gas*, *Phys. Rev. Lett.* **84** (Mar, 2000) pp. 2056–2059. xix

[44] M. J. Wright, S. Riedl, A. Altmeyer, C. Kohstall, E. R. S. Guajardo, J. H. Denschlag, and R. Grimm, *Finite-temperature collective dynamics of a fermi gas in the bec-bcs crossover*, *Phys. Rev. Lett.* **99** (Oct, 2007) p. 150403. xix, xxii

[45] M. Goossens, R. Erdélyi, and M. S. Ruderman, *Resonant mhd waves in the solar atmosphere*, *Space Science Reviews* **158** (2010), no. 2 pp. 289–338. xx

[46] T. Schäfer, *The Shear Viscosity to Entropy Density Ratio of Trapped Fermions in the Unitarity Limit*, *Phys. Rev.* **A76** (2007) p. 063618, [cond-mat/0701251]. xxi

[47] M. J. H. Ku, A. T. Sommer, L. W. Cheuk, and M. W. Zwierlein, *Revealing the superfluid lambda transition in the universal thermodynamics of a unitary fermi gas*, *Science* **335** (2012), no. 6068 pp. 563–567, [http://science.sciencemag.org/content/335/6068/563.full.pdf]. xxi

[48] J. A. Joseph, E. Elliott, and J. E. Thomas, *Shear viscosity of a unitary fermi gas near the superfluid phase transition*, *Phys. Rev. Lett.* **115** (Jul, 2015) p. 020401. xxi

[49] M. Guchait, A. M. Iyer, and R. Samanta, *Looking for lepton flavor violation in supersymmetry at the lhc*, *Phys. Rev. D* **93** (Jan, 2016) p. 015018. xxii

[50] S. Bhattacharyya, V. E. Hubeny, S. Minwalla, and M. Rangamani, *Nonlinear Fluid Dynamics from Gravity*, *JHEP* **0802** (2008) p. 045, [arXiv:0712.2456]. xxiii

[51] S. Bhattacharyya, V. E. Hubeny, R. Loganayagam, G. Mandal, S. Minwalla, *et. al.*, *Local Fluid Dynamical Entropy from Gravity*, *JHEP* **0806** (2008) p. 055, [arXiv:0803.2526]. xxiii

[52] J. Bhattacharya, S. Bhattacharyya, S. Minwalla, and A. Yarom, *A Theory of first order dissipative superfluid dynamics*, *JHEP* **1405** (2014) p. 147, [arXiv:1105.3733]. xxiii

[53] V. E. Hubeny, S. Minwalla, and M. Rangamani, *The fluid/gravity correspondence*, arXiv:1107.5780. xxiii

[54] O. Ovdat and A. Yarom, *A modulated shear to entropy ratio*, *JHEP* **1411** (2014) p. 019, [arXiv:1407.6372].

[55] S. Chakraborty and R. Samanta, "Viscosity for anisotropic reissner-nordström black branes," *Phys. Rev. D*, vol. 95, p. 106012, May 2017.

xxiii

xxiii

List of Publications

Papers relevant to the thesis work:

- *"Interpolating from Bianchi Attractors to Lifshitz and AdS Spacetimes"*;
  Shamit Kachru, Nilay Kundu, Arpan Saha, Rickmoy Samanta, Sandip P. Trivedi;
  JHEP 1403 (2014) 074; arXiv:1310.5740 [hep-th];

- *" Stable Bianchi III attractor in $U(1)_R$ gauged supergravity "*;
  Karthik Insbasekar , Rickmoy Samanta;
  JHEP 1408 (2014) 055; arXiv:1310.5740 [hep-th];

- *"The Shear Viscosity in anisotropic phases "*;
  Sachin Jain, Rickmoy Samanta, Sandip Trivedi;
  JHEP 1510 (2015) 028; arXiv:1506.01899 [hep-th];

- *"Looking for lepton flavour violation in SUSY at the LHC "*;
  Monoranjan Guchait, Abhishek Iyer, Rickmoy Samanta;
  Phys. Rev. D 93, 015018, Published 27 January 2016;

- *"The Shear Viscosity in an Anisotropic Unitary Fermi Gas "*;
  Rickmoy Samanta, Rishi Sharma, Sandip Trivedi;
  Phys. Rev. A 96, 053601, 2017. ;

Contents

Chapter 1

Introduction

A Roadmap of the Thesis:

The lessons from string theory, in particular the AdS/CFT correspondence suggest that fascinating connections exist between the study of gravity and the study of strongly coupled field theories. Motivated by the large number of interesting phases seen in nature, new brane solutions have been discovered in gravity. The earliest works mostly focused on horizons with translational and rotational symmetry, but more recently examples of black brane horizons dual to field theories with further reduced space-time symmetries have been discussed. Extremal branes are particularly interesting, since they correspond to ground states of the dual field theory in the presence of a chemical potential or doping. Their near-horizon geometries often exhibit a type of attractor behavior, and as a result, are quite universal. Of particular interest for this thesis are the brane solutions in classical gravity which correspond to phases of matter which are homogeneous but not isotropic. It was shown (see [1, 2]) that in $4 + 1$ dimensions, such brane solutions can be classified using the Bianchi classification developed earlier for studying homogeneous cosmologies. These near-horizon solutions were given the name "Bianchi attractors". Bianchi attractors have a non-trivial geometry along the field theory directions. It is therefore worth asking whether these attractors can arise in situations where the dual field theory lives in flat space, as opposed to the more exotic scenario where the ultraviolet (UV) field theory itself must be placed in a non-trivial geometry of the appropriate Bianchi Type. This question maps to constructing interpolating extremal black brane solutions that asymptote to Anti-De Sitter space (AdS) and asking whether the non-normalizable deformations for the metric can be asymptotically turned off near the AdS boundary which lies at the ultraviolet end.

In the first part of the doctoral work in Chapter 2, we tried to interpolate these attractor geometries with generalized translational symmetry to asymptotic anti de sitter space in Einstein gravity. While we did not obtain the interpolating metrics as solutions to Einstein's equations, we showed that were they to arise as solutions, the required matter will satisfy the weak and null energy conditions. We also tried to realize some of these near horizon attractor geometries as solutions to gauged supergravity theories and examined the stability and supersymmetry of one of the solutions (Bianchi Type III) in Chapter 3.

In the next part of the doctoral work in Chapter 4, we turn to a study of transport properties of such anisotropic blackbranes, with a view towards strongly coupled field theories in the presence of an anisotropic driving force. Using techniques from AdS/CFT, our calculations indicate that one may obtain parametric violations of the KSS bound ($\eta/s \geq 1/4\pi$) proposed by Kovtun, Son and Starinets, in such strongly coupled systems in presence of anisotropy. This feature seems to be quite general and holds true for situations where the driving force responsible for breaking rotational symmetry is spatially constant. In particular, we find a general formula for the shear viscosity over the entropy density in terms of the ratio of metric components evaluated at the horizon leading to a parametric violation of the bound proposed by KSS.

If the phenomenon of small shear viscosity components in presence of anisotropy also carries over to the unitary Fermi gases, it may be possible to measure these small viscosities in experiments with trapped ultra-cold Fermi gases. We thus propose a set-up in Chapter 5 involving trapped, ultracold fermions in the unitary regime of the BEC-BCS crossover, where the above suppression of some components of the anisotropic shear viscosity tensor may be observed experimentally. We present the relevant hydrodynamic modes and the trap parameters where this effect is likely to be seen. To the best of our knowledge, this is the first proposal to probe anisotropic shear viscosity in trapped fermions at low temperatures.

In a parallel exploration in this doctoral work, which is independent of the earlier chapters, we considered models of supersymmetry which can incorporate sizeable mixing between different generations of sfermions and performed a detailed collider analysis to devise a signal to probe the lepton flavour violating parameter in such models relevant for the LHC. This is discussed in Chapter 6 and can be read independent of the earlier chapters.

In the following section, we present a non-technical introduction to the basics of AdS/CFT since this is the primary tool we will be using in our computations. Wherever possible, we refer the reader to more elaborate and detailed reviews on the subject.

1.1 Basics of AdS/CFT

Suppose we are interested in a strongly interacting quantum field theory at a finite temperature and finite charge density. Our aim is to investigate the transport properties of such a system. Needless to say, this presents a tough problem in quantum field theory. However, string theory teaches us that there exist classes of quantum field theories which have a dual description in terms of gravitational theories in higher dimensions. This duality is the celebrated AdS/CFT correspondence or, sometimes called holography (see [3] and the references therein). Holography can be used to learn a lot about strongly coupled interacting field theories.

Let us list a few review materials in this context : [4, 5, 6, 7] for applications of holography to condensed matter physics and [8] for holography applied to QCD.

Holography is basically an equivalence between two very different looking theories:

- Strongly interacting quantum field theories in d spacetime dimensions
- Theories of gravity in (d + 1) spacetime dimensions

The quantum field theory resides in the boundary of the spacetime in which gravity lives. The boundary theory is strongly interacting matter involving quantum fields with spin zero, half or one. The boundary quantum field theory does not include gravity. Stretching away from the boundary is the larger space called the bulk. This is the space where the gravity theory lives. In practice this usually is Einstein gravity with a negative cosmological constant and a collection of other fields coupled to gravity. Holography tells us that gravity in the bulk and QFT on the boundary are equivalent. Anything that happens in the bulk is equivalently captured in the boundary theory and vice versa.

Usually in a quantum field theory, we are interested to compute the generating function

$$Z_{QFT}[\phi_0] = \int DA\ exp\left(i[S_{QFT} + \int \phi_0\ \mathcal{O}[A]]\right) \tag{1.1}$$

where A represents all fundamental fields of the theory, S_{QFT} is the action which is a functional of the fields. $\mathcal{O}[A]$ is a gauge invariant operator built from the fields. $\phi_0(x)$ is under our control in a QFT and we usually compute the correlators by taking derivatives with respect to ϕ_0 and ultimately setting it to zero. The key point is that in holographic calculations we make $\phi_0(x)$ dynamical in the bulk and demand $\phi_0(x,u) \to \phi_0(x)$ as one approaches the boundary (The extra radial co-ordinate in the bulk is "u"). The holographic equivalence can be stated in terms of partition functions as

$$Z_{QFT}[\phi_0] \sim Z_{Quantum\ gravity}[\phi_0(x,u) \to \phi_0(x)] \tag{1.2}$$

In the limit of large degrees of freedom in the field theory,

$$Z_{QFT}[\phi_0] \sim e^{iS_{bulk}}\big|_{\phi_0(x,u)\to\phi_0(x)} \tag{1.3}$$

where S_{bulk} is the classical gravity bulk action. Corresponding to the nature of the spin and charge of the operators in the boundary theory, we introduce the bulk fields of similar type, with the dimension of the field theory operators corresponding to the mass of the bulk fields. For example, a scalar operator corresponds to a scalar field in the bulk $\phi(x,u) \to \mathcal{O}(x)$, for a vector we introduce gauge field $A_\mu(x,u) \to J_\mu(x)$, the metric $g_{AB}(x,u) \to T_{\mu\nu}(x)$

corresponds to the stress tensor of the boundary theory.

Typically we are interested in extracting the response due to these sources. In our classical bulk gravity picture, this just boils down to solving classical Einstein Gravity differential equations in the bulk with appropriate boundary conditions. For example, a very quick way to extract the response $<\mathcal{O}(x)>$ due to ϕ_0 goes as follows (using the equivalence of the bulk and boundary partition functions) :

$$<\mathcal{O}(x)>=\frac{1}{Z_{QFT}[\phi_0]}\frac{\partial Z_{QFT}}{\partial\phi_0}\sim\frac{\partial\left(logZ_{QFT}\right)}{\partial\phi_0}\sim\frac{\partial S_{bulk}^{OnShell}}{\partial\phi_0} \tag{1.4}$$

The object on the right is highly reminiscent of Hamilton Jacobi formalism in classical mechanics. One can show that in a QFT this response to the source is just the radial canonical momentum in the bulk evaluated at the boundary and this can be easily found by solving the differential equations for the source field in the bulk.

With this working knowledge of holography, we proceed into the core of the thesis according to the roadmap supplied at the beginning of this introduction.

Chapter 2

Interpolating from Bianchi Attractors to Lifshitz and AdS spacetimes

2.1 Introduction

In the last few years, we have witnessed a beautiful connection develop between gravity and condensed matter physics, or more specifically the study of strongly coupled field theories at finite density. For nice reviews on the subject, we refer to [5, 6, 7, 9]. On the gravity side, motivated by the new and beautiful phases found in nature, new brane solutions have been discovered. These branes have new kinds of hair, or have horizons with reduced symmetry. For example, [10, 11, 12, 13]has discussions on how black hole no-hair theorems can be violated in AdS space in the context of holographic superconductivity; [14, 15, 16] discusses how emergent horizons with properties reflecting dynamical scaling in the dual field theory ("Lifshitz solutions") can arise; and [17, 18, 19, 20, 21, 22, 23] has discussions of horizons exhibiting both dynamical scaling and hyperscaling violation.[1] The earliest work mostly focused on horizons with translational and rotational symmetry, but more recently examples of black brane horizons dual to field theories with further reduced space-time symmetries have been discussed in e.g. [31, 32, 33, 34, 35, 36, 37, 38, 39, 40, 41, 42, 43, 44, 45, 46, 47].

Extremal branes are particularly interesting, since they correspond to ground states of the dual field theory in the presence of a chemical potential or doping. Their near-horizon geometries often exhibit a type of attractor behavior, and as a result, are quite universal and independent of many details. There has been considerable work regarding the attractor mechanism, starting with the pioneering work in [48], ([49] has a nice review). For a review of work on non-supersymmetric attractor mechanism, relevant for our studies, please have

[1] Embeddings of such solutions in string theory have also been discussed in many papers, such as [22, 23, 24, 25, 26, 27, 28, 29, 30].

a look at[50, 51, 52, 53, 54, 55].

Of particular interest to us in this chapter are the brane solutions studied in [34, 35], which correspond to phases of matter which are homogeneous but not isotropic. It was shown that in $4+1$ dimensions, such brane solutions can be classified using the Bianchi classification developed earlier for studying homogeneous cosmologies. In [34, 35], it was found that for extremal black branes of this kind, the near-horizon geometry itself often arises as an exact solution for a system consisting of Einstein gravity coupled to (simple) suitable matter in the presence of a negative cosmological constant. These near-horizon solutions were given the name “Bianchi attractors”.

The attractor nature mentioned above makes the Bianchi attractor geometries more universal, and therefore in many ways more interesting, than the complete extremal black brane solutions from which they arise in the IR. However, some examples of more complete solutions, interpolating between asymptotically AdS space and Bianchi attractors of various Types, are well worth constructing and could lead to a better understanding of the attractor mechanism.

For example, Bianchi attractors have a non-trivial geometry along the field theory directions. It is therefore interesting to ask whether these attractors can arise in situations where the dual field theory lives in flat space, as opposed to the more exotic possibility that the UV field theory itself must be placed in a non-trivial geometry of the appropriate Bianchi Type. This question maps to constructing interpolating extremal black brane solutions and asking whether the non-normalizable deformations for the metric can be asymptotically turned off near the AdS boundary which lies at the ultraviolet end.

For one case, Bianchi Type VII, an explicit interpolating solution of this type was indeed found in [34]. More precisely, it was seen that, in the presence of suitable matter, a solution exists which interpolates between the Bianchi attractor region and $AdS_2 \times R^3$. The latter in turn is well known to arise as the near-horizon region of an extremal Reissner–Nordstrom black brane which is asymptotically AdS_5. In this way, it was shown that Bianchi Type VII can arise as the near-horizon limit of an asymptotically AdS brane. In this solution, no non-normalizable mode for the metric is turned on near the AdS_5 boundary, and therefore the field theory lives in flat $3+1$ dimensional spacetime. Sources are turned on for some of the field theory operators (but none dual to non-normalizable metric modes), and these operators are responsible for the breaking of UV symmetries that leads to Bianchi Type VII.

For the other Bianchi classes, finding such interpolating extremal brane solutions has proved difficult so far. The main complication is a calculational one. It is easy to write down a continuous and sufficiently smooth metric which interpolates between the near-horizon region and asymptotic AdS space, with no non-normalizable metric deformations turned on, for any of the other Bianchi classes. But it is not easy to find such a metric as an explicit solution to the Einstein equations for gravity coupled to some simple matter field theory.

The symmetries of Type VII are a subgroup of the three translations and the rotations in R^3; this allows the equations for the full interpolating solution in the Type VII case to be reduced to algebraic ones, and solved. On the other hand, the symmetries in the other Bianchi Types cannot be embedded in those of R^3, and thus the equations cannot be reduced to merely algebraic ones.

Here, we take a partial step towards finding such interpolating solutions for some of the other Bianchi classes. We start with a particular smoothly varying metric which interpolates between the near-horizon region and Lifshitz spacetime. The metric is chosen so that the non-normalizable deformations of the metric near the Lifshitz boundary are turned off. While we do not obtain these metrics as solutions of Einstein gravity coupled to a specific simple matter field theory, we demonstrate that were they to arise as solutions, the required matter would satisfy the weak energy condition. In this way, we establish that there is no fundamental barrier, at least at the level of reasonable energy conditions, to having such an interpolating solution.

In turn, it is well known that Lifshitz spacetimes, now thought of as the IR end, can be connected to AdS space in the UV. Solutions of this type to Einstein's equations coupled with reasonable matter satisfying the energy conditions have been obtained, see, e.g., [56], [57], [16], [27], [29], [30], [58], [59], [60]. In these solutions often no non-normalisable metric deformations are turned on in the AdS region, although a source for other operators can be present. Taking these solutions together with the interpolating metrics we study, one can then conclude that interpolating geometries exist which connect some of the Bianchi classes to asymptotic AdS space. These interpolations do not violate the energy conditions, and they do not have any non-normalisable deformations for the metric turned on in the asymptotic AdS region. This establishes one of the main results of this chapter.

Hopefully, our result will provide motivation for finding solutions of Einstein's equations sourced by suitable specific matter field theories, which interpolate between the Bianchi classes and Lifshitz or AdS spaces, in the near future. The weak energy condition implies the null energy condition. Thus, our results also imply that no violations of the null energy condition are necessary for the required interpolations. While violations of the null-energy condition are known to be possible, they usually require either quantum effects or exotic objects like orientifold planes in string theory. Our result suggests that these are not required, and that standard matter fields should suffice as sources in constructing these interpolating solutions. Once constructed, these solutions will allow us to ask whether, from the field theory perspective, the symmetries of various Bianchi classes can emerge in the IR, either spontaneously or in response to some suitable source not involving the metric.

Near the end of the chapter, in §6, we also explore the existence of C-functions in flows between Bianchi attractors. We find that if the matter sourcing the geometry satisfies the null energy condition, a function does exist, for a large class of flows, which is monotonically decreasing from the UV to the IR. But unless the attractors meet a special condition, this function does not attain a finite, non-vanishing constant value at the end points. We also show that the area element of the three-dimensional submanifold generated by the Bianchi isometries in the attractor spacetimes monotonically decreases from the UV to the IR.

The plan of the chapter is as follows. In §2, we discuss the weak and null energy conditions. §3 outlines the general procedure we follow in constructing the interpolating metrics and illustrates this for the particular case of Bianchi Type II. Bianchi Type VI and the closely related classes of Type III and V are discussed in §4, and Type IX, for which the interpolation is to $AdS_2 \times S^3$, is discussed in §5. In §6, we explore the existence of a C-function. We end with some conclusions in §7. The appendix contains a more complete discussion of the energy conditions.

2.2 Energy Conditions

We will work in $4+1$ dimensional spacetime and adopt the mostly positive convention for the metric, so that the flat metric is $\eta_{\mu\nu} = \mathrm{diag}(-1, 1, 1, 1, 1)$.

Let us consider a coordinate system x^μ, $\mu = 0, 1, \ldots, d$, with the metric being $g_{\mu\nu}$. We denote the stress energy tensor, as in the standard notation, by $T_{\mu\nu}$, and let n_μ be a null vector, with $n_\mu n_\nu g^{\mu\nu} = 0$. Then the null energy condition (NEC) is satisfied iff

$$T_{\mu\nu} n^\mu n^\nu \geq 0 \tag{2.1}$$

for any future directed null vector, see [61], [62]. Here we will only consider spacetimes which are time reversal invariant, i.e., with a $t \to -t$ symmetry. For such spacetimes the requirement of n^μ being future directed can be dropped.

For the purposes of our analysis it is convenient to state this condition as follows. T^μ_ν can be regarded as a linear operator acting on tangent vectors. Let the orthonormal eigenvectors of this operator be denoted by $\{u_0, u_1, u_2, u_3, u_4\}$, with eigenvalues, $\{\lambda_0, \lambda_1, \lambda_2, \lambda_3, \lambda_4\}$ respectively. Note that orthonormality implies $\langle u_a, u_b \rangle \equiv u_{a\mu} u_{b\nu} g^{\mu\nu} = \eta_{ab}$, so that u_0 is time-like and the other eigenvectors, u_c, $c = 1, \ldots, 4$, are space-like.

Then, as discussed in Appendix A.2, the NEC requires that

$$-\lambda_0 + \lambda_c \geq 0 \tag{2.2}$$

for $c = 1, 2, 3, 4$.

In contrast, the weak energy condition (WEC) requires that

$$T_{\mu\nu} u^\mu u^\nu \geq 0, \tag{2.3}$$

for any future directed time-like vector u^μ [61], [62]. As in the discussion of the NEC above, for the time reversal invariant backgrounds we consider here, the requirement that u^μ is future directed need not be imposed. In terms of the eigenvalues $\{\lambda_0, \lambda_c\}$ of T^μ_ν, this leads to two conditions:

$$\lambda_0 \leq 0 \tag{2.4}$$
$$\lambda_c - \lambda_0 \geq 0, \quad \text{for } c = 1,2,3,4. \tag{2.5}$$

From eq.(2.5) and eq.(2.2) we see that the weak energy condition implies the null energy condition. Thus, the weak energy condition is stronger.

We make two final comments before we end this section. In this chapter, we will follow the conventions of [34], where the action takes the form (see equation (3.4) of [34])

$$S = \int d^5x\sqrt{-g}\,\{R + \Lambda + \cdots\}. \tag{2.6}$$

The ellipsis on the RHS denotes the contribution to the action from matter fields. In these conventions, AdS_5 spacetime is a solution to the Einstein equations, in the absence of matter, for $\Lambda > 0$. It follows then that the cosmological constant required for AdS space violates eq.(2.4) and thus the weak energy condition, but it satisfies eq.(2.2) as an equality, thereby meeting the null energy condition.

Secondly, we have assumed above that the linear operator T^μ_ν is diagonalizable and that its eigenvalues are real. These properties do not have to be true, since T^μ_ν, unlike, $T_{\mu\nu}$, need not be symmetric, and moreover since the inner product is Lorentzian (see [63]). However, for the interpolations we consider, it will turn out that T^μ_ν is indeed diagonalizable with real eigenvalues and therefore we will not have to consider this more general possibility.

2.3 Outline Of Procedure

In this section, we will outline the basic ideas that we follow to find metrics with the required properties that interpolate between the near-horizon attractor region and an asymptotic Lifshitz spacetime. We will illustrate this procedure in the context of one concrete example, which we will take to be Bianchi Type II. Holography in this particular Bianchi attractor was recently studied in depth in [46].

The metrics we consider in general have the form

$$ds^2 = -g_{tt}(r)dt^2 + g_{rr}(r)dr^2 + \sum_{i,j=1,2,3} g_{ij}(r,x^i)dx^i dx^j. \tag{2.7}$$

In the Bianchi attractor region which occurs in the deep IR, for $r \to -\infty$, the metric takes the form,

$$ds_B^2 = -e^{2\beta_t r}dt^2 + dr^2 + \sum_{i=1,2,3} e^{2\beta_i r}(\omega^i)^2, \tag{2.8}$$

where ω^i are one-forms invariant under the Bianchi symmetries generated by the Killing fields ξ_i, $i = 1, 2, 3$ (More generally, off-diagonal terms are also allowed in eq.(2.8) but we will not consider this possibility here.) The commutation relations of the Killing vectors [2]

$$[\xi_i, \xi_j] = C^k_{ij} \xi_k \tag{2.9}$$

give rise to the corresponding Bianchi algebra.

In the far UV on the other hand, which occurs for $r \to \infty$, the metric becomes of Lifshitz form,

$$ds^2_L = -e^{2\tilde{\beta}_t r} dt^2 + dr^2 + e^{2\tilde{\beta} r} \sum_{i=1,2,3} dx_i^2. \tag{2.10}$$

Here for simplicity, we only consider the case where all the spatial directions have the same scaling exponent, $\tilde{\beta}$, more generally this exponent can be different for the different spatial directions. Also, to avoid unnecessary complications we take the exponent in the time direction $\tilde{\beta}_t$ in the Lifshitz region to satisfy the condition

$$\tilde{\beta}_t = \beta_t, \tag{2.11}$$

where β_t is the value for the exponent in the Bianchi attractor region, eq.(2.8). The metric eq.(2.10) then becomes

$$ds^2_L = -e^{2\beta_t r} dt^2 + dr^2 + e^{2\tilde{\beta} r} \sum_{i=1,2,3} (dx^i)^2. \tag{2.12}$$

The metric which interpolates between these two regions is taken to have the form

$$ds^2 = \left(\frac{1 - \tanh \sigma r}{2} \right) ds^2_B + \left(\frac{1 + \tanh \sigma r}{2} \right) ds^2_L, \tag{2.13}$$

where ds^2_B and ds^2_L are defined in eq.(2.8) and eq.(2.10) respectively. σ is a positive constant which characterizes how rapid or gradual the interpolation is. One can show, and this will become clearer in the specific examples we consider below, that as long as σ is sufficiently big the metric becomes of the Bianchi attractor form as $r \to -\infty$. Also, for sufficiently large σ the metric becomes of Lifshitz type as $r \to \infty$. More correctly, for this latter statement to be true the limit $r \to \infty$ must be taken keeping the spatial coordinates $x^i, i = 1, 2, 3$ fixed. We will also comment on this order of limits in more detail below.

We should emphasize that we do not obtain the interpolating metric in eq.(2.13) as a solution to Einstein's equations coupled to suitable matter. Instead, what we will do is to construct from the metric, via the Einstein equations, a stress energy tensor for matter and then examine whether this stress energy satisfies the energy conditions.

[2] The Bianchi classification is described in [64], [65], including the symmetry generators and invariant one-forms; also see A.1 of Appendix.

Let us mention that one can try to obtain a full interpolating solution using simple gauge field matter content. For example, the metric which interpolates between these two regions may be taken to have the form

$$ds^2 = f(r)ds_B^2 + g(r)ds_L^2, \tag{2.14}$$

where ds_B^2 and ds_L^2 are defined in eq.(2.8) and eq.(2.10) respectively.

The gauge field may be taken to be of the form

$$A = \sqrt{A_t}\, e^{\beta_t r} h(r) + \sqrt{\tilde{A}_t}\, e^{\tilde{\beta}_t r} k(r) dt. \tag{2.15}$$

Here f(r),g(r),h(r) and k(r) are appropriate interpolating functions such that the geometry interpolates from Lifshitz in the UV to respective Bianchi attractor in the IR. However, the resulting differential equations are too complicated to solve. However, such a technique is worthy of further exploration.

Below, we will analyze cases where the interpolation is from attractor geometries of Bianchi Type II, III, V, or VI to Lifshitz geometry. In addition, using a different strategy, we will also consider the interpolation from Type IX to $AdS_2 \times S^3$.

2.3.1 More Details for the Type II Case

Let us now give more details for how the analysis proceeds in the Type II case.

It will be convenient in the analysis to take the Bianchi attractor geometry and the Lifshitz geometry which arise in the IR and UV ends of the interpolation as solutions of Einstein's equations coupled to reasonable matter. This ensures that the energy conditions will be satisfied at least asymptotically. In fact the Bianchi attractor geometry and the Lifshitz geometry can both arise as solutions in a system of gravity coupled to a massive Abelian gauge field in the presence of a cosmological constant, with an action of the form,

$$S = \int d^5x\sqrt{-g}\left(R + \Lambda - \frac{1}{4}F^2 - \frac{1}{4}m^2 A^2\right). \tag{2.16}$$

The Type II solutions which arise from this action were discussed in [34] and we will mostly follow the same conventions here. The invariant one-forms for Type II are given by

$$\omega^1 = dy - x\,dz, \quad \omega^2 = dz, \quad \omega^3 = dx. \tag{2.17}$$

The solutions of Type II obtained from eq.(2.16) were described in eq.(4.2), (4.3) and (4.10), (4.11) in [34]. The metric and gauge field in these solutions take the form

$$ds_B^2 = R^2[dr^2 - e^{2\beta_t r}dt^2 + e^{2(\beta_2+\beta_3)r}(\omega^1)^2 + e^{2\beta_2 r}(\omega^2)^2 + e^{2\beta_3 r}(\omega^3)^2] \tag{2.18}$$

and

$$A = \sqrt{A_t}\, e^{\beta_t r} dt. \tag{2.19}$$

These solutions are characterized by five parameters, R, β_t, β_2, β_3, A_t. The equations of motion give rise to five independent equations which determine these parameters in terms of m^2, Λ. For our purposes it will be convenient to work in units where $R = 1$ and to use the equations of motion to express β_t, β_1, β_2, A_t and m^2 in terms of Λ. The resulting relations are,

$$\beta_t = v, \tag{2.20}$$

$$\beta_2 = \beta_3 = -\frac{(3 - \Lambda + u)v}{36 - 8\Lambda}, \tag{2.21}$$

$$m^2 = \frac{8}{11}(6 - \Lambda + u), \tag{2.22}$$

$$A_t = \frac{-11v^2 + 3u}{18 - 4\Lambda}, \tag{2.23}$$

where

$$u = \sqrt{-63 + 10\Lambda + \Lambda^2},$$
$$v = \left[\frac{-81 + 19\Lambda + 3u}{22}\right]^{\frac{1}{2}}.$$

Demanding that $A_t, m^2, \beta_t, \beta_2, \beta_3$ be positive and u be real, we get $\Lambda > \frac{9}{2}$. The Lifshitz metric which we are interested in near the boundary also arises as a solution from the action in eq.(2.16). The metric and gauge field in this solution take the form

$$ds_L^2 = dr^2 - e^{2\beta_t r} dt^2 + e^{2\tilde{\beta} r} dx^2 + e^{2\tilde{\beta} r} dy^2 + e^{2\tilde{\beta} r} dz^2 \tag{2.24}$$

and

$$A = \sqrt{A_t}\, e^{\beta_t r} dt. \tag{2.25}$$

The solution is characterized by three parameters, β_t, $\tilde{\beta}, A_t$ which are determined in terms of m^2 and Λ. For our purposes it is more convenient to express $\tilde{\beta}, A_t$ and m^2 in terms of β_t and Λ. These relations, which arise due to the equations of motion, are

$$\tilde{\beta} = \frac{1}{9}\left(-\beta_t + \sqrt{-8\beta_t^2 + 9\Lambda}\right), \tag{2.26}$$

$$m^2 = \frac{2}{3}\beta_t\left(-\beta_t + \sqrt{-8\beta_t^2 + 9\Lambda}\right), \tag{2.27}$$

$$A_t = \frac{2}{9}\left(10 - \frac{1}{\beta_t}\sqrt{-8\beta_t^2 + 9\Lambda}\right). \tag{2.28}$$

In order to ensure that $\tilde{\beta}, A_t, m^2$ are all nonnegative, we must have $\beta_t > 0$, $\beta_t^2 \leq \Lambda \leq 12\beta_t^2$. We will consider Lifshitz metric where these conditions hold.

The Type II and Lifshitz solutions we consider correspond to the same value of the cosmological constant. It will also be convenient to take the exponent β_t along the time direction in the Type II and Lifshitz cases to be the same as discussed in eq.(2.11). This will mean that the mass parameter m^2 for the Type II and Lifshitz cases will be different in general.

A negative cosmological constant (in our conventions $\Lambda > 0$) violates the weak energy condition, thus in studying the violations of this condition it is useful to separate the contributions of the cosmological constant from the matter in the stress energy. Since the two asymptotic geometries we consider arise as solutions with the same value of the cosmological constant we can consistently take the cosmological constant to have this same value throughout the interpolation. Using the Einstein equations we can then define a matter stress tensor, minus the cosmological constant, and then study its behavior with respect to the weak energy condition. The null energy condition, in contrast to the weak energy condition, does not receive contributions from the cosmological constant, and so for studying its possible violations such a separation between matter and the cosmological constant components is not necessary.

We now turn to the full interpolating metric. As discussed in the previous subsection this takes the form

$$\begin{aligned} ds^2 = dr^2 &- e^{2\beta_t r} dt^2 \\ &+ \left[\left(\frac{1-\tanh\sigma r}{2}\right) e^{2\beta_3 r} + \left(\frac{1+\tanh\sigma r}{2}\right) e^{2\tilde{\beta} r}\right] dx^2 \\ &+ \left[\left(\frac{1-\tanh\sigma r}{2}\right) e^{2(\beta_2+\beta_3) r} + \left(\frac{1+\tanh\sigma r}{2}\right) e^{2\tilde{\beta} r}\right] dy^2 \\ &+ \left[\left(\frac{1-\tanh\sigma r}{2}\right) (x^2 e^{2(\beta_2+\beta_3) r} + e^{2\beta_2 r}) + \left(\frac{1+\tanh\sigma r}{2}\right) e^{2\tilde{\beta} r}\right] dz^2 \\ &- x\left(\frac{1-\tanh\sigma r}{2}\right) e^{2(\beta_2+\beta_3) r}(dy\otimes dz + dz\otimes dy). \end{aligned} \tag{2.29}$$

We note that in the limit of r becoming very large, the above may be approximated by

$$\begin{aligned} ds^2 = dr^2 - e^{2\beta_t r} dt^2 &+ \left[e^{2(\beta_3-\sigma) r} + e^{2\tilde{\beta} r}\right] dx^2 \\ &+ \left[e^{2(\beta_2+\beta_3-\sigma) r} + e^{2\tilde{\beta} r}\right] dy^2 \\ &+ \left[x^2 e^{2(\beta_2+\beta_3-\sigma) r} + e^{2(\beta_2-\sigma) r} + e^{2\tilde{\beta} r}\right] dz^2 \\ &- x e^{2(\beta_2+\beta_3-\sigma) r}(dy\otimes dz + dz\otimes dy). \end{aligned} \tag{2.30}$$

To ensure that this metric approaches the Lifshitz geometry as $r \to \infty$, with exponentially small corrections, the terms arising from the Lifshitz metric, eq(2.24), must dominate in every component of the metric. It is easy to see that this condition is met when

$$\sigma > \beta_2 + \beta_3. \tag{2.31}$$

Similarly, one finds that the conditions requiring the metric to become of the Bianchi II type, eq.(2.18), in the IR are also met when σ satisfies the condition in eq.(2.31).

Actually, the $r \to +\infty$ limit is a bit subtle. As one can see from the coefficient of the dz^2 and the $(dy \otimes dz + dz \otimes dy)$ terms in eq.(2.30), eq.(2.31) ensures that the metric becomes of Lifshitz type when $r \to \infty$, as long as x is constant, or at least for $|x|$ growing sufficiently slowly in this limit. This is in fact the limit we will consider in our discussion.

Taking the limit in this way is well motivated physically. It is quite reasonable to place the dual field theory whose properties we are interested in studying in a box of finite size. In fact this is always the case in any experimental situation. In such a finite box the range of the spatial coordinates is finite ensuring that the $r \to \infty$ limit is of the required type. As long as the box is sufficiently big, compared to the other scales, e.g. the temperature, the properties of the system, e.g. its thermodynamics, do not depend in a sensitive way on the size of the box.

While the requirement for getting the correct asymptotic behavior imposes a lower bound on σ, eq.(2.31), meeting the energy conditions give rise to an upper bound on σ, as we will see below. It will turn out that there is a finite region for the allowed values of σ between these two bounds, for the Type II case, and by choosing σ to lie in this region an acceptable interpolation meeting the energy conditions can be obtained.

Energy Conditions for the Type II Interpolation

With the interpolating metric in hand, we can now test the various energy conditions. We do so numerically.

From the metric, eq.(2.29), we define a stress tensor, assuming that the Einstein equations are valid. This gives

$$T_{\mu\nu} \equiv R_{\mu\nu} - \frac{1}{2} g_{\mu\nu} R. \tag{2.32}$$

(We set $\kappa = 8\pi G_N = 1$.) This stress energy tensor in turn is separated into a matter and a cosmological constant contribution. With our conventions, eq.(2.6), we get

$$T_{\mu\nu} = \frac{\Lambda}{2} g_{\mu\nu} + T^{(\text{matter})}_{\mu\nu}. \tag{2.33}$$

Combining these two equations gives

$$T^{(\text{matter})}_{\mu\nu} = R_{\mu\nu} - \frac{1}{2} g_{\mu\nu} R - \frac{\Lambda}{2} g_{\mu\nu}. \tag{2.34}$$

To analyze whether the energy conditions are valid, we first note that owing to the form we have chosen for the interpolating metric, eq.(2.29), $T^{(\text{matter})\mu}_{\nu}$ is block diagonal. Therefore, its eigenvalues take the simple form

$$\lambda_0 = -\frac{\Lambda}{2} + T_t^t, \tag{2.35}$$
$$\lambda_1 = \frac{1}{2}\left[-\Lambda + T_r^r + T_x^x + \left[(T_r^r - T_x^x)^2 + 4T_r^x T_x^r\right]^{\frac{1}{2}}\right], \tag{2.36}$$
$$\lambda_2 = \frac{1}{2}\left[-\Lambda + T_r^r + T_x^x - \left[(T_r^r - T_x^x)^2 + 4T_r^x T_x^r\right]^{\frac{1}{2}}\right], \tag{2.37}$$
$$\lambda_3 = \frac{1}{2}\left[-\Lambda + T_y^y + T_z^z + \left[\left(T_y^y - T_z^z\right)^2 + 4T_y^z T_z^y\right]^{\frac{1}{2}}\right], \tag{2.38}$$
$$\lambda_4 = \frac{1}{2}\left[-\Lambda + T_y^y + T_z^z - \left[\left(T_y^y - T_z^z\right)^2 + 4T_y^z T_z^y\right]^{\frac{1}{2}}\right]. \tag{2.39}$$

Since we obviously have $\lambda_1 \geq \lambda_2$ and $\lambda_3 \geq \lambda_4$, the criteria discussed in §2 above reduces to just checking whether the following conditions hold:

$$\lambda_0 \leq 0, \lambda_2 - \lambda_0 \geq 0, \lambda_4 - \lambda_0 \geq 0. \tag{2.40}$$

For the numerics, we set

$$\Lambda = 12. \tag{2.41}$$

(In $R = 1$ units).

From eq.(2.21) we can now determine β_2, β_3 and thus the lower bound on σ, eq.(2.11), which turns out to be $\sigma_{\text{lower}} = 0.5065$. As we increase σ we find in the numerical analysis that violations of the null energy condition start setting in around $\sigma = 1.05026$. The weak energy condition is not violated before this. Thus, there is a finite interval $0.5065 < \sigma < 1.05$, within which both the correct asymptotic behavior for the metric is obtained and the null and weak energy conditions are met.

To illustrate this, we consider the case where $\sigma = 1$ in more detail. It turns out that $\lambda_2 < \lambda_4$, where the eigenvalues are defined in eq.(2.35), eq.(2.36), eq.(2.37), eq.(2.38), eq.(2.39).

The plots of λ_0 and $\min(\lambda_c - \lambda_0) = \lambda_2 - \lambda_0$, are given in fig. 2.1, 2.2. From fig. 2.1 we see that λ_0 is always negative. In fig. 2.2 we see that $\min(\lambda_c - \lambda_0) > 0$ but there is a region around $r \sim 3$ where it becomes very small. We have investigated this region further in much more detail numerically and find that even after going out to arbitrarily large values of x, $\min(\lambda_c - \lambda_0)$ continues to be positive in the worrisome range $2 < r < 8$. For a fixed value of r, in this range, as we go out to larger x the value of $\min(\lambda_c - \lambda_0)$ decreases reaching a minimum value for $|x| \to \infty$. For example, the resulting plot for $r = 3$, as a function of x, is given in fig. 2.3 where we see that the minimum value obtained for $\min(\lambda_c - \lambda_0)$ is positive. For other values of r in this range a qualitatively similar plot is obtained as x is varied with the minimum value of $\min(\lambda_c - \lambda_0)$ again being positive. As an additional check, we have analytically computed the value of $\min(\lambda_c - \lambda_0)$ in the limit where $|x| \to \infty$. In the worrisome region $2 < r < 8$ we find that this value is positive. We show this in fig.

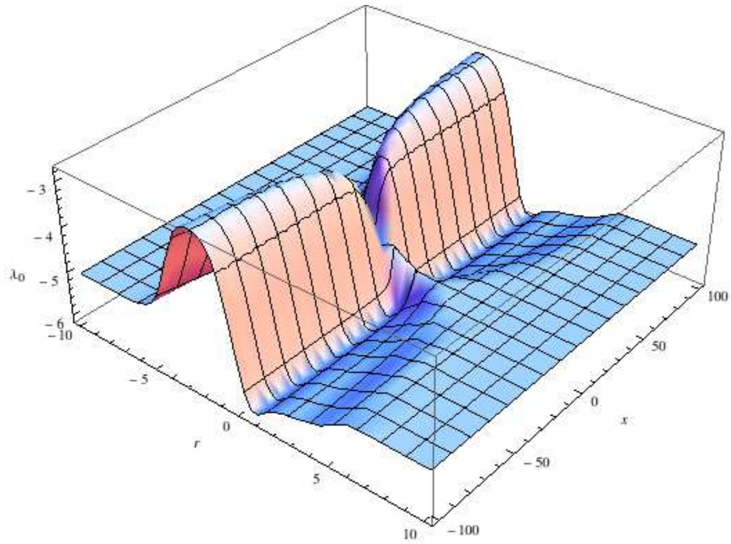

Figure 2.1: Type II 3D plot of λ_0 (time-like eigenvalue) versus r and x for $\sigma = 1,\ \Lambda = 12$.

2.4 where the limiting value of $\min(\lambda_c - \lambda_0)$, as $|x| \to \infty$, is plotted as a function of r. We see that as r increases, this limiting value at first decreases, reaching a minimum at around $r = 5$, and then increases again. The minimum value is clearly positive showing that the null energy condition is indeed met everywhere in the interpolating metric.

Let us end this section with one comment. Because of the upper bound on σ, which arises in order to meet the energy conditions, the metric cannot approach that of Lifshitz space arbitrarily rapidly. The reader might worry that the values of σ allowed by this bound are too small to be physically acceptable. To explain this, consider as an example the more familiar case of asymptotically AdS_5 spacetime. Since a domain wall in AdS_5 ought to carry positive energy density and pressure, one might expect that the rate at which the metric of such a solution approaches AdS_5 is governed by the normalizable metric deformations of AdS_5, and should not be slower. A similar type of argument should also apply to Lifshitz spaces. However, this expectation need not be valid if other fields are also turned on, since these fields can source the metric, and this can lead to a fall-off slower than that expected from the normalizable mode of the metric itself.

2.4 Types VI, V and III

We now turn to constructing metrics which interpolate from Bianchi Types VI, III and V to Lifshitz. Since our discussion will closely parallel that for Type II above, we will skip some details. We will find that an analysis along the lines above will successfully lead to a class of interpolating metrics for Type VI and Type III, meeting the weak and null energy conditions. However, for reasons which will become clearer below, we do not succeed in finding such an interpolating metric for Type V.

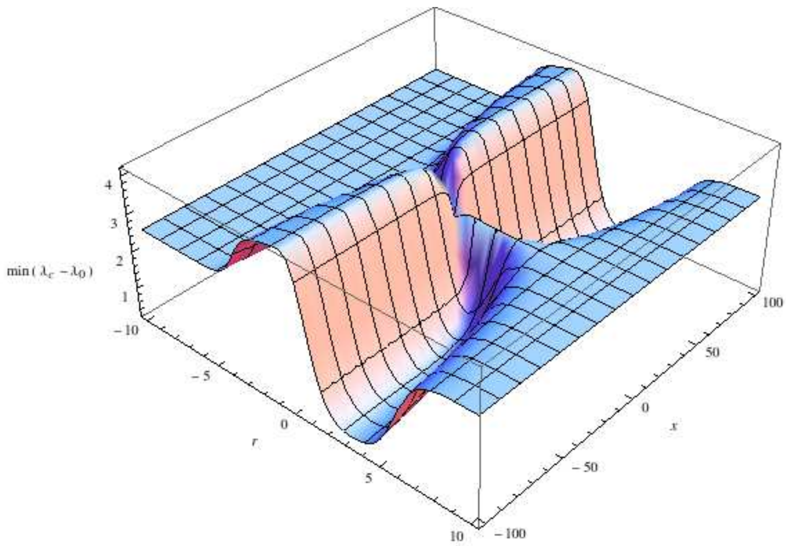

Figure 2.2: Type II 3D plot of $\min(\lambda_c - \lambda_0)$ versus r and x for $\sigma = 1,\ \Lambda = 12$.

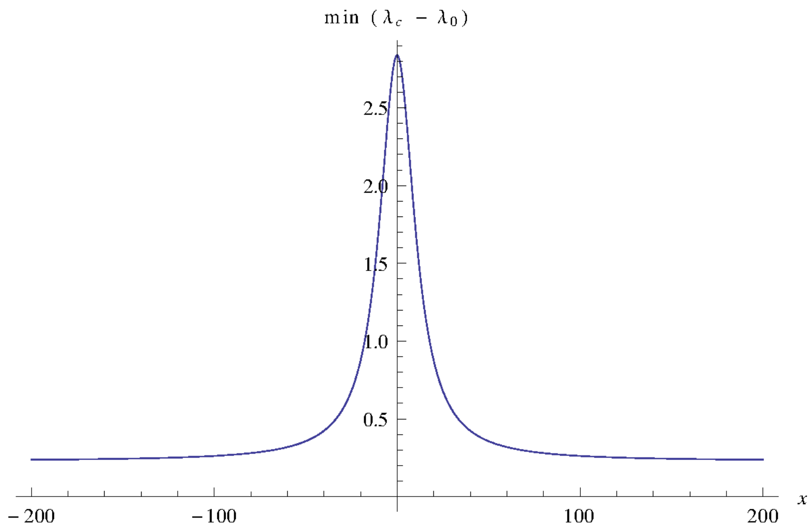

Figure 2.3: Type II plot of $\min(\lambda_c - \lambda_0)$ versus x at $r = 3$ for $\sigma = 1,\ \Lambda = 12$.

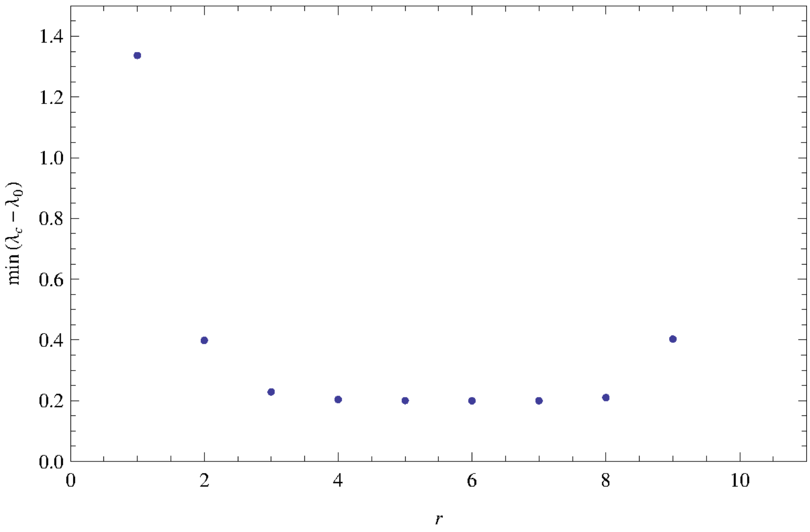

Figure 2.4: Type II list plot of $\min(\lambda_c - \lambda_0)$ versus r as $x \to \pm\infty$ for for $\sigma = 1,\ \Lambda = 12$.

The algebra for a general Type VI spacetime is characterized by one parameter 'h'. Killing vectors and invariant one-forms for Type VI are given in Appendix A of [34] (see also [65]),

$$\xi_1 = \partial_y, \quad \xi_2 = \partial_z, \quad \xi_3 = \partial_x + y\partial_y + hz\partial_z \tag{2.42}$$

and

$$\omega^1 = e^{-x}dy, \quad \omega^2 = e^{-hx}dz, \quad \omega^3 = dx\ . \tag{2.43}$$

These depend on the parameter h.

The Type V algebra is a special case of Type VI, and is obtained by setting $h = 1$. The Killing vectors and invariant one-forms can then be obtained from eq.(2.42) and eq.(2.43) by setting $h = 1$. Similarly the Type III algebra is also a special case obtained by setting $h = 0$, with the Killing vectors and one-forms given by setting $h = 0$ in the equations above.

To keep the discussion simple, we restrict ourselves to only considering the case $h = -1$ for Type VI, besides also considering the Type V and Type III cases.

The invariant one-forms for Type VI with $h = -1$ are

$$\omega^1 = e^{-x}dy, \quad \omega^2 = e^{x}dz, \quad \omega^3 = dx. \tag{2.44}$$

Bianchi Type VI attractor solutions, for the case $h = -1$, were obtained in Section 4.2 of [34] for a system of gravity coupled with a massive gauge field, with an action eq.(2.16). The solution has a metric,

$$ds_B^2 = R^2[dr^2 - e^{2\beta_t r}dt^2 + e^{2\beta_1 r}(\omega^1)^2 + e^{2\beta_2 r}(\omega^2)^2 + e^{2\beta_3 r}(\omega^3)^2] \tag{2.45}$$

and a gauge field, eq.(2.19), with the invariant one-forms being given in eq.(2.44). As in the discussion for Type II we will work in $R = 1$ units below. The exponents β_t, β_1, β_2, β_3 in the solution are then given in terms of Λ by

$$\beta_t = v, \tag{2.46}$$

$$\beta_1 = \beta_2 = \frac{(-4 + \Lambda - u)v}{24 - 4\Lambda}, \tag{2.47}$$

$$\beta_3 = 0, \tag{2.48}$$

while the mass and A_t are

$$m^2 = \frac{2}{3}(8 - \Lambda + u), \tag{2.49}$$

$$A_t = \frac{-3v^2 + u}{6 - \Lambda}, \tag{2.50}$$

where

$$u = \sqrt{-80 + 8\Lambda + \Lambda^2}, \tag{2.51}$$

$$v = \left[\frac{-28 + 5\Lambda + u}{6}\right]^{\frac{1}{2}}. \tag{2.52}$$

Demanding that $A_t, m^2, \beta_t, \beta_1, \beta_2$ be positive and u be real, we get $\Lambda > 6$. The Lifshitz spacetime in the UV is also obtained as a solution of the same system, eq.(2.16). The metric is given by eq.(2.24) and the gauge field by eq.(2.25). The exponent $\beta_t, \tilde{\beta}$ and A_t are given in eq.(2.26), (2.27) and (2.28) in terms of m^2, Λ. We will take the value of Λ to be the same in the IR Type VI and the UV Lifshitz theories. For simplicity we will also take condition eq.(2.11) to hold so that the exponents along the time direction are the same, accordingly we have denoted both of them as β_t above.

The strategy we now follow is similar to the Type II case. The interpolating metric is given by eq.(2.13), which when written out in full becomes

$$\begin{aligned}
ds^2 = dr^2 &- e^{2\beta_t r}dt^2 \\
&+ \left[\left(\frac{1 - \tanh \sigma r}{2}\right) + \left(\frac{1 + \tanh \sigma r}{2}\right) e^{2\tilde{\beta} r}\right] dx^2 \\
&+ \left[\left(\frac{1 - \tanh \sigma r}{2}\right) e^{2\beta_1 r - 2x} + \left(\frac{1 + \tanh \sigma r}{2}\right) e^{2\tilde{\beta} r}\right] dy^2 \\
&+ \left[\left(\frac{1 - \tanh \sigma r}{2}\right) e^{2\beta_2 r + 2x} + \left(\frac{1 + \tanh \sigma r}{2}\right) e^{2\tilde{\beta} r}\right] dz^2.
\end{aligned} \tag{2.53}$$

As in the Type II case, we again require that the interpolating metric correctly asymptotes to Type VI in the IR and Lifshitz in the UV. This now imposes the lower bound

$$\sigma > \beta_1 - \tilde{\beta} = \beta_2 - \tilde{\beta}. \tag{2.54}$$

We remind the reader again that the $r \to +\infty$ limit is taken while keeping x fixed to obtain this bound.

We take Λ (in $R = 1$ units) to have the value given in eq.(2.41). The lower bound for σ then becomes, $\sigma > 0.0579912$. The matter stress tensor is then calculated as given in eq.(2.34) and we examine its properties with respect to the energy conditions numerically.

The numerical analysis shows that as σ is increased violations of the null energy condition start setting in around $\sigma = 1.15993$. The weak energy condition is not violated for smaller values of σ. Thus, as in the the Type II case, there is a non-vanishing interval for σ within which the metric has the correct asymptotic behavior and the weak and null energy conditions are both met.

To illustrate this, consider the case when $\sigma = 1$, which lies within this interval. The minimum of the eigenvalues of the spatial eigenvectors turns out to be λ_2, where the eigenvalues are defined in eq.(2.35)–eq.(2.39). The plots of λ_0 and $\min(\lambda_c - \lambda_0) = \lambda_2 - \lambda_0$, are given in fig. 2.5, 2.6, as a function of the r, x coordinates. We see that the qualitative behavior is similar to that in Type II. λ_0 is always negative. And $\lambda_2 - \lambda_0$ is positive but there is a worrisome region around $r = 5$ where this difference of eigenvalues becomes small. We have analyzed this region more carefully further. One finds that for any fixed $r \in [4, 9]$ the minimum value for $\lambda_2 - \lambda_0$ is attained as $|x| \to \infty$ and moreover this minimum value is positive. An analytic expression for this minimum value was also obtained and agrees with the numerical results. This is shown in fig. 2.7 where this minimum value is plotted as a function of r and shown to be positive. These results establish that the interpolating metric eq.(2.53) satisfies both the weak and the null energy conditions when σ takes values within a suitable range.

2.4.1 Type III

Since the analysis follows that of the Type VI case closely we will be more brief for this case.

The invariant one-forms for Type III, see Appendix A of [34], are given by

$$\omega^1 = e^{-x} dy, \quad \omega^2 = dz, \quad \omega^3 = dx. \tag{2.55}$$

Solutions of Type III for the system described by the action eq.(2.16) exist and have been discussed in section 4.2.2 of [34]. These take the form eq.(2.45), eq.(2.19) for the metric and gauge field. The exponents β_t, β_1, β_2, the gauge field A_t and m^2 (in $R = 1$ units) are

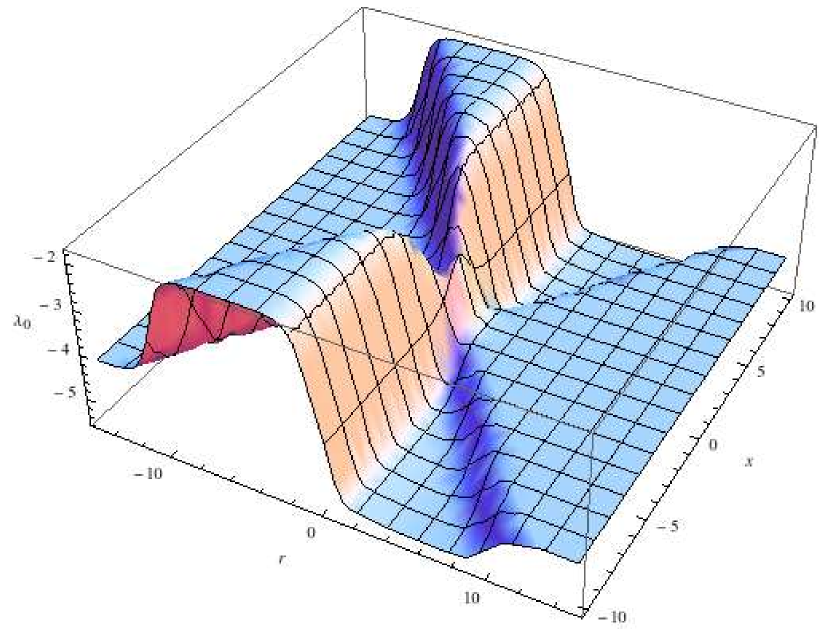

Figure 2.5: Type VI 3D plot of λ_0 (time-like eigenvalue) versus r and x for $\sigma = 1,\ \Lambda = 12$.

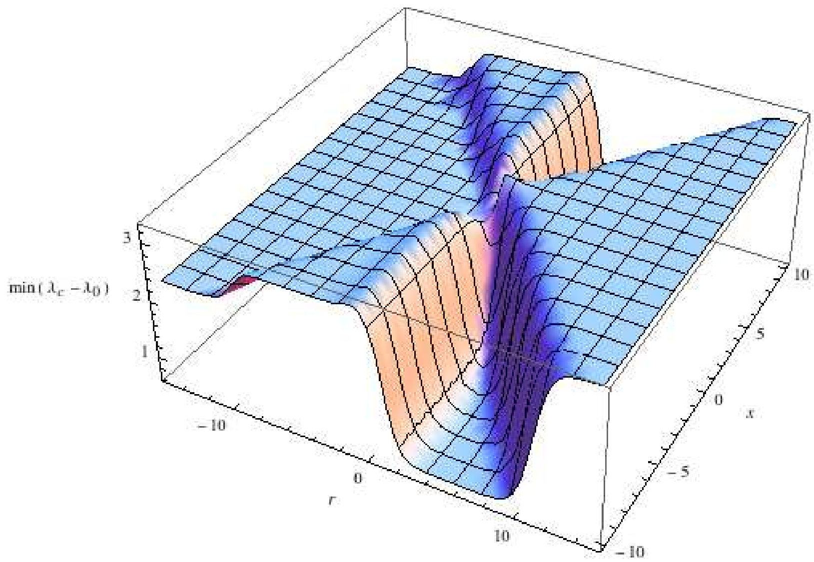

Figure 2.6: Type VI 3D plot of $\min(\lambda_c - \lambda_0)$ versus r and x for $\sigma = 1,\ \Lambda = 12$.

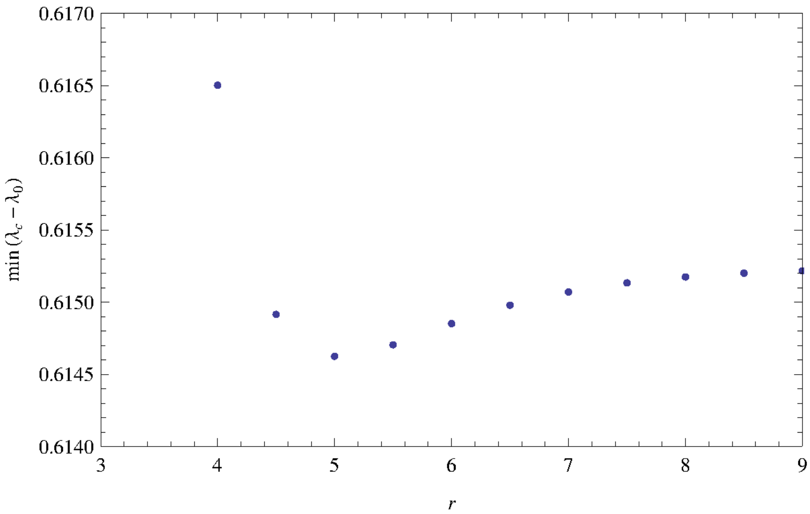

Figure 2.7: Type VI list plot of $\min(\lambda_c - \lambda_0)$ versus r as $x \to \pm\infty$ for $\sigma = 1,\ \Lambda = 12$.

given by

$$\beta_t = v, \tag{2.56}$$

$$\beta_1 = \beta_3 = 0, \tag{2.57}$$

$$\beta_2 = \frac{(-2+\Lambda-u)v}{6-2\Lambda}, \tag{2.58}$$

$$m^2 = \frac{1}{2}(4-\Lambda+u), \tag{2.59}$$

$$A_t = \frac{-4v^2+2u}{3-\Lambda}, \tag{2.60}$$

where

$$u = \sqrt{-8+\Lambda^2}, \tag{2.61}$$

$$v = \frac{\sqrt{-8+3\Lambda+u}}{2}. \tag{2.62}$$

Demanding that $A_t, m^2, \beta_t, \beta_2$ be positive and u to be real, we get $\Lambda > 3$. To obtain the desired interpolation from a Bianchi Type III solution to Lifshitz, we follow the strategy adopted in case of Type II, VI, above, and consider the following interpolating metric:

$$\begin{aligned} ds^2 = {} & dr^2 - e^{2\beta_t r} dt^2 \\ & + \left[\left(\frac{1-\tanh\sigma r}{2} \right) + \left(\frac{1+\tanh\sigma r}{2} \right) e^{2\tilde{\beta} r} \right] dx^2 \\ & + \left[\left(\frac{1-\tanh\sigma r}{2} \right) e^{-2x} + \left(\frac{1+\tanh\sigma r}{2} \right) e^{2\tilde{\beta} r} \right] dy^2 \\ & + \left[\left(\frac{1-\tanh\sigma r}{2} \right) e^{2\beta_2 r} + \left(\frac{1+\tanh\sigma r}{2} \right) e^{2\tilde{\beta} r} \right] dz^2. \end{aligned} \tag{2.63}$$

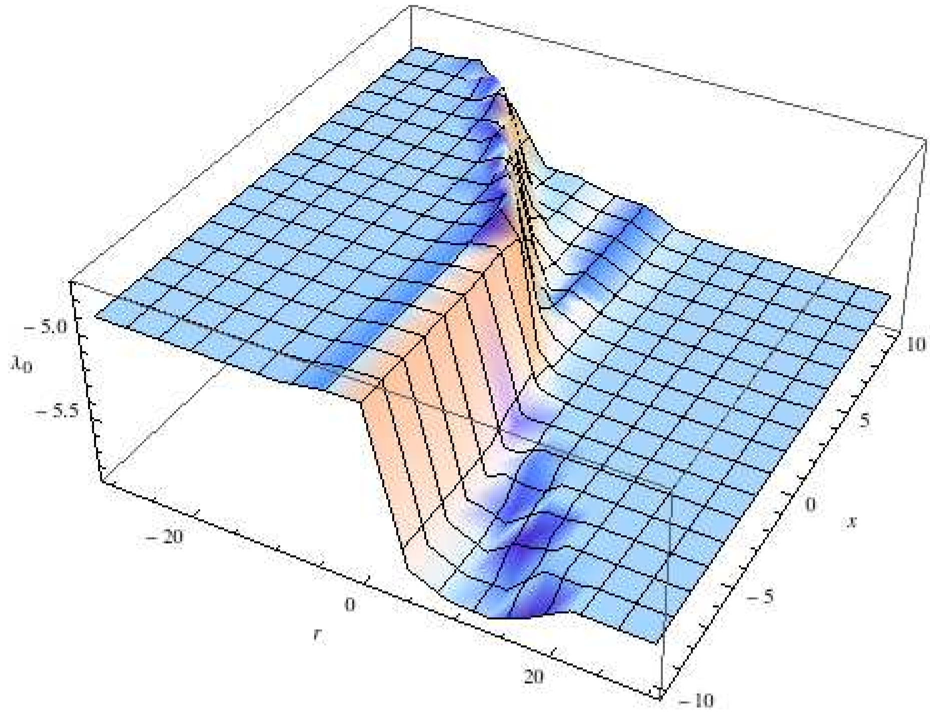

Figure 2.8: Type III 3D plot of λ_0 (time-like eigenvalue) versus r and x for $\sigma = 0.3,\ \Lambda = 12$.

Requiring this interpolating metric to correctly asymptote to Type VI in the IR and Lifshitz in the UV imposes the following lower bound: $\sigma > \beta_2 - \tilde{\beta}$. We choose $\Lambda = 12$ in $R = 1$ units. The lower bound for σ then becomes, $\sigma > 0.0456046$.

Furthermore, we numerically find that violations of the null energy condition start setting in around $\sigma = 0.40108$. The weak energy condition is not violated for smaller values of σ. Thus, we find once again that there is a range of values for σ for which the metric asymptotes to the required forms and for which the weak and null energy conditions are preserved.

To illustrate this, we choose $\sigma = 0.3$ which lies in the allowed region. The plots of λ_0 and $\min(\lambda_c - \lambda_0) = \lambda_2 - \lambda_0$, where λ_0 and λ_2 are as defined in eq.(2.35) and eq.(2.37), are given in fig. 2.8 and fig. 2.9. We see that λ_0 is always negative. And $\lambda_2 - \lambda_0$ is positive but this difference becomes small near $r \sim 10 - 15$ as $x \to -\infty$. We examined this region in more detail and find that for any fixed r in this region $\lambda_2 - \lambda_0$ attains its minimum value as x is varied for $x \to -\infty$ and this minimum value is indeed positive. An analytic expression for this minimum value was obtained, and agrees with the numerical analysis. In fig 2.10 we plot this minimum value, attained when $x \to -\infty$, for $\lambda_2 - \lambda_0$ against r. We see that the minimum value is positive. These results establish that the interpolating metric eq.(2.63) in the Type III case also meets the weak and null energy conditions for a suitable range of σ values.

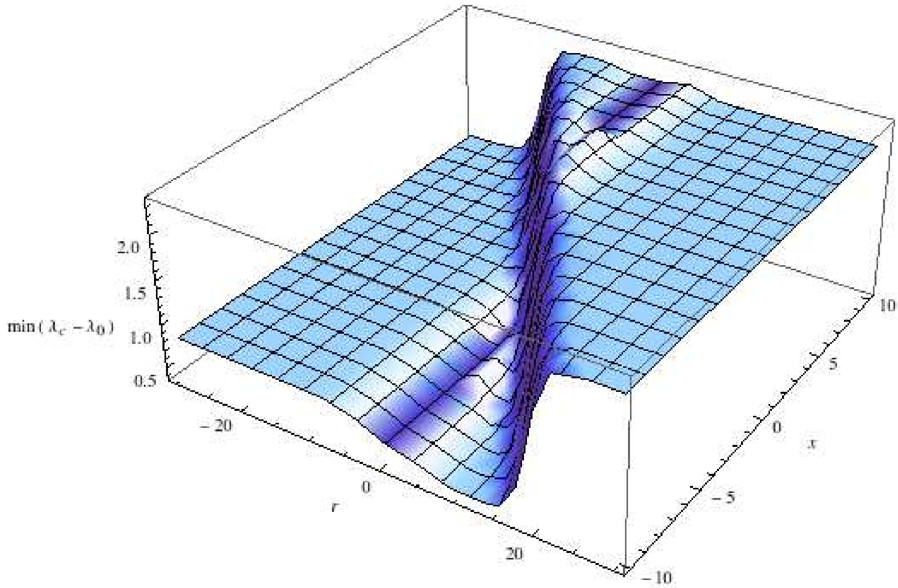

Figure 2.9: Type III 3D plot of $\min(\lambda_c - \lambda_0)$ versus r and x for $\sigma = 0.3,\ \Lambda = 12$.

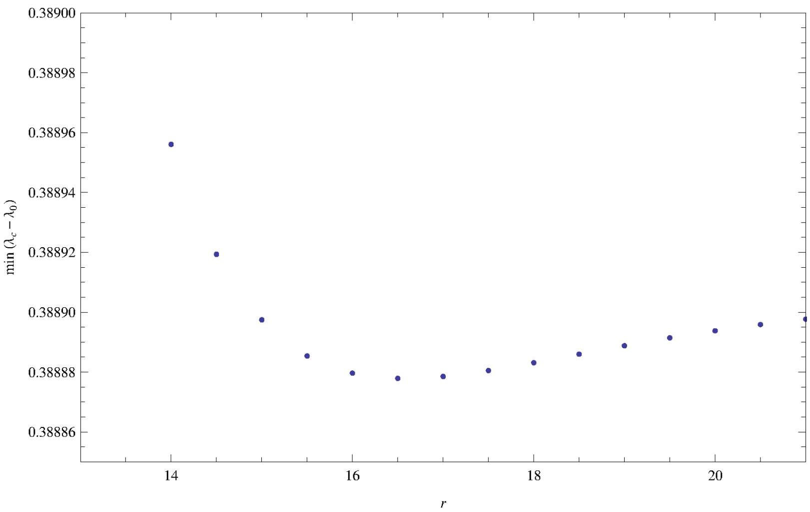

Figure 2.10: Type III list plot of $\min(\lambda_c - \lambda_0)$ versus r as $x \to -\infty$ for $\sigma = 0.3,\ \Lambda = 12$.

2.4.2 Type V

The invariant one-forms in the Type V case are

$$\omega^1 = e^{-x}dy, \quad \omega^2 = e^{-x}dz, \quad \omega^3 = dx. \tag{2.64}$$

Solutions of Type V for the system, eq.(2.16) take the form eq.(2.8), eq.(2.19). The parameters, β_t, β_1, β_2, m^2, A_t, are given by

$$\beta_t = \sqrt{-4+\Lambda}, \tag{2.65}$$

$$\beta_1 = \beta_2 = \beta_3 = 0, \tag{2.66}$$

$$m^2 = 0, \tag{2.67}$$

$$A_t = \frac{2(6-\Lambda)}{4-\Lambda}. \tag{2.68}$$

Demanding that A_t, β_t be positive and real respectively, we get $\Lambda > 6$. Starting from this metric in the IR one would like to consider a metric of the form eq.(2.13) which interpolates to Lifshitz space in the UV. However, it turns out that in this case interpolations of the the type eq.(2.63) violate the null energy condition for all values of σ.

The failure of the interpolating metric to work in this case can in fact be understood analytically. It is tied to the fact that the Type V solution has one important difference with the other kinds of solutions, Type II, VI, III, studied above. Here, it turns out that the smallest eigenvalue of $T_\nu^{(\mathrm{matter})\mu}$ corresponding to a space-like eigenvector, $\min(\lambda_c), c = 1,2,3,4$, is exactly equal to the eigenvalue corresponding to the time-like eigenvector, λ_0, and thus the null energy condition eq.(2.2) is met as an equality. This case is therefore much more delicate.

In fact, a perturbative analysis reveals that once the Type V metric is deformed by considering the full interpolating metric given in eq.(2.63), the splitting which results as $r \to -\infty$ goes in the wrong direction, making $\min(\lambda_c) - \lambda_0 < 0$ for any value of σ, leading to a violation of the null energy condition.

2.5 From Type IX To $AdS_2 \times S^3$

The symmetry algebra for Bianchi Type IX is $SO(3)$ and its natural action is on a compact space corresponding to a squashed S^3. Therefore, for Type IX it is natural to explore interpolations going from a Type IX attractor geometry to $AdS_2 \times S^3$ instead of $AdS_2 \times R^3$ or Lifshitz.

The strategy we use for finding such an interpolation is different from what was used in the cases above. It is motivated by the fact that the $SO(3)$ symmetry for Type IX is a subgroup of the symmetries of S^3, $SO(3) \times SO(3)$. The interpolating metric we consider will therefore be obtained by introducing a deformation parameter which allows the spatial components of the metric to go from that of a squashed S^3 in the IR to the round S^3 in the UV. This is somewhat akin to what was done in [34] to find an interpolation between Type VII and Type I.

The invariant one-forms for Bianchi Type IX are

$$\begin{aligned}
\omega^1 &= -\sin(z)\, dx + \sin(x)\cos(z)\, dy, \\
\omega^2 &= \cos(z)\, dx + \sin(x)\sin(z)\, dy, \\
\omega^3 &= \cos(x)\, dy + dz.
\end{aligned}$$

One finds that a Type IX attractor solution arises in a system of Einstein gravity with the cosmological constant Λ, coupled to two gauge fields, A_1, A_2 with action

$$S = \int d^5x\sqrt{-g}\left(R + \Lambda - \frac{1}{4}F_1^2 - \frac{1}{4}F_2^2 - \frac{1}{4}m^2A_2^2\right). \tag{2.69}$$

Note that A_1 is massless while A_2 has $(\text{mass})^2 = m^2$.

In this solution the metric is given by

$$ds^2 = R^2[dr^2 - e^{2\beta_t r}dt^2 + (\omega^1)^2 + (\omega^2)^2 + \ \lambda\ (\omega^3)^2] \tag{2.70}$$

and the two gauge fields are

$$A_1 = \sqrt{A_t}\, e^{\beta_t r}dt, \qquad A_2 = \sqrt{A_s}\, \omega^3 = \sqrt{A_s}\, (\cos(x)dy + dz). \tag{2.71}$$

Note that λ in eq.(2.70) is the deformation parameter we had mentioned above.

In $R = 1$ units, the equations of motion which follow from eq.(2.69) give rise to the following relations,

$$m^2 = -2\lambda, \qquad A_t = \frac{2(-\lambda + 2\Lambda + 4)}{-\lambda + 2\Lambda + 3}, \tag{2.72}$$

$$A_s = 1 - \lambda, \qquad \beta_t = \left[\frac{-\lambda + 2\Lambda + 3}{2}\right]^{\frac{1}{2}}. \tag{2.73}$$

These relations can be thought of as determining $A_s, A_t, \beta_t, \lambda$ in terms of Λ and m^2.

Note that the conditions $A_s, A_t \geq 0$, $\Lambda > 0$ imply, from eq.(2.72) and eq.(2.73), the relation

$$\lambda \leq 1. \tag{2.74}$$

It is easy to see that for $\lambda = 1$, this solution becomes[3] $AdS_2 \times S^3$, and for any other value of λ between 0 and 1, it is Type IX.

[3] We note that $(\omega^1)^2 + (\omega^2)^2 + (\omega^3)^2$ may be obtained as the pullback of the standard Euclidean metric

Let us make one comment before proceeding. Eq.(2.72) and Eq.(2.73) give four relations and at first it might seem that they determine the four parameters $A_t, A_s, \lambda, \beta_t$ and therefore determine the solution completely. However, since we have set the radius $R = 1$, this is not the case and the solution in fact contains one undetermined parameter. This becomes clear if we consider the $\lambda = 1$ case, where $A_s = 0$ and the massive gauge field vanishes. The resulting solution is $AdS_2 \times S^3$ which is the near-horizon extremal RN solution. This solution has one free parameter, which we can take to be A_t, the value of the massless gauge field which determines the electric field of this gauge field. Or we can take it to be R. In the interpolation below, we will take the free parameter to be R, and set $R = 1$, keeping its value fixed as the radial coordinate r varies.

It turns out that for the solution given above in eq.(2.70), eq.(2.71), eq.(2.72), eq.(2.73), for any given λ, the null energy condition is satisfied but as an equality, with the smallest eigenvalue of a space-like eigenvector of $T_{\nu}^{(\text{matter})\mu}$, $\min(\lambda_c)$, being equal to the eigenvalue for the time-like eigenvector, λ_0. This is analogous to what we saw above in the Type V case. However, here because the symmetries involved are different, we can choose another kind of interpolation, as mentioned in the beginning of this section.

We do this by taking λ to be a function of r of the form

$$\lambda(r) = C + (1 - C)\left(\frac{1 + \tanh(\sigma r)}{2}\right) \tag{2.75}$$

where C, and σ are constants, with $0 < C < 1$, to meet eq.(2.74). We find that the degeneracy between $\min(\lambda_c), \lambda_0$ is now lifted. Unlike the Type V case though, this lifting occurs so that $\min(\lambda_c) - \lambda_0 > 0$, if σ is sufficiently small, thus preserving the null energy condition, eq.(2.2). If σ becomes bigger than a critical value, violations of the NEC set in.

For example, for the choice of $\Lambda = 12$, and $C = 0.5$ we find that the energy conditions are met for a range of σ up to $\sigma_{\text{crit}} = 1.82$. For $0 < \sigma \leq 1.82$ and $C = 0.5$ both eq.(2.4), eq.(2.5) are met, so that the interpolating metric above satisfies the WEC and hence also the NEC.

For $C = 0.5$, $\sigma = 0.5$, the results are summarized in fig. 2.11 and 2.12. Fig. 2.11 shows that λ_0 satisfies the condition $\lambda_0 < 0$. And fig. 2.12 shows that $\min(\lambda_c - \lambda_0) > 0$. As $r \to \pm\infty$ the interpolation approaches a solution of the type considered in eq.(2.70), eq.(2.71), and the value of $\min(\lambda_c - \lambda_0) \to 0$. However, we have verified that at both ends, $r \to \pm\infty$, $\min(\lambda_c - \lambda_0)$ approaches zero from above so that the NEC continues to hold. Together, these results imply that $T_{\nu}^{(\text{matter})\mu}$ satisfies the weak energy condition, and therefore also the null energy condition.

on R^4 (with coordinates W, X, Y, Z) under the following S^3 embedding:

$$W = \cos\left(\frac{x}{2}\right)\cos\left(\frac{y+z}{2}\right), \qquad X = \cos\left(\frac{x}{2}\right)\sin\left(\frac{y+z}{2}\right),$$
$$Y = \sin\left(\frac{x}{2}\right)\cos\left(\frac{y-z}{2}\right), \qquad Z = \sin\left(\frac{x}{2}\right)\sin\left(\frac{y-z}{2}\right).$$

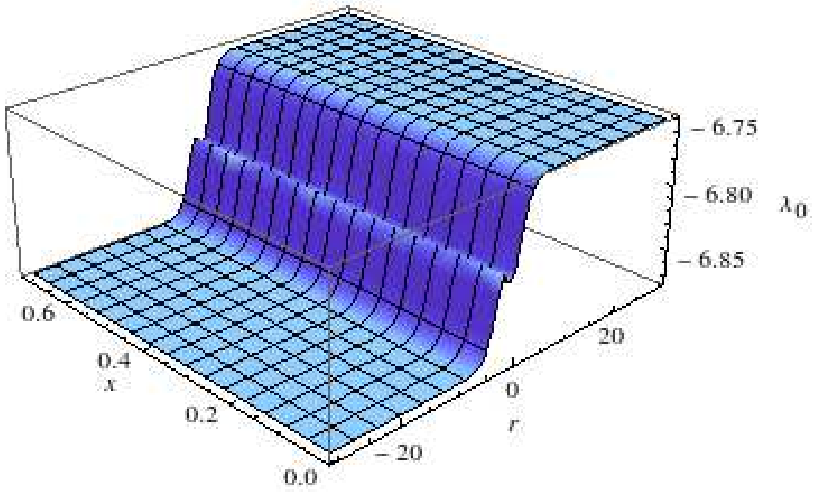

Figure 2.11: Type IX 3D plot of λ_0 (time-like eigenvalue) versus r and x for $C = 0.5,\ \sigma = 0.5,\ \Lambda = 12$.

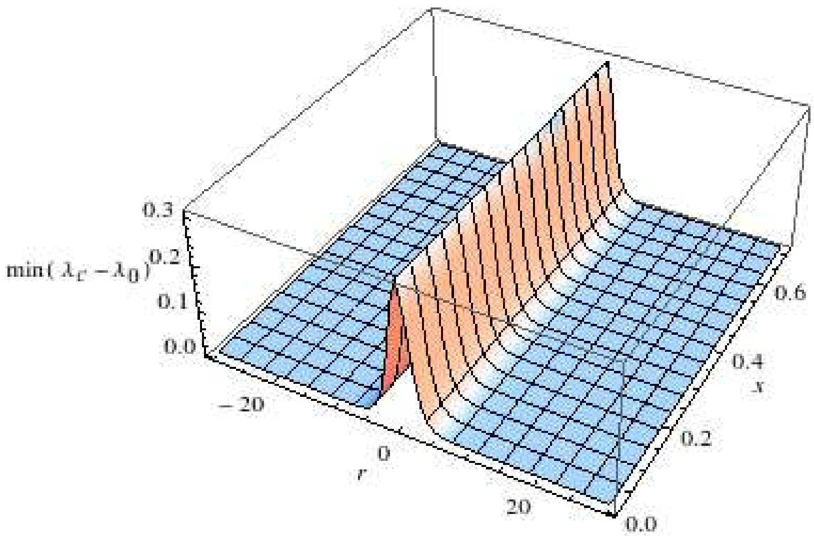

Figure 2.12: Type IX 3D plot of $\min(\lambda_c - \lambda_0)$ versus r and x for $C = 0.5,\ \sigma = 0.5,\ \Lambda = 12$.

2.6 C-function

In this section, we investigate a large class of geometries of the form

$$ds^2 = -g_{tt}(r)dt^2 + dr^2 + g_{ij}(x^i, r)dx^i dx^j \tag{2.76}$$

which interpolate between two Bianchi attractor spacetimes. The Bianchi attractors arise at the UV and IR ends, $r \to \pm\infty$ respectively, where the geometry takes the scale invariant form, eq.(2.8), with the exponents β_t, β_i being constant and positive. The UV and IR ends are defined by the redshift factor, g_{tt}, which decreases from the UV to the IR.

We find that as long as the matter sourcing the geometry satisfies the null energy condition, the area element of the submanifold spanned by the x^i coordinates (at constant t, r) monotonically decreases with r, obtaining its minimum value in the IR. For a Bianchi attractor, eq.(2.8), the area element is proportional to $e^{\sum_i \beta_i r}$ and diverges in the UV, $r \to \infty$, while vanishing in the IR, $r \to -\infty$. The only exception is when the exponents β_i all vanish, as happens for example in $AdS_2 \times R^3$ space, in which case the area element becomes a non-zero constant. We also find an additional function, which we will refer to as the C-function below, which is monotonically decreasing from the UV to the IR. For an AdS attractor, this function attains a constant value and is the central charge. For other Bianchi attractors meeting a specific condition, given in eq.(2.93) below, this function also flows to a constant in the near-horizon region. More generally, when this specific condition is not met, the function either vanishes or diverges as $r \to \pm\infty$. All of these results are most easily derived by applying Raychaudhuri's equation to an appropriately chosen set of null geodesics in the geometry, eq.(2.76).

Let us note that the flows we study include interpolations between two AdS spacetimes which at intermediate values of r can break not only Lorentz invariance but also spatial rotational invariance and translational invariance. As long as the UV and IR geometries are AdS, our results imply that the IR central charge must be smaller than the UV one. Our results therefore lead to a generalization of the holographic C-theorem for flows between conformally invariant theories which can also break boost, rotational and translational symmetries. This is in contrast to much of the discussion in the literature so far, which has considered only Lorentz invariant flows.

Besides the area element and the C-function mentioned above, and of course monotonic functions of these, for example, powers of the area element or the C-function, we do not find any other function which in general would necessarily be monotonic as a consequence of the null energy condition. As was mentioned above, both the area element and the C-function do not in general attain finite non-vanishing values in the asymptotic Bianchi attractor regions. This suggests that for Bianchi attractors in general, no analogue of a finite, non-vanishing, central charge can be defined which is monotonic under RG flow. This conclusion should apply for example to general Lifshitz spacetimes (see also a discussion of these cases in [66]). When the Bianchi attractor meets the specific condition of eq.(2.93), the C-function does become a finite constant and the analogue of the central charge can be defined. Understanding this constant in the field theory dual to the Bianchi attractor would be a worthwhile thing to do.

2.6.1 The Analysis

We now turn to describing the analysis in more detail. Our notation will follow that of [67], Section 9.2. The analysis is also connected to the discussion of a C-function in [68]. A nice discussion of the C-function in AdS space can be found in Section 4.3.2 of [69]. For discussions of renormalization group flows in the context of the AdS/CFT correspondence, see [70, 71, 72, 73, 74]. The earliest proofs of holographic C-theorems appear in [75], [76], and our strategy is a generalization of the one employed there.

We start with a spacetime described by the metric, eq.(2.76), and consider a 3-dimensional submanifold spanned by the x^i coordinates for any fixed r, t. Next, we consider a family of null geodesics which emanate from all points of this submanifold. If n^a is the tangent vector of the null geodesic, with a taking the values $a = t, r, i = 1, 2, 3$, then the geodesics we consider have $n^i = 0$ so that they correspond to motion only in the radial direction. Both the radially in-going and out-going families of this type form a congruence. To arrive at our results, it is enough to consider any one of them and we consider the radial out-going geodesics below. The time-like component of the vectors in this congruence, n_t, is a constant which we can set to unity,

$$n_t = 1. \tag{2.77}$$

Then for the radially outgoing geodesics

$$n^r = \frac{dr}{d\lambda} = \frac{1}{\sqrt{g_{tt}}}, \tag{2.78}$$

where λ is the affine parameter along the geodesic.

Now we take the tensor field

$$B_{ab} = \nabla_b n_a \tag{2.79}$$

and consider its components for $a, b = i, j = 1, 2, 3$. In the notation of [67], this gives us the components of $\hat{B}_{ab}$. It is easy to see that

$$B_{ij} = -\Gamma^c_{ij} n_c = \frac{1}{2}\frac{\partial_r g_{ij}}{g_{tt}} \tag{2.80}$$

and thus B_{ij} is symmetric so that the twist of the congruence vanishes. The expansion of the congruence, denoted by θ, is then

$$\theta = \frac{1}{2}\partial_r g_{ij}\frac{g^{ij}}{\sqrt{g_{tt}}} = \partial_r(\ln A)\frac{1}{\sqrt{g_{tt}}}, \tag{2.81}$$

where we have introduced the notation

$$A \equiv \sqrt{\det(g_{ij})} \tag{2.82}$$

to denote the area element of the hypersurface spanned by the x^i coordinates for any constant r, t.

From eq.(2.81) and eq.(2.78) we get that

$$\frac{d\theta}{d\lambda} = \frac{1}{\sqrt{g_{tt}}}\partial_r \left(\frac{\partial_r \ln A}{\sqrt{g_{tt}}}\right). \tag{2.83}$$

Raychaudhuri's equation then gives

$$\frac{d\theta}{d\lambda} = -\frac{1}{3}\theta^2 - \hat{\sigma}_{ab}\hat{\sigma}^{ab} - R_{cd}n^c n^d \tag{2.84}$$

since the twist $\hat{\omega}_{ab} = 0$. Note that the coefficient of the first term on the RHS is $\frac{1}{3}$ and not $\frac{1}{2}$ since we are in $4+1$ dimensions and not $3+1$ dimensions.

If the matter sourcing the geometry satisfies the null energy condition, the Ricci curvature satisfies the relation $R_{cd}n^c n^d \geq 0$, leading to the conclusion from eq.(2.84) that $\frac{d\theta}{d\lambda} < 0$. From eq.(2.83), this in turn leads to

$$\partial_r \left(\frac{\partial_r \ln A}{\sqrt{g_{tt}}}\right) < 0. \tag{2.85}$$

In the UV, $r \to \infty$,

$$\frac{\partial_r \ln A}{\sqrt{g_{tt}}} = \sum_i \beta_i e^{-\beta_t r} > 0 \tag{2.86}$$

where β_i, β_t are the exponents corresponding to the UV attractor. It then follows from eq.(2.85) that for all values of r, $\frac{\partial_r \ln A}{\sqrt{g_{tt}}} > 0$, and thus

$$\partial_r \ln A > 0. \tag{2.87}$$

This leads to our first result: the area element A, defined in eq.(2.82), decreases monotonically from the UV, $r \to \infty$, to the IR, $r \to -\infty$.

Raychaudhuri's equation, eq.(2.84) also leads to the conclusion that

$$\frac{d\theta}{d\lambda} + \frac{1}{3}\theta^2 \leq 0, \tag{2.88}$$

if the matter satisfies the null energy condition. From eq.(2.81), eq.(2.83) this leads to

$$\partial_r \left(\frac{(\partial_r \ln A)A^{1/3}}{\sqrt{g_{tt}}}\right) < 0. \tag{2.89}$$

A monotonically decreasing function from the UV to the IR is therefore given by

$$C = \left(\frac{\sqrt{g_{tt}}}{(\partial_r \ln A) A^{1/3}} \right)^3 . \tag{2.90}$$

For a Bianchi attractor with exponents β_t, β_i, C becomes

$$C \propto \left(\frac{e^{(\beta_t - \bar{\beta})r}}{3\bar{\beta}} \right)^3 , \tag{2.91}$$

where we have defined

$$\bar{\beta} = \frac{1}{3} \sum_i \beta_i . \tag{2.92}$$

The overall power of 3 in the definition of C, eq.(2.90), is chosen so that in AdS space, where $\beta_i = \beta_t$ and C is a constant, it agrees with the usual definition of the central charge up to an overall coefficient. More generally, C also becomes a constant for any Bianchi attractor meeting the condition

$$\beta_t = \bar{\beta} = \frac{1}{3} \sum_i \beta_i \tag{2.93}$$

and now takes a value

$$C \propto \frac{1}{(\sum_i \beta_i)^3} . \tag{2.94}$$

However, for the general case of a Bianchi attractor which does not meet the condition in eq.(2.93), C does not attain a constant value. In such situations, for C to be monotonically decreasing towards the IR or constant, we need $(\beta_t - \bar{\beta}) \geq 0$. Thus, we find that if the attractor arises in the IR, then our C vanishes. On the other hand, if the attractor arises in the UV, it diverges.

2.7 Comments and discussions

In this chapter, we constructed a class of smooth metrics which interpolate from various Bianchi attractor geometries in the IR to Lifshitz spaces or $AdS_2 \times S^3$ in the UV. We did not show that these interpolating metrics arise as solutions to Einstein gravity coupled with suitable matter field theories. However, for Bianchi Types II, VI (with parameter $h = -1$), III and IX, we did show that *were* these geometries to arise as solutions to Einstein's equations, the required matter would not violate the weak or null energy conditions. It is well known that the Lifshitz spaces (which are in fact attractors of Bianchi Type I) or $AdS_2 \times S^3$ geometry in turn can be connected to AdS_5 in the ultraviolet, with no non-normalizable deformation for the metric being turned on in the asymptotic AdS_5 region. Thus, our results establish that there is no barrier, at least at the level of energy conditions, to having a smooth interpolating metric arise as a solution of the Einstein equations sourced by reasonable matter, which connects the various Bianchi classes mentioned above with asymptotic AdS_5 space. We should mention here that for Type VII geometries, which were not investigated in this chapter, solutions with reasonable matter which interpolate from the attractor region to $AdS_2 \times R^3$ or AdS_5 are already known to exist [34].

The absence of any non-normalizable metric deformations in the asymptotic AdS_5 region in our interpolations suggests that the Bianchi attractor geometries can arise as the dual description in the IR of field theories which live in flat space. The anisotropic and homogeneous phases in these field theories, described by the Bianchi attractor regions, could arise either due to a spontaneous breaking of rotational invariance or due to its breaking by sources other than the metric in the field theory. We expect both possibilities to be borne out. For spin density waves, which correspond to Type VII, indeed this is already known to be true [33, 34].

Finding such interpolating metrics as solutions to Einstein's equations is not easy, as was mentioned in the introduction, since it requires solving coupled partial differential equations in at least two variables. We hope that the results presented here will provide some further motivation to try and address this challenging problem. Perhaps it might be best to first look for supersymmetric domain walls interpolating between different Bianchi types, since for such solutions, working with first-order equations often suffices.

We also note that our smooth interpolating metric which interpolates from Bianchi Type V to Lifshitz failed to satisfy the null energy conditions. Our failure in this case may be due to the restricted class of functions we used to construct the interpolating metrics or it might suggest a more fundamental constraint. We leave a more detailed exploration of this issue for the future.

Towards the end of the chapter, we explored whether a C-function exists for flows between two Bianchi attractor geometries. As long as the matter sourcing the geometry meets the null energy condition, we found that a function can be defined which is monotonically decreasing from the UV to the IR. In AdS space, this function becomes the usual central charge. More generally though, unless the Bianchi attractor meets a specific condition relating the exponents β_i, β_t which characterize it, the function we have identified does not attain a finite, non-vanishing constant value in the attractor geometry. The absence of a general monotonic function which is non-vanishing and finite in the attractor spacetime suggests that no analogue of a central charge, which is monotonic under RG flow, can be defined in general for field theories dual to the Bianchi attractors. For flows between AdS spacetimes, on the other hand, our analysis implies that the central charge decreases even under RG flows which break boost, rotational and translational invariance.

Chapter 3

Bianchi III attractor in Gauged Supergravity

3.1 Introduction

In the last chapter, we saw how the Bianchi type metrics can be shown to numerically interpolate to Lifshitz or $AdS_2 \times S^3$ from which they can be connected to AdS_5 [77]. In particular, we have been able to show that the matter sourcing these interpolating geometries obeys reasonable energy conditions. This provides some evidence towards the expectation that they are attractor geometries.

The attractor mechanism has been thoroughly studied for extremal black holes in supergravity theories [78, 79].[1] Originally studied for supersymmetric black holes, it was understood later that the attractor mechanism is a consequence of extremality rather than supersymmetry [82], and has been shown to work for extremal non-supersymmetric black holes [83, 84]. Recently much progress has been made towards the generalization of attractor mechanism for gauged supergravity theories [85, 86, 87, 88, 89, 90, 91, 92, 93, 94, 95]. The simplest Bianchi type I geometries such as Lifshitz geometries have already been embedded in gauged supergravity [96, 97].

A prescription fairly general enough to capture the essential features of homogeneous geometries as generalised attractor solutions of gauged supergravity was given in [89]. The generalised attractors are defined as solutions to equation of motion when all the fields and curvature tensors are constants in tangent space. These solutions are characterised by constant anholonomy coefficients and are regular by construction. Following this prescription some of the Bianchi type geometries were embedded in five dimensional gauged supergravity [95].

The generalised attractor solutions existed at critical points rather than an absolute min-

[1] See [80, 81] for recent reviews on the subject.

imum of the attractor potential. The stability of such solutions for small perturbations of the scalar fields about the attractor value were studied [94]. By stability, we mean an investigation on the response of a system subject to linearized perturbations of the fields about their fixed point values. If the perturbations are regular as opposed to being divergent when one approaches the fixed point, then it is a stable attractor. There is also the notion of stability as described by the B.F. bound [98, 99]. However, we do not discuss this here.

It was found in [94], that the stress energy tensor in gauged supergravity depends on linearized scalar fluctuations due to the interaction terms. Therefore, for back-reaction to be small as one approaches the attractor geometry, the scalar fluctuations are required to be regular near the horizon. For the solutions constructed in [94, 95], the scalar fluctuations about the critical values were regular near the horizon only when the Bianchi geometries factorized as $AdS_2 \times M$, where M is a homogeneous space of dimension three. The factorized geometries have the unphysical property that the entropy does not vanish as the temperature goes to zero.

In this chapter, we seek to construct interesting class of Bianchi type solutions which do not factorize and are stable under linearized scalar fluctuations. Our strategy is to rely on the conventional wisdom of the physics of stable attractor points for extremal black holes. Namely, there are two sufficient conditions for the attractor mechanism [84]. First, there must exist a critical point of the effective potential. Second, the Hessian of the effective potential evaluated at the solution must have positive eigenvalues. These two conditions are always met by supersymmetric solutions. For non-supersymmetric extremal black hole solutions the above two conditions are sufficient to guarantee a stable attractor.

Keeping the above strategy in mind, we construct a new magnetic Bianchi type III solution in Einstein-Maxwell theory with massless gauge fields. We show that it can be embedded in $U(1)_R$ gauged supergravity via the generalised attractor procedure. We find that there are a large class of type III solutions that exist at a critical point corresponding to a minimum of the attractor potential. We do a linearized fluctuation analysis of the scalar field about its attractor value. For the scalar fluctuations sufficient conditions for a stable attractor discussed in the above paragraph guarantees the existence of a solution which dies out at the horizon. We then determine the gauge field and metric fluctuations that are sourced by scalar fluctuations. We find that the simplicity of the solution causes the source term in the gauge field fluctuations to vanish. Hence there are no gauge field fluctuations sourced by the scalar fluctuations in this case. As a result the metric fluctuations are sourced purely by scalar fluctuations. We solve the equations for the metric fluctuations with the source terms and show that they vanish as one approaches the horizon. Thus, the type III example we have constructed is a stable attractor.

The results of the stability analysis are as follows. The Bianchi type III metric

$$ds^2 = -\hat{r}^{2\beta_t} d\hat{t}^2 + \frac{d\hat{r}^2}{\hat{r}^2} + d\hat{x}^2 + e^{-2\hat{x}} d\hat{y}^2 + \hat{r}^{2\beta_t} d\hat{z}^2 \tag{3.1}$$

which has the scaling symmetries

$$\hat{t} \to \frac{\hat{t}}{\alpha^{\beta_t}} \ , \quad \hat{r} \to \alpha\hat{r} \ , \quad \hat{x} \to \hat{x} \ , \quad \hat{y} \to \hat{y} \ , \quad \hat{z} \to \frac{\hat{z}}{\alpha^{\beta_t}} \ , \tag{3.2}$$

is a generalised attractor solution in gauged supergravity. The solution exists at a critical point ϕ_c such that

$$\left.\frac{\partial \mathcal{V}_{attr}}{\partial \phi}\right|_{\phi_c} = 0 \ , \quad \left.\frac{\partial^2 \mathcal{V}_{attr}}{\partial \phi^2}\right|_{\phi_c} > 0 \ , \tag{3.3}$$

where $\mathcal{V}_{attr}$ is the attractor potential. The above conditions are expressed in terms of some free parameters in gauged supergravity that are not fixed by any symmetries and are met for a wide range of values. Thus a class of solutions exists at a minimum of the attractor potential and the Hessian has a positive eigenvalue. The scalar field fluctuations $\delta\phi$ about the attractor values are of the form

$$\delta\phi \sim \hat{r}^{\Delta} \ , \quad \Delta > 0 \ . \tag{3.4}$$

The scalar fluctuations are regular near the horizon $\hat{r} \to 0$. All the metric fluctuations $\gamma_{\mu\nu}$ are of the form

$$\gamma_{\mu\nu} \sim g_{\mu\nu}\hat{r}^{\Delta} \tag{3.5}$$

and are regular near the horizon. Thus, we have a class of Bianchi III solutions which are stable with respect to linearized fluctuations of scalar, gauge field and metric fluctuations about the attractor value. The solution is an example of a stable Bianchi attractor in gauged supergravity.

Given that the solution is a stable Bianchi attractor, we also investigate its supersymmetry properties. The study of supersymmetry of Bianchi attractors is very interesting since it can lead to solutions such as domain walls interpolating between Bianchi attractors and AdS. Besides, supersymmetry equations are first order differential equations and are often easier to solve. Earlier studies on supersymmetry of Bianchi type metrics have focused on the Bianchi I class. The simplest of which is AdS space. In this case, there are two types of Killing spinors, one which is purely radial and the other which depends on all coordinates [100, 101]. The radial spinor generates the Poincaré supersymmetries while the other spinor generates the conformal supersymmetries. The earliest works were on supersymmetric black string solutions whose near horizon geometries take the form $AdS_3 \times \mathbb{H}^2$ [102, 103]. The Supersymmetry of the Bianchi I metrics such as Lifshitz, have also been studied in four dimensional gauged supergravity [96, 97]. In five dimensional $U(1)^3$ gauged supergravity Bianchi I types such as $AdS_2 \times \mathbb{R}^3$, $AdS_3 \times \mathbb{R}^2$ have been found to be supersymmetric [104]. In the above cases the geometries preserve $1/4$ of the supersymmetry and the Killing spinor equations were solved for a spinor which depended only on the radial direction.

In this spirit, we study the Killing spinor equations of $\mathcal{N} = 2, U(1)_R$ gauged supergravity in the background of the Bianchi type III metric. We choose the radial ansatz for the Killing spinor, since it preserves the time translation symmetries and homogeneous symmetries of the type III metric. However, we find that the radial ansatz breaks all the supersymmetries. This suggests that the stable type III solution that we have constructed may be a non-supersymmetric attractor.

The chapter is organised as follows. In §3.2 we construct a magnetic Bianchi type III solution in Einstein-Maxwell theory with massless gauge fields. Following that, we provide some background in $U(1)_R$ gauged supergravity and generalised attractors in §3.3.1 and §3.3.2. In the next subsection §3.3.3 we embed the Bianchi type III solution in the $U(1)_R$ gauged supergravity. We discuss the linearized fluctuation analysis of the gauge field, scalar field and metric in §3.4. We analyze the Killing spinor equation in gauged supergravity with the background Bianchi type III metric in §3.5. We conclude and summarize our results in §3.6. We summarize some of the notations and conventions in §B.1. We provide some details regarding the linearized Einstein equations in §B.2 and list the coefficients that appear in the metric fluctuations in §B.3.

3.2 Bianchi III solution in Einstein-Maxwell theory

We begin with a quick review of some elements of the Bianchi III symmetry. The Bianchi classification of real Lie algebras in three dimensions is well known in the literature [105, 106]. There are nine types of such algebras. In three dimensional Euclidean space, Killing vectors that generate homogeneous symmetries close to form Lie algebras that are isomorphic to the Bianchi classification.

The Bianchi III algebra is generated by the Killing vectors X_i

$$X_1 = \partial_{\hat{y}} \ , \quad X_2 = \partial_{\hat{z}} \ , \quad X_3 = \partial_{\hat{x}} + \hat{y}\partial_{\hat{y}} \ , \tag{3.6}$$

$$[X_1, X_3] = X_1 \ . \tag{3.7}$$

The only non trivial Killing vector is the translation in the $\hat{x}$ direction that is accompanied by a unit weight scaling in the $\hat{y}$ direction. To write a metric which is manifestly invariant under this symmetry, one identifies the vector fields $\tilde{e}_i$ that commute with the Killing vectors

$$[\tilde{e}_i, X_j] = 0 \ . \tag{3.8}$$

The invariant vector fields for the type III case are

$$\tilde{e}_1 = e^{\hat{x}}\partial_{\hat{y}} \ , \quad \tilde{e}_2 = \partial_{\hat{z}} \ , \quad \tilde{e}_3 = \partial_{\hat{x}} \ , \tag{3.9}$$

$$[\tilde{e}_1, \tilde{e}_3] = -\tilde{e}_1 \ , [\tilde{e}_1, \tilde{e}_2] = 0 \ , [\tilde{e}_2, \tilde{e}_3] = 0 \ . \tag{3.10}$$

Note that $\tilde{e}_1$ and $\tilde{e}_3$ form a sub-algebra. This sub-algebra is generated by the Killing vectors of the hyperbolic space $\mathbb{H}^2$ in two dimensions. The two dimensional analogue of the Bianchi classification consists of two distinct algebras. One is a trivial algebra with commuting generators corresponding to $\mathbb{R}^2$ and the other is the algebra that corresponds to $\mathbb{H}^2$ [106].

The duals of the $\tilde{e}_i$ are one forms ω^i

$$\omega^1 = e^{-\hat{x}} d\hat{y} \ , \quad \omega^2 = d\hat{z} \ , \quad \omega^3 = d\hat{x} \ , \tag{3.11}$$

that are invariant under the type III homogeneous symmetry. The invariant one forms satisfy the relation

$$d\omega^1 = \omega^1 \wedge \omega^3 \ . \tag{3.12}$$

The metric written in terms of the invariant one forms

$$ds_3^2 = (\omega^1)^2 + (\omega^2)^2 + (\omega^3)^2 \tag{3.13}$$

is manifestly invariant under the homogeneous type III symmetries.

We are interested in five dimensional black brane horizons with homogeneous symmetries in the spatial directions. These geometries are obtained from gravity coupled to simple matter in the presence of a cosmological constant and are known as the Bianchi attractors [2, 107]. For the purposes of this article, we construct a simple type III solution in Einstein-Maxwell theory sourced by a single massless gauge field and a cosmological constant. We take the type III metric to be of the form

$$ds^2 = -\hat{r}^{2\beta_t} d\hat{t}^2 + \frac{d\hat{r}^2}{\hat{r}^2} + (\omega^3)^2 + (\omega^1)^2 + \hat{r}^{2\beta_2} (\omega^2)^2 \ , \tag{3.14}$$

where β_t, β_2 are positive exponents. For the case $\beta_t = \beta_2$, the metric becomes $AdS_3 \times EAdS_2$. To see this we substitute for the invariant one forms from (3.11) and make the coordinate transformation $\hat{x} = \ln \hat{\rho}$ to get,

$$ds^2 = \left(-\hat{r}^{2\beta_t} d\hat{t}^2 + \frac{d\hat{r}^2}{\hat{r}^2} + \hat{r}^{2\beta_t} d\hat{z}^2\right) + \left(\frac{d\hat{y}^2 + d\hat{\rho}^2}{\hat{\rho}^2}\right) \ . \tag{3.15}$$

When one performs a Kaluza-Klein reduction of the above solution one gets the $AdS_2 \times EAdS_2$ solution in four dimensions with hyper scale violation [2].

We now construct the Type III solution (3.14) in Einstein-Maxwell theory. The action is of the form

$$S = \int d^5x \sqrt{-g} (R - \frac{1}{4} F^{\mu\nu} F_{\mu\nu} + \Lambda) \ , \tag{3.16}$$

where $\Lambda > 0$ corresponds to Anti de-Sitter space in our conventions. We are interested in a magnetic solution and we choose the gauge field to have components along the ω^1 direction

$$A = A_3 \omega^1, \tag{3.17}$$

where A_3 is a constant.[2] The gauge field equations are automatically satisfied with this ansatz and the independent trace reversed Einstein equations are

$$\begin{aligned} A_3^2 - 6\beta_t(\beta_2+\beta_t) + 2\Lambda = 0 \ , \\ A_3^2 - 6(\beta_2^2+\beta_t^2) + 2\Lambda = 0 \ , \\ -A_3^2 - 3 + \Lambda = 0 \ , \\ A_3^2 - 6\beta_2(\beta_2+\beta_t) + 2\Lambda = 0 \ . \end{aligned} \tag{3.18}$$

The $\hat{t}\hat{t}$ and $\hat{z}\hat{z}$ equations imply

$$\beta_2 = \beta_t \tag{3.19}$$

and the rest of the equations give the solution

$$\Lambda = 1 + 4\beta_t^2 \ , \quad A_3 = \sqrt{-2+4\beta_t^2} \ . \tag{3.20}$$

Thus we have a magnetic type III solution sourced by a massless gauge field and parametrized by β_t, which satisfies the condition

$$\beta_t^2 > \frac{1}{2} \ , \tag{3.21}$$

such that A_3 is real. In the following section, we construct a similar solution in $U(1)_R$ gauged supergravity.

3.3 Gauged supergravity and generalised attractors

3.3.1 Gauged supergravity

In this section, we review essential material in $\mathcal{N}=2, d=5$ gauged supergravity relevant for our purpose. The general supergravity coupled to vector, tensor, hyper multiplets with a gauging of the symmetries of the scalar manifold and R symmetry is discussed in [108]. We work with the $\mathcal{N}=2, d=5$ gauged supergravity coupled to a single vector multiplet and a gauging of the $U(1)_R$ symmetry [109, 110, 111, 112].

The gravity multiplet consists of two gravitinos ψ^i_μ, $i=1,2$, and a graviphoton. The vector multiplet consists of a vector A_μ, a real scalar ϕ and the gaugini λ_i. The vector in the vector multiplet and the graviphoton are collectively represented by A^I_μ, $I=0,1$.

The scalars in the theory parametrize a very special manifold described by the cubic surface (see for eg [113])

$$N \equiv C_{IJK}h^I h^J h^k = 1 \ , \quad h^I \equiv h^I(\phi) \ . \tag{3.22}$$

The constants C_{IJK} are real and symmetric. The condition (3.22) is solved by going to a

[2] The notation A_3 is just chosen for convenience.

basis [109, 110], with $h^I = \sqrt{\frac{2}{3}}\xi^I|_{N=1}$ such that,

$$N(\xi) = \sqrt{2}\xi^0(\xi^1)^2 = 1 \ , \tag{3.23}$$

where,

$$\xi^0 = \frac{1}{\sqrt{2}\phi^2}, \quad \xi^1 = \phi \ . \tag{3.24}$$

From the definition of the basis, we find that the h^I are related to the scalars ϕ in the Lagrangian through

$$h^0 = \frac{1}{\sqrt{3}\phi^2}, \quad h^1 = \sqrt{\frac{2}{3}}\phi \ . \tag{3.25}$$

It is clear from the scalar parametrization that the only non-zero coefficients for C_{IJK} are $C_{011} = \sqrt{3}/2$ and its permutations.

The ambient metric used to raise and lower the index I is defined through

$$a_{IJ} = -\frac{1}{2}\frac{\partial}{\partial h^I}\frac{\partial}{\partial h^J}\ln N|_{N=1} \ , \tag{3.26}$$

and takes the form

$$a_{IJ} = \begin{bmatrix} \phi^4 & 0 \\ 0 & \frac{1}{\phi^2} \end{bmatrix} \ . \tag{3.27}$$

The metric on the scalar manifold is obtained from the ambient metric (3.26) through

$$g_{xy} = h^I_x h^J_y a_{IJ} \ , \quad h^I_x = -\frac{\sqrt{3}}{2}\frac{\partial h^I}{\partial \phi^x} \ . \tag{3.28}$$

Since we only have a single scalar field, using the equations (3.25) and (3.26) we obtain

$$g(\phi) = \frac{3}{\phi^2} \ . \tag{3.29}$$

The field content and the various definitions above are identical to the ungauged theory. The difference in the gauged theory is the presence of a scalar potential. The process of gauging converts some of the global symmetries of the Lagrangian into local symmetries. One of the global symmetries enjoyed by the fermions in a $\mathcal{N} = 2$ theory is the $SU(2)_R$ symmetry. For the case of interest, we consider the gauging of the abelian $U(1)_R \subset SU(2)_R$. The R symmetry is gauged by replacing the usual Lorentz covariant derivative acting on the fermions with $U(1)_R$ gauge covariant derivative as follows

$$\begin{aligned} \nabla_\mu \lambda^i &\rightarrow \nabla_\mu \lambda^i + g_R A_\mu(U(1)_R)\delta^{ij}\lambda_j \ , \\ \nabla_\mu \psi^i_\nu &\rightarrow \nabla_\mu \psi^i_\nu + g_R A_\mu(U(1)_R)\delta^{ij}\psi_{\nu j} \ . \end{aligned} \tag{3.30}$$

We refer the reader to §B.1 for conventions on raising and lowering of the $SU(2)$ indices. The δ_{ij} in the covariant derivatives are the usual Kronecker delta symbols and g_R is the

$U(1)_R$ gauge coupling constant. The $U(1)_R$ gauge field is a linear combination of the gauge fields in the theory

$$A_\mu(U(1)_R) = V_I A^I_\mu \ , \tag{3.31}$$

where the parameters $V_I \in \mathbb{R}$ are free.[3]

The $U(1)_R$ covariantization breaks the supersymmetry and therefore compensating terms are added to the Lagrangian for supersymmetric closure [112]. These terms result in the form of a potential for the scalar fields,

$$\mathcal{V}(\phi) = -2g_R^2 V_1 \left[\frac{2\sqrt{2}V_0}{\phi} + \phi^2 V_1\right] . \tag{3.32}$$

The potential has a critical point at

$$\phi_* = \left(\sqrt{2}\frac{V_0}{V_1}\right)^{1/3} . \tag{3.33}$$

The vacuum solution at this critical point is a supersymmetric Anti de-Sitter space with a cosmological constant $\mathcal{V}(\phi_*) = -6g_R^2 V_1^2 \phi_*^2$.

The bosonic part of the Lagrangian is

$$\begin{aligned}\hat{e}^{-1}\mathcal{L} = &-\frac{1}{2}R - \frac{1}{4}a_{IJ}F^I_{\mu\nu}F^{J\mu\nu} - \frac{1}{2}g(\phi)\partial_\mu\phi\partial^\mu\phi \\ &- \mathcal{V}(\phi) + \frac{\hat{e}^{-1}}{6\sqrt{6}}C_{IJK}\epsilon^{\mu\nu\rho\sigma\tau}F^I_{\mu\nu}F^J_{\rho\sigma}A^K_\tau \ ,\end{aligned} \tag{3.34}$$

where $\hat{e} = \sqrt{-detg_{\mu\nu}}$ and C_{IJK} are the constant symmetric coefficients that appeared in the definition of the scalar manifold (3.22).

We also list the various field equations for reference. The gauge field equations are

$$\partial_\mu(\hat{e}a_{IJ}F^{J\mu\nu}) = -\frac{1}{2\sqrt{6}}\epsilon^{\nu\lambda\rho\sigma\tau}F^J_{\lambda\rho}F^K_{\sigma\tau} \ . \tag{3.35}$$

The scalar field equations are

$$\frac{1}{\hat{e}}\partial_\mu(\hat{e}g(\phi)\partial^\mu\phi) - \frac{1}{2}\frac{\partial g(\phi)}{\partial\phi}\partial_\mu\phi\partial^\mu\phi - \frac{\partial}{\partial\phi}\left[\frac{1}{4}a_{IJ}F^I_{\mu\nu}F^{J\mu\nu} + \mathcal{V}(\phi)\right] = 0 \tag{3.36}$$

and the Einstein equations are

$$R_{\mu\nu} - \frac{1}{2}Rg_{\mu\nu} = T_{\mu\nu} \ , \tag{3.37}$$

[3] When the gauging of R symmetry is accompanied by gauging of a non-abelian symmetry group K of the scalar manifold, the V_I are constrained by $f^I_{JK}V_I = 0$, where f^I_{JK} are structure constants of K.

where the stress energy tensor is

$$T_{\mu\nu} = g_{\mu\nu}\big[\frac{1}{4}a_{IJ}F^I_{\mu\nu}F^{J\mu\nu} + \mathcal{V}(\phi) + \frac{1}{2}g(\phi)\partial_\mu\phi\partial^\mu\phi\big] - \big[a_{IJ}F^I_{\mu\lambda}F^{J\ \lambda}_{\nu} + g(\phi)\partial_\mu\phi\partial_\nu\phi\big]\ . \quad (3.38)$$

3.3.2 Generalised attractors

We now outline a brief discussion on a class of solutions to the field equations known as generalised attractors [89]. For a $\mathcal{N} = 2, d = 5$ gauged supergravity with generic gauging of scalar manifolds and in the presence of hyper/tensor multiplets, the generalised attractor equations were shown to be algebraic in [95]. The $U(1)_R$ gauged supergravity discussed in §3.3.1 is a special case of the general gauged theory. The relevant field equations which follow from (3.34) can be simply obtained by setting the tensors, hyperscalars and the coupling constant associated with gauging of the scalar manifold to zero in the field equations derived in [95].

Generalised attractors are defined as solutions to equations of motion that reduce to algebraic equations when all the fields and Riemann tensor components are constants in tangent space

$$\phi = const\ , \qquad A^I_a = const\ , \qquad c_{ab}{}^c = const\ , \quad (3.39)$$

where $a = 0, 1, \dots, 4$, are tangent space indices. The $c_{ab}{}^c$, referred to as anholonomy coefficients are structure constants that appear in the Lie bracket of the vielbeins

$$[e_a, e_b] = c_{ab}{}^c e_c\ , \quad e_a \equiv e^\mu_a\partial_\mu\ . \quad (3.40)$$

In the absence of torsion, the spin connections are expressed in terms of the anholonomy coefficients

$$\omega_{abc} = \frac{1}{2}(c_{abc} - c_{acb} - c_{bca})\ , \quad (3.41)$$

which are constants.[4] Thus the curvature tensor components expressed in terms of the spin connections as

$$R_{abc}{}^d = -\omega_{ac}{}^e\omega_{be}{}^d + \omega_{bc}{}^e\omega_{ae}{}^d - c_{ab}{}^e\omega_{ec}{}^d \quad (3.42)$$

are constants in tangent space. Hence, the generalised attractor solutions characterised by constant anholonomy coefficients and are regular.

At the attractor points defined by (3.39) the scalar field equation (3.36) reduces to the condition

$$\frac{\partial\mathcal{V}_{attr}(\phi, A)}{\partial\phi} = 0 \quad (3.43)$$

[4]The antisymmetry properties of the spin connection and anholonomy coefficients are $\omega_a{}^{bc} = -\omega_a{}^{cb}$ and $c_{ab}{}^c = -c_{ba}{}^c$ respectively.

on an attractor potential

$$\mathcal{V}_{attr}(\phi, A) = \frac{1}{4} a_{IJ} F^I_{\mu\nu} F^{J\mu\nu} + \mathcal{V}(\phi) \ . \tag{3.44}$$

Solving (3.43) gives the critical value of the scalar ϕ_c in terms of the charges A. The critical point is a minimum when the Hessian has positive eigenvalues, which is also the condition for a stable attractor solution [84].

We also list the tangent space generalised attractor equations for the gauge and Einstein equations for reference. The gauge field equations are

$$a_{IJ}(\omega_a{}^a{}_c F^{Jbc} + \omega_a{}^b{}_c F^{Jac}) = 0 \ , \tag{3.45}$$

where the the field strength is

$$F^I_{ab} \equiv e^\mu_b e^\nu_a (\partial_\mu e^c_\nu - \partial_\nu e^c_\mu) A^I_c = c^c_{ab} A^I_c \ , \tag{3.46}$$

and the Chern-Simons term vanishes for the Bianchi attractors [95]. The Einstein equations are

$$R_{ab} - \frac{1}{2} R \eta_{ab} = T^{attr}_{ab} \ , \tag{3.47}$$

where

$$T^{attr}_{ab} = \mathcal{V}_{attr}(\phi, A)\eta_{ab} - a_{IJ} F^I_{ac} F^{Jc}_{\ \ b} \ . \tag{3.48}$$

In the following section we solve the algebraic attractor equations and find a Bianchi type III solution.

3.3.3 Bianchi III solution in $U(1)_R$ gauged supergravity

We choose the Bianchi type III ansatz as before in eq.(3.14). The gauge field ansatz is also same as before,

$$A^I_{\hat{y}} = e^{-x} A^I_3 \ , \quad A^0_3 \equiv A_3 \ , \tag{3.49}$$

where we have turned on only the graviphoton $I = 0$ for simplicity. Similar to the Einstein-Maxwell case studied in §3.2 earlier, the gauge field equations (3.45) are trivially satisfied in the $U(1)_R$ gauged supergravity as expected.

At the attractor point the scalars are constant. Hence the scalar equations reduce to extremization of the attractor potential (3.43). The attractor potential has the form

$$\mathcal{V}_{attr}(\phi, A) = \frac{1}{2\phi}\left(A_3^2 \phi^5 - 4 g_R^2 V_1 (2\sqrt{2} V_0 + V_1 \phi^3)\right) \ . \tag{3.50}$$

The second term is the contribution of the potential (3.32). We would like to briefly contrast the nature of the possible critical points possible from (3.50) as compared to some of the earlier works [94, 95]. The Bianchi attractors constructed in gauged supergravity were attractor solutions such that the critical points of the attractor potential coincided with the critical points of the scalar potential (3.32). This was a simplification which was possible because the attractor potential had additional terms due to gauging of the scalar manifold or with multiple field strengths in the absence of such gauging. For the $U(1)_R$ case with just one gauge field considered here, the attractor potential (3.50) does not allow such critical points for non-trivial gauge fields. It is also important to note that in [95], the Bianchi III solution could not be obtained from the Bianchi VI$_h$ solution by taking the limit $h \to 0$ since it resulted in a singular gauge field.[5]

The scalar field equation then reduces to,

$$\frac{\partial \mathcal{V}_{attr}(\phi, A)}{\partial \phi} = \frac{2}{\phi^2}\left(A_3^2\phi^5 + 4g_R^2 V_1(\sqrt{2}V_0 - V_1\phi^3)\right) = 0 \ . \tag{3.51}$$

In principle, one can solve for ϕ from the above equation. In practice, it is much easier to solve the scalar equation simultaneously with the Einstein equation to get nice compact expressions.

The independent Einstein equations (3.37) are

$$\begin{aligned} 2(1+\beta_2^2)\phi + A_3^2\phi^5 - 4g_R^2 V_1(2\sqrt{2}V_0 + V_1\phi^3) &= 0 \ , \\ 2(1+\beta_2\beta_t)\phi + A_3^2\phi^5 - 4g_R^2 V_1(2\sqrt{2}V_0 + V_1\phi^3) &= 0 \ , \\ 2(\beta_2^2 + \beta_2\beta_t + \beta_t^2)\phi - A_3^2\phi^5 - 4g_R^2 V_1(2\sqrt{2}V_0 + V_1\phi^3) &= 0 \ , \\ 2(1+\beta_t^2)\phi + A_3^2\phi^5 - 4g_R^2 V_1(2\sqrt{2}V_0 + V_1\phi^3) &= 0 \ . \end{aligned} \tag{3.52}$$

From the $\hat{t}\hat{t}$ and the $\hat{z}\hat{z}$ equations we get

$$\beta_2 = \beta_t \ . \tag{3.53}$$

The equations now simplify to

$$\begin{aligned} 2(1+\beta_t^2)\phi + A_3^2\phi^5 - 4g_R^2 V_1(2\sqrt{2}V_0 + V_1\phi^3) &= 0 \ , \\ 6\beta_t^2\phi - A_3^2\phi^5 - 4g_R^2 V_1(2\sqrt{2}V_0 + V_1\phi^3) &= 0 \ . \end{aligned} \tag{3.54}$$

We solve for A_3 from the above equations to obtain

$$A_3 = \frac{\sqrt{-1+2\beta_t^2}}{\phi^2} \ , \tag{3.55}$$

and

$$(1+4\beta_2^2)\phi - 4g_R^2 V_1(2\sqrt{2}V_0 + V_1\phi^3) = 0 \ . \tag{3.56}$$

This equation can be solved together with the scalar equation (3.51) to determine the critical

[5] The Bianchi VI$_h$ algebra has a free parameter h. The Bianchi V algebra is obtained in the limit $h \to 1$, while the Bianchi III algebra is obtained in the limit $h \to 0$ [105, 106].

point

$$\phi_c = 4\sqrt{2}g_R^2 V_0 V_1 \ , \quad \beta_t = \frac{1}{2}\sqrt{1+128 g_R^6 V_0^2 V_1^4} \tag{3.57}$$

For the gauge field to be real we require

$$\beta_t^2 > \frac{1}{2}. \tag{3.58}$$

We note that the same condition was obtained for the Type III solution in Einstein-Maxwell theory (3.21). It is also clear from (3.57) that the condition is satisfied for arbitrary values of the gauged supergravity parameters g_R, V_0, V_1.

We now examine the nature of the critical point given by eqs.(3.57) and (3.55). The Hessian evaluated at the critical point

$$\left.\frac{\partial^2 \mathcal{V}_{attr}(\phi, A)}{\partial \phi^2}\right|_{\phi_c} = \frac{-7+8\beta_t^2}{\phi_c^2} \tag{3.59}$$

is positive provided we choose

$$\beta_t^2 > \frac{7}{8} \ . \tag{3.60}$$

We choose this condition for β_t^2, since above this bound we also satisfy the general condition for a stable attractor solution. In terms of the gauged supergravity parameters the condition on β_t^2 translates to

$$g_R^6 V_0^2 V_1^4 > \frac{5}{256} \ , \tag{3.61}$$

which can be satisfied for a wide range of values for the parameters g_R, V_0, V_1, since none of them are constrained in anyway. Thus, for various values of g_R, V_0, V_1 satisfying (3.61) we find a class of type III Bianchi metrics as generalised attractor solutions in $U(1)_R$ gauged supergravity.

The attractor potential evaluated at the critical point given by (3.55) and (3.57) takes a remarkably simple form

$$\mathcal{V}_{attr}|_{\phi_c} = -(1+\beta_t^2) \ , \tag{3.62}$$

which will be useful later. To summarize, the type III solution is

$$\begin{aligned}
ds^2 &= -\hat{r}^{2\beta_t} d\hat{t}^2 + \frac{d\hat{r}^2}{\hat{r}^2} + (\omega^3)^2 + (\omega^1)^2 + \hat{r}^{2\beta_2}(\omega^2)^2 \ , \\
A_3 &= \frac{\sqrt{-1+2\beta_t^2}}{\phi_c^2}, \quad \phi_c = 4\sqrt{2} g_R^2 V_0 V_1, \\
\beta_2 &= \beta_t, \quad \beta_t = \frac{1}{2}\sqrt{1+128 g_R^6 V_0^2 V_1^4}, \quad \beta_t^2 > \frac{7}{8} \ .
\end{aligned} \tag{3.63}$$

We have seen that the Hessian of the effective potential evaluated on this solution has a positive eigenvalue suggesting that it is a stable attractor. In the following section we provide more evidence by considering linearized fluctuations of the scalar, gauge and metric fields about their attractor values and showing that they are well behaved near the horizon.

3.4 Linearized fluctuations about attractor value

In this section, we study the linearized fluctuations of the gauge field, scalar field and metric about their attractor values. For $\mathcal{N} = 2, d = 5$ gauged supergravity coupled to vector multiplets with a generic gauging of the scalar manifold and gauging of R symmetry the linearized equations were derived in [94]. The corresponding equations for the $U(1)_R$ case that follow from (3.34) can be simply obtained by setting the coupling constant associated with gauging of the scalar manifold to zero.

The linearized fluctuations about the attractor values are of the following form,

$$\begin{aligned} &\phi_c + \epsilon\delta\phi(\hat{r}) \ , \\ &A_\mu + \epsilon\delta A_\mu(\hat{r}) \ , \\ &g_{\mu\nu} + \epsilon\gamma_{\mu\nu}(\hat{r}) \ , \end{aligned} \tag{3.64}$$

where $\epsilon < 1$. The attractor values of the scalar field and gauge field are ϕ_c, A_μ, respectively. We take the near horizon metric $g_{\mu\nu}$ as the type III Bianchi metric (3.63). We have chosen all the fluctuations to depend purely on the radial direction $\hat{r}$, since it is this behavior that is most interesting from the point of view of an RG flow. Also, this is the first thing to attempt before going to much complicated cases. The magnetic type III solution (3.63) offers lot of simplifications. In particular, we will see that the source term in the gauge field fluctuations vanishes and this simplifies the procedure of solving for the metric fluctuations later on.

3.4.1 Gauge field fluctuations

The equation satisfied by the linearized gauge field fluctuations is

$$a_{IJ}|_{\phi_c}\nabla_\mu F_\delta^{\mu\nu J} = -\left.\frac{\partial a_{IJ}}{\partial\phi}\right|_{\phi_c}\nabla_\mu(F^{\mu\nu J}\delta\phi) \ , \tag{3.65}$$

where

$$F_\delta^{\mu\nu J} = \partial^\mu\delta A^\nu - \partial^\nu\delta A^\mu \ , \tag{3.66}$$

and $F^{\mu\nu J}$ is the field strength corresponding to the attractor solution. We can simplify (3.65) using the attractor equation for the gauge field (3.35), where the Chern-Simons term vanishes and the scalars are independent of spacetime coordinates at the attractor point. Thus we have

$$a_{IJ}|_{\phi_c}\nabla_\mu F_\delta^{\mu\nu J} = -\left.\frac{\partial a_{IJ}}{\partial\phi}\right|_{\phi_c}F^{\mu\nu J}\partial_\mu\delta\phi \ . \tag{3.67}$$

For the gauge field ansatz (3.49), the non-trivial field strength component is only along the $F^{\hat{x}\hat{y}}$ direction. Since the scalar field fluctuation in (3.64) depends only on the radial direction, the right hand side of (3.67) vanishes. Hence, there are no gauge field fluctuations that are sourced by the scalar fluctuations in this case. Thus the linearized fluctuations of the gauge field about the attractor value satisfy the attractor equation

$$a_{IJ}|_{\phi_c}\nabla_\mu F_\delta^{\mu\nu J} = 0 \; . \tag{3.68}$$

From the point of view of the attractor mechanism in supergravity [78, 79], it is the behavior of the scalar fields that is most relevant for our case. Hence, we do not consider any independent gauge field fluctuations here. Thus, we can drop the gauge field fluctuations for the rest of the analysis in the following sections.

In a general situation as opposed to the simple example considered here, the source term in (3.67) need not vanish. In such a case, however one may still be able to solve the problem in certain situations where the scalar fluctuation equations decouple from gauge field fluctuations at linearized level [94]. So solving the linearized equation for scalar fluctuations determines the source term in the gauge field fluctuation, which can then in principle be solved. However, the situation becomes more complicated for the metric fluctuations since both the gauge field and scalar fluctuations will enter through the stress tensor.

Another notable simplification is that currently we are working with the $U(1)_R$ gauged supergravity. When the gauging of the symmetries of scalar manifold is also considered there are additional terms in (3.65) and solving for the gauge field fluctuations is much harder in the presence of additional scalar source terms.[6]

3.4.2 Scalar fluctuations

We will now solve the linearized equations for the scalar fluctuations about the attractor value ϕ_c. The linearized equation for the scalar field obtained from (3.34) takes a remarkably simple form,

$$g(\phi_c)\nabla_\mu\nabla^\mu\delta\phi - \left.\frac{\partial^2\mathcal{V}_{attr}}{\partial\phi^2}\right|_{\phi_c}\delta\phi = 0, \tag{3.69}$$

where $g(\phi)$ and the attractor potential are defined in (3.29) and (3.50) respectively. Using (3.59), we define

$$\lambda = \frac{1}{g(\phi_c)}\left.\frac{\partial^2\mathcal{V}_{attr}}{\partial\phi^2}\right|_{\phi_c} = \frac{-7+8\beta_t^2}{3} \tag{3.70}$$

[6] See for example, eq 3.5 of [94].

which is positive for the solution of interest, since $\beta_t^2 > \frac{7}{8}$. Using the expression for the metric (3.3.3), equation (3.69) can be simplified as

$$\left[\hat{r}^2\partial_{\hat{r}}^2 + (1+2\beta_t)\hat{r}\partial_{\hat{r}} - \lambda\right]\delta\phi = 0\ . \tag{3.71}$$

The general solution for this equation is of the form

$$\delta\phi = C_1\hat{r}^{\sqrt{\lambda+\beta_t^2}-\beta_t} + C_2\hat{r}^{-\sqrt{\lambda+\beta_t^2}-\beta_t}\ . \tag{3.72}$$

The type III metric (3.14) is written in a coordinate system such that the horizon is located at $\hat{r} = 0$. We require the scalar fluctuations (3.64) to vanish as $\hat{r}^\Delta$ for $\Delta > 0$ such that the scalar field approaches its attractor value as $\hat{r} \to 0$. Therefore, we choose $C_2 = 0$. The other constant C_1 cannot be fixed at this stage as the equation (3.69) is valid only near the horizon. However, we can choose $C_1 = C_s \in \mathbb{R}$ since the scalar fields in five dimensional gauged supergravity are real. In addition, for non-trivial fluctuations $C_s \neq 0$. Thus the scalar fluctuations which are well behaved near the horizon are of the form

$$\delta\phi = C_s\hat{r}^\Delta\ , \quad \Delta = \sqrt{\lambda+\beta_t^2} - \beta_t\ . \tag{3.73}$$

Note that, the condition obtained from (3.59) indeed ensures that the scalar fluctuations are well behaved as $\hat{r} \to 0$ near the horizon.

To fix the constants in the solution completely, one has to solve the scalar equation in the background of a solution which interpolates from Bianchi III to AdS with appropriate boundary conditions. Such interpolating metrics obeying reasonable energy conditions that interpolate to Lifshitz or $AdS_2 \times S^3$ which can then be connected to AdS have been constructed numerically in [77]. However, they are not yet known to arise as solutions to Einstein gravity coupled to some simple matter theory.

3.4.3 Metric fluctuations

In this section, we solve the linearized metric fluctuations about the type III metric, that are sourced by scalar fluctuations (3.73). The linearized fluctuation equations of the metric have the form [94],

$$\begin{aligned}\nabla^\alpha\nabla_\alpha\bar{\gamma}_{\mu\nu} + 2R_{(\mu\ \nu)}^{\ \ \alpha\ \ \beta}\bar{\gamma}_{\beta\alpha} - 2R_{(\mu}^{\ \ \beta}\bar{\gamma}_{\nu)\beta} + g_{\mu\nu}(R_{\alpha\beta}\bar{\gamma}^{\alpha\beta} - \frac{2}{3}R\bar{\gamma}) + R\bar{\gamma}_{\mu\nu} \\ +2(\dot{T}^{attr}_{\mu\nu}(g_{\alpha\beta} + \epsilon\gamma_{\alpha\beta})|_{\epsilon=0} + \dot{T}^{attr}_{\mu\nu}(\phi_c + \epsilon\delta\phi)|_{\epsilon=0}) = 0,\end{aligned} \tag{3.74}$$

where

$$\bar{\gamma}_{\mu\nu} = \gamma_{\mu\nu} - \frac{1}{2}\gamma g_{\mu\nu}\ , \quad \gamma = g^{\mu\nu}\gamma_{\mu\nu}\ , \quad \bar{\gamma} = -\frac{3}{2}\gamma\ . \tag{3.75}$$

The dots indicate derivatives with respect to ϵ. The covariant derivatives, raising and lowering are with respect to the near horizon metric $g_{\mu\nu}$. The Riemann tensor, Ricci tensor and curvature that appear in (3.74) are also with respect to $g_{\mu\nu}$.

The contribution of the linearized metric fluctuations from the stress energy tensor are

$$\begin{aligned}\dot{T}^{attr}_{\mu\nu}(g_{\alpha\beta}+\epsilon\gamma_{\alpha\beta})|_{\epsilon=0} =&\mathcal{V}_{attr}|_{\phi_c}(\bar{\gamma}_{\mu\nu}-\frac{2\bar{\gamma}}{3}g_{\mu\nu}) \\ &-(\bar{\gamma}_{\lambda\sigma}-\frac{\bar{\gamma}}{3}g_{\lambda\sigma})(\frac{1}{2}T^{\lambda\sigma}_{attr}|_{\phi_c}g_{\mu\nu}+a_{IJ}|_{\phi_c}F^{I\ \lambda}_{\mu}F^{J\ \sigma}_{\nu}).\end{aligned} \tag{3.76}$$

where

$$T^{attr}_{\mu\nu} = \mathcal{V}_{attr}|_{\phi_c}g_{\mu\nu} - a_{IJ}|_{\phi_c}F^I_{\mu\lambda}F_\nu^{\ \lambda J} \tag{3.77}$$

and $V_{attr}|_{\phi_c}$ is defined by (3.62). The contribution of the linearized scalar fluctuations from the stress energy tensor are

$$\dot{T}^{attr}_{\mu\nu}(\phi_c+\epsilon\delta\phi)|_{\epsilon=0} = \left.\frac{\partial\mathcal{V}_{attr}}{\partial\phi}\right|_{\phi_c} g_{\mu\nu}\delta\phi - \left.\frac{\partial a_{IJ}}{\partial\phi}\right|_{\phi_c} F^I_{\mu\lambda}F_\nu^{\ \lambda J}\delta\phi\ , \tag{3.78}$$

which can be further simplified using the attractor equation (3.43) to get

$$\dot{T}^{attr}_{\mu\nu}(\phi_c+\epsilon\delta\phi)|_{\epsilon=0} = -\left.\frac{\partial a_{IJ}}{\partial\phi}\right|_{\phi_c} F^I_{\mu\lambda}F_\nu^{\ \lambda J}\delta\phi\ . \tag{3.79}$$

We can now solve for the metric fluctuations by plugging in the scalar fluctuations (3.73). First, let us simplify the form of (3.74) by making a few observations. We note that the type III metric in its explicit form

$$ds^2 = -\hat{r}^{2\beta_t}d\hat{t}^2 + \frac{d\hat{r}^2}{\hat{r}^2} + d\hat{x}^2 + e^{-2\hat{x}}d\hat{y}^2 + \hat{r}^{2\beta_t}d\hat{z}^2 \tag{3.80}$$

is diagonal. Therefore, It is reasonable to expect fluctuations only along the diagonal directions. Hence we can choose the fluctuations $\gamma_{\mu\nu}$ to be symmetric. As a result the antisymmetrized terms in (3.74) vanish, as can be checked explicitly. Thus we have

$$\begin{aligned}\nabla^\alpha\nabla_\alpha\bar{\gamma}_{\mu\nu} + g_{\mu\nu}(R_{\alpha\beta}\bar{\gamma}^{\alpha\beta}-\frac{2}{3}R\bar{\gamma}) + R\bar{\gamma}_{\mu\nu} +& 2(\dot{T}^{attr}_{\mu\nu}(g_{\alpha\beta}+\epsilon\gamma_{\alpha\beta})|_{\epsilon=0} \\ &+\dot{T}^{attr}_{\mu\nu}(\phi_c+\epsilon\delta\phi)|_{\epsilon=0}) = 0,\end{aligned} \tag{3.81}$$

with the contributions from the stress energy tensor corresponding to metric and scalar fluctuations as given by (3.76) and (3.79) respectively.

We choose the fluctuation terms of the metric in $g_{\mu\nu} + \epsilon\gamma_{\mu\nu}(\hat{r})$ to be of the form

$$\begin{aligned}
\gamma_{\hat{t}\hat{t}} &= C_{\hat{t}}\hat{r}^{2\beta_t}\tilde{\gamma}_{\hat{t}\hat{t}}(\hat{r}) \ , \\
\gamma_{\hat{r}\hat{r}} &= C_{\hat{r}}\frac{1}{\hat{r}^2}\tilde{\gamma}_{\hat{r}\hat{r}}(\hat{r}) \ , \\
\gamma_{\hat{x}\hat{x}} &= C_{\hat{x}}\tilde{\gamma}_{\hat{x}\hat{x}}(\hat{r}) \ , \\
\gamma_{\hat{y}\hat{y}} &= C_{\hat{y}}e^{-2\hat{x}}\tilde{\gamma}_{\hat{y}\hat{y}}(\hat{r}) \ , \\
\gamma_{\hat{z}\hat{z}} &= C_{\hat{z}}\hat{r}^{2\beta_t}\tilde{\gamma}_{\hat{z}\hat{z}}(\hat{r}) \ ,
\end{aligned} \tag{3.82}$$

where $C_{\hat{t}}, C_{\hat{r}}, C_{\hat{x}}, C_{\hat{y}}, C_{\hat{z}}$ are constants which are to be determined in terms of the gauged supergravity parameters g_R, V_0, V_1, and the coefficient C_s in the scalar fluctuation (3.73).

Because of the way the perturbations have been chosen in (3.82), one can contract the Einstein equations with the vielbeins and write the final expressions in terms of the $\tilde{\gamma}_{\mu\nu}(\hat{r})$. We also observe that the source term from the scalar fluctuation (3.79) appears only in the $\hat{x}\hat{x}$ and $\hat{y}\hat{y}$ directions. While the source goes like $\hat{r}^{\Delta}$, the Einstein equations will contain terms like $\hat{r}^2\partial_{\hat{r}}^2\tilde{\gamma}_{\mu\nu}$, $\hat{r}\partial_{\hat{r}}\tilde{\gamma}_{\mu\nu}$, $\tilde{\gamma}_{\mu\nu}$. Hence one expects the fluctuations $\tilde{\gamma}_{\mu\nu}$ to also go like $\hat{r}^{\Delta}$. This can be checked by observing the explicit equations, which are rather messy. We refer the reader to the appendix §B.2 for more details. Thus all the metric fluctuations should have the behavior

$$\tilde{\gamma}_{\hat{t}\hat{t}} = \tilde{\gamma}_{\hat{r}\hat{r}} = \tilde{\gamma}_{\hat{x}\hat{x}} = \tilde{\gamma}_{\hat{y}\hat{y}} = \tilde{\gamma}_{\hat{z}\hat{z}} = \hat{r}^{\Delta} \ . \tag{3.83}$$

We now substitute (3.83) in eqs. (3.81) and reduce them to an algebraic system,

$$\begin{aligned}
&4({\beta_t}^2(3C_{\hat{r}} + 3C_{\hat{t}} + C_{\hat{x}} + C_{\hat{y}} + 3C_{\hat{z}}) + 2C_{\hat{t}} + C_{\hat{x}} + C_{\hat{y}}) \\
&\qquad + 6\beta_t\Delta(C_{\hat{r}} - C_{\hat{t}} + C_{\hat{x}} + C_{\hat{y}} + C_{\hat{z}}) + \Delta^2(C_{\hat{r}} - C_{\hat{t}} + C_{\hat{x}} + C_{\hat{y}} + C_{\hat{z}}) = 0 \ ,
\end{aligned}$$

$$\begin{aligned}
&C_{\hat{r}}(-4(5{\beta_t}^2 + \beta_t{+}1) + 2(\beta_t - 2)\Delta + \Delta^2) - 2(\beta_t - 2)\Delta(C_{\hat{t}} + C_{\hat{x}} + C_{\hat{y}} + C_{\hat{z}}) \\
&\qquad + 4\beta_t(\beta_t(-C_{\hat{t}} + C_{\hat{x}} + C_{\hat{y}} - C_{\hat{z}}) + C_{\hat{t}} + C_{\hat{x}} + C_{\hat{y}} + C_{\hat{z}}) \\
&\qquad + \Delta^2(-(C_{\hat{t}} + C_{\hat{x}} + C_{\hat{y}} + C_{\hat{z}})) - 4(C_{\hat{t}} + 2(C_{\hat{x}} + C_{\hat{y}}) + C_{\hat{z}}) = 0 \ ,
\end{aligned}$$

$$\begin{aligned}
&(16 - 32{\beta_t}^2)C_s - \phi_c((4{\beta_t}^2 + 2\beta_t\Delta + \Delta^2)(C_{\hat{r}} + C_{\hat{t}} + C_{\hat{y}} + C_{\hat{z}}) \\
&\qquad + C_{\hat{x}}(12{\beta_t}^2 - 2\beta_t\Delta - \Delta^2 + 12)) = 0 \ ,
\end{aligned}$$

$$\begin{aligned}
&(16 - 32{\beta_t}^2)C_s - \phi_c\big(4{\beta_t}^2(C_{\hat{r}} + C_{\hat{t}} + C_{\hat{x}} + 3C_{\hat{y}} + C_{\hat{z}}) + 2\beta_t\Delta(C_{\hat{r}} + C_{\hat{t}} + C_{\hat{x}} - C_{\hat{y}} + C_{\hat{z}}) \\
&\qquad + \Delta^2(C_{\hat{r}} + C_{\hat{t}} + C_{\hat{x}} - C_{\hat{y}} + C_{\hat{z}}) + 6(C_{\hat{r}} + C_{\hat{t}} + C_{\hat{x}} + C_{\hat{y}} + C_{\hat{z}})\big) = 0 \ ,
\end{aligned}$$

$$-4{\beta_t}^2(3C_{\hat{r}}+3C_{\hat{t}}+C_{\hat{x}}+C_{\hat{y}}+3C_{\hat{z}})-6\beta_t\Delta(C_{\hat{r}}+C_{\hat{t}}+C_{\hat{x}}+C_{\hat{y}}-C_{\hat{z}})$$
$$-\Delta^2(C_{\hat{r}}+C_{\hat{t}}+C_{\hat{x}}+C_{\hat{y}}-C_{\hat{z}})-4(C_{\hat{x}}+C_{\hat{y}}+2C_{\hat{z}})=0\ , \quad (3.84)$$

which can be solved to determine the coefficients. Note that the other parameters ϕ_c, Δ, β_t that enter the equations are all expressible in terms of the gauged supergravity parameters g_R, V_0, V_1 from eqs (3.57) and (3.73). However, we will express everything in terms of β_t for convenience. Thus the solution for the coefficients are,

$$\begin{aligned}
C_{\hat{t}} &= \frac{C_s}{\phi_c}F_0(\beta_t)\ ,\\
C_{\hat{r}} &= \frac{C_s}{\phi_c}F_1(\beta_t)\ ,\\
C_{\hat{x}} &= \frac{C_s}{\phi_c}F_2(\beta_t)\ ,\\
C_{\hat{y}} &= \frac{C_s}{\phi_c}F_3(\beta_t)\ ,\\
C_{\hat{z}} &= \frac{C_s}{\phi_c}F_4(\beta_t)\ .
\end{aligned} \quad (3.85)$$

where $F_i(\beta_t), i=0,\ldots 4$ are complicated functions of β_t which are given in §B.3. Note that all the coefficients are proportional to the coefficient C_s. This is a consistency check that the metric fluctuations considered in the analysis are sourced by the scalar fluctuations.

Thus the full metric along with the fluctuations is

$$ds^2=-\left(1+C_{\hat{t}}\hat{r}^{\Delta}\right)\hat{r}^{2\beta_t}d\hat{t}^2+\left(1+C_{\hat{r}}\hat{r}^{\Delta}\right)\frac{d\hat{r}^2}{\hat{r}^2}+\left(1+C_{\hat{x}}\hat{r}^{\Delta}\right)d\hat{x}^2$$
$$+\left(1+C_{\hat{y}}\hat{r}^{\Delta}\right)e^{-2\hat{x}}d\hat{y}^2+\left(1+C_{\hat{r}}\hat{r}^{\Delta}\right)\hat{r}^{2\beta_t}d\hat{z}^2\ . \quad (3.86)$$

From eq (3.70) and eq (3.73), we see that positivity of λ implies Δ is positive for the solution (3.63). Hence, all the metric fluctuations are well behaved and the metric approaches the type III attractor metric as one approaches the horizon $\hat{r}\to 0$. The reader may worry that the perturbation in $\hat{r}\hat{r}$ is well behaved only if $\Delta>2$. However there is no need to put any additional condition, since the behavior at $\hat{r}\to 0$ is dictated by the $\frac{1}{\hat{r}^2}$ term owing to Δ being positive. Thus we have constructed a stable Bianchi III attractor solution in gauged supergravity. In the following section, we investigate the supersymmetry of this solution.

3.5 Supersymmetry analysis

In this section, we analyze the Killing spinor equations for the $U(1)_R$ gauged supergravity with the Bianchi type III solution (3.63) as the background. The Killing spinor equation is obtained by setting the supersymmetric variation of the gravitino to zero. For the $\mathcal{N}=$

$2, U(1)_R$ gauged supergravity the gravitino variation is [111],

$$\delta\psi_{\mu i} = \nabla_\mu(\omega)\epsilon_i + \frac{i}{4\sqrt{6}}h_I(\gamma_{\mu\nu\rho} - 4g_{\mu\nu}\gamma_\rho)F^{I\nu\rho}\epsilon_i + \delta'\psi_{\mu i} \ . \tag{3.87}$$

Our notations and conventions are summarized in §B.1. The indices I label the number of vectors and the scalars h_I are as defined in §3.3.1. Although we have only one gauge field for the solution (3.63), we will keep the I indices for the gauge fields to avoid introducing the explicit form of h_I in the equations. The term $\delta'\psi_{\mu i}$ is the modification in the supersymmetry variations as a result of the $U(1)_R$ gauging. Explicitly it takes the form,

$$\delta'\psi_{\mu i} = -\frac{i}{\sqrt{6}}g_R h^I V_I \gamma_\mu \delta_{ij}\epsilon^j \ , \tag{3.88}$$

where V_I are the parameters that appear in the $U(1)_R$ gauging. Note that the δ_{ij} is not used to raise or lower the $SU(2)$ index.

We now proceed to analyze the Killing spinor equations. The vielbeins and spin connections of the metric (3.63) are

$$\begin{aligned} &e^0_{\hat{t}} = r^{\beta_t} \ , \ e^1_{\hat{r}} = \frac{1}{\hat{r}} \ , \ e^2_{\hat{x}} = 1 \ , \ e^3_{\hat{y}} = e^{-\hat{x}} \ , \ e^4_{\hat{z}} = \hat{r}^{\beta_t} \ , \\ &\omega^{01}{}_{\hat{t}} = \beta_t \hat{r}^{\beta_t} \ , \ \omega^{32}{}_{\hat{y}} = -e^{-\hat{x}} \ , \ \omega^{41}{}_{\hat{z}} = \beta_t \hat{r}^{\beta_t} \ . \end{aligned} \tag{3.89}$$

Substituting the above in (3.87), the Killing spinor equations can be written as

$$\begin{aligned} &\gamma_0 \hat{r}^{-\beta_t}\partial_{\hat{t}}\epsilon_i - \frac{\beta_t}{2}\gamma_1\epsilon_i + \frac{i}{2\sqrt{6}}A^I_3 h_I \gamma_{23}\epsilon_i + \frac{i}{\sqrt{6}}g_R h^I V_I \delta_{ij}\epsilon^j = 0 \ , \\ &\gamma_1 \hat{r}\partial_{\hat{r}}\epsilon_i - \frac{i}{2\sqrt{6}}A^I_3 h_I \gamma_{23}\epsilon_i - \frac{i}{\sqrt{6}}g_R h^I V_I \delta_{ij}\epsilon^j = 0 \ , \\ &\gamma_2 \partial_{\hat{x}}\epsilon_i + \frac{i}{\sqrt{6}}A^I_3 h_I \gamma_{23}\epsilon_i - \frac{i}{\sqrt{6}}g_R h^I V_I \delta_{ij}\epsilon^j = 0 \ , \\ &\gamma_3 e^{\hat{x}}\partial_{\hat{y}}\epsilon_i - \frac{1}{2}\gamma_2\epsilon_i + \frac{i}{\sqrt{6}}A^I_3 h_I \gamma_{23}\epsilon_i - \frac{i}{\sqrt{6}}g_R h^I V_I \delta_{ij}\epsilon^j = 0 \ , \\ &\gamma_4 \hat{r}^{-\beta_t}\partial_{\hat{z}}\epsilon_i + \frac{\beta_t}{2}\gamma_1\epsilon_i - \frac{i}{2\sqrt{6}}A^I_3 h_I \gamma_{23}\epsilon_i - \frac{i}{\sqrt{6}}g_R h^I V_I \delta_{ij}\epsilon^j = 0 \ . \end{aligned} \tag{3.90}$$

The γ_a matrices that appear in the above set of equations are in tangent space.

We choose a radial profile for the Killing spinor. This is motivated by the fact that the radial spinor preserves the time translation and homogeneous symmetries of the type III metric (3.14). Moreover, it is well known that the radially dependent spinor generates the Poincaré supersymmetries in AdS [100, 101]. Furthermore, some of the Bianchi type I solutions such as the Lifshitz and $AdS_3 \times \mathbb{R}^2$ solutions in gauged supergravity preserve $1/4$ of the supersymmetries for the radial spinor [96, 97, 104].

We choose the spinor ansatz

$$\epsilon_i = f(\hat{r})\chi_i \ , \tag{3.91}$$

where χ_i is a constant symplectic majorana spinor. Substituting (3.91) in the Killing spinor equation (3.90), we see that $\hat{t}, \hat{z}$ equations become identical. Adding the $\hat{t}$ equation and the radial equation we get

$$\hat{r}\partial_{\hat{r}} f(\hat{r}) - \frac{\beta_t}{2} f(\hat{r}) = 0 \ , \tag{3.92}$$

which is solved by

$$f(\hat{r}) = \hat{r}^{\frac{\beta_t}{2}}. \tag{3.93}$$

Using the above in (3.91) and substituting it in the Killing spinor equation (3.90) we get,

$$\begin{aligned}
&\frac{\beta_t}{2}\gamma_1\chi_i - \frac{i}{2\sqrt{6}}A_3^I h_I \gamma_{23}\chi_i - \frac{i}{\sqrt{6}} g_R h^I V_I \delta_{ij}\chi^j = 0 \ , \\
&\frac{i}{\sqrt{6}}A_3^I h_I \gamma_{23}\chi_i - \frac{i}{\sqrt{6}} g_R h^I V_I \delta_{ij}\chi^j = 0 \ , \\
&\frac{1}{2}\gamma_2\chi_i - \frac{i}{\sqrt{6}}A_3^I h_I \gamma_{23}\chi_i + \frac{i}{\sqrt{6}} g_R h^I V_I \delta_{ij}\chi^j = 0 \ .
\end{aligned} \tag{3.94}$$

From the last two of the above equations, it follows that

$$\gamma_2\chi_i = 0 \ . \tag{3.95}$$

This condition breaks all of the supersymmetry. The origin of the γ_2 term is the spin connection term due to the $EAdS_2$ (3.15) part of the type III metric. Thus, a naive radial spinor does not preserve supersymmetry in this case. This suggests that the stable Bianchi III metric we have constructed may be a non-supersymmetric attractor. However, it is possible that there may be a more general ansatz for the Killing spinor which could preserve some supersymmetry. We hope to study this in future works.

3.6 Comments and discussions

In this chapter, we constructed a new Bianchi type III solution in Einstein-Maxwell theory with massless gauge fields. We embedded this solution in a $U(1)_R$ gauged supergravity with one vector multiplet. We found that there exist a class of type III solutions parametrized by g_R, V_0, V_1 that satisfied the two sufficient requirements for the attractor mechanism, namely the existence of a critical point of the attractor potential and that the Hessian of the attractor potential should have a positive eigenvalue.

We investigated the stability of the Bianchi type III solution in gauged supergravity by studying the linearized fluctuations of the gauge field, scalar field, metric about their attractor values. The stress energy tensor in gauged supergravity depends on linearized fluctuations of scalars and gauge fields [94]. In order to avoid backreaction and deviation from the attractor geometry, all the fluctuations have to be well behaved as one approaches the horizon.

For the solution (3.63), we showed that the source term in the gauge field fluctuations vanishes. Thus there are no gauge field fluctuations sourced by scalar fluctuations. The metric fluctuation equations are sourced completely by the scalar perturbations. We showed that for the type III solution satisfying the sufficient conditions for the attractor mechanism, the scalar fluctuations are well behaved near the horizon. We also solved the metric fluctuations and showed that all the fluctuations are regular. Since all the linearized fluctuations are well behaved near the horizon, we infer that the type III Bianchi solution is a stable attractor solution at the linearized level.

One of the simplifications that aided us in the stability analysis was that there were no gauge field fluctuations which are sourced by scalar fluctuations. As we commented before in §3.4.1, this need not happen in general. For more complicated situations we expect that as long as the solution satisfies the sufficient conditions for the attractor mechanism [84], the Bianchi type geometries might be stable with respect to linearized fluctuations about the attractor values. We hope to explore these aspects and look for more interesting solutions in future.

In the long run, we hope our stability analysis will provide motivation to explore the possibility of construction of analytic black brane solutions which interpolate between IR and UV attractor geometries. In particular, it will be very interesting to construct solutions that are asymptotically AdS. Such interpolating solutions will be helpful to explore the holographic duals of Bianchi attractors. In the last chapter 2 we saw some progress in this direction (Ref. [77]). It will be valuable to construct analytic interpolating solutions in a simple theory of gravity coupled to suitable matter.

In this chapter, we also investigate the supersymmetry of the Bianchi type III solution. We study the Killing spinor equations of $\mathcal{N} = 2, U(1)_R$ gauged supergravity with the background Bianchi type III solution. We chose a radial profile for the Killing spinor since it preserves the time translations and homogeneous symmetries of the metric. However, we found that the naive radial spinor which gives supersymmetric Bianchi I spaces such as AdS and Lifshitz fails for the type III case. This suggests that the stable type III solution we have constructed may be a non-supersymmetric attractor. However, there could be more general spinors than the radial one we have considered. We leave a systematic analysis of this issue for future work.

Chapter 4

The Shear Viscosity in Anisotropic Phases

4.1 Introduction

In the last few chapters, we have spent some time on understanding how anisotropic blackbrane geometries arise in theories of Einstein gravity and also in gauged supergravity theories. In this chapter, we are now prepared to study the transport properties of anisotropic strongly coupled fluids. Via holography, this maps to an investigation of the anisotropic blackbrane geometries in the bulk. Let us first make a few general comments on the existing results in the literature and set up our main goals for this chapter.

The AdS/CFT correspondence has emerged as an important tool in the analysis of strongly coupled systems, especially for the study of transport properties of such systems. Neither analytical nor numerical methods are convenient for calculating these properties on the field theory side since they require an understanding of the real time response at finite temperature. In contrast, they can be calculated with relative ease on the gravity side, often by solving simple linear equations. An important insight which has come out of these studies pertains to the behaviour of the viscosity. It was found in KSS [114, 115, 116], that for systems having a gravity description that can be well approximated by classical Einstein gravity, the ratio of the shear viscosity, η, to the entropy density, s, takes the universal value

$$\frac{\eta}{s} = \frac{1}{4\pi}. \tag{4.1}$$

This is a small value, compared to weak coupling where the ratio diverges. It was also initially suggested that this value is a bound, and the ratio can never become smaller. We now know that this is not true [117, 118, 119, 120], see also [121, 122], but in all controlled counter-examples the bound is violated at best by a numerical factor, and not in a parametric manner. Attempts to produce bigger violations lead to physically unacceptable situations, e.g., to causality violations, for example, see [123, 124]. However, there is some discussion of a violation of the bound in metastable states, see [125]. Also, see [126] for a discussion of violations in a superfluid phase described by higher derivative gravity.

The behaviour of the viscosity discussed above refers to isotropic and homogeneous phases, which on the gravity side at finite temperature are described by the Schwarzschild black brane geometry. Gravitational backgrounds which correspond to anisotropic phases in field theory have also been studied (see [121, 127, 128, 129, 130, 131, 132, 133] and the behaviour of the viscosity in some of these anisotropic phases has also been analysed, see [134, 135] and [136, 137, 138, 139, 140, 141]. The viscosity in the anisotropic case is a tensor, which in the most general case, with no rotational invariance, has 21 independent components (when the field theory lives in $3+1$ dimensions). In [134, 135, 139], where some simple cases were considered, it was found that some components of the viscosity tensor can become much smaller, parametrically violating the bound in eq.(4.1). For example, in [139], a gravitational solution was considered where the rotational invariance of the three space dimensions in which the field theory lives was broken from $SO(3)$ to $SO(2)$, due to a linearly varying dilaton . In the solution, the dilaton varies along the z direction and rotational invariance in the remaining x, y, spatial directions was left unbroken. The component of the viscosity, called $\eta_{||}$ in [139], which measures the shear force in the $x-y$ plane, was still found to satisfy the relation, eq.(4.1). However, other components of the viscosity did not satisfy it. In particular, it was found that a component called $\eta_{\perp}$, which measures the shear force in the $x-z$ or $y-z$ plane, could become much smaller, going like

$$\frac{\eta_{\perp}}{s} = \frac{8\pi}{3}\frac{T^2}{\rho^2}, \tag{4.2}$$

where T is the temperature and ρ is the anisotropy parameter. The result, eq.(4.2) is valid in the extremely anisotropic limit, when $T \ll \rho$. A detailed study was also carried out in [139] of this extreme anisotropic regime and no instabilities were found to be present.

For the case of low anisotropy, spin 1 component of the shear viscosity $\eta_{xz} = \eta_{yz} \equiv \eta_{\perp}$ behave as follows:

Low anisotropy regime ($\rho/T \ll 1$):

$$\frac{\eta_{\perp}}{s} = \frac{1}{4\pi} - \frac{\rho^2 \log 2}{16\pi^3 T^2} + \frac{(6-\pi^2+54(\log 2)^2)\rho^4}{2304\pi^5 T^4} + \mathcal{O}\left[\left(\frac{\rho}{T}\right)^6\right] . \tag{4.3}$$

We see that a small anisotropy at order $(\rho/T)^2$ already reduces this component of the viscosity and makes it smaller than the KSS bound. In the limit of zero anisotropy, we recover the KSS bound

$$\frac{\eta_{\perp}}{s} \to \frac{1}{4\pi}. \tag{4.4}$$

In this chapter we study many other examples where anisotropic phases arise and show that in all of them components of the viscosity can become parametrically small, in units of the entropy density, when the anisotropy becomes sufficiently large compared to the temperature. Depending on the example, the factor of T^2 in eq.(4.2) can be replaced by some other positive power of T.

A common feature of all our examples is that the breaking of anisotropy is due to an externally applied force which is translationally invariant. For example, the linearly varying dilaton considered in [139], and also in section (4.2) gives rise to such a spatially constant forcing function. This follows from the fact that the boundary theory stress tensor is no longer conserved in the presence of the dilaton and instead satisfies the equation

$$\partial_\mu < T^{\mu\nu} >=< \hat{O} > \partial^\nu \phi, \tag{4.5}$$

where $\hat{O}$ is the operator dual to the dilaton, see eq.(6.9) of [139]. Similarly, we consider linearly varying axions in section 4.4.3 and 4.4.4, and a constant magnetic field in section 4.4.2.

Another common feature in our examples is that some residual Lorentz symmetry survives, at zero temperature, after incorporating the breaking of rotational invariance. Fluid mechanics then corresponds to the dynamics of the goldstone modes associated with the boost symmetries of this Lorentz group which are broken at finite temperature.

In the second half of this chapter we give an argument, based on a Kaluza Klein decomposition of modes, which shows quite generally that in all situations sharing these features, in particular where the forcing function does not break translational invariance, appropriate components of the viscosity tensor become parametrically small. These components correspond to perturbations of the metric which carry spin 1 with respect to the surviving Lorentz symmetry. Let z be a spatial direction in the boundary theory along which there is anisotropy and x be a spatial direction along which the boost symmetry is left unbroken, then we show that the viscosity component η_{xz}, which couples to the h_{xz} component of the metric perturbation, satisfies the relation,

$$\frac{\eta_{xz}}{s} = \frac{1}{4\pi}\frac{g_{xx}}{g_{zz}}\Big|_{u=u_h}, \tag{4.6}$$

where $g_{xx}|_{u=u_h}, g_{zz}|_{u=u_h}$ refer to the components of the background metric at the horizon. Eq.(4.6) is one of the main results of this chapter. It also agrees with the behaviour seen in all the explicit examples we consider. This result was first derived for an anisotropic axion-dilaton-gravity system in [134].

In the isotropic case the ratio $\frac{g_{xx}}{g_{zz}}\Big|_{u=u_h}$ is unity and we see that the KSS result is obtained. However, in anisotropic cases this ratio can become very different from unity and in fact much smaller, leading to the parametric violation of the bound, eq.(4.1).

Let us note that the result, eq.(4.6), is true for conformally invariant systems, as well as systems with a mass gap, when subjected to a constant driving force. Examples of massive

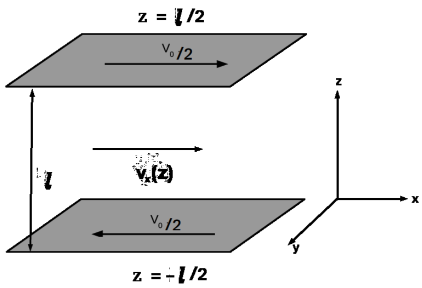

Figure 4.1: Picture showing flow of fluid enclosed between two parallel plates separated along the z-direction.

systems include, for example, gravitational duals of confining gauge theories, [142] and [143]. For these cases the temperature should be bigger than the confining scale so that the gravity dual is described by a black brane. Also, for some components of the viscosity to become significantly smaller than the bound, the anisotropy must be bigger than the temperature.

Physically a component like η_{xz} measures the resistance to shear. For example, if the fluid is enclosed between two parallel plates which are separated along the z direction and moving with a relative velocity v_x along the x direction in a non-relativistic fashion, they will experience a friction force due to the fluid, proportional to $\eta_{xz}\partial_z v_x$. See Fig (4.1) and the more extensive discussion in section 6 of [139]. Thus the parametrically small values obtained here correspond to a very small resistance to shear in anisotropic systems.

Our results which are quite general, open up the exciting possibility that in nature too, strongly coupled anisotropic systems may have a very small value for components of the viscosity. It would be very exciting if this behaviour can be probed in experimental situations, realised perhaps in cold atom systems, or in the context of QCD. We will explore this in detail later in Chapter 5.

This chapter is structured as follows. In section 4.2 we review the earlier discussion of a system with one linearly varying dilaton. Some general aspects involved in the calculation of viscosity are discussed in section 4.3. Several examples of anisotropic systems realised in gravity are then discussed, including the case with two dilatons in section 4.4.1, a magnetic field in section 4.4.2, and axions and dilatons, section 4.4.3 and section 4.4.4. The general argument based on a Kaluza Klein truncation is given in section 4.5. We end with conclusions in section 4.6. The appendices C.1, C.2 and C.3 contain additional important details.

4.2 Brief Review of The System With One Dilaton

Here we briefly summarise some of the key results in [139] which considered a linearly varying dilaton $\phi = \rho\, z$ in asymptotically AdS_5, for a theory with action

$$S_{bulk} = \frac{1}{2\kappa^2} \int d^5x\sqrt{-g}\, \left(R + 12\Lambda - \frac{1}{2}(\partial\phi)^2 \right). \tag{4.7}$$

Here $2\kappa^2 = 16\pi G$ is the gravitational coupling and G is the Newton's Constant in 5-dimensions. At zero temperature the near horizon solution was found to be $AdS_4 \times R$,

$$ds^2 = -\frac{4}{3}u^2dt^2 + \frac{du^2}{\frac{4}{3}u^2} + \frac{4}{3}\, u^2(dx^2 + dy^2) + \frac{\rho^2}{8}dz^2. \tag{4.8}$$

The radius of AdS_4, $R_4^2 = 3/4$, in units where $\Lambda = 1$. We see in eq.(4.8) that the metric component g_{zz} becomes constant due to the extra stress energy provided by the linearly varying dilaton. The $AdS_4 \times R$ solution is in fact an exact solution to the equations of motion.

At small temperature, $T \ll \rho$, the geometry is that of a Schwarzschild black brane in $AdS_4 \times R$. The viscosity is related, using linear response, to the retarded two point function of components of the stress tensor, and the latter, using Ads/CFT, can be calculated from the behaviour of appropriate metric perturbations in the bulk. The answer for η_{xy}, which is denoted as $\eta_{||}$ and for η_{xz}, η_{yz}, which are equal and denoted as $\eta_\perp$, is given in eq.(4.9) and eq.(4.10) below:

$$\frac{\eta_{||}}{s} = \frac{1}{4\pi}, \tag{4.9}$$

$$\frac{\eta_\perp}{s} = \frac{8\pi T^2}{3\rho^2}, \tag{4.10}$$

with s being the entropy density.

We see that $\eta_\perp$ in units of the entropy density becomes parametrically small in the limit of high anisotropy. The fluid mechanics in this high anisotropy limit was also systematically set up in [139] and it was shown that, as expected, this small viscosity component results in a very small shear force on two suitably oriented parallel plates which are moving with a relative velocity and enclose the fluid.

4.3 More Details On The Calculation Of Viscosity

Before proceeding, we provide some more details on the calculation of the viscosity for the one dilaton system above. These features, as we will see, will be shared by all the examples we consider subsequently in this chapter. The analysis that follows will also reveal the central reason for why the viscosity in units of the entropy density can become so small in anisotropic systems.

With anisotropy, the viscosity is a tensor, η_{ijkl}, in general with 21 components. Using the Kubo formula these can be related to the two point function of the stress energy tensor as follows ,

$$\eta_{ij,kl} = -\lim_{\omega \to 0} \frac{1}{\omega} \mathbf{Im}\left[G^R_{ij,kl}(\omega)\right], \tag{4.11}$$

where

$$G^R_{ij,kl}(\omega, 0) = \int dt\ d\mathbf{x}\, e^{i\omega t}\, \theta(t)\, \langle [T_{ij}(t, \mathbf{x}), T_{kl}(0, 0)]\rangle, \tag{4.12}$$

and **Im** denotes the imaginary part of the retarded Green's function.
From the AdS/CFT correspondence the two point function of T_{ij} can be calculated in terms of the behaviour of metric perturbations, and in this way the viscosity can be obtained.

In the one dilaton system considered in section 4.2 , the solution has an $SO(2)$ rotational invariance in the $x - y$ plane, as is evident from the metric (4.8). For simplicity we denote the $\eta_{xz,xz}$ component as η_{xz}, and $\eta_{yz,yz}$ as η_{yz} etc. Due to the $SO(2)$ invariance we get that $\eta_{xz} = \eta_{yz} \equiv \eta_{\perp}$. These components are related to the behaviour of the h_{xz}, h_{yz} components of metric perturbations, which carry spin 1 with respect to $SO(2)$ symmetry.

We now proceed to introduce the h_{xz} perturbation in the metric as follows

$$\begin{aligned} ds^2 = -g_{tt}(u)dt^2 + g_{uu}(u)du^2 &+ g_{xx}(u)dx^2 + g_{yy}dy^2 + g_{zz}(u)dz^2 \\ &+ 2e^{-i\omega t} Z(u) g_{xx}(u) dx\ dz, \end{aligned} \tag{4.13}$$

where $Z(u)$ is the required perturbation of interest. We can show that the other modes decouple from $Z(u)$ and hence we can consistently set them to zero. Here we follow closely [144].

One finds that the mode $Z(u)$ obeys an equation of the form

$$\partial_u \left(\sqrt{-g} P(u) g^{uu} \partial_u Z(u)\right) - \omega^2 N(u) g^{tt} Z(u) = 0, \tag{4.14}$$

The functions $P(u), N(u)$ are given in terms of the background metric , with

$$P(u) = g^{zz} g_{xx}. \tag{4.15}$$

In effect, eq.(4.14) arises from an action

$$S = -\int \sqrt{-g} \frac{1}{16\pi G} [P(u) \frac{1}{2} g^{uu} (\partial_u Z)^2 - \frac{1}{2} N(u) g^{tt} (\partial_t Z)^2] \tag{4.16}$$

(we are neglecting the dependence on the spatial x^i coordinates here). Using AdS/CFT we can find the response in terms of the canonical momentum

$$\Pi(u, \omega) = -\frac{1}{16\pi G} \sqrt{-g} P(u) g^{uu} \partial_u Z(u). \tag{4.17}$$

The retarded Green's function is then given by the ratio of the response over the source,

$$G^{\text{ret}} = -\frac{\Pi(u,\omega)}{Z(u,\omega)}\bigg|_{u\to\infty} . \tag{4.18}$$

leading to the result from eq.(4.11)

$$\eta_\perp = \lim_{\omega\to 0} \frac{\Pi(u,\omega)}{i\omega Z(u,\omega)}\bigg|_{u\to\infty} . \tag{4.19}$$

We now show that the RHS of eq.(4.19) can also be evaluated near the horizon, $u = u_H$, instead of $u \to \infty$. Since we are interested in the limit $\omega \to 0$ we can neglect the second term in eq.(4.14) leading to

$$\partial_u \Pi = 0 \tag{4.20}$$

upto $O(\omega)^2$. This gives

$$\Pi = C, \tag{4.21}$$

where C is independent of u . Next, it is easy to see that there is a solution of eq.(4.14) in the $\omega \to 0$ limit in which Z is simply a constant. This solution also meets the correct boundary condition at $u \to \infty$, since, as can be seen from eq.(4.13), the non-normalisable mode must go to a constant at $u \to \infty$. Putting all this together we find that to leading order in the $\omega \to 0$ limit both Π and Z are constant and thus the ratio in eq.(4.19) being independent of u can also be evaluated at the horizon.

As a result we get

$$\eta_\perp = \lim_{\omega\to 0} \frac{\Pi(u,\omega)}{i\,\omega\, Z(u,\omega)}\bigg|_{u\to u_H} . \tag{4.22}$$

Demanding regularity at the future horizon , we can approximate the behaviour of Z as follows

$$Z \sim e^{-i\omega(t+r_*)}, \tag{4.23}$$

where r_* is the tortoise coordinate,

$$r_* = \int \sqrt{\frac{g_{uu}}{g_{tt}}}\, du. \tag{4.24}$$

It then follows that

$$\eta_\perp = \frac{1}{16\pi G} P(u_H) \sqrt{\frac{-g}{g_{tt} g_{uu}}}\bigg|_{u\to u_H} . \tag{4.25}$$

The entropy density is

$$s = \frac{1}{4G} \frac{\sqrt{-g}}{\sqrt{g_{uu} g_{tt}}}\bigg|_{u_H} . \tag{4.26}$$

Using the value of P(u) from (4.15) and using eq.(4.25) and eq.(4.26) this finally leads to

$$\frac{\eta_\perp}{s} = \frac{1}{4\pi}\frac{g_{xx}}{g_{zz}}\bigg|_{u_H}. \tag{4.27}$$

We now see why anisotropic systems will generically be different from isotropic ones. For an isotropic system rotational invariance makes the ratio $\frac{g_{xx}}{g_{zz}} = 1$, leading to the KSS bound, eq.(4.1). However in the anisotropic case in general this ratio will not be unity and thus the ratio of η/s can become smaller than $\frac{1}{4\pi}$. In the one dilaton system this is what happens leading to the result, eq.(4.27). In the rest of this chapter we will find many more examples of this type, where anisotropy will allow different metric components to shrink at different rates and attain different values at the horizon, thereby leading to violations of the KSS bound.

4.4 Additional examples with anisotropy

4.4.1 Anisotropic solution in two dilaton gravity system

To generalise the example in section 4.2, we consider next the case of gravity, with a negative cosmological constant, two massless scalar fields, ϕ_1 and ϕ_2 , both of which we now call dilatons, in 5 spacetime dimensions with action,

$$S_{bulk} = \frac{1}{2\kappa^2}\int d^5x\sqrt{-g}\,\left(R + 12\Lambda - \frac{1}{2}(\partial\phi_1)^2 - \frac{1}{2}(\partial\phi_2)^2\right). \tag{4.28}$$

Both the dilatons are turned on to be linearly varying, but along different directions:

$$\phi_1 = \rho_1 y, \quad \phi_2 = \rho_2 z. \tag{4.29}$$

The zero temperature near horizon solution is now given by $AdS_3 \times R \times R$ (we have set Λ=1):

$$ds^2 = -2u^2dt^2 + \frac{1}{2u^2}du^2 + 2u^2dx^2 + \frac{\rho_1^2}{8}dy^2 + \frac{\rho_2^2}{8}dz^2. \tag{4.30}$$

We see that there are now two different mass scales, ρ_1, ρ_2 which characterise the anisotropy. In appendix C.1 we show that this near horizon geometry interpolates smoothly to asymptotically AdS_5. The $SO(2,2)$ symmetry of AdS_3 is preserved all along this interpolation.

At small temperature, $T \ll \rho_1, \rho_2$, the near-horizon solution is given by :

$$ds^2 = -2u^2(1-\frac{\pi^2T^2}{u^2})dt^2 + \frac{1}{2u^2(1-\frac{T^2\pi^2}{u^2})}du^2 + 2u^2dx^2 + \frac{\rho_1^2}{8}dy^2 + \frac{\rho_2^2}{8}dz^2. \tag{4.31}$$

The horizon lies at

$$u = u_h = \pi T. \tag{4.32}$$

The computation of the shear viscosity follows the discussion in [139] quite closely. The near-horizon AdS_3 has $SO(1,1)$ Lorentz invariance in the t, x directions. The metric perturbations can be classified in terms of different spins with respect to this $SO(1,1)$ symmetry. The viscosity component η_{xz}, given by,

$$\eta_{xz} = -\lim_{\omega \to 0} \frac{1}{\omega} Im\big[G^R_{xz,xz}(\omega)\big], \tag{4.33}$$

can be calculated by considering a metric perturbation $Z(u)$ defined so that the full metric with the perturbation takes the form,

$$\begin{aligned} ds^2 = -g_{tt}(u)dt^2 + g_{uu}(u)du^2 + &g_{xx}(u)dx^2 + g_{yy}dy^2 + g_{zz}(u)dz^2 \\ &+ 2e^{-i\omega t} Z(u) g_{xx}(u) dx dz. \end{aligned} \tag{4.34}$$

This component has spin 1 with respect to the $SO(1,1)$ symmetry. It turns out that resulting analysis is quite similar to that in section 4.3 and this perturbation satisfies an equation of the type given in eq.(4.14), with $P(u)$ given by eq.(4.15). The conjugate momentum Π is also given by eq.(4.17) with $P(u)$ given by eq.(4.15). As a result η_{xz} is given by eq.(4.25).

The entropy density is given by

$$s = \frac{1}{4G} \frac{\sqrt{-g}}{\sqrt{g_{uu} g_{tt}}}\bigg|_{u_H}. \tag{4.35}$$

This gives,

$$\frac{\eta_{xz}}{s} = \frac{1}{4\pi} \frac{g_{xx}}{g_{zz}}\bigg|_{u_H}. \tag{4.36}$$

which using eq.(4.31) becomes

$$\frac{\eta_{xz}}{s} = \frac{4\pi T^2}{\rho_2^2}. \tag{4.37}$$

Similarly, for η_{xy} we get

$$\frac{\eta_{xy}}{s} = \frac{1}{4\pi} \frac{g_{xx}}{g_{yy}}\bigg|_{u_H} = \frac{4\pi T^2}{\rho_1^2}. \tag{4.38}$$

We see from eq.(4.36), eq.(4.38) that the relative ratio of η/s for these components is determined by the ratio of the metric components as one approaches the horizon.

4.4.2 Viscosity in the Presence of a Uniform Magnetic Field

Here, for completeness, we briefly review a situation where the anisotropy is generated due to a magnetic field which has been studied in considerable depth in [140]. We refer to [140] for details. We start with a system with the action

$$S = \int d^5x\sqrt{-g}(R + 12\Lambda - \frac{1}{4}F^2), \tag{4.39}$$

and consider a solution where the magnetic field

$$F_{yz} = B, \tag{4.40}$$

with B being a constant. Such a system was also considered in [145].
The resulting near horizon solution at zero temperature is now again $AdS_3 \times R \times R$, just as in the two dilaton system, with rotational invariance also preserved in the yz plane.

The metric is (we have set Λ=1)

$$ds^2 = -3u^2dt^2 + \frac{1}{3u^2}du^2 + 3u^2dx^2 + \frac{1}{2\sqrt{3}}|B|dy^2 + \frac{1}{2\sqrt{3}}|B|dz^2. \tag{4.41}$$

The radius of AdS_3, $R_3^2 = 1/3$, in units where $\Lambda = 1$.

At small temperature, $T \ll B$ the solution is a black brane in $AdS_3 \times R \times R$ with metric

$$ds^2 = -3u^2(1 - \frac{c}{u^2})dt^2 + \frac{1}{3u^2(1-\frac{c}{u^2})}du^2 + 3u^2dx^2 + \frac{1}{2\sqrt{3}}|B|dy^2 + \frac{1}{2\sqrt{3}}|B|dz^2, \tag{4.42}$$

where c is given in terms of T as follows

$$c = \frac{4\pi^2T^2}{9}. \tag{4.43}$$

The horizon lies at

$$u = u_h = \frac{2}{3}\pi T. \tag{4.44}$$

The viscosity components $\eta_{xy} = \eta_{xz} \equiv \eta_\perp$. To calculate $\eta_\perp$ we consider the h_{xz} component of metric perturbation, so that the full metric is of the form

$$\begin{aligned} ds^2 = -g_{tt}(u)dt^2 + g_{rr}(u)dr^2 + g_{xx}(u)dx^2 + g_{yy}(u)dy^2 + g_{zz}(u)dz^2 \\ + 2e^{-i\omega t}Z(u)g_{xx}(u)dxdz, \end{aligned} \tag{4.45}$$

with $Z(u)$ being the perturbation that we need to study. We can easily show that the other modes decouples from $Z(u)$ and so can be consistently set to zero.

We find that the resulting analysis is again quite similar to that in section 4.3 . This perturbation satisfies an equation of the type given in eq.(4.14), with $P(u)$ given by eq.(4.15).

The conjugate momentum Π is also given by eq.(4.17) with $P(u)$ given by eq.(4.15).

The resulting value for the viscosity is given by

$$\frac{\eta_\perp}{s} = \frac{1}{4\pi}\frac{g_{xx}}{g_{zz}}\bigg|_{u_H}. \tag{4.46}$$

Substituting the metric components from (4.42) above we get that

$$\frac{\eta_\perp}{s} = \frac{2}{\sqrt{3}}\pi\frac{T^2}{|B|}. \tag{4.47}$$

As discussed in [140], this example may be relevant in the study of QCD, perhaps for heavy ion collisions, and also in the core of neutron stars where strong magnetic fields can arise.

4.4.3 The Dilaton-Axion System

In the examples considered so far, the near horizon geometry was of the form, $AdS \times R^n$, with the metric components along the R^n directions not contracting as one gets to the horizon. It is worth considering other situations where the near horizon geometry is of Lifshitz type instead, with metric components along all the directions contracting as one approaches the horizon but at different rates.

An easy way to construct such an example involves a system consisting of gravity with an axion and dilaton with action,

$$S_{bulk} = \frac{1}{2\kappa^2}\int d^5x\sqrt{-g}\,\left(R + 12\Lambda - \frac{1}{2}(\partial\phi)^2 - \frac{1}{2}e^{2\alpha\phi}(\partial\chi)^2\right), \tag{4.48}$$

containing the parameter α which enters in the dilaton dependence of the axion kinetic energy term. Earlier work in [134] considered the case with $\alpha = 1$. The case $\alpha = -1$ has $SL(2, R)$ invariance.

It is easy to see that by turning on a linear profile for the axion one obtains an extremal solution whose near horizon limit is given by (setting Λ=1)

$$ds^2 = R^2\left(-u^2dt^2 + \frac{du^2}{u^2} + u^2dx^2 + u^2dy^2 + \rho^2\, u^{\frac{4\alpha^2}{1+2\alpha^2}}dz^2\right), \tag{4.49}$$

$$\chi = c_1\ \rho\ z, \tag{4.50}$$

$$\phi = \frac{2\alpha}{1+2\alpha^2}\log(u), \tag{4.51}$$

$$c_1 = \frac{\sqrt{2(3+8\alpha^2)}}{(1+2\alpha^2)}, \tag{4.52}$$

$$R^2 = \frac{3+8\alpha^2}{4+8\alpha^2}. \tag{4.53}$$

This solution breaks rotational invariance along the z direction due to the linearly varying axion, and ρ is the mass scale which characterises this breaking of anisotropy. We see that all components of the metric along the spatial directions now shrink as one approaches the far IR, but the rate at which the g_{zz} component vanishes is different from the other spatial components, g_{xx}, g_{yy}. Let us also note that for $\alpha = 1$ the solution above agrees with [128].

At small temperature $T \ll \rho$ the resulting solution has a metric given by

$$ds^2 = R^2 \left(-u^2 f(u) dt^2 + \frac{du^2}{u^2 f(u)} + u^2 dx^2 + u^2 dy^2 + \rho^2 u^{\frac{4\alpha^2}{1+2\alpha^2}} dz^2 \right), \tag{4.54}$$

where R^2 is as given in eq(4.53) above and f(u) is given as

$$1 - \left(\frac{16\pi T}{p^2 u} \right)^p, \tag{4.55}$$

where p $= \frac{3+8\alpha^2}{1+2\alpha^2}$. The axion continues to be linear as in the solution eq.(4.50) and the dilaton is given by eq.(4.51).

The horizon in eq.(4.54) is at

$$u = u_h = \frac{16\pi T}{p^2}. \tag{4.56}$$

Let us now turn to computing the viscosity. The shear viscosity component η_{xy} satisfies the KSS bound in eq.(4.9) . Next consider the component $\eta_{xz} = \eta_{yz}$. To compute this component we can consider the h_{xz} component of metric perturbation, so that the full metric is of the form

$$\begin{aligned} ds^2 = -g_{tt}(u)dt^2 + g_{uu}(u)du^2 + &g_{xx}(u)dx^2 + g_{yy}(u)dy^2 + g_{zz}(u)dz^2 \\ &+ 2e^{-i\omega t} Z(u) g_{xx}(u) dx dz, \end{aligned} \tag{4.57}$$

where $Z(u)$ is the perturbation that we need to study. The dilaton and axion are unchanged and are given by eq (4.51) and eq (4.50) respectively. We can easily show that the other modes decouples from $Z(u)$ and so can be consistently set to zero.

We again find that resulting analysis is similar to that in section 4.3 and the perturbation satisfies an equation of the type given in eq.(4.14), with $P(u)$ given by eq.(4.15). The conjugate momentum Π is also given by eq.(4.17) with $P(u)$ given by eq.(4.15). As a result η_{xz} is given by eq.(4.25).

Thus, substituting the metric components for the finite temperature solution (4.54) we get

$$\frac{\eta_\perp}{s} = \frac{1}{4\pi} \frac{g_{xx}}{g_{zz}} \sim \left(\frac{T}{\rho}\right)^{\frac{2}{1+2\alpha^2}}. \tag{4.58}$$

The dependence on T in eq.(4.58) follows from the metric eq.(4.54) and the dependence on ρ is then obtained on dimensional grounds. Let us note that the temperature T which appears in eq.(4.55) could be related to the temperature as measured in the asymptotic AdS

coordinates by a rescaling. By the asymptotic AdS coordinates we mean those in which the metric takes the standard form:

$$ds^2 = \Big[-u^2 dt^2 + \frac{du^2}{u^2} + u^2(dx^2 + dy^2 + dz^2) \Big], \tag{4.59}$$

This is also true for the x, y coordinates in eq.(4.54) and the corresponding coordinates which appear in eq.(4.59). and also for the z coordinate in eq.(4.54) which is related to the corresponding coordinate in eq.(4.59) by a ρ dependent rescaling in general. These rescaling factors have to be determined if the coefficient in eq.(4.58) is to be fixed. To do so, one needs to find the full interpolating geometry from the near horizon region, described by eq.(4.54) , to the asymptotic AdS region, eq.(4.59).

We have carried out such a numerical interpolation for $\alpha = \pm 1$, for which, eq.(4.58) becomes,

$$\frac{\eta_\perp}{s} \sim (\frac{T}{\rho})^{2/3}. \tag{4.60}$$

We find, within the accuracy of our numerical calculation, that there is no rescaling of the T, x, y coordinates while the z coordinate is rescaled by a non-trivial ρ dependent factor. One consequence is that the temperature T which appears in eq.(4.58) is the same as the temperature measured in the field theory.

4.4.4 The two Axion-one Dilaton System

For good measure, as another example, we consider a system consisting of gravity with two axions and one dilaton described by the action

$$S_{bulk} = \frac{1}{2\kappa^2} \int d^5x \sqrt{-g} \left(R + 12\Lambda - \frac{1}{2}(\partial\phi)^2 - \frac{1}{2}e^{2\alpha\phi}(\partial\chi_1)^2 - \frac{1}{2}e^{2\alpha\phi}(\partial\chi_2)^2 \right). \tag{4.61}$$

In this case we will see that for a suitable profile for the two axions, the AdS_4 symmetry of the near-horizon geometry is broken further to AdS_3, with now two of the spatial directions, y, z, being characterised by non-trivial Lifshitz exponents.

The linear profiles for the two axons and resulting near horizon solution is given by (setting

Λ=1)

$$ds^2 = R^2 \left(-u^2 dt^2 + \frac{du^2}{u^2} + u^2 dx^2 + \rho^2\ u^{\frac{8\alpha^2}{1+4\alpha^2}} dy^2 + \rho^2\ u^{\frac{8\alpha^2}{1+4\alpha^2}} dz^2 \right), \tag{4.62}$$

$$\chi_1 = c\ \rho\ y, \tag{4.63}$$

$$\chi_2 = c\ \rho\ z, \tag{4.64}$$

$$\phi = \frac{4\ \alpha \log(u)}{1+4\alpha^2}, \tag{4.65}$$

$$c = \frac{2}{1+4\alpha^2}\sqrt{1+8\alpha^2}, \tag{4.66}$$

$$R^2 = \frac{1+8\alpha^2}{2+8\alpha^2}. \tag{4.67}$$

This metric in this solution has AdS_3 invariance, and also a scaling symmetry under which y, z transform with a non-trivial exponent. The linearly varying axions break this scaling symmetry, and also the rotational invariance along the y and z directions, with ρ being the mass scale which characterise the breaking.

At small temperature $T \ll \rho$ the resulting solution has a metric

$$R^2 \left(-u^2 f(u) dt^2 + \frac{du^2}{u^2 f(u)} + u^2 dx^2 + \rho^2\ u^{\frac{8\alpha^2}{1+4\alpha^2}} dy^2 + \rho^2\ u^{\frac{8\alpha^2}{1+4\alpha^2}} dz^2 \right), \tag{4.68}$$

where R^2 is as given in eq.(4.67) above and f(u) is given as

$$1 - \left(\frac{16\pi T}{p^2 u} \right)^p, \tag{4.69}$$

where p $= \frac{2(1+8\alpha^2)}{1+4\alpha^2}$.

The two axions continue to be linear as in the solution eq.(4.63), eq.(4.64) and the dilaton is given by eq.(4.65).

The horizon in eq.(4.68) is at

$$u = u_h = \frac{16\pi T}{p^2}. \tag{4.70}$$

The η_{xy} and η_{xz} components of the viscosity are the same., we denote them by $\eta_\perp$. To calculate these components we consider the h_{xz} component of metric perturbation, so that the full metric is of the form

$$\begin{aligned} ds^2 = -g_{tt}(u)dt^2 + g_{uu}(u)du^2 + &g_{xx}(u)dx^2 + g_{yy}(u)dy^2 + g_{zz}(u)dz^2 \\ &+ 2e^{-i\omega t} Z(u) g_{xx}(u) dx dz, \end{aligned} \tag{4.71}$$

where $Z(u)$ is the perturbation that we need to study.
The dilaton and axions are unchanged and are given by eq (4.65) and eq (4.63) , eq (4.64) respectively. We can easily show that the other modes decouples from $Z(u)$ and so can be

consistently set to zero.

As in the previous cases , the analysis here is similar to that in section 4.3 and this perturbation satisfies an equation of the type given in eq.(4.14), with $P(u)$ given by eq.(4.15). The conjugate momentum Π is also given by eq.(4.17) with $P(u)$ given by eq.(4.15). As a result η_{xz} is given by eq.(4.25).

Thus, substituting the metric components for the finite temperature solution (4.68) we get

$$\frac{\eta_\perp}{s} = \frac{1}{4\pi}\frac{g_{xx}}{g_{zz}} \sim \left(\frac{T}{\rho}\right)^{\frac{2}{1+4\alpha^2}} . \tag{4.72}$$

For the case $\alpha = \pm 1$, eq.(4.72) becomes,

$$\frac{\eta_\perp}{s} \sim \left(\frac{T}{\rho}\right)^{2/5} . \tag{4.73}$$

Interestingly, both in eq.(4.58) for the one axion case, and in eq.(4.72) above we see that the maximum value the exponent governing the temperature dependence can take is 2, and the minimum value, for $\alpha = \infty$, is 0.

4.5 Kaluza Klein Reduction

The previous sections dealt with a number of examples where anisotropic situations gave rise to small values for the viscosity to entropy ratio. One common feature of all these examples was that the breaking of isotropy was due to a spatially constant driving force. For example, the dilaton considered in section 4.2, gives rise to a force proportional to the gradient of the dilaton which is a constant since the dilaton varies linearly. One way to see this is by noting that the stress tensor is no longer conserved and satisfies the equation

$$\partial_\mu < T^{\mu\nu} > \;\; = \;\; < \hat{O} > \partial^\nu \phi, \tag{4.74}$$

as discussed in eq.(6.9) of [139]. Similarly, we consider linearly varying axions in section 4.4.3 and 4.4.4, and a constant magnetic field in section 4.4.2.

In this section we will present a general argument which should apply to all such situations where the breaking of isotropy occurs due to matter fields which give rise to a spatially constant driving force. We will also assume that a residual AdS symmetry is preserved in the bulk, and a corresponding Lorentz symmetry is left intact in the boundary theory. Fluid mechanics then corresponds to the dynamics of the goldstone modes associated with the boost symmetries of this Lorentz group. The components of the viscosity which give rise to the violation of the KSS bound in the examples considered above correspond to metric perturbations which have spin 1 with respect to the surviving Lorentz symmetry. Let z

be a spatial direction in the boundary theory along which there is anisotropy and x be a spatial direction along which the boost symmetry is left unbroken then we will present a general argument below showing that the viscosity component η_{xz}, which couples to the h_{xz} component of the metric perturbation. satisfies the relation,

$$\frac{\eta_{xz}}{s} = \frac{1}{4\pi}\frac{g_{xx}}{g_{zz}}\Big|_{u=u_h}. \tag{4.75}$$

where $g_{xx}|_{u=u_h}, g_{zz}|_{u=u_h}$ refer to the components of the background metric at the horizon. Eq.(4.75) is the main result of this section and one of the main results of this chapter. We note that it also agrees with all the examples considered above. This result was first obtained for an anisotropic axion-dilaton-gravity system in [134]. An analysis using RG flow and KK reduction, for this system, was carried out in [138] along the lines of [115, 144].

For a case with a residual AdS_{d+1} factor in the metric, the basic idea behind the general analysis will be to consider a dimensionally reduced description, starting from the original $D+1$ dimensional theory and going down to the AdS_{d+1} space-time. Different Kaluza Klein (KK) modes in the extra dimensions will not mix with each other since the effects breaking rotational invariance are in effect spatially constant. For example, for cases where there are linearly varying fields, like axions or dilatons, this will be true since the equations of motion involve only gradients of these fields which are spatially constant. The non-mixing of the KK modes will greatly ease in the analysis, since we can use the standard formulae of KK reduction and moreover truncate the analysis to the zero modes in the extra dimensions. The off diagonal components of the metric, whose perturbations carry spin 1 and which are related to the viscosity components of interest, will give rise to gauge fields in the dimensionally reduced theory. By studying the conductivity of these gauge fields, which can be related easily to the spin 1 viscosity components we will derive the result in eq.(4.75).

The study of more complicated situations where the breaking of rotational invariance is due to a driving force that also breaks translational invariance is left for the future.

4.5.1 The Dimensionally Reduced Theory

To start, we will consider the case where $D = 4$ and $d = 3$, so that a residual AdS_4 symmetry survives, and the asymptotic geometry, towards the boundary, is AdS_5. In this case we start with 5 dimensions with a gravitational action :

$$S = \frac{1}{2\hat{\kappa}^2}\int d^5x\sqrt{-\hat{g}}\;(\hat{R}+12\Lambda). \tag{4.76}$$

Here $2\hat{\kappa}^2 = 16\pi\hat{G}$ is the gravitational coupling with $\hat{G}$ being Newton's Constant in 5-dimension and we set Λ=1.

Parametrising the 5 dimensional metric by

$$(\hat{g}_{AB}) = \begin{pmatrix} e^{-\psi(u)} g_{\mu\nu} + e^{2\psi(u)} A_\mu A_\nu & e^{2\psi(u)} A_\mu \\ e^{2\psi(u)} A_\nu & e^{2\psi(u)} \end{pmatrix} \quad , \tag{4.77}$$

and taking all components to be independent of the z direction which we take to be the compactification direction, gives

$$S = \frac{1}{2\kappa^2} \int d^4x \sqrt{-g} \left(R - \frac{3}{2} (\partial\psi)^2 - \frac{e^{3\psi}}{4} F^2 + 12 e^{-\psi} \right), \tag{4.78}$$

where we have dropped total derivatives .
We also note that in our choice of parametrisation ,

$$\hat{g}_{zz} = e^{2\psi}. \tag{4.79}$$

The coefficient of the first term in the matrix in eq.(4.77) was taken to be $e^{-\psi}$ so that the resulting 4 dimensional action is in the Einstein frame. κ which appears above is related to the 5 dimensional gravitational coupling $\hat{\kappa}$ by

$$\frac{L}{2\hat{\kappa}^2} = \frac{1}{2\kappa^2}, \tag{4.80}$$

where L is the length of the compactified z direction.

So far we have neglected any matter fields. Consider for concreteness the case of the axion-dilaton system considered in section 4.4.3 with action eq.(4.48) with α=1. Inserting the background solution for the axion

$$\chi = a\ z, \tag{4.81}$$

and taking the dilaton to be independent of z we get from the kinetic energies of the dilaton and axion,

$$S = \frac{1}{2\kappa^2} \int d^4x \sqrt{-g} \left(-\frac{a^2 e^{2\phi} A^2}{2} - \frac{1}{2} (\partial\phi)^2 - \frac{1}{2} a^2 e^{2\phi - 3\psi} \right). \tag{4.82}$$

We see that there is an extra term which depends on the gauge field and which gives rise to a mass for it. This term arises due to the linearly varying axion, eq.(4.81) and is tied to the breaking of translational invariance due to this linear variation. We see that the terms in eq.(4.78) and eq.(4.82) involving the gauge field are quadratic in this field and can be written as

$$S = \frac{1}{2\kappa^2} \int d^4x \sqrt{-g} \left(\frac{-1}{4 g_{\text{eff}}^2(u)} F^2 - \frac{1}{4} m^2(u) A^2 \right), \tag{4.83}$$

where

$$m^2(u) = 2a^2 e^{2\phi(u)}, \tag{4.84}$$

and

$$\frac{1}{g_{\text{eff}}^2(u)} = e^{3\psi} = (\hat{g}_{zz}(u))^{\frac{3}{2}}\,. \tag{4.85}$$

The solution in the near horizon region for this dilaton-axion system was given in eq.(4.49) with α=1. It is easy to see from this solution that

$$\frac{1}{g_{\text{eff}}^2}(u) = \rho^3 u^2, \tag{4.86}$$

and

$$m^2(u) = \frac{44}{9}\rho^2 u^{\frac{4}{3}}, \tag{4.87}$$

and therefore that the gauge coupling and mass vary with the radial coordinate.

Similarly, in other cases where there is also a breaking of translational invariance we will get both a kinetic energy term and a mass term, and in general both the gauge coupling and the mass will vary in the radial direction. For the subsequent analysis we will analyse the perturbations of the gauge fields in the 4 dimensional theory given in eq.(4.83). Such a system was considered in [146, 147] and our subsequent discussion closely follows this reference. As we will see later, the conductivity of these gauge fields can be related easily to the spin 1 viscosity components using which we will derive the result in eq.(4.75). Let us mention for now that the essential reason for this is that the two-point correlator of the current operator gives the conductivity of the gauge field, while the two-point stress tensor in the higher dimensional theory is related to the viscosity. Since the gauge field is obtained from the spin 1 component of the metric in the higher dimensional theory, these two correlators are closely related.

The 3+1 dimensions, include time, t, the radial direction u, and additional space directions, one of which we denote by x. To study the conductivity we consider a perturbation for the x component of the gauge field,

$$A_x(\vec{x}, t, u) = \int \frac{d\omega d^3\vec{k}}{(2\pi)^4} e^{-i\omega t + \vec{k}.\vec{x}} Z(u, \omega). \tag{4.88}$$

This gauge field perturbation decouples from the rest (we have set perturbations of the axion to vanish even before the KK reduction in the example above, this turns out to be a consistent thing to do). $Z(u, \omega)$ satisfies the equation

$$\frac{d}{du}(N(u)\frac{d}{du}Z(u,\omega)) - \omega^2 N(u)\; g_{uu}g^{tt}Z(u,\omega) + M(u)Z(u,\omega) = 0, \tag{4.89}$$

with

$$N(u) = \sqrt{-g}\frac{1}{g_{\text{eff}}^2}g^{xx}g^{uu}, \tag{4.90}$$

and

$$M(u) = -\frac{m^2(u)\sqrt{-g}}{2\ g_{xx}}. \tag{4.91}$$

Treating the radial coordinate u as the analogue of time we can read off the "momentum" conjugate to Z from eq.(4.83) to be

$$\Pi(u,\omega) = \frac{\delta S}{\delta Z'(u,-\omega)} = -\frac{1}{2\kappa^2} N(u) Z'(u,\omega), \tag{4.92}$$

where $Z' = \frac{d}{du} Z(u,\omega)$ and N(u) as given in eq(4.90).

The conductivity is given by

$$\sigma(u,\omega) = \frac{\Pi(u,\omega)}{i\omega Z(u,\omega)}\Big|_{u\to\infty,\omega\to 0}, \tag{4.93}$$

where Z and Π are the asymptotic values of the perturbation and conjugate momentum defined in eq.(4.92) in the region $u \to \infty$.

We assume that the underlying higher dimensional geometry is asymptotically AdS_5 space and that the back reaction due to the matter fields which break the rotational invariance dies out compared to the cosmological constant in this asymptotic region. This is true in all the examples studied above where the geometry becomes AdS_5 when $u \to \infty$. It is then easy to check, as discussed in appendix C.2 that the ratio on the RHS in eq.(4.93) becomes independent of u when $u \to \infty$.

We can write $\sigma(u,\omega)$ as the sum of real and imaginary parts as $\mathrm{Re}\,(\sigma(u,\omega)) + i\ \mathrm{Im}\,(\sigma(u,\omega))$. We will be interested in the real part $\mathrm{Re}\,(\sigma)$ since that is related to the viscosity components of interest. It is easy to see from our definition, eq.(4.93) that

$$\mathrm{Re}\,(\sigma(u,\omega)) \quad = \quad \mathrm{Im}\left(\frac{\Pi(u,\omega) Z(u,-\omega)}{\omega Z(u,\omega) Z(u,-\omega)}\right)\Big|_{u\to\infty,\ \omega\to 0}. \tag{4.94}$$

where $\Pi(u,\omega)$ is defined in eq.(4.92).
To evaluate the RHS in the limit $\omega \to 0$, it will be sufficient to consider the leading order behaviour of the denominator. Since $Z(u,\omega)$ is real to leading order when $\omega \to 0$ we obtain

$$\mathrm{Re}\,(\sigma) = \frac{\mathrm{Im}\,(\Pi(u,\omega) Z(u,-\omega))}{\omega\ Z^2(u)}\Big|_{u\to\infty,\ \omega\to 0}. \tag{4.95}$$

The numerator of RHS of eq.(4.95) is independent of u (appendix C.3) and can therefore be evaluated at $u = u_h$ instead of $u \to \infty$. After some more simplification this gives

$$\mathrm{Re}\,(\sigma) = \sigma_H \ \left(\frac{Z(u_h)}{Z(u\to\infty)}\right)^2\Big|_{\omega\to 0}, \tag{4.96}$$

where σ_H is the conductivity evaluated at the horizon and its expression is given by,

$$\sigma_H = \frac{1}{2\kappa^2 g_{\text{eff}}^2}\Big|_{u=u_h}. \tag{4.97}$$

See appendix C.3 for more details.

To proceed we need to evaluate the ratio $\frac{Z(u_h)}{Z(u\to\infty)}$. For this purpose we go back to the underlying higher dimensional theory with which we started in which the gauge field is actually an off diagonal component of the metric, eq.(4.77). The background about which we are calculating the behaviour of the perturbation is diagonal in the metric with all components being only a function of u. Now consider a coordinate transformation $x \to x + \alpha z$, with all the other coordinates remaining the same. It is easy to see that under this transformation the metric now acquires an off-diagonal component

$$\delta \hat{g}_{xz} = \alpha \hat{g}_{xx}, \tag{4.98}$$

with all the other components of the background metric staying the same. Note that in our notation the hatted metric refers to the 5 dimensional one while the unhatted metric refers to the 4 dimensional Einstein frame metric, see eq.(4.77).

Since we have merely carried out a coordinate transformation it is clear that $\delta\hat{g}_{xz}$ in eq.(4.98) must satisfy the equations of motion for small perturbations about the starting background. Comparing with eq.(4.77) we find that this corresponds to turning on a gauge field

$$A_x = \alpha \frac{\hat{g}_{xx}}{e^{2\psi}}, \tag{4.99}$$

which must therefore solve the equation (4.89) in the limit $\omega \to 0$ with

$$Z(u) = \alpha \frac{\hat{g}_{xx}}{e^{2\psi}}. \tag{4.100}$$

In this way we can exploit the co-ordinate invariance of the underlying higher dimensional theory to obtain a solution for $Z(u)$ in the $\omega \to 0$ limit. More over it is easy to see that this solution meets the correct boundary condition at $u \to \infty$. As was mentioned above, we are assuming that the higher dimensional metric is asymptotically AdS_5 space. The ratio $\frac{\hat{g}_{xx}}{e^{2\psi}}$ therefore goes to unity and $Z(u)$ goes to a constant which is the correct behaviour needed, as is also discussed in appendix C.2.

With the solution eq.(4.100) at hand we can now evaluate the ratio $\frac{Z(u_h)}{Z(u\to\infty)}$. The arbitrary constant α drops out and we get that

$$\frac{Z(u_h)}{Z(u\to\infty)} = \frac{\hat{g}_{xx}}{e^{2\psi}}\Big|_{u=u_h}. \tag{4.101}$$

Substituting in eq.(4.96) and using eq.(4.97) we get that the conductivity is given in terms of $g^2_{\rm eff}$ and various metric opponents at the horizon by

$$\sigma = \frac{1}{2\kappa^2 g^2_{\rm eff}} \left(\frac{\hat{g}_{xx}}{e^{2\psi}}\right)^2 \Big|_{u=u_h}. \tag{4.102}$$

From eq.(4.85) and using eq.(4.79) from our parametrisation eq.(4.77) , we finally get that

$$\sigma = \frac{1}{2\kappa^2}\frac{\hat{g}^2_{xx}}{\sqrt{\hat{g}_{zz}}}. \tag{4.103}$$

Note that we have been able to obtain an expression independent of m^2 that only depends on the metric components $\hat{g}_{xx}, \hat{g}_{zz}$ in the 5 dimensional theory. In the subsequent discussion we somewhat loosely denote $Re(\sigma)$ by σ itself.

4.5.2 The Viscosity To Entropy Ratio

The next step is to relate the conductivity obtained above to the viscosity. This is in fact straightforward. Kubo's formula relates the components of the viscosity to the two point function of corresponding components of the stress tensor T_{ij} in eq.(4.11). This two point function is obtained by calculating the response to turning on suitable metric perturbations in the bulk. We will be assuming, as was mentioned above, that asymptotically the background metric is AdS_5. Thus as $u \to \infty$, $\hat{g}_{\mu\nu} \to u^2\delta_{\mu\nu}$ for all components other than along the u direction, as discussed in appendix C.2. The off - diagonal metric perturbations required for the shear viscosity then behave like

$$\delta\hat{g}_{\mu\nu} = u^2 h_{\mu\nu}$$

as $u \to \infty$, where $h_{\mu\nu}$ is independent of u. The viscosity component η_{xz} is then given by

$$\eta_{xz} = -\frac{1}{\omega}\mathrm{Im}\left(< T_{xz}(\vec{k_1},\omega)T_{xz}(\vec{k_2},\omega) >'\right)|_{\vec{k_1},\vec{k_2}\to 0,\omega\to 0}, \tag{4.104}$$

where the prime subscript on the RHS means that the overall energy momentum conserving delta function has been removed. From AdS/CFT we have that

$$< T_{xz}(\vec{k_1})T_{xz}(\vec{k_2}) > \;\; = \frac{\delta^2 S}{\delta h_{xz}(\vec{k_1})\delta h_{xz}(\vec{k_2})}. \tag{4.105}$$

The conductivity in an analogous way is given by

$$\sigma = -\frac{1}{\omega}\mathrm{Im}\left(< J_x(\vec{k_1},\omega)J_x(\vec{k_2},\omega) >'\right)|_{\vec{k_1},\vec{k_2}\to 0,\omega\to 0}, \tag{4.106}$$

which in turn can be calculated from the bulk response since

$$< J_x(\vec{k_1}) J_x(\vec{k_2}) > \;\; = \frac{\delta^2 S}{\delta A_x(\vec{k_1})\ \delta A_x(\vec{k_2})}. \tag{4.107}$$

On comparing with eq.(4.77) we see that the zero mode of h_{zx} in the z direction is in fact A_x. This shows that η_{xz} and σ are essentially the same upto one minor factor of L the size of the z direction. This factor arises because the prime subscript in eq. (4.104) and eq.(4.106) are different, in the first case the momentum conservation delta function removed includes a delta function in the z direction, whereas in the case of the conductivity it does not include this delta function. Accounting for the difference gives

$$\eta_{xz} = \frac{\sigma}{L}. \tag{4.108}$$

The entropy density in the 5 dimensional theory is given by

$$s = \frac{2\pi}{\hat{\kappa}^2} A = \frac{2\pi}{\hat{\kappa}^2} \sqrt{\hat{g}_{xx}\hat{g}_{yy}\hat{g}_{zz}}, \tag{4.109}$$

(this is also the same as the entropy density in the 4 dimensional theory divided by L). From eq.(4.108) , eq.(4.102), eq.(4.79), eq.(4.109)and eq.(4.80), we can now write the ratio

$$\frac{\eta_{xz}}{s} = \frac{\frac{\sigma}{L}}{s} = \frac{1}{4\pi} \frac{\frac{1}{g_{\text{eff}}^2} \left(\frac{\hat{g}_{xx}}{\hat{g}_{zz}}\right)^2}{\sqrt{\hat{g}_{xx}\hat{g}_{yy}\hat{g}_{zz}}}\Big|_{u=u_h}. \tag{4.110}$$

Using eq.(4.85), eq.(4.79) in the above expression and using isotropy along x and y, we arrive at the following result

$$\frac{\eta_{xz}}{s} = \frac{1}{4\pi} \frac{\hat{g}_{xx}}{\hat{g}_{zz}}\Big|_{u=u_h}. \tag{4.111}$$

This general result agrees with the ones we obtained in all the examples we studied in the previous sections. We see that independent of the details of the matter fields which were responsible for the breaking of the rotational symmetry we get a general result in eq.(4.110). This result shows that when the ratio of the metric components $\frac{\hat{g}_{xx}}{\hat{g}_{zz}}$ at the horizon becomes smaller than unity the KSS bound will be violated.

4.5.3 Generalisation To Case with Additional Directions

In the preceding discussion of this section we have considered the dimensional reduction from 5 to 4 dimensions. However, it is easy to generalise these results for the case where we start with $D+1$ dimensions and KK reduce to $d+1$ dimensions. In fact, this generalisation is needed for the situation discussed earlier with a magnetic field where the residual symmetry arises due to an AdS_3 factor instead of an AdS_4 in the geometry. Our analysis closely follows [148]. The dimensional reduction in this case will give rise to $D-d$ gauge fields .

Following [148], we parametrize the higher dimensional metric as :

$$(\hat{g}_{AB}) = \begin{pmatrix} g_{\mu\nu} + A^{(1)\gamma}_{\mu} A^{(1)}_{\nu\gamma} & A^{(1)}_{\mu\beta} \\ A^{(1)}_{\nu\alpha} & G_{\alpha\beta} \end{pmatrix} \quad , \tag{4.112}$$

where the $D+1$ dimensional vielbein is given by

$$\left(\hat{e}^{\hat{r}}_{\hat{\mu}}\right) = \begin{pmatrix} e^{r}_{\mu} & A^{(1)\beta}_{\mu} E^{a}_{\beta} \\ 0 & E^{a}_{\alpha} \end{pmatrix} \quad , \tag{4.113}$$

with $G_{\alpha\beta} = E^a_\alpha \delta_{ab} E^b_\beta$ and $g_{\mu\nu} = e^r_\mu \eta_{rs} e^s_\nu$. Here $\alpha, \beta = 1, ..D-d$ denote the directions over which the reduction has been carried out and $\mu, \nu = 0, 1, \cdots d$ are the ones left in the lower dimensional theory. It also follows from the parametrisation that

$$\sqrt{-\hat{g}} = \sqrt{-g}\sqrt{G}, \tag{4.114}$$

where G is the determinant of the internal metric $G_{\alpha\beta}$. Additional matter fields required for breaking rotational invariance which also break the translational invariance in the compactified directions give mass terms for the gauge fields, which will vary in general in the radial direction. Neglecting these additional matter fields for now we start with the action

$$S_{\hat{g}} = \frac{1}{2\hat{\kappa}^2} \int d^{D+1}x \, \sqrt{-\hat{g}} \, \left[\hat{R} + \Lambda\right]$$

As shown in [148] the dimensionally reduced action in $d+1$ dimensions becomes

$$\begin{aligned} S = \frac{1}{2\kappa^2} \int d^{d+1}x \sqrt{-g} \, e^{-\phi} \Big(& R + \Lambda + g^{\mu\nu}\partial_\mu\phi\partial_\nu\phi + \frac{1}{4} g^{\mu\nu}\partial_\mu G_{\alpha\beta}\partial_\nu G^{\alpha\beta} \\ & - \frac{1}{4} g^{\mu\rho} g^{\nu\lambda} G_{\alpha\beta} F^{(1)\alpha}_{\mu\nu} F^{(1)\beta}_{\rho\lambda} \Big) , \end{aligned} \tag{4.115}$$

where

$$\phi = -\frac{1}{2} \log \, \det\left(G_{\alpha\beta}\right) \Rightarrow e^{-\phi} = \sqrt{G}, \tag{4.116}$$

where G is the determinant of the internal metric $G_{\alpha\beta}$,

$$F^{(1)\alpha}_{\mu\nu} = \partial_\mu A^{(1)\alpha}_{\nu} - \partial_\nu A^{(1)\alpha}_{\mu}, \tag{4.117}$$

and κ which appears above is related to the 5 dimensional gravitational coupling $\hat{\kappa}$ by

$$\frac{L^{D-d}}{2\hat{\kappa}^2} = \frac{1}{2\kappa^2}, \tag{4.118}$$

where L^{D-d} is the volume of the compactified directions .

For simplicity we assume that the internal metric $G_{\alpha\beta}$ is diagonal and focus on the $\hat{g}_{xz}$ component of the metric perturbation (where x represents a spatial direction along which the boost symmetry is left unbroken and z represents an anisotropy direction in the boundary field theory). Comparing the last term in the action eq.(4.115) with the kinetic energy term, $\sqrt{-g}\left(\frac{-1}{4g_{\text{eff}}^2(u)}F^2\right)$, as given in eq.(4.83), we then find the effective gauge coupling, for the corresponding gauge field A is

$$\frac{1}{g_{\text{eff}}^2} = e^{-\phi} g_{zz}. \tag{4.119}$$

As mentioned above, additional matter fields give rise to mass terms for the gauge fields. We will also take these mass terms to be diagonal for simplicity. The resulting equation for the x component of the gauge field A_x is then of the form given in eq.(4.89), where we have expanded A_x as given in eq.(4.88). It can then be argued (see Appendix C.3 for details) that the conductivity in the lower $d+1$ dimensional theory [1] is given by

$$\begin{aligned}
\text{Re}\,(\sigma) &= \frac{1}{2\kappa^2}\left(\sqrt{\frac{g_{uu}}{g_{tt}}}\,N(u)\right)_{u=u_h}\left(\frac{Z(u_h)}{Z(u\to\infty)}\right)^2 \\
&= \frac{1}{2\kappa^2}\left(\sqrt{\frac{g_{uu}}{g_{tt}}}\,\sqrt{-\,g}\frac{1}{g_{\text{eff}}^2}\,g^{xx}\,g^{uu}\right)_{u=u_h}\left(\frac{Z(u_h)}{Z(u\to\infty)}\right)^2
\end{aligned}$$

Thus we find

$$\text{Re}\,(\sigma) = \sigma_H\,\left(\frac{Z(u_h)}{Z(u\to\infty)}\right)^2, \tag{4.120}$$

where σ_H is the conductivity evaluated at the horizon and its expression is given by,

$$\sigma_H = \frac{1}{2\kappa^2\,g_{\text{eff}}^2}\,\frac{g_{xx}^{\frac{d-1}{2}}}{g_{xx}}\Big|_{u=u_h}, \tag{4.121}$$

where we have used isotropy along the spatial directions (besides u) in the lower dimensional theory. Using eq.(4.120), eq.(4.119), eq.(4.116) we get

$$\begin{aligned}
\text{Re}\,(\sigma) &= \frac{1}{2\kappa^2 g_{\text{eff}}^2}\,\frac{g_{xx}^{\frac{d-1}{2}}}{g_{xx}}\Big|_{u=u_h}\,\left(\frac{Z(u_h)}{Z(u\to\infty)}\right)^2 \\
&= \frac{1}{2\kappa^2}\,e^{-\phi}g_{zz}\frac{g_{xx}^{\frac{d-1}{2}}}{g_{xx}}\Big|_{u=u_h}\,\left(\frac{Z(u_h)}{Z(u\to\infty)}\right)^2 \\
&= \frac{1}{2\kappa^2}\sqrt{G}\,g_{xx}^{\frac{d-1}{2}}\,\frac{g_{zz}}{g_{xx}}\left(\frac{Z(u_h)}{Z(u\to\infty)}\right)^2.
\end{aligned} \tag{4.122}$$

We can now repeat the analysis done in the previous section to evaluate the ratio $\frac{Z(u_h)}{Z(u\to\infty)}$, by using general coordinate invariance in the underlying higher dimensional theory and noting

[1] With our choice, eq.(4.112), the dimensional reduction results in an action which is not in Einstein frame. We could have performed a conformal transformation to bring the lower dimensional action back to the Einstein frame. Our end result however will be independent of this choice.

that the gauge field is an off-diagonal component of the metric, eq.(4.112) (for details see eq.(4.101)).
Thus we get

$$\begin{aligned}
\mathrm{Re}\,(\sigma) &= \frac{1}{2\kappa^2}\sqrt{G}\; g_{xx}^{\frac{d-1}{2}}\,\frac{g_{zz}}{g_{xx}} Z(u_h)^2\Big|_{u=u_h} \\
&= \frac{1}{2\kappa^2}\sqrt{G}\; g_{xx}^{\frac{d-1}{2}}\,\frac{g_{zz}}{g_{xx}}\,\frac{g_{xx}^2}{g_{zz}^2}\Big|_{u=u_h} \\
&= \frac{1}{2\kappa^2}\sqrt{G}\; g_{xx}^{\frac{d-1}{2}}\;\frac{g_{xx}}{g_{zz}}\Big|_{u=u_h}. \qquad (4.123)
\end{aligned}$$

The higher dimensional entropy density is

$$s = \frac{2\pi}{\hat{\kappa}^2}\sqrt{G}\; g_{xx}^{\frac{d-1}{2}}. \qquad (4.124)$$

Hence we arrive at the result

$$\frac{\sigma}{s} = L^{D-d}\frac{1}{4\pi}\frac{g_{xx}}{g_{zz}}\Big|_{u=u_h}. \qquad (4.125)$$

Finally, the arguments given in subsection 4.5.2 allows us to connect η_{xz} computed in the higher dimension to σ in the following way

$$\eta_{xz} = \frac{\sigma}{L^{D-d}}. \qquad (4.126)$$

Thus we find

$$\frac{\eta_{xz}}{s} = \frac{\frac{\sigma}{L^{D-d}}}{s} = \frac{1}{4\pi}\frac{g_{xx}}{g_{zz}}\Big|_{u=u_h}, \qquad (4.127)$$

which agrees with the examples we have studied in the previous sections.

4.6 Comments and discussions

In this chapter we have considered a variety of anisotropic examples, and have shown that suitable components of the viscosity can become very small in the highly anisotropic case and can parametrically violate the bound, eq.(4.1). All our examples have the feature that the breaking of rotational invariance is due to an externally imposed forcing function which is translationally invariant. E.g. due to linearly varying scalars which give rise to a constant forcing function, or due to a spatially constant magnetic field, which was studied earlier in [140]. Another common feature in all our examples is that some residual Lorentz symmetry survives at zero temperature. In the second half of the chapter we show in considerable generality that for all cases with these two features, the components of the viscosity tensor, which correspond to metric perturbations which carry spin 1 with respect to the unbroken Lorentz symmetry, satisfy the relation eq.(4.6). In the anisotropic case the ratio of the metric components on the RHS of eq.(4.6) can become very small as $T \to 0$, resulting in a parametrically large violation of the KSS bound. This is indeed true for the examples we consider, all of which satisfy eq.(4.6) .

Besides allowing for a computation of the viscosity with relative ease, the gravitational description also provides an intuitive understanding of why such violation of the KSS bound may arise. In the absence of isotropy the different metric perturbations break up into components with different values of spin with respect to the remaining Lorentz symmetry. Spin 2 components, if present, give rise to viscosity coefficients which satisfy the KSS bound. But spin 1 components can violate it. In fact the spin 1 components are akin to gauge fields, and the corresponding calculations for these components of the viscosity therefore becomes similar to those for conductivity. These are well known in several AdS/CFT examples, and also in nature, to sometimes become very small.

In weakly coupled theories, with well defined quasi particles, we would expect, [149], [150], that

$$\frac{\eta}{s} \sim \frac{l_{mfp}}{\lambda_{dB}}, \tag{4.128}$$

where l_{mfp}, λ_{dB} refer to the mean free path and the de Broglie wave length for the quasi particles. This leads to the intuitive expectation that at strong coupling the ratio $\eta/s \sim O(1)$. However, here we see that at strong coupling, where the gravity description is valid, some components of the viscosity tensor in the anisotropic case violate this relation and can become parametrically smaller.

The generality of our result suggests the possibility that this behaviour might happen in nature too. It would be very exciting if this can be probed in experiments, perhaps on cold atom systems, or in QCD.

Ordinarily, QCD at finite temperature is described by a homogeneous and isotropic phase for which the calculations discussed here are not relevant. This is true even when we consider situations which come about due to anisotropic initial conditions, as might arise in heavy ion collisions. The behaviour of the QCD fluid in these situations is still governed by rotationally invariant Navier Stokes equations with appropriate viscosity coefficients. However, this could change if a sufficiently big magnetic field is turned on breaking rotational invariance [2]. The resulting equilibrium phase could then be highly anisotropic and our results, and earlier work, [140], hint that suitable components of the viscosity might become small. It has been suggested that such an intense magnetic field might perhaps arise in the interior of some highly magnetised neutron stars [3], see [151], [152] and [153]. It has also been suggested that strong magnetic fields might actually arise in the highly relativistic heavy ion collisions (see [154], [155] and [156]), although in this case the transitory nature of these fields must also then be taken into account.

Turning to cold atom systems, the unitary Fermi gas has also been observed to have a value

[2] A magnetic field of order 10^{16} Tesla or so is needed in order to contribute an energy density comparable to the QCD scale ~ 200 Mev.

[3] We thank Gergely Endrödi and Gunnar Bali for a discussion on this issue.

of η/s close to the KSS bound. As we will explore in Chapter 5, we can introduce the breaking of rotational invariance in this system. It is thus very interesting to examine the resulting behaviour of the viscosity tensor. Even at small anisotropy one might hope to see a trend where some components start getting smaller than the bound. A natural way to incorporate anisotropy in this case might be to consider the effects of an asymmetric trap [4] which we will describe in Chapter 5 .

It is worth mentioning that the spin 1 viscosity components, which become very small in our work, govern the diffusion of the momentum components oriented transverse to the direction in which the initial inhomogeneity is set up. For example, take a case with anisotropy in the z direction. If the momentum along the x direction, p_x, is now taken to have an initial gradient along the z direction, then its diffusion is governed by the viscosity component η_{xz}, with diffusion length

$$D_\perp = \frac{\eta_{xz}}{sT}, \tag{4.129}$$

where s is the entropy density. A small value of $\frac{\eta_{xz}}{s}$ then gives rise to a small value for the diffusion constant [5]$D_\perp$ in units of temperature.

It is perhaps worth mentioning in this context that there have been some recent measurements of spin diffusion in the unitary fermi gas system [6]. In three space dimensions, with rotational invariance intact, the transverse spin diffusion constant is measured to be close to the bound which arises from standard Boltzmann transport theory based on quasi particles, see [157]. However, in a quasi-two space dimensions [158], it was found that the transverse spin diffusion constant is about three orders of magnitude smaller than this bound. It would be worth exploring if these observations can be related to the results presented here.

We have not analysed the stability of the anisotropic solutions discussed in this chapter in any detail. For the one dilaton case this question was analysed at considerable length in [139] and no instabilities were found. This suggests that some examples studied here, e.g., the two dilation case, also could be stable. We leave a more detailed analysis of this question for the future. It is worth noticing that if an instability appears, it will be when the temperature $T \sim \rho$, where ρ is the scale of the anisotropy. As a result one expects $\mathcal{O}(1)$ violations of the bound for such systems as well, although not violations where the viscosity becomes parametrically small. On a more theoretical note, it would be worth obtaining string theory embeddings of the anisotropic systems we have studied here and examining if they are stable. Some embeddings for the axion dilaton system were studied in [128] and for the one dilaton case in [139] and were found to be unstable, since they contained fields which lay below the BF bound of the near horizon geometry. In another instance, e.g.

[4]We thank Mohit Randeria for very helpful discussions in this regard and also for his comments about the spin diffusion experiments.

[5]The anisotropy force in this case would act in the z direction. This force does not directly enter in the diffusion equation for p_x. For significant anisotropy, $\rho/T \gg 1$, the force is big, and as a result the fluid cannot move in the z direction at all. This follows from the bulk geometry, e.g. $AdS_4 \times R$ in the case considered in section 4.2, where Lorentz invariance along the z direction is manifestly broken.

[6]We thank Sean Hartnoll for bringing these experiments to our notice.

[135], though, a stable supersymmetric system with anisotropy was found where suitable components of the viscosity become vanishingly small at low temperatures, just as in our analysis here.

We have discussed situations where the breaking of rotational invariance is explicit, due to an externally applied source. It would also be interesting to extend this analysis to cases where the breaking is spontaneous. Another direction is to consider Bianchi spaces which have been discussed in [1, 2], and which describe homogeneous but anisotropic phases in general. Some discussion of transport coefficients in such phases using the gravity description can be found in [159].

Chapter 5

The Shear Viscosity in an Anisotropic Unitary Fermi Gas

5.1 Introduction

The calculation of the transport properties of strongly coupled quantum theories is an interesting problem for theorists working on a wide range of systems including ultra-cold Fermi gases at unitarity [160, 161], heavy ion collisions [160, 162], and neutron stars [163, 164].

At strong coupling, perturbative expansions fail to give reliable answers. Sophisticated Monte-Carlo techniques which are used to study such theories non-perturbatively by evaluating path-integrals in imaginary time, while very successful for calculating equilibrium properties (in the Fermi gas context see Ref. [165] and Refs therein; for heavy ion collisions see Ref. [166] and Refs therein) cannot be easily generalized to study transport (in the Fermi gas context see Ref. [167, 168]; for heavy ion collisions see Ref. [169] and Refs therein).

Within the framework of AdS/CFT however, a class of strongly interacting quantum field theories in d dimensions in some limits can be related to weakly coupled theories of gravity in $(d+1)$ dimensions. This correspondence [170] allows us to compute dynamical properties of these theories, often with relative ease.

While the theories describing ultra-cold Fermi gases and heavy ion collisions do not have known gravitational duals and controlled calculations are difficult, beautiful experiments have managed to measure the value of η/s in the two systems. The value of η/s of the quark gluon plasma created in heavy ion collisions, required for hydrodynamic simulations to be consistent with the experimentally measured spectrum of low energy particles (see Ref. [171] for a review), seems to be close to $1/(4\pi)$. Remarkably, η/s has been measured for ultra-cold fermions at unitarity for a wide range of temperatures and the minimum value (see Refs. [172, 173, 174]) is about six times the KSS bound.

Interestingly, the shear viscosity tensor for many interesting systems is often anisotropic. For example, it has been suggested that the highly anisotropic initial states in heavy ion collisions (the direction parallel to the collision axes is fundamentally different from the transverse directions) may give rise to anisotropic transport properties [175]. Furthermore, many interesting states of matter, eg. spin density waves and spatially modulated phases, are anisotropic. Another possibility, that we shall explore in detail in this chapter, is that an externally applied field can pick a particular direction and give rise to anisotropies in the shear viscosity. This possibility has been explored extensively for the case of weakly coupled theories in the presence of a background magnetic field. (See Ref. [149] for a classic treatment, Ref. [176] for applications to heavy ion collisions and Ref. [177] for applications to neutron stars.) The behavior of strongly coupled theories in the presence of an external field is less well explored. Our results in the last chapter (Chapter 4) indicate that one may expect parametric violations of the KSS bound in such anisotropic scenarios. As we saw, this feature arises in a wide variety of examples and seems to be quite general. In particular, for a spatially constant driving force which breaks rotational invariance, we found that by increasing the strength of the driving force compared to the temperature, the ratio for appropriate components of the shear viscosity to entropy density can be made arbitrarily small, violating the KSS bound.
If this phenomenon also carries over to the unitary Fermi gases, it may be possible to measure these small viscosities in experiments with trapped ultra-cold Fermi gases. For this purpose, it is helpful to consider traps which share the essential features of the systems we have considered in gravity listed at the end of Sec. 5.2 of this chapter. The goal of this chapter is to give a concrete proposal for the trap geometry and parameters where this effect is likely to be seen.

While typical trap potentials are harmonic, [quadratic (Eq. 5.14) rather than linear in the distance] by using existing results for the thermodynamics of unitary Fermi gases, we show that for a range of temperatures the dominant contribution to the damping of collective modes due to viscosity arises from a narrow region in the trap not near the center, where the trapping potential can be approximately considered as linear. In analogy with Ref. [139, 178] it is desirable to have traps that are highly anisotropic, which can be simulated by taking the trapping frequencies [179] in one of the directions (say ω_z) to be much larger than the frequencies in the other directions.
We describe two hydrodynamic modes whose dissipation is governed by the components of viscosity which are expected to become small in the anisotropic situation considered here. One of them is known in the literature as the scissor mode which has been well studied for bosonic superfluids at $T = 0$ theoretically [180] and has also been experimentally excited in both bosonic [181] and fermionic [182] superfluids. The second mode is a new quasi-stationary solution to the hydrodynamic equations. Especially for the scissor mode, we show that for experimentally reasonable values of trap parameters, the damping rate of the mode lies within an experimentally accessible range. It should therefore be possible to study

this mode, measure the relevant component of the viscosity and its possible suppression.

To gain some additional understanding of how the anisotropic system might behave, we also make a rough estimate of the viscosity components in the presence of an anisotropic trapping potential using the Boltzmann equation. We find that as the anisotropy increases, due to an increase in the trapping frequency ω_z in one of the directions, some components of the viscosity tensor decrease, compared to their value in the isotropic case.

The outline for the chapter is as follows. First, using the knowledge we have gained in the previous chapters in the gravity picture, we summarize the essential features required in a system to exhibit the suppression of η/s.

Next, we consider the unitary Fermi gas in an anisotropic harmonic trapping potential and describe the two hydrodynamic modes which couple to the small components of the shear viscosity tensor in Sec. 5.3.1. In Sec. 5.3.3 and Sec. 5.3.4 we show that these two hydrodynamic modes satisfy the equations of superfluid hydrodynamics. Sec. 5.3.5 discusses the energy dissipation due to shear viscosity in these two modes we have studied. In Sec. 5.3.6 we examine the constraints on the mode amplitudes by demanding validity of fluid mechanics and in Sec. 5.3.7 we discuss the damping in the outer regions of the cloud. Next we review the thermodynamics of the system in Sec.5.3.8. In Sec. 5.3.9 we give parameter values for traps (the trapping potential, the temperature and the chemical potential at the center of the trap) which are tuned such that the system possesses the required essential features, and show that by measuring the damping rate of fluid modes (described in Sec. 5.3.1) one can measure the shear viscosity. This section contains some of the key results in the chapter. Sec. 5.4 discusses an analysis in a weakly coupled anisotropic theory using the Boltzmann equation. We conclude our discussion in Sec. 5.5.

The solution of the Boltzmann equation used to estimate the values of the trap potentials for which we expect the corrections to the viscosity to be substantial is given in Appendix D.2. In Appendix D.1 we compare the modes (discussed in Sec. 5.3.1) with the well known breathing modes.

5.2 Brief recap of the main results from gravity and conditions for suppression of η/s

In Chapter 4 (Ref. [178]), several anisotropic theories in $3+1$ dimensional space-time (the boundary with coordinates (t, x, y, z)), which are dual to a gravitational theory living in $4+1$ dimensional space-time (the bulk with an additional coordinate u) were studied. Isotropy was broken by considering states where some of the fields have a background value that depended on some of the spatial coordinates x , y , z, explicitly breaking rotational symmetry between them.

All the examples studied in Chapter 4 (Ref. [178]) share the common feature that the force responsible for breaking isotropy in the boundary theory is translation invariant as we shall explain via an example below.

Chapter 4 (Ref. [178]) built on the results of Ref. [139], which studied a simple system consisting of a linearly varying dilaton. The dilaton field ϕ couples to the graviton in the bulk via the Lagrangian

$$S = \frac{1}{16\pi G}\int d^5x\sqrt{g}\,\left[R + 12\Lambda - \frac{1}{2}\partial_\mu\phi\partial^\mu\phi\right] , \tag{5.1}$$

where G is Newton's constant in 5 dimensions and Λ is a cosmological constant. The boundary theory in the absence of anisotropy is a $3+1$ dimensional conformal field theory.

In this system we can clarify what we mean by saying that the driving force is constant. The dilaton field in the background solution here has the profile

$$\phi(t,x,y,z) = \rho z \; . \tag{5.2}$$

Clearly this choice of the background singles out the z direction, breaking isotropy. In the presence of the dilaton the conservation equations for the stress tensor get modified to be,

$$\partial_\mu T^{\mu\nu} = \langle O\rangle\partial^\nu\phi \quad , \tag{5.3}$$

where O is the operator dual to the field ϕ. The right hand side arises because the varying dilaton results in a driving force on the system. We see that a linear profile results in a constant value for $\partial^\nu\phi$ and thus a constant driving force.

Let us also mention that in this example, on the gravity side the linearly varying dilaton gives rise to a translationally invariant stress tensor and thus a black brane solution which preserves translational invariance. This corresponds to the fact that in the field theory the equilibrium stress tensor features only derivatives of ϕ and is thus space-time invariant.

We shall see that the cold-atom system we consider will not be invariant under translations in equilibrium. However the equations of hydrodynamics (Eq. 5.20) in the presence of a driving force associated with a space varying potential look similar to Eq. 5.3, where the operator O in the cold-atom system corresponds to the density, and the driving force is proportional to the gradient of the potential $\phi(\mathbf{r})$.

The example considered in Ref. [139] also shares the property that an $SO(2,1)$ residual Lorentz symmetry survives, at zero temperature, after breaking isotropy. This residual Lorentz symmetry corresponds to the t, x, y directions in the boundary theory. Fluid mechanics corresponds to the dynamics of the Goldstone modes associated with the boost symmetries of this residual Lorentz group, which are broken at finite temperature.

In a general system the viscosity η is a fourth order tensor under rotations relating the deviation of the stress-energy tensor from its equilibrium value, to the velocity gradient. If

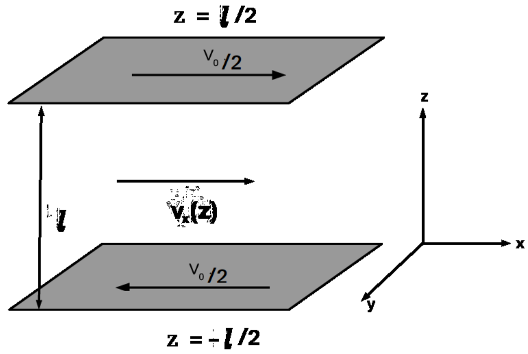

Figure 5.1: Fluid flow between two parallel plates. For $\phi = \rho z$ the driving force is in the z direction and is proportional to ρ. Parametrically small values of the viscosity (Eq. 5.12) govern the dynamics for flows in the x (or y) direction with a gradient in the z direction (for Eg. $v_x = v_0 z$).

the local fluid velocity is $\mathbf{v} = (v_x, v_y, v_z)$, we have

$$\delta T^{ij} = \eta^{ijkl}\frac{1}{2}(\partial_k v_l + \partial_l v_k) \; . \tag{5.4}$$

Since we are only considering the effects of the shear components,

$$\eta^{ijkl}\delta_{kl} = 0 \; . \tag{5.5}$$

In the example in Ref. [139], with dilaton profile given by Eq. 5.2, the viscosity components that become small correspond to the η^{xzxz}, η^{yzyz} components of the viscosity tensor. In the subsequent discussion we shall use an abbreviated notation,

$$\eta^{xzxz} = \eta_{xz}, \;\; \eta^{yzyz} = \eta_{yz}. \tag{5.6}$$

In the gravity description these components correspond to perturbations of the metric which carry spin 1 with respect to the surviving $SO(2,1)$ residual Lorentz symmetry.

A fluid flow configuration where the frictional force (and therefore the resulting dissipation) is governed by a spin 1 viscosity component arises as follows. Consider the fluid enclosed between ([178, 183]) two parallel plates separated along z axis by a distance L with the top plate moving with a speed $v_0/2$ along x direction while the lower plate moves with a speed $v_0/2$ along $-x$ direction, see Fig.5.1.

The resulting steady state solution of the Navier Stokes equation, even for the anisotropic case, is remarkably simple, with

$$v_y = 0, \;\; v_z = 0, \tag{5.7}$$

the temperature T being a constant, and v_x being a linear function of z

$$v_x = \frac{v_0}{L} z, \; z \in (-L/2, L/2) \tag{5.8}$$

(we have chosen coordinates so that $z = 0$ lies at the midpoint between the plates). A constant force per unit area is exerted by the fluid on both the upper and lower plates, $T^{xz} = \eta_{xz}\, \partial_z v_x$, in this solution (we are compactly writing η_{xzxz} as η_{xz}). This frictional force retards the relative motion of the plates and must be counteracted by an equal and opposite force acting on both plates externally to sustain the steady state solution. We also note that for this solution, in the gravity theory under discussion, hydrodynamics is valid as long as the velocity gradient $\frac{v_0}{L}$ is small compared to the temperature T.

Using results from the gauge-gravity duality [170] it was shown in Chapter 4 (Ref. [178]) quite generally that the viscosity component η_{xz} behaves like

$$\frac{\eta_{xz}}{s} = \frac{1}{4\pi} \frac{g_{xx}}{g_{zz}} \Big|_{u=u_h}, \tag{5.9}$$

where $g_{xx}|_{u=u_h}, g_{zz}|_{u=u_h}$ refer to the components of the background metric evaluated at the horizon which we denote by u_h. 's' refers to the entropy density which in the bulk picture corresponds to the area of the event horizon.

In the isotropic case the ratio $\frac{g_{xx}}{g_{zz}}\Big|_{u=u_h}$ is unity and we see that the KSS result is obtained. However, in anisotropic cases this ratio can become very different from unity and in fact much smaller, leading to the parametric violation of the KSS bound, where the relevant dimensionless parameter is the ratio of the strength of the anisotropic interaction and an appropriate microscopic energy scale of the system.

The general result Eq. 5.9, for the behavior of the spin 1 shear viscosity components $\eta_{xz} = \eta_{yz} \equiv \eta_\perp$ was studied in the example of Ref. [139] for two cases — one in the low anisotropy regime and the other in the high anisotropy regime. In this example, there are two scales of interest, ρ, which enters in the dilaton profile, Eq. 5.2 and determines the anisotropy, and the temperature T (while this theory does not have quasi-particles at finite T, one can roughly think of the mean free path as being of the order of $1/T$). Whether the anisotropy is large or small is determined by the ratio ρ/T which is dimensionless. Simple results can be obtained in the limit of low and high anisotropy which correspond to $\rho/T \ll 1$ and $\rho/T \gg 1$ respectively.

For the spin 1 component of the shear viscosity $\eta_{xz} = \eta_{yz} \equiv \eta_\perp$ the results are as follows:

1. Low anisotropy regime ($\rho/T \ll 1$):

$$\frac{\eta_\perp}{s} = \frac{1}{4\pi} - \frac{\rho^2 \log 2}{16\pi^3 T^2} + \frac{(6 - \pi^2 + 54(\log 2)^2)\rho^4}{2304\pi^5 T^4} + \mathcal{O}\left[\left(\frac{\rho}{T}\right)^6\right] . \tag{5.10}$$

We see that a small anisotropy at order $(\rho/T)^2$ already reduces this component of the viscosity and makes it smaller than the KSS bound. In the limit of zero anisotropy, we recover the KSS bound

$$\frac{\eta_\perp}{s} \to \frac{1}{4\pi}. \tag{5.11}$$

We also note that the driving force in the conservation equation for the stress tensor (Eq. 5.3) is proportional to $\nabla\phi \sim \rho$ (Eq. 5.2) and the analogue of the mean free path is T. Thus the corrections go like $\frac{(\nabla\phi)^2}{T^2}$.

2. High anisotropy regime ($\rho/T \gg 1$):

$$\frac{\eta_\perp}{s} = \frac{8\pi T^2}{3\rho^2}\ . \tag{5.12}$$

We see that in this limit the ratio can be made arbitrarily small, with $\frac{\eta_\perp}{s} \to 0$, as $T \to 0$ keeping ρ fixed. [1]

In contrast the η_{xyxy} component (which couples to a spin 2 metric perturbation) was found to be unchanged from its value in the isotropic case,

$$\frac{\eta_{xyxy}}{s} = \frac{1}{4\pi} \tag{5.13}$$

and thus continues to meet the KSS bound.

Motivated by the results in the gravity side, we may hope to find parametrically suppressed viscosities compared to the KSS bound in systems where the following basic requirements are met.

1. The system is strongly interacting and in the absence of anisotropy have a viscosity close to the KSS bound.

2. The equations of hydrodynamics for the system admits modes sensitive to the spin one viscosity components as described above and in Ref. [139, 178].

3. Sufficient anisotropy needs to be introduced in the system (say in the z direction with rotational symmetry preserved along the $x-y$ plane), such that these spin one components of the viscosity, when measured in units of the entropy density, show an experimentally measurable decreasing tendency from its lowest value observed so far in ultracold Fermi gases.

4. The force responsible for breaking of isotropy is approximately spatially constant.

5. The velocity gradients are small enough (compared to say the inverse mean free path) ensuring that hydrodynamics is the appropriate effective theory to describe the system.

[1] In this regime $\eta_\perp \sim \frac{T^4}{\rho}$ and $s \sim T^2\rho$, whereas for the isotropic case ($\rho = 0$) $\eta_\perp \sim T^3$ and $s \sim T^3$. Thus we see that for $T \ll \rho$, $\eta_\perp$ is smaller than its value in the isotropic case while s is bigger, resulting in the parametric violation in Eq. 5.12.

In the next section (Sec. 5.3) we explore a system of trapped ultra-cold Fermi gases, chosen so as to explore anisotropic fluid dynamics. While some of the details of this system are different from the systems with dual gravitational theories discussed above, it is possible to choose a set of parameters such that the system has the five features listed above. It can therefore be used to explore the behavior of the viscosity in the anisotropic regime.

While gravitational duals for the ultra-cold Fermi gases are not yet known and hence we can not calculate the anisotropic viscosity coefficients in this strongly coupled system, if the main feature that η_{xz} is smaller than the KSS bound holds true for these, one could potentially measure this phenomenon in experiments.

5.3 Anisotropic viscosity in trapped anisotropic Fermi gases

Trapped ultra-cold Fermi gas with their scattering length tuned to be near the unitarity limit [179, 184], are strongly interacting systems for which η/s [172, 173, 174], was measured to be close to the KSS bound $1/(4\pi)$. In this section we shall explore the properties of this system, when it is placed in an anisotropic trap. We identify suitable hydrodynamic modes which probe the viscosity component expected to be suppressed due to the potential in a highly anisotropic harmonic trap and find that for reasonable choices of parameters the five criterion referred to above, (see Sec.5.2), can be met in these modes. This leads us to suggest that an anisotropic shear viscosity can arise in such systems and appropriate components of the viscosity may show a reduction from the isotropic values in an experimentally accessible way.

One method [174] to measure the viscosity is by starting with an initial state where the fluid is trapped in an anisotropic harmonic trap. On removing the trapping potential, the fluid experiences elliptic flow and the extent of the flow is related to the initial anisotropy and the viscosity. The relevant bulk viscosity of the system vanishes [185, 186], which allows one to cleanly extract the shear viscosity. Note that even though the initial state of the fluid is anisotropic, the experiment does not probe anisotropic shear viscosities: after the trap potential is removed, the viscosity tensor at any point is isotropic.

An alternative technique is to measure the damping rate of breathing modes [172, 173] which is related to the loss of energy due to the viscosity. The experiments we propose in this chapter use this alternative technique and propose to measure the relevant component of the shear viscosity by measuring the damping of appropriate hydrodynamic modes.

The unitary Fermi gas system we consider here shares important features with the gravitational system described in Sec. 5.2. The role of a linear potential was emphasized in Sec. 5.2. While such a linear potential cannot arise in the trapped fermion system we consider, we shall see below that if we choose the velocity profile and the trap parameters carefully, the dominant contribution to shear viscosity comes from a region of the trap where the confining force is approximately constant: satisfying the fourth criterion listed in Sec. 5.2.

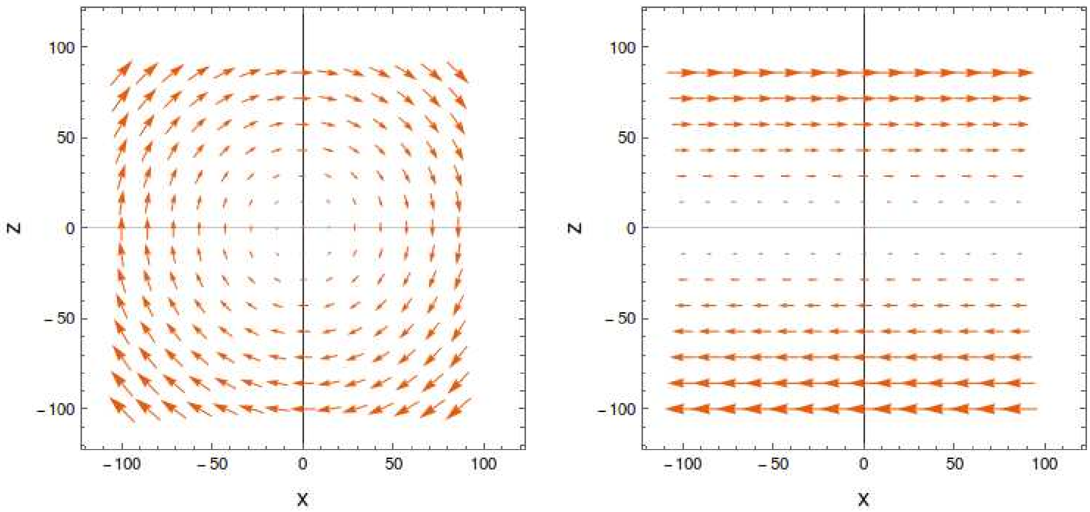

Figure 5.2: (Arbitrary units for coordinates) The flow profile in the $x - z$ plane for the Elliptic mode, ie. $\mathbf{v} = z\ \hat{x} - x\ \hat{z}$ (left panel, corresponding to $\omega_x/\omega_z = 1$ in Eq. 5.16) and $\mathbf{v} = z\ \hat{x} - 0.001\ x\ \hat{z}$ (right panel, corresponding to $\omega_x/\omega_z = 0.03$ in Eq. 5.16).

The system we consider consists of an ultra-cold Fermi gas under harmonic confinement described by the potential

$$\phi(\mathbf{r}) = \sum_i \frac{1}{2} m\omega_i^2 x_i^2 \tag{5.14}$$

where i runs over x, y, z and m denotes the mass of the fermionic species. The trap is anisotropic if ω_i's are unequal. For example, $\omega_z \gg \omega_x, \omega_y$ gives rise to a pancake like trap: thin in the z direction. This can lead to an anisotropic shear viscosity tensor as described in Sec. 5.4. The potential gradient in the x and y directions is small in most of the trap.

This section is organized as follows. After a general discussion we describe the two modes of interest (referred to as the Elliptic mode and the Scissor mode) in subsection 5.3.1. The equations of superfluid hydrodynamics are described next in subsection 5.3.2, following which, in subsection 5.3.3 and 5.3.4 respectively we show that the Scissor mode and the Elliptic mode satisfy these equations. The fluid flow profile in the Elliptic mode is similar to that considered in Chapter 4: a velocity in the x direction with a gradient in the z direction. The scissor mode is well known in the literature. In subsection 5.3.5 we show that the dissipation of energy in the two modes of interest is determined by the relevant components of the viscosity tensor (the spin 1 components described in the previous section). In Subsection 5.3.6 we find a constraint on the magnitude of the velocity for the two modes by demanding the validity of fluid mechanics. The thermodynamics of the system is discussed in subsection 5.3.8. Finally in subsection 5.3.9 we bring this understanding together and show that for reasonable values of parameters the required criterion listed in Sec. 5.2 can indeed be met.

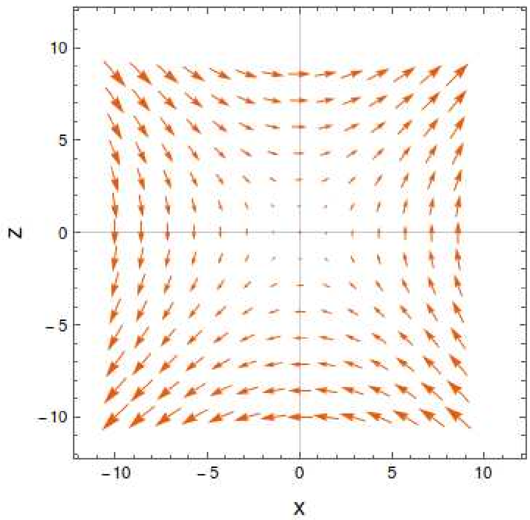

Figure 5.3: (Arbitrary units for coordinates) The flow profile in the $x - z$ plane at time $t = 0$ for the Scissor mode, ie. $v = z\ \hat{x} + x\ \hat{z}$ (Eq. 5.17)

5.3.1 Choice of Velocity Profile

Here we first describe the two modes of interest which arise as solutions to the equations of ideal superfluid hydrodynamics. Each of these modes is characterized by the superfluid and the normal components, which we denote by $\mathbf{v}_s$ and $\mathbf{v}_n$ respectively.
The first mode, which we call the Elliptic mode has $\mathbf{v}_s = 0$ and $\mathbf{v}_n = \mathbf{v}$ given by

$$\mathbf{v} \ = e^{i\omega t}(\alpha_x z\ \hat{x} + \alpha_z x\ \hat{z}) \tag{5.15}$$

with the following relations:

$$\textbf{Elliptic mode}: \ \ \omega = 0,\ \ \alpha_z = -\frac{\omega_x^2}{\omega_z^2}\alpha_x \tag{5.16}$$

The other mode of interest, denoted by the Scissor mode, has $\mathbf{v}_s = \mathbf{v}_n = \mathbf{v}$ given by Eq. 5.15 with

$$\textbf{Scissor mode}: \ \ \omega = \sqrt{\omega_x^2 + \omega_z^2},\ \ \alpha_z = \alpha_x. \tag{5.17}$$

From the right panel in Fig. 5.2 we see that in the high anisotropy limit $\omega_z \gg \omega_x$, $\alpha_z \to 0$ for the Elliptic mode, and hence we recover a flow profile similar to that considered in Chapter 4; namely a time independent (in the limit of small viscosity) velocity ($\mathbf{v} \propto z\hat{x}$) linearly increasing with the coordinate in the direction of the gradient of the external potential (z), pointing ($\hat{x}$) in the direction perpendicular to the gradient of the external potential (neglecting ω_x, ω_y. The gradient is in the $\hat{z}$ direction). To the best of our knowledge, the Elliptic mode has not been studied in ultra-cold gas experiments. The scissors mode which has been studied extensively (for example see Refs. [180, 181, 182]).

In what follows, we will first show that the Elliptic mode and the Scissor mode satisfy the equations of superfluid hydrodynamics in the presence of a harmonic trap. There are viscous corrections to the hydrodynamic equations, but we work in a limit where viscous corrections are small and therefore the solutions to the ideal hydrodynamics can be used to calculate the energy loss rate due to viscosity in a perturbative manner.

5.3.2 Equations of superfluid hydrodynamics

Neglecting viscosity, the superfluid equations are given by the conservation laws of entropy, mass (particle number), momentum and an additional equation for the superfluid velocity. In the presence of the external potential $\phi(\mathbf{r})$ they are listed below :

$$\frac{\partial(\rho s)}{\partial t} + \nabla \cdot (\rho s \mathbf{v}_n) = 0, \tag{5.18}$$

$$\frac{\partial \rho}{\partial t} + \nabla \cdot \mathbf{g} = 0\,, \tag{5.19}$$

$$\frac{\partial g_i}{\partial t} + \nabla_j \Pi_{ij} = -n\nabla\phi(\mathbf{r}), \tag{5.20}$$

$$\frac{\partial \mathbf{v}_s}{\partial t} = -\nabla\Big(\frac{\mathbf{v}_s^2}{2} + \frac{\phi(\mathbf{r})}{m} + \frac{\mu(\mathbf{r})}{m}\Big)\,. \tag{5.21}$$

Here ρ is the total mass density (where ρ_n and ρ_s are the normal and superfluid mass density of the system and the total mass density $\rho = \rho_n + \rho_s$). We have not written out the dependence of the velocity on position and time. $\mu(\mathbf{r})$ can be thought of as the local chemical potential. n (not in the subscript) denotes the total number density (which is related to the total mass density ρ via the relation $\rho = mn$), $\mathbf{g}$ is the momentum density, and Π_{ij} is the stress tensor, given as follows

$$\begin{aligned} \mathbf{g} &= \rho_n \mathbf{v}_n + \rho_s \mathbf{v}_s\,, \\ \Pi_{ij} &= P\delta_{ij} + \rho_n \mathbf{v}_{n,i}\mathbf{v}_{n,j} + \rho_s \mathbf{v}_{s,i}\mathbf{v}_{s,j}\,. \end{aligned} \tag{5.22}$$

Let us note that the equation for energy conservation can be derived from the set of equations above, and is not an additional independent constraint.

Altogether there are 8 equations above and they can be solved for the 8 independent variables - 6 components of $(\mathbf{v_s},\ \mathbf{v_n})$ and $T,\ \mu(\mathbf{r})$. We can then express all thermodynamic variables as functions of $(T,\ \mu(\mathbf{r}))$ like $P(T,\ \mu(\mathbf{r}))$, $s(T,\ \mu(\mathbf{r}))$ etc. In the trap geometries we consider, the center of the trap is superfluid and the outer trap is in the normal phase. The equations for a normal fluid can be obtained by simply substituting $\rho_s = 0$ and ignoring Eq. 5.21.

Let us first look at the equilibrium situation $\mathbf{v_n} = \mathbf{v_s} = \mathbf{0}$ in the absence of external potential ϕ. Eqns. 5.18, 5.19, 5.20, 5.21 are satisfied with $\mu(\mathbf{r})$ and P spatially constant.

Before we consider the effects of an external potential let us also note that the pressure and number density in the absence of the trap, which we denote as $P_{\phi=0}, n_{\phi=0}$ respectively, satisfy the Gibbs-Duhem relation

$$\frac{\partial P_{\phi=0}}{\partial \mu} = n_{\phi=0}. \tag{5.23}$$

In the presence of the external potential $\phi(\mathbf{r})$ with $\mathbf{v}_s = \mathbf{v}_n = 0$, only Eq. 5.20 and Eq. 5.21 changes. Eq. 5.21 is satisfied by taking

$$\mu(\mathbf{r}) = \mu - \phi(\mathbf{r}), \tag{5.24}$$

where μ is a global constant that determines the total number of particles in the system. Eq. 5.20 in the presence of $\phi(\mathbf{r})$ becomes

$$\partial_i P(\mathbf{r}) = -n\ \partial_i \phi(\mathbf{r}). \tag{5.25}$$

This is consistent with the replacement $\mu(\mathbf{r}) \to \mu - \phi(\mathbf{r})$ if we take the pressure P at a point $\mathbf{r}$ in the presence of the trap to be equal to $P_{\phi=0}(T, \mu - \phi(\mathbf{r}))$ and the number density to be $n_{\phi=0}(T, \mu - \phi(\mathbf{r}))$. This follows from Eq. (5.23), since $\partial_i P = -\frac{\partial P_{\phi=0}}{\partial \mu} \partial_i \phi = -n_{\phi=0}\ \partial_i \phi$. This is also known as LDA (Local Density Approximation). Generally LDA corresponds to the conditions,

$$f(\mu(\mathbf{r}),\ T) := f_{\phi=0}\ \ (\mu - \phi(\mathbf{r}),\ T) \tag{5.26}$$

where f is P, n, ρ or s. In all the subsequent discussions, a subscript 0 indicates that the conditions for LDA are valid in equilibrium. Note that in equilibrium T is a constant.

5.3.3 Scissor mode solution to linear order

First we look for solutions of the form

$$\mathbf{v}_n = \mathbf{v}_s = \mathbf{v} \tag{5.27}$$

and $\nabla \times \mathbf{v} = \mathbf{0}$. We restrict ourselves to small velocities and linearize the above equations. For the scissor mode we see from Eq. 5.15 and Eq. 5.17 that $\mathbf{v}$ is given by

$$\mathbf{v} = \alpha\ e^{i\omega t}(z\hat{x} + x\hat{z}) \tag{5.28}$$

where $\alpha = \alpha_x = \alpha_z$ is a constant. We will solve the equations to linear order in α.

Let us first explore Eq. 5.21. Out of equilibrium ($\mathbf{v} \neq 0$), $\mu(\mathbf{r})$ has an extra correction associated with $\mathbf{v}$,

$$\mu(\mathbf{r}) = \mu - \phi(\mathbf{r}) + \epsilon(\mathbf{r}, t)\ . \tag{5.29}$$

Eq. 5.21 then gives

$$\epsilon = -\alpha mxz\ i\omega\ e^{i\omega t}. \tag{5.30}$$

Once we are out of equilibrium, we will see that the remaining equations are self consistently solved by letting

$$f_{\phi\neq 0}(\mu(\mathbf{r}),\ T) := f_{\phi=0}\ \ (\mu - \phi(\mathbf{r}) + \epsilon(\mathbf{r},t),\ T) \tag{5.31}$$

where f is P, n, ρ or s.

The mass and momentum conservation equations, with the condition Eq. (5.27), give

$$\frac{\partial \rho}{\partial t} + \nabla\cdot(\rho\mathbf{v}) = 0\,, \tag{5.32}$$

$$\rho\frac{\partial \mathbf{v}}{\partial t} + \rho(\mathbf{v}.\nabla)\mathbf{v} = -\nabla P - n\nabla\phi \tag{5.33}$$

where $\phi(\mathbf{r})$ is the external potential and ρ is the total mass density $(\rho_n+\rho_s)$. Linearizing these equations to order α [2] using Eq. 5.31 we get,

$$\frac{\partial \rho_0}{\partial \mu}\frac{\partial \epsilon}{\partial t} + \nabla\cdot(\rho_0\mathbf{v}) = 0\,, \tag{5.34}$$

$$\rho_0\frac{\partial \mathbf{v}}{\partial t} = -\nabla(\frac{\partial P_0}{\partial \mu}\epsilon) - (\frac{\partial n_0}{\partial \mu}\epsilon)\nabla\phi\,. \tag{5.35}$$

Using $\partial_i\rho_0 = -\frac{\partial\rho_0}{\partial\mu}\partial_i\phi$ and using the fact that for the modes we consider in this chapter $\nabla.\mathbf{v} = 0$ we get from Eq. 5.34

$$\frac{\partial \epsilon}{\partial t} - \partial_i\phi\ \mathbf{v}_i = 0\,. \tag{5.36}$$

Plugging in the harmonic potential and the solution Eq. 5.30, we find that the above equation is solved by the Scissor mode which satisfies the condition, Eq. 5.17. Now taking time derivative of the Euler equation Eq. 5.35 and using Eq. 5.34 in the second term on R.H.S of Eq. 5.35 and $\frac{\partial P_0}{\partial \mu} = n_0$ (total number density at equilibrium),

$$\begin{aligned}
&\rho_0\frac{\partial^2 \mathbf{v}_i}{\partial t^2} = -\partial_i(n_0\frac{\partial \epsilon}{\partial t}) + \partial_j(n_0\mathbf{v}_j)\partial_i\phi \\
&\Rightarrow \rho_0\frac{\partial^2 \mathbf{v}_i}{\partial t^2} + n_0\partial_i(\frac{\partial \epsilon}{\partial t}) = -\partial_i n_0(\frac{\partial \epsilon}{\partial t}) + \partial_j n_0\mathbf{v}_j\partial_i\phi \\
&\Rightarrow \rho_0\frac{\partial^2 \mathbf{v}_i}{\partial t^2} + n_0\partial_i(\frac{\partial \epsilon}{\partial t}) = \frac{\partial n_0}{\partial \mu}\partial_i\phi(\frac{\partial \epsilon}{\partial t}) - \frac{\partial n_0}{\partial \mu}\ \partial_j\phi\ \mathbf{v}_j\ \partial_i\phi\,.
\end{aligned} \tag{5.37}$$

We see from Eq. 5.36 that the RHS of the above equation vanishes. For the scissor mode, it follows from Eq. 5.17 and Eq. 5.30 that the LHS also vanishes, and thus the equation is met.

[2] Note that ϵ in Eq. 5.30 is of order α

For the time dependent scissor mode, the mass conservation equation is

$$\frac{\partial \rho}{\partial t} + \nabla \cdot (\rho \mathbf{v}) = 0 \tag{5.38}$$

for $\mathbf{v}_s = \mathbf{v}_n = \mathbf{v}$.

Starting with Eq. 5.18 and using Eq. 5.38 we get

$$\frac{\partial s}{\partial t} + \mathbf{v} \cdot \boldsymbol{\nabla} s = 0\,. \tag{5.39}$$

Assuming that the entropy is of the form $s(\mu - \phi(\mathbf{r}) + \epsilon(\mathbf{r}, t))$ as given in Eq. 5.31 and linearizing in α we get

$$\frac{\partial s_0}{\partial \mu}\frac{\partial \epsilon}{\partial t} - \frac{\partial s_0}{\partial \mu}\partial_i \phi \; \mathbf{v}_i = 0\,. \tag{5.40}$$

This equation is valid when Eq. 5.36 is met. Hence we find that the ansatz Eq. 5.31 with Eq. 5.30 meets all the equations self consistently.

5.3.4 Elliptic mode solution to linear order

Next we verify that the Elliptic mode, Eq.5.16, solves the superfluid equations to linear order in the velocity. Note that this mode is a stationary solution ($\omega = 0$). Like in the previous case we take T to be a constant in this mode. Note that in this solution $\mathbf{v}_n$ has a non-zero curl, $\nabla \times \mathbf{v}_n \neq 0$, and therefore in the absence of vortices $\mathbf{v}_s \neq \mathbf{v}_n$. We will denote $\mathbf{v}_n = \mathbf{v}$ below.

We start with Eq. 5.21. Since $\mathbf{v}_s = 0$ in this mode, we see that this equation is met if

$$\mu(r) = \mu - \phi(r) \tag{5.41}$$

where μ on the RHS is an $\mathbf{r}$ independent constant.

Next, with $\mathbf{v}_s = 0$ the mass and momentum conservation equations simplify to

$$\frac{\partial \rho}{\partial t} + \boldsymbol{\nabla} \cdot (\rho_n \mathbf{v}) = 0\,, \tag{5.42}$$

$$\frac{\partial (\rho_n \mathbf{v_i})}{\partial t} + \boldsymbol{\nabla}_j (\rho_n \mathbf{v_i} \mathbf{v_j}) = -\,\boldsymbol{\nabla}_i P - n \nabla_i \phi\,. \tag{5.43}$$

The time derivatives in these equations can be dropped. The Euler equation, Eq. 5.43, is met to order $\mathbf{v}$ if P and n take their form in the LDA approximation, Eq. 5.26. We will also assume that the other thermodynamic values, ρ_n, s take this LDA form and denote them with a subscript 0. Using the fact that $\nabla \cdot \mathbf{v} = 0$, the other equation, Eq. 5.42, becomes,

$$\boldsymbol{\nabla} \cdot (\rho_{0n} \mathbf{v}) = 0 \Rightarrow -\frac{\partial \rho_{0n}}{\partial \mu} \; \partial_i \phi \; \mathbf{v}_i = 0 \tag{5.44}$$

where we have used the ansatz Eq. 5.26 for the mass density of the normal component. For our mode $\alpha_x z\ \hat{x} + \alpha_z x\ \hat{z}$ with $\alpha_z = -\frac{\omega_x^2}{\omega_z^2}\alpha_x$ (see Eq. 5.16) one can easily check that

$$\partial_i \phi\ \mathbf{v}_i = 0, \tag{5.45}$$

so that this equation is satisfied.
Finally, the entropy conservation equation (after replacing ρ, s by their LDA values) becomes

$$\boldsymbol{\nabla} \cdot (\rho_0 s_0 \mathbf{v}) = 0. \tag{5.46}$$

Using the fact that our mode is free of divergence, and $\rho_0 s_0$ is a function of $\mu - \phi(\mathbf{r})$, we see that this equation is also met when Eq. 5.45 is satisfied.

It is interesting to note that the fact that the Elliptic mode and the Scissor mode also solve the equations of one component fluid mechanics in the normal phase. Since the temperature is a constant in these modes, and the chemical potential varies as given in Eq. 5.24, up to possible corrections of order ϵ, Eq. 5.29, as one moves from the center of the trap to its edges the ratio $\mu(r)/T$ becomes smaller and the system will transit from the superfluid to normal phase. The solutions we have found above, for both modes, will continue to hold in such situations as well.

5.3.5 Energy dissipation due to viscosity

The energy dissipated due to viscosity is given by

$$\dot{E}_{\text{kinetic}} = -\frac{1}{2}\int d^3\mathbf{r}\, \eta_{ijij}(\mathbf{r}) \left(\partial_i v_j + \partial_j v_i - \frac{2}{3}\delta_{ij}\partial_k v_k\right)^2 - \int d^3\mathbf{r}\, \zeta(\mathbf{r}) \left(\partial_i v_i\right)^2 \tag{5.47}$$

where $\eta_{ijij} \equiv \eta_{ij}$ is the relevant component of the shear viscosity and ζ is the bulk viscosity. We note that for our chosen velocity profiles, the bulk viscosity contribution vanishes. Also in the traps we will consider, the temperature T is constant throughout the trap. Hence we also ignored contributions from thermal conductivity.

Thus,

$$\dot{E}_{\text{kinetic}} = -\int d^3\mathbf{r}\, \eta_{xz}(\mathbf{r})\ \alpha_x^2 (1 - \frac{\omega_x^2}{\omega_z^2})^2 \tag{5.48}$$

is the energy dissipation rate for the Elliptic mode, where we have simply written η_{xzxz} as η_{xz}.

The energy dissipated per unit cycle for the oscillatory time dependent scissor mode is

$$\dot{E}_{\text{kinetic}} = -2\int d^3\mathbf{r}\, \eta_{xz}(\mathbf{r})\ \alpha_x^2. \tag{5.49}$$

5.3.6 Validity of hydrodynamics

One expects that hydrodynamics is a valid description of the system as long as the viscous correction to the stress tensor is small compared to its value in an ideal fluid (for eg. see Ref. [183] or Sec. 10.3.4 in Ref. [187]).

For the Elliptic mode the contribution to the stress energy tensor from viscosity is

$$\eta_{xz}\frac{1}{2}(\alpha_x + \alpha_z) \approx \eta_{xz}\frac{1}{2}(\alpha_x) \tag{5.50}$$

where we have assumed $\omega_z \gg \omega_{x,\,y}$ and neglected the contribution from α_z (see Eq. 5.16).

For the Scissor mode the magnitude of the contribution to the stress energy tensor from viscosity is

$$\eta_{xz}\frac{1}{2}(\alpha_x + \alpha_z) = \eta_{xz}(\alpha_x) \tag{5.51}$$

where we have $\alpha_z = \alpha_x$ for the Scissor mode.

At any point $\mathbf{r}$, hydrodynamics is expected to be valid if the viscosity contribution is smaller than the pressure $P(\mathbf{r})$,

$$\alpha_x \eta_{xz}(\mathbf{r}) \ll P(\mathbf{r}) \quad . \tag{5.52}$$

In the outer edges of the trap the pressure becomes small while η tends to a constant [188, 189, 190] and Eq. 5.52 is necessarily violated regardless of how small α_x is chosen. The contribution of this region to the total energy loss is typically small however. (Note that the expression Eq. 5.47 can not be used to evaluate the energy loss if Eq. 5.52 is not satisfied [190].) What we desire is that hydrodynamics should be a good theory in the region where the energy loss is substantial. When we consider specific numerical values for the parameters of the trap in Subsection 5.3.9, we will identify a point $\mathbf{r_{max}}$ close to the edge of the trap, such that the integral Eq. 5.47 receives most of its contribution for $r < \mathbf{r_{max}}$.

We can then define $\alpha_x^{\max}$ by the condition that for this amplitude the viscosity contribution to the stress energy tensor is equal to the pressure at the point $\mathbf{r}_{\max}$

$$\alpha_x^{\max} = \frac{P(\mathbf{r}_{\max})}{\eta_{xz}(\mathbf{r}_{\max})}. \tag{5.53}$$

For $\alpha_x < \alpha_x^{\max}$ hydrodynamics is valid in the region of interest. This constraint limits how large α_x and consequently $\dot{E}_{\text{kinetic}}$ can be. As long as this dominates over other processes of energy loss (interaction with the environment) this damping can be measured. In Table. 5.3 in Sec. 5.3.9 we show this numerical limit for the traps described in that Section.

5.3.7 The outer core

It has been noted that a naive application of hydrodynamics at the outer region of the trap where the density of the atoms is very low leads to an unphysical result. Since the shear viscosity in the ultra-dilute regime has the form $\eta \sim (mkT)^{3/2}$, (m is the mass, k is the Boltzmann's constant and T is the temperature) the contribution from the tail (or the outer cloud) is independent of the density, and hence is divergent [[190, 191, 192, 193, 194, 195]]. The unphysical result arises because in the outer part of the trap collisions are rare and hydrodynamics breaks down. In fact the better approximation in this region is assuming that atom dynamics in this ultra-dilute region is collisionless and hence does not contribute significantly to damping.

Here we use a simple procedure to take this physics into account. We only consider traps where the chemical potential at the center is positive and cutoff the damping contribution from the outer cloud by integrating the viscosity contribution only from the center of the trap up to $\mathbf{r}_{\max}$ which is defined as the surface where $\mu - V(\mathbf{r}_{\max}) = T$. Similar prescriptions have been followed previously by [173, 174] (see [195] for an overview).

One can also perform a more careful estimate of the contribution from the outer cloud. To be concrete, let us consider the scissor mode. We follow the procedure described in Ref. [192] which solves the Boltzmann equation in the dilute regime, rather than assuming that hydrodynamics is accurate in this region. Their important result is that for the scissor mode [3] the energy loss rate in the dilute regime can be written as the integral over η divided by a suppression factor that increases exponentially as a function of the trapping potential. More precisely,

$$\langle \dot{E}_{\text{kinetic}} \rangle| = -2\alpha^2 \int_{\mathbf{r}>\mathbf{r}_{\max}} d^3\mathbf{r} \frac{\eta}{1+\omega^2\tau_\eta^2(\mathbf{r})}, \tag{5.54}$$

where in the dilute regime (or the "classical limit")

$$\tau_\eta(\mathbf{r}) = \frac{4.17}{N\bar{\omega}} \left(\frac{kT}{\hbar\bar{\omega}}\right)^2 e^{V(\mathbf{r})/kT} , \tag{5.55}$$

and the viscosity η is given by

$$\eta = \frac{15}{32\sqrt{\pi}} \frac{(mkT)^{3/2}}{\hbar^2} . \tag{5.56}$$

The scissor mode frequency is given by,

$$\omega = \sqrt{\omega_x^2 + \omega_z^2} , \tag{5.57}$$

and the geometric mean $\bar{\omega} = (\omega_x \omega_y \omega_z)^{\frac{1}{3}}$.

[3] Let us also note that the scissor mode is excited in the $x - y$ plane in Ref. [192]. We have taken care of this fact in our calculations and comparisons.

T	$\Gamma\ (s^{-1})$	$\Gamma\ (s^{-1})$
$4T_c/5$	23.03	0.0044
$2T_c/3$	18.32	0.00009
$4T_c/7$	14.6	2.14×10^{-6}
$T_c/2$	11.86	4.69×10^{-8}

Table 5.1: Comparison of contributions to the damping rates for the scissor mode from the core [Γ(c) Eq. 5.64], and the outer core [Γ(oc) Eq. 5.63] for the trap parameters we will explore in our chapter.

The integral Eq. 5.54 is convergent because of the exponential increase in the relaxation time $\tau_\eta(\mathbf{r})$ even if we take the upper limit of the integral to ∞ but for the numerical evaluation we take the upper limit of the x-integration to be $x_{\max} + L$, for the y-integration to be $y_{\max} + L$, and z-integration to be $z_{\max} + L$ with $L \gg |\mathbf{r}_{\max}|$.

At the core of the trap hydrodynamics is a good approximation (unless $T \ll T_c$ where the superfluid phonons can move out of equilibrium). This is a crucial point because Boltzmann transport is not a valid approximation at the core where the density of atoms is high. As we explained in the last section, as long as $\alpha_x = \alpha_z = \alpha < \alpha_x^{\max}$, hydrodynamics is a good approximation and the local contribution from the viscosity to the stress energy tensor

$$\alpha\ \eta(\mathbf{r}) \tag{5.58}$$

is smaller than the pressure

$$P(\mathbf{r}) \tag{5.59}$$

for $\mathbf{r} < \mathbf{r}_{\max}$. Therefore, using hydrodynamics to evaluate the damping contribution from the core, we get

$$\langle \dot{E}_{\text{kinetic}} \rangle| = -2\alpha^2 \int_{\mathbf{r}<\mathbf{r}_{\max}} d^3\mathbf{r}\ \eta(\mathbf{r})\ , \tag{5.60}$$

where the local value of $\eta(\mathbf{r})$ is calculated using the data for η from [174]. The integration is performed over $x < x_{\max}$, $y < y_{\max}$ and $z < z_{\max}$. This approximates the actual ellipsoidal region with a rectangular shape, but we see that this will not change the results substantially since the contribution from the outer cloud is small.

The amplitude decay rate is given by

$$\Gamma = \frac{|\langle \dot{E}_{\text{kinetic}} \rangle|}{2\langle E \rangle} \tag{5.61}$$

$\langle E \rangle$ is the total mechanical energy averaged over a cycle,

$$\begin{aligned}\langle E \rangle &= \frac{1}{2}\int d^3 r m n(\mathbf{r})|v|^2(\mathbf{r}) \\ &= \frac{1}{2} m\alpha^2 \int d^3 r m n(\mathbf{r})(z^2 + x^2) \;,\end{aligned} \tag{5.62}$$

where $v = \alpha e^{i\sqrt{\omega_x^2+\omega_z^2}t}(z\hat{x} + x\hat{z})$. In Eq. 5.64, α^2 cancels out and we only need $n(\mathbf{r})$ which is obtained from experiments as explained in detail in Sec.5.3.8.

The damping rate contribution from the outer cloud is given by

$$\Gamma = \frac{|\langle \dot{E}_{\text{kinetic}} \rangle|}{2\langle E \rangle} \tag{5.63}$$

and the contribution from the core is given by

$$\Gamma = \frac{|\langle \dot{E}_{\text{kinetic}} \rangle|}{2\langle E \rangle} \;, \tag{5.64}$$

and the total damping rate Eq. 5.61 is the sum of the two.

In Table. 5.1, for the representative trap parameters which we will be considering later ($\omega_z = 2\pi \times 10^4$ rads/s, $\omega_x = \omega_y = 2\pi \times 385$ rads/s and $\mu = 10\mu$K and T/T_c values as given in the table), we present the comparison of the contribution to damping from the outer cloud and the core in Table. 5.1. We see that the damping contribution from the outer cloud is small, especially for the low temperatures, justifying our approach. A direct comparison using our technique (where we cut off the integral for $\dot{E}_{\text{kinetic}}$ at the point of the trap where hydrodynamics breaks down) can only be made for the lowest temperature ($T/T_F = 0.1$) of Ref. [182]. Our calculations (using the trap parameters of [182])give a damping rate of 250 s^{-1} which agrees with experiments (255 $\pm$ 40 s^{-1}, [182]). This is a non-trivial check of our methodology and gives us confidence in our approach in this regime.

5.3.8 Thermodynamics

The evaluation of the energy loss from Eq. 5.48 and Eq. 5.49 requires the viscosity η as a function of the position $\mathbf{r}$ in the trap. In the highly anisotropic traps we are considering the viscosity is actually a tensor and the different components of the shear viscosity can acquire different values, in contrast with the isotropic case. For the modes of interest, Eq. 5.15 we need to determine the behavior of the component (η_{xz}).

To get a first estimate of the region of the trap which gives a dominant contribution to the integral in Eq. 5.47, we use the local density approximation (LDA) and estimate the resulting viscosity. More specifically, we assume in this approximation that thermodynamic variables like the number density n, the entropy density s depend only on the local value of T

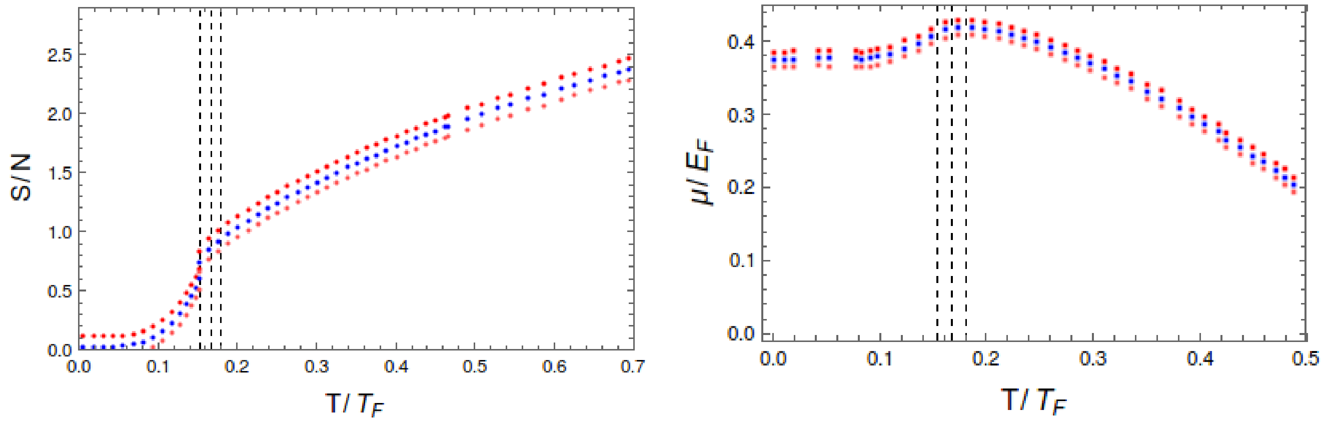

Figure 5.4: (Color online) Data of $\frac{S}{N}$ as a function of T/T_F (left panel) and μ/E_F versus T/T_F (right panel) from Ref. [196]. The central curves (blue online) correspond to the central values and the band gives an error estimate (Ref. [196]). The band denoted by the dashed vertical lines corresponds to the phase transition between the normal and the superfluid phase. The error bands represent the maximum error chosen from a set of representative error bars given in Ref. [196].

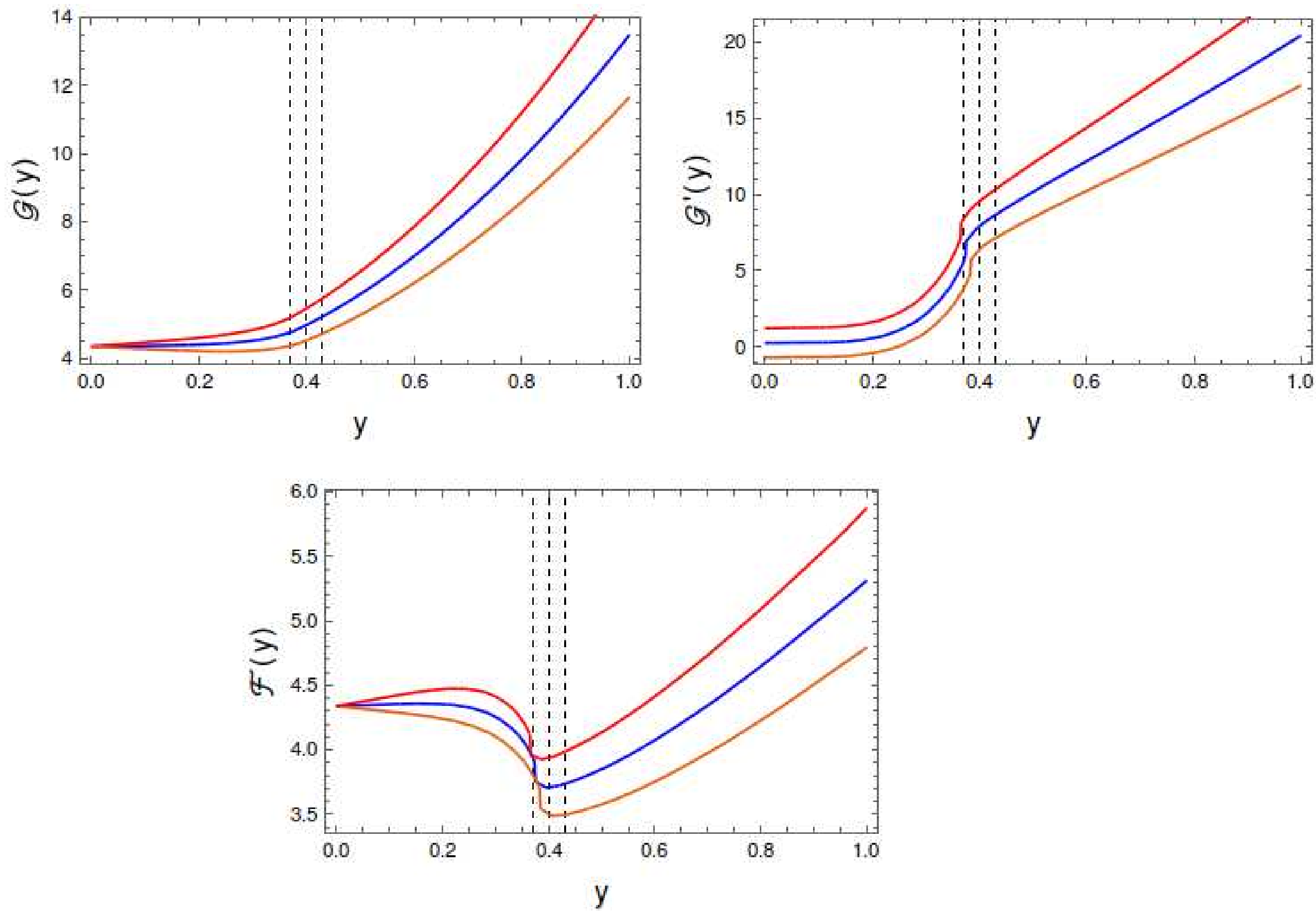

Figure 5.5: (Color online) The thermodynamic function $\mathcal{G}$ (top left panel) and its derivative (top right panel) as a function of $\frac{T}{\mu}$. The lower panel shows $\mathcal{F}$. These dimensionless functions are defined in Eq. 5.65. The error bands follow from the error bands in Fig. 5.4.

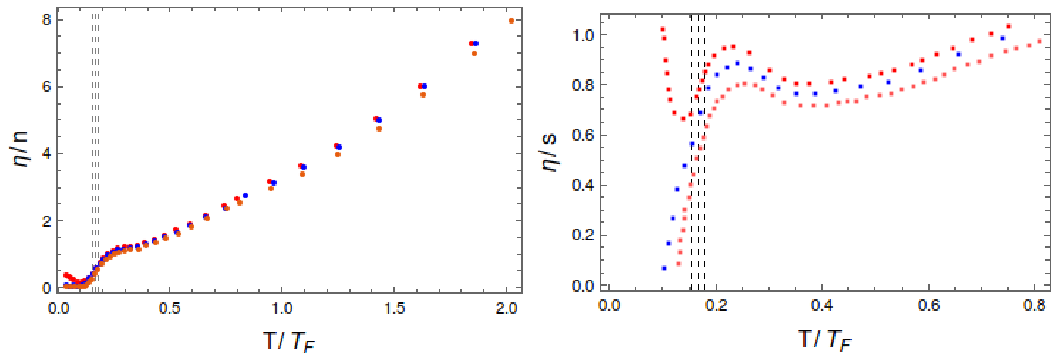

Figure 5.6: (Color online) The left panel shows $\frac{\eta}{n}$ versus T/T_F from Figs. 2 and 3 of [174]. The right panel shows $\frac{\eta}{s}$ versus T/T_F from Fig. 5 of [174].

and μ. The viscosity is also then taken to be given by these local values of T, μ, neglecting any effects of anisotropy which could make the different components of the tensor take different values.

The effect of anisotropy on the viscosity tensor are estimated using Eq. 5.102, in a following section (Sec. 5.4). While we cannot reliably compute them, the key point of our analysis here is that they may be experimentally measured and could lie below the KSS bound.

To apply the LDA approximation mentioned above, we start first by considering a homogeneous system characterized by temperature T, μ and review the behavior of the thermodynamical parameters and the viscosity as a function of these parameters. This is covered in this subsection. In the presence of the trap μ varies in the equilibrium configuration. The effects of the trap, in this approximation, are then incorporated by using the resulting local value for μ and T in the behavior for the homogeneous case. The next subsection will then incorporate the effects of the trap.

In certain thermodynamic regimes, the viscosity of a uniform unitary Fermi gas can be computed in a controlled manner. At temperatures much smaller than the chemical potential, transport is dominated by the Goldstone mode associated with superfluidity and the viscosity can be computed by solving the Boltzmann transport equations [197]. At temperatures large compared to the chemical potential, the density of fermions is small and a kinetic estimate of the viscosity, $\eta = \text{const.} \times (mT)^{3/2}$, is adequate [188, 189, 190]. But we shall see that the largest contribution to damping arises from the regime where T and μ are comparable, and a theoretical evaluation of the viscosity is difficult. Monte Carlo [167, 168] methods, microscopic approaches [198], and $T-$matrix techniques [199] have been used to calculate the viscosity in this regime but presently the best estimate for the viscosity in this intermediate regime comes from experiments.

In Refs. [172, 173], η/s was measured for the first time. Recently, this measurement was refined in Ref. [174] and the result for the dimensionless ratio η/n was measured for a wide range of T/μ, which we show in Fig. 5.6. Therefore, to obtain the LDA value of the viscosity, we just need $n(\mu, T)$.

In the next few paragraphs we describe how to obtain $n(\mu, T)$ using the scaling properties of the unitary Fermi gas. With that understanding at hand we will then return to a discussion of how to obtain the viscosity in the approximation described above. In the unitary Fermi gas, the chemical potential μ and the temperature T are the only energy scales in the problem. Therefore, we can express various thermodynamic quantities as a function of the dimensionless quantity $y = T/\mu$ multiplied by an appropriate dimensionful function of only one of the two variables. Following [172] we write,

$$\begin{aligned} n(\mu,\ T) &= n_f(\mu)\mathcal{F}(y), \\ s(\mu,\ T) &= \frac{2}{5} n_f(\mu)\mathcal{G}'(y)\ , \end{aligned} \tag{5.65}$$

where n is the number density, s is the entropy density, and $\mathcal{F}(y) = \mathcal{G}(y) - 2\ y\ \mathcal{G}'(y)/5$, $n_f(\mu) = \frac{1}{3\pi^2}(2m\mu)^{\frac{3}{2}}$ is the number density of a free Fermi gas. Therefore one can compute the desired thermodynamic quantities if the function $\mathcal{G}(y)$ is known. For example, one can write the pressure as

$$P(\mu,\ T) = \frac{2}{5}\mu\ n_f(\mu)\ \mathcal{G}(y). \tag{5.66}$$

In the following discussion, we use the usual definitions

$$k_F = (3\pi^2 n)^{1/3},\ E_F = \frac{k_F^2}{2m},\ T_F = E_F/k_B,\ v_F = \frac{k_F}{m}\ . \tag{5.67}$$

At low temperatures ($\frac{T}{T_F} \lesssim 0.6$) we use the $\frac{S}{N}$ data from Fig. 3(b) of Ref. [196] to obtain $\mathcal{G}(y)$. Data from two graphs obtained from Ref. [196] are shown here in the two panels of Fig. 5.4 for convenience. The left panel shows $S/N = s/n$ as a function of T/T_F and the right panel shows μ/E_F as a function of T/T_F.

In order to solve Eq. 5.65 we need to get $\frac{S}{N}$ as a function of y. We use Fig. 3(a) of Ref. [196] to convert the $\frac{S}{N}$ data in terms of $y = \frac{T}{\mu}$ rather than $\frac{T}{T_F}$. We obtain the function $\mathcal{G}(y)$ by numerically solving Eq. 5.65, subject to the boundary condition $\mathcal{G}(0) = 1/\xi^{3/2}$ at $T = 0$. We use $\xi = 0.376 \pm 0.0075$. (The value of ξ quoted here is from [196]. Various theoretical calculations can be found in [165, 200, 201, 202, 203, 204, 205].) Fig. 5.5 shows the numerically extracted function $\mathcal{G}$, its first derivative and the function $\mathcal{F}$. In Fig. 5.5 and the rest of the figures, the band denoted by the dashed vertical lines corresponds to the phase transition between the normal and the superfluid phase.

The data in Ref. [196] stops at $T/T_F \approx 0.6$. For higher temperatures the density is small and as far as thermodynamics is concerned, we can model the system as a gas of weakly interacting fermions with a self energy correction in the chemical potential associated with self interactions in the normal phase. Therefore n and s have the same form as in a Fermi gas, (Ref. [206])

$$
\begin{aligned}
n_{\text{norm}} &= -g\,(mT)^{\frac{3}{2}}\frac{\text{PolyLog}\left(\frac{3}{2},-e^{\frac{\mu}{T}}\right)}{2\sqrt{2}\pi^{3/2}} \\
s_{\text{norm}} &= \frac{\sqrt{T}\left(2\;\mu\;\text{PolyLog}\left(\frac{3}{2},-e^{\frac{\mu}{T}}\right)-5\;T\;\text{PolyLog}\left(\frac{5}{2},-e^{\frac{\mu}{T}}\right)\right)}{2\sqrt{2}\pi^{3/2}}\;,
\end{aligned}
\tag{5.68}
$$

where n_{norm}, s_{norm} denote the number density and entropy in the normal phase, $g = 2$ is the energy level degeneracy, and μ with self energy corrections is replaced by $\mu - \frac{3^{2/3}n^{2/3}\pi^{4/3}(\xi_n-1)}{2m}$. Fitting to high temperature data gives $\xi_n \approx 0.45$ [196]. This description works well all the way down to temperatures $T/T_F \gtrsim 0.5$ or equivalently $\frac{T}{\mu} \gtrsim 3.2$ as one can check by comparing the values of S/N as a function of T/T_F in this approximation with the results from [206]. These results match smoothly to the low temperature measurements in Ref. [196]. Therefore for $\frac{T}{\mu} > 3.2$ we use Eq. 5.68 to compute the thermodynamics.

Now that we have understood how to obtain $n(T,\mu)$ we can return to our discussion of the viscosity. To evaluate η at a given μ and T we simply multiply $\frac{\eta}{n}$ from Fig. 3 of Ref. [174] (shown here in the left panel of Fig. 5.6) with the number density that can be found using Eq. 5.65. One could alternatively multiply $\frac{\eta}{s}$ from Fig. 5 of Ref. [174] (shown here in the right panel of Fig. 5.6) with the entropy that can be found using Eq. 5.65. The former works better because of the smaller error bars.

As we shall see in the next section when we describe the fermions in a trap, the dominant contribution to the energy loss arises from the region in the trap where T/μ is about 0.54. This is just above the critical temperature T_c given by the relation

$$
T_c/T_F = 0.167 \pm 0.013\;, \tag{5.69}
$$

or equivalently

$$
\frac{T_c}{\mu} = 0.4 \pm 0.03\;. \tag{5.70}
$$

From the right panel of Fig. 5.6 we see that just above $\frac{T_c}{\mu} \approx 0.4$, $\eta/s \approx 0.7 \approx 8(\frac{1}{4\pi})$. This fact will be relevant in the next section.

5.3.9 Results for the trap

Having understood the thermodynamics in the absence of the trap, we now turn to incorporating the trap potential in the discussion. We first use the LDA approximation to calculate how thermodynamic quantities like s, n etc. vary along the trap. It turns out that on starting at the center of the trap at a sufficiently low temperature, the entropy density has a peak, z_0, close to the point where the superfluid-normal transition occurs. In turn, this leads to the viscosity and damping effects for the fluid modes of interest receiving their contribution from a region close to the peak and with a width, δz that can be made narrow,

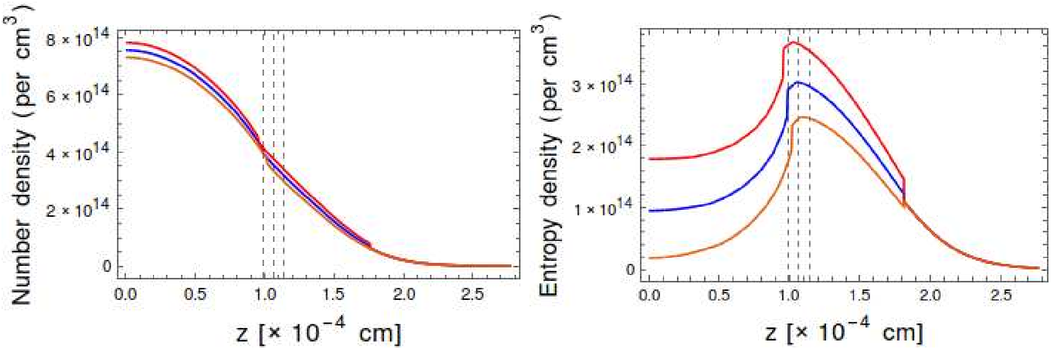

Figure 5.7: (Color online) Variation of number density (left panel) and the entropy density (right panel) with respect to z for $T = \frac{2T_c}{3}$ at $\omega_z = 2\pi \times 10^4$ rads/s with chemical potential at the trap center 10μK. The vertical lines denote the band in z where $T = (0.4 \pm 0.03)(\mu - \phi(z))$ (Eq. 5.70).

$\delta z/z_0 < 1$. Finally, in this subsection we examine the resulting behavior of the system for a range of reasonable values of parameters and show that the five conditions listed at the end of Section 5.2 can be met. It turns out that both the time scales for energy loss, and the magnitude of the total energy, lie in the range of experimentally accessible values.

Before we start let us note that there are three energy scales, T, μ, ω_z in the system (μ without an argument refers to the chemical potential at the center of the trap, and we are neglecting ω_x, ω_y here). These give rise to two dimensionless ratios, $T/\mu, \omega_z/\mu$. Length scales can be obtained from these energy scales using the mass, via the relation, $L = \frac{1}{\sqrt{2mE}}$.

Thermodynamics in the Trap:

As discussed in Subsection 5.3.2 in the presence of a trap the equations for superfluid dynamics can be solved at equilibrium by taking the chemical potential to have a local value which varies along the trap, as given by [4] Eq. 5.24. The temperature T in equilibrium is a constant.

Once we have the function $\mathcal{G}$ as discussed in Sec. 5.3.8, one can then use LDA to express all quantities of interest as a function of the displacement from the trap center (which we denote by $\mathbf{r}$). Thus, within LDA, we can write the number density as

$$n(\mathbf{r}) = n\left(\mu(\mathbf{r}),\ T\right). \tag{5.71}$$

We can also express energy and entropy density in the same fashion as a function of the distance from the trap center. Some comments on the conditions for the violation of LDA will be made in the end of the section.

To set the scales we show (see Fig. C.1) the number density and the entropy density as

[4]From now on μ without the argument $\mathbf{r}$ refers to the chemical potential at the center of the trap and $\mu(\mathbf{r}) = \mu - \phi(\mathbf{r})$.

a function of the distance z from the trap center at $x = 0, y = 0$, for a typical trap configuration that we consider. In all the examples we consider, we will take Li_6 as the fermionic species.

In making Fig. C.1, the chemical potential at the center of the trap is chosen to be 10μK which is typical for experiments performed with fermionic cold atoms [173, 207]. The potential is taken to be harmonic (Eq. 5.14), with the confinement frequency along z direction, $\omega_z = 2\pi \times 10^4$ rads/s which is about 10 times that chosen in Ref. [207]. [5] Since we are taking $x = y = 0$, ω_x and ω_y do not matter in drawing Fig. C.1. However, since we will be exploring anisotropic traps we keep in mind the condition that $\omega_x = \omega_y \ll \omega_z$.

The temperature throughout the trap is taken to be $T = \frac{2T_c}{3}$, where T_c is the critical temperature (Eq. 5.70) associated with the chemical potential (μ) at the center of the trap defined by

$$T_c \equiv 0.4\ \mu\ . \tag{5.72}$$

To avoid confusion we note that T_c is the temperature at which the superfluid to normal phase transition would have occurred at the center of the trap. In the system under consideration with $T = \frac{2T_c}{3}$, since T at the center of the trap is below the local critical temperature at the center of the trap, the transition actually occurs away from the center of the trap, at a location $z = z_c$, where the local chemical potential $\mu(z_c) = \frac{T}{(0.4)}$ [where we have abbreviated $\mu((0, 0, z_c))$ as $\mu(z_c)$] corresponding to the phase transition to the normal phase. In Fig. C.1 we have denoted it by dashed (gray online) vertical lines corresponding to the central value and the error bands.

The error bands to the densities (marked by red curves online) are associated with the errors in $\mathcal{G}$ (Fig. 5.5). They are discontinued from $z = 17 \times 10^{-5}$ cm corresponding to the point where we switch to Eq. 5.68 to calculate the thermodynamics.

In the other trap geometries we consider below, we will keep the chemical potential at the center, μ, unchanged as it will set the overall scale of the problem, and only change the temperature of the trap and the confining frequency ω_z, in order to explore traps which satisfy criteria listed in Sec. 5.2. The strategy we follow is given below.

As explained in the last section, we estimate the η at a given location $\mathbf{r}$ corresponding to the local chemical potential $\mu(\mathbf{r})$ and temperature T by simply multiplying the local number density n we find using Eq. 5.65 with $\frac{\eta}{n}$ from Fig. 3 of Ref. [174]. (We have reproduced it here in Fig. 5.6 for convenience.) This estimate assumes that not only thermodynamic but also the transport quantities are determined by the local chemical potential and the temperature. This estimate necessarily implies that the viscosity is isotropic. Nonetheless this will help us identify the values of T/μ for which the energy loss of the hydrodynamic shear modes is dominated by a region where the potential can be approximated as a linear potential. Having done that, we will increase ω_z to induce anisotropy in the transport

[5] For conversions to energy units, we use 1 eV^{-1} = 1.97×10^{-7} m, 1 eV= 1.78×10^{-36} kg, 1 eV^{-1} = 6.58×10^{-16} s, 1 eV= 1.16×10^4 K. The mass of Li_6 in natural units is 5.6×10^9 eV.

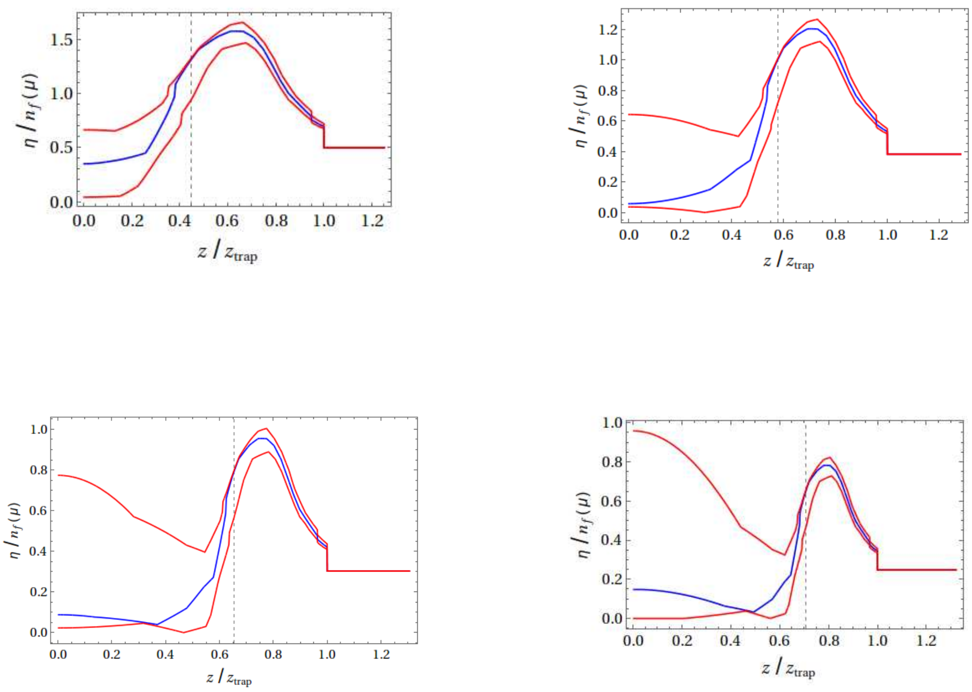

Figure 5.8: (Color online) Local shear viscosity with respect to z for $T = \frac{4T_c}{5}$ (top left), $T = \frac{2T_c}{3}$ (top right) $T = \frac{4T_c}{7}$ (bottom left) and $T = \frac{T_c}{2}$ (bottom right) at $\omega_z = 2\pi \times 10^4$ rads/s and $\mu = 10\mu$K. The red curves denote the error estimate which include errors in the measurement of η/n [174] as well as errors in $\mathcal{G}$ due to errors in the measurements of thermodynamics [196]. The black dashed vertical line is at z_c.

coefficients.

Let us consider the four panels in Fig. 5.8. They show the local shear viscosity (in units of $(2m\mu)^{3/2}/(3\pi^2)$ where μ is the central chemical potential) as a function of z for $x = 0, y = 0$ for four different temperatures at $\omega_z = 2\pi \times 10^4$ rads/s. The chemical potential at the center is taken to be 10μK. The temperatures are $T = \frac{4T_c}{5}$ (top left panel), $T = \frac{2T_c}{3}$ (top right panel) and $T = \frac{4T_c}{7}$ (bottom left panel) and $T = \frac{T_c}{2}$ (bottom right panel). Like Fig. C.1, the vertical line (gray online) corresponds to z_c where $T = 0.4\mu(z_c)$. The error bands of the curves are associated with the errors in $\mathcal{G}$ — which impact n — as well as the errors in the measured η/n. The x-axes of the plots is the z coordinate scaled by the trap size

$$z_{\text{trap}} = \sqrt{\frac{2\mu}{m\omega_z^2}}\,. \tag{5.73}$$

One can also define a characteristic distance z_{max} where $T/\mu(z) = 1$ given by

$$z_{\text{max}} = \sqrt{\frac{2(\mu - T)}{m\omega_z^2}} \,. \tag{5.74}$$

For $\mu = 10\mu$K at the center of the trap and $\omega_z = 2\pi \times 10^4$ rads/s, z_{trap} is about 18.3×10^{-5} cm and z_{max} is about 15.7×10^{-5} cm. Beyond the distance z_{trap}, we assume the viscosity to behave like $\frac{15}{32\sqrt{\pi}}(mT)^{\frac{3}{2}}$ as predicted by the two-body Boltzmann equation [189].

Note that within LDA the plots in Fig. 5.8 are independent of ω_z if we keep T/T_c fixed. This is because scaling ω_z by a factor f can be undone by scaling z by a factor $1/f$. Since z_{trap} is scaled by the same factor, z/z_{trap} at any point on the curve remains unchanged.

To understand the behavior of viscosity along the trap, first consider the central values in Fig. 5.8 (blue curve online). For all temperatures given above (notice that they are all below T_c meaning that the centre of the trap is superfluid), we find the presence of a peak in the middle region of the trap length. Qualitatively we understand this from the fact that the local entropy (see Eq. 5.65) is the product of $n_f(\mu(\mathbf{r}))$ which decreases along the length of the trap, while the function $\mathcal{G}'$ increases along the length of the trap, hence it is natural to expect a peak for the entropy density somewhere along the length of the trap. It is clearly seen in the right panel of Fig. C.1. Since the local shear viscosity over entropy density is relatively slowly varying in this region (the peak location is just above the critical region), it is not surprising that the local shear viscosity shows a similar behavior. Henceforth, we will denote the position of this peak by z_0. We also denote the full width at half maximum of the peak by δz.

The existence of the peak allows us to construct a system where the dominant contribution comes from a region where the potential approximately varies linearly, modeling the theories (Sec. 5.2) where the force that breaks rotational invariance is spatially constant. Here, the trap potential is harmonic, but the dominant contribution to the integral in Eq. 5.48 and Eq. 5.49 comes from an interval δz near z_0. If we expand the confinement potential as a Taylor series around z_0 as

$$\phi(z_0) + \phi^{'}(z_0)(\delta z) + \frac{1}{2}\phi^{''}(z_0)(\delta z)^2 + ... \tag{5.75}$$

The linearity approximation will hold as long as the confinement potential satisfies

$$\frac{\phi^{''}(z)}{\phi^{'}(z)}\,\delta z \ll 1 \Rightarrow l \equiv \frac{\delta z}{z_0} \ll 1 \,. \tag{5.76}$$

Since we are using a harmonic trap, there are no higher order terms. Our criterion for constant driving force is therefore straightforward. We desire that the dimensionless ratio $l \equiv \frac{\delta z}{z_0}$ be less than 1.

There are other motivations to choose the dominant contribution to shear viscosity to arise from such a localized region. We are interested in extracting the value of η/s, for suitable components of the viscosity tensor, for particular values of T, μ (in particular, close to the critical temperature T_c where η/s is known to be close to the KSS bound). Due to the varying trap potential, $\mu(z)$ and therefore the entropy density at equilibrium also vary along the trap. The change resulting in the viscosity due to anisotropy should be bigger than the effect due to the variation of the trap potential on s, thereby giving rise to the condition,

$$\frac{\delta\eta}{\eta} > \frac{\partial s}{\partial z}\frac{\delta z}{s}\,. \tag{5.77}$$

As we saw in Sec. 5.2 after Eq. 5.10 the corrections to the viscosity due to anisotropy go like square of the force that generates the anisotropy. For the system at hand this leads to the expectation

$$\frac{\delta\eta}{\eta} \sim \frac{(\nabla\phi)^2}{(\mu(z)^2 k_F(z)^2)}. \tag{5.78}$$

This estimate agrees with the analysis based on the Boltzmann equation as discussed later in Sec.5.4 (see Eq. 5.102). The RHS in Eq. 5.77 goes like $\frac{\partial s}{\partial z}\frac{\delta z}{s} \sim \delta z/z_0 = l$, and this gives rise to the condition

$$\kappa_{\rm LDA}^2 > l \tag{5.79}$$

where we have introduced the notation

$$\kappa_{\rm LDA} = \frac{(\nabla\phi)}{(\mu(z_0)\ k_F(z_0))}\,. \tag{5.80}$$

It is easy to see that $\kappa_{\rm LDA}$ roughly scales as

$$\kappa_{\rm LDA} \sim \frac{\omega_z}{\mu} \tag{5.81}$$

so that Eq. 5.79 leads to the condition

$$\frac{\omega_z^2}{\mu^2} > l. \tag{5.82}$$

For fixed T, μ one can show that l does not change as ω_z changes. Thus the left hand side is independent of the ratio $\frac{\omega_z}{\mu}$ for fixed T/μ, and the inequality can be met for sufficiently large $\frac{\omega_z}{\mu}$.

Let us also mention that the gravity results apply to situations with only linearly varying potential (Eq. 5.2) leading to only $|\nabla\phi|^2$ corrections due to the anisotropy. In general we would expect that there are additional corrections proportional to $\nabla^2\phi$. There is little guidance on what these corrections do, for the kind of strongly coupled system we are dealing with here. Thus, to the extent we are trying to stay close to situations where gravitational systems give at least some guidance, it is desirable to choose the dominant contribution to shear viscosity to arise from a narrow localized region.

T	$z_{\text{trap}}\sqrt{\frac{\mu}{10\mu\text{K}}\frac{2\pi\times10^4}{\omega}}$ cm	$\frac{z_0}{z_{\text{trap}}}$	l	$\frac{T}{\mu(z)}\vert_{z_0}$	$\frac{\eta}{n}\vert_{z_0}$	$\frac{\eta}{s}\vert_{z_0}$	$\kappa_{\text{LDA}}\frac{10\mu\text{K}}{\mu}\frac{\omega_z}{2\pi\times10^4 rad/s}$
$4T_c/5$	18.3×10^{-5}	0.63	0.98	0.54	0.89	0.85	0.05
$2T_c/3$	18.3×10^{-5}	0.71	0.62	0.54	0.89	0.85	0.08
$4T_c/7$	18.3×10^{-5}	0.76	0.46	0.54	0.89	0.85	0.11
$T_c/2$	18.3×10^{-5}	0.8	0.37	0.55	0.91	0.85	0.13

Table 5.2: Trap characteristics for various T/T_c. The scaling behavior of various quantities with ω_z are also shown. The entries were calculated for $\mu = 10\mu$K, $T_c = 0.4\mu$. $l = \frac{\delta z}{z_0}$ (Eq. 5.76) tests how well the potential can be approximated as a linear potential in the regime of interest. κ_{LDA} (Eq. 5.96) tests how well LDA is expected to work at z_0.

T	$\alpha_x^{\max}(10^{-10}\text{eV})$	$\dot{E}_{kin}$(j/s)(**a**)	E(j) (**a**)	$\tau_0(s)$(**a**)	$\dot{E}_{kin}$(j/s)(**b**)	E(j) (**b**)	$\tau_0(s)$(**b**)
$4T_c/5$	2.83	2.37×10^{-16}	3×10^{-20}	0.0002	4.7×10^{-16}	10^{-17}	0.04
$2T_c/3$	2.35	1.25×10^{-16}	2×10^{-20}	0.0003	2.5×10^{-16}	6.8×10^{-18}	0.05
$4T_c/7$	2.02	7.12×10^{-17}	1.4×10^{-20}	0.0004	1.4×10^{-16}	4.8×10^{-18}	0.07
$T_c/2$	1.77	4.33×10^{-17}	1.1×10^{-20}	0.0005	8.65×10^{-17}	3.6×10^{-18}	0.08

Table 5.3: Additional trap characteristics for various T/T_c at $\omega_z = 2\pi\times10^4$ rads/s, $\omega_x = \omega_y = 2\pi\times385$ rads/s and $\mu = 10\mu$K. The energy is given in joules abbreviated as 'j' and energy loss rate in joules per second, (j/s). For a fixed T/μ, the energy of the Elliptic mode scales as $\sim\frac{1}{\omega_x\omega_y\omega_z^3}$ and that of the Scissor mode scales as $\sim\frac{1}{\omega_x^3\omega_y\omega_z}$. The characteristic time τ_0 (given in seconds 's' in the table and defined in Eq.5.87) of the Elliptic mode scales as $\sim\frac{\mu}{\omega_z^2}$ and that of the Scissor mode scales as $\sim\frac{\mu}{\omega_x^2}$. For the Elliptic mode to account for the fact that only the normal component of the velocity is non-zero near the trap centre, we assume that the normal component density in this region is $\frac{T}{T_c}$ times the total density in this region. For the Scissor mode we have the full number density.

Viscosity and Other Properties For Varying Trap Parameters: Table 5.2

We now turn to examining the behavior of η, η/s, and $l = \frac{\delta z}{z_0}$ as trap parameters are varied. In Table 5.2 we keep ω, μ fixed to take the values $\omega_z = 2\pi\times10^4$ rads/s, $\mu = 10\mu$K and vary T. As mentioned at the beginning of Subsection 5.3.9 there are two dimensionless ratios that characterize the energy scales in this system. The different rows corresponding to different values of T in units of T_c show how various quantities vary with T/μ. The scaling of these quantities with ω_z/μ is given in the first line on top of the Table. 5.2. Thus κ_{LDA} scales like ω_z/μ. z_0, z_{trap} and δz scale like $1/\omega_z$ for fixed T, μ, as was discussed above after Eq. 5.74. Thus their ratios, $\frac{z_o}{z_{\text{trap}}}, l = \frac{\delta z}{z_0}$ etc. are independent of ω_z/μ. The third column of the Table. 5.2 tests the linearity of the potential, which is a good approximation near the peak if $l = \delta z/z_0 \ll 1$.

The ratio l is governed by the temperature of the trap divided by the chemical potential or equivalently T_c at the center. As we decrease T/T_c, z_0 increases and δz decreases. This consideration would suggest that to obtain $\frac{\delta z}{z_0}$ as small as possible we should consider as small a temperature as possible. But this conclusion is not correct as is clear from the upper error band in Fig. 5.8 (red online).

The errors bands on η are fairly narrow in the region near z_0. However, the errors grow near $z \to 0$, in particular for smaller T/T_c (Fig. 5.8). The reason is the large errors in the measured η/n in the superfluid regime (see the region $T/T_F \lesssim 0.16$ in Fig. 5.6). Indeed, we expect that for $T \ll T_F$, the viscosity is dominated by superfluid phonons whose contribution diverges as $T \to 0$ as $\eta \approx (9.3 \times 10^{-6})\ \xi^5\ (T_F^8/v^3T^5)$ where v is the speed of superfluid phonons [197]. Numerically, $\eta/n \approx 2.5 \times 10^{-5}\ \frac{T_F^5}{T^5}$. Therefore, to avoid a large contribution from the center of the trap rather than from near z_0, we do not consider temperatures below $T_c/2$. Within this constrained temperature regime between $T_c/2$ and T_c we find that the linearity condition $\delta z/z_0 < 1$ is satisfied, although it is not possible to generate traps where $\delta z/z_0$ is parametrically small. In the narrow range of temperatures, it turns out that the location of z_0 is such that $T/\mu(z_0) \approx 0.54$, just off to the right of the phase transition at $T/\mu(z_c) \approx 0.4$.

Note that, as explained in the discussion above, a few paragraphs after Eq. 5.72, the value for the viscosity η/s which appears in the Table 5.2 is an approximate one, obtained by taking the value in the isotropic situation corresponding to the local value for μ, T at the location z_0. By a similar argument as before, this value is independent of the ratio ω_z/μ for a fixed T/T_c. We note that the values of η/s in the Table 5.2 are about 10 times the KSS bound. One would expect that various components of the viscosity tensor deviate from this rough value by a fraction of order κ_{LDA}^2. The parameter κ_{LDA} which was introduced in Eq. 5.80 above, when computed at the location of the peak z_0, has the more exact form

$$\kappa_{\text{LDA}} = \frac{m\omega_z^2 z_0}{(3\pi^2 n(z_0))^{\frac{1}{3}}\mu(z_0)} = \frac{\sqrt{\frac{m}{2}}\omega_z^2 z_0}{[\mathcal{F}(\frac{T}{\mu(z_0)})]^{1/3}[\mu(z_0)]^{\frac{3}{2}}} \tag{5.83}$$

as one can easily check by using Eq. 5.65.

Energy Damping For Varying Values of Trap Parameters: Table 5.3

We now turn to considering the effects of varying the trap parameters on various quantities like the total energy E_{kinetic}, the damping rate of this energy $\dot{E}_{\text{kinetic}}$, etc. In Table 5.3 we again keep μ, ω_z fixed to take values $\omega_z = 2\pi \times 10^4$ rads/s, $\mu = 10\mu$K and consider the effects of varying T. In addition, we also need to consider the effects of the harmonic trap in the x, y directions. We keep ω_x, ω_y to be fixed to take values $\omega_x = \omega_y = 2\pi \times 385$ rads/s. The different rows then give how various quantities vary as T/μ changes. We note that for the range of temperatures considered the total number of atoms in the trap is approximately, $\sim 10^6$.

The energy which appears in this Table is the total mechanical energy E given by

$$E = 2E_{\text{kinetic}} \tag{5.84}$$

where

$$E_{\text{kinetic}} = \langle \frac{1}{2} \int d^3\mathbf{r}\, mn(\mathbf{r})\mathbf{v}^2 \rangle\ , \tag{5.85}$$

where $\mathbf{v}$ is the velocity of either mode and the average is taken over one cycle for the scissor mode (the elliptic mode is non-oscillatory). For the Elliptic mode and the Scissor mode with amplitude $\alpha_x^{\max}$, the kinetic energy is given as follows:

$$\begin{aligned}\text{For }\textbf{Elliptic},\ E_{\text{kinetic}}(\mathbf{a}) &= \int d^3\mathbf{r}\, \frac{1}{2} m\, n_{normal}\, (\alpha_x^{max})^2 [\frac{\omega_x^4}{\omega_z^4} x^2 + z^2] \\ \text{For }\textbf{Scissor},\ E_{\text{kinetic}}(\mathbf{b}) &= \int d^3\mathbf{r}\, \frac{1}{4} m\, n\, (\alpha_x^{max})^2 [x^2 + z^2]\,.\end{aligned} \tag{5.86}$$

$\dot{E}_{\text{kinetic}}$ is the rate of energy loss due to viscosity induced dissipation, Eq. 5.47. The energy loss, $\dot{E}_{\text{kinetic}}$ in these modes is given by Eqns. 5.48, 5.49.

Note that for the Scissor mode the expression corresponds to the kinetic energy averaged over an oscillation cycle. Also, for the Elliptic mode, $v_s = 0$, Eq. 5.16, and only the normal component contributes to the kinetic energy. The density in the normal phase is estimated in the region close to the centre, where both the superfluid and normal components are present, as being $\frac{T}{T_c}$ times the total density in this region and we have denoted it by n_{normal} in Eq. 5.86. For the Scissor mode we have the full number density denoted by n in the above formulas.

The validity of hydrodynamics imposes a condition on how big α_x can become, the resulting maximum value, α_x^{max} was estimated in Eq. 5.53. The quantities E_{kinetic}, $\dot{E}_{\text{kinetic}}$ which appear in Table 5.3 are obtained from Eq. 5.47, Eq. 5.86 by setting $\alpha_x = \alpha_x^{max}$.

A convenient quantity with which to compare $\alpha_x^{\max}$ is the ratio of the speed of sound at the centre $c_s = \sqrt{\frac{2\mu}{3m}}$ to a measure of the trap size z_{trap}. For comparison, let us note that for $\omega_z = 2\pi \times 10^4$ rads/s we obtain $\frac{c_s}{z_{\text{trap}}} = \frac{\omega_z}{\sqrt{3}} = 3.63 \times 10^{-11}$ eV.

The (amplitude) damping time τ_0, which appears in Table 5.3, is defined as

$$\tau_0 = 2E/\dot{E}_{kinetic} \tag{5.87}$$

As mentioned above, the table considers the effects of varying the temperature while keeping $\mu, \omega_z, \omega_x, \omega_y$ fixed. For fixed T/μ one can also consider what happens as the angular frequencies are varied. In the highly anisotropic situations $\omega_z \gg \omega_x, \omega_y$, one finds that the total energy E_{kinetic} for the Elliptic mode approximately scales like

$$E_{\text{kinetic}}(a) \sim \mu \frac{\mu}{\omega_x} \frac{\mu}{\omega_y} \left(\frac{\mu}{\omega_z}\right)^3 \tag{5.88}$$

and the damping time τ_0 for the Elliptic mode approximately scales like

$$\tau_0(a) \sim \frac{\mu}{\omega_z^2}\,. \tag{5.89}$$

Similarly for the Scissor mode we get

$$E_{\text{kinetic}}(b) \sim \mu \frac{\mu}{\omega_y} \frac{\mu}{\omega_z} \left(\frac{\mu}{\omega_x} \right)^3 , \tag{5.90}$$

$$\tau_0(b) \sim \frac{\mu}{\omega_x^2} . \tag{5.91}$$

These scalings are obtained by noting that $\alpha_x^{\max} \sim \mu$ for fixed T/μ, and also that the trap potential is unchanged under a rescaling $\omega_z \to \lambda\, \omega_z, z \to z/\lambda$ and similarly for x, y. We have also assumed that $\omega_z \gg \omega_x, \omega_y$. Some of these scalings are summarized in the caption below Table 5.3. For example, the scalings of the scissor mode, can be derived as follows: $E \sim \int dxdydz[mnv^2] \sim L_x L_y L_z[mn\alpha^2 L_x^2] \sim \frac{\mu^6}{\omega_x^3 \omega_y \omega_z}$, where we have assumed that at the center of the trap $\mu > 0$ and $L_i = \sqrt{2\mu/(m\omega_i^2)}$.) In a similar manner, one can derive the approximate scalings for energy dissipation rates: $\dot{E} \sim \frac{\mu^5}{\omega_x \omega_y \omega_z}$ for both the modes (assuming η scales the same way as n ie. $\sim (m\mu)^{\frac{3}{2}}$.

The approximate value of T, μ, ω_z we consider here are of the same order as those considered in [173] where the viscosity of a unitary Fermi gas was measured, using a radial breathing mode. The Scissor mode has been considered in the literature before. The damping rate has been measured for cold atoms system in this mode in superfluid bosonic (see Ref. [181] and Refs. therein) and in fermionic systems [182]. In particular [182] carries out these measurements in the unitary Fermi gas. The values for trap parameters we consider are similar to those considered for example in [173] and not very different from those considered in [182]. The maximum angular amplitude of the the scissor mode is determined by the velocity amplitude α_x (Eqs. 5.17, 5.15) which is bounded above by $\alpha_x^{\max}$ in Table 5.3. One can show that the angular amplitude (in radians) of the oscillation executed by the deformed cloud in the scissor mode is given by

$$\theta = \tan^{-1} \left(\frac{e^{\frac{2\alpha_x}{\omega}} - 1}{e^{\frac{2\alpha_x}{\omega}} + 1} \right) , \tag{5.92}$$

where $\omega = \sqrt{\omega_x^2 + \omega_z^2}$. Taking α_x to be the maximum value $\alpha_x^{\max} \sim 10^{-10}$ eV and ω to be $2\pi \times 10^4$ rads/s $\equiv 4.16 \times 10^{-11}$ eV, we find $\theta_{\max} \sim \tan^{-1}[1] \equiv 45°$. For a frequency 10 times larger, $\theta_{\max} \sim \tan^{-1}[0.4] \equiv 24°$. It is satisfying that these amplitudes are larger than those measured in [182] for the scissor mode and hence the condition for hydrodynamics (Eq. 5.53) does not force the amplitudes to be so small as to preclude observation using existing techniques. For $\mu = 10\mu K$, $\omega_x = \omega_y = 2\pi \times 385$ rads/s and $\omega_z = 2\pi \times 10^4$ rads/s, τ_0 ranges from roughly 0.04 sec to 0.08 sec. The damping of the scissor mode has been observed for slightly different parameters values, $\mu \approx 1\mu K$, $\omega_x = 2\pi \times 830$ Hz, $\omega_y = 2\pi \times 415$ Hz and $\omega_z = 2\pi \times 22$ Hz in Ref. [182] where the damping time scales measured are of the order of milliseconds.

Summary:

Now we come to the punch line of this section. The effects of anisotropy can cause a fractional change in components of the viscosity tensor, potentially lowering some of them. This effect is expected to go like, $\delta\eta/\eta \sim \kappa_{\text{LDA}}^2$, as mentioned in Eq. 5.78. We see from Table 5.2 that, for fixed ω_z/μ, κ_{LDA} increases as T decreases (i.e. T/μ decreases), with the maximum value, within the range of allowed temperatures, being of order $\kappa_{\text{LDA}} \sim 10\%$. This would lead, one expects, to a fractional change in components of the viscosity of order $\delta\eta/\eta \sim (\text{few}) \times 1\%$, which is quite small. However note that increasing ω_z will increase κ_{LDA} with a linear dependence $\kappa_{\text{LDA}} \sim \omega_z/\mu$ as noted in Eq. 5.81 and also in the first row of Table 5.2. In turn this should lead to a quadratic fractional change in $\delta\eta/\eta \sim (\frac{\omega_z}{\mu})^2$. We can carry out this change while keeping ω_x, ω_y fixed thereby increasing the anisotropy. Note that this change of ω_z will decrease the total energy of this mode $E_{\text{kinetic}}(b) \sim 1/\omega_z$, Eq.5.90, but it does not change τ_0 significantly, since τ_0 depends to a good approximation on ω_x and not ω_z as seen from Eq. 5.91. Also note that changing ω_z while keeping T/μ fixed will not change l and thus the localized nature of the region from which the damping arise. In fact it will make it easier to meet the condition Eq. 5.82.

Also it is worth commenting that it is easy to see from Eq. 5.81, Eq. 5.90 and Eq. 5.91 that if one want to keep τ_0 and E_{kinetic} for the scissor mode both fixed and increase $\kappa_{\text{LDA}} \to \lambda\, \kappa_{\text{LDA}}$ one could do this (while keeping $\omega_x = \omega_y$) by scaling

$$\omega_x \to \lambda^{\frac{1}{6}}\ \omega_x,\ \omega_y \to \lambda^{\frac{1}{6}}\ \omega_y,\ \omega_z \to \lambda^{\frac{4}{3}}\ \omega_z,\ \mu \to \lambda^{\frac{1}{3}}\ \mu,\ T \to \lambda^{\frac{1}{3}}\ T. \tag{5.93}$$

This keeps $\frac{T}{\mu}$, τ_0 and E_{kinetic} fixed, increases the overall magnitude of μ, increases ω_z and also ω_x, ω_y.

The discussion of the previous two paragraphs suggests that one can quite plausibly keep the damping time scale and the total energy in the experimentally accessible range, while gradually increasing ω_z making $\kappa_{\text{LDA}} \sim \mathcal{O}(1)$ and the effects of anisotropy significant. While some of the theoretical approximations made will break down in this limit it is possible that the effects of anisotropy would get more pronounced, and potentially even dramatic, driving the spin one components of the viscosity to be much smaller than their values in the isotropic case, and potentially even violating the KSS bound.

We have not discussed the Elliptic mode in as much detail. One reason is that unlike the scissor mode, this mode has not been experimentally realized in cold atom systems yet.[6] Also we see from Table 5.3 that the damping time τ_0 in this case is about two orders of magnitude smaller, and this too might be an issue of some experimental concern. It may of course turn out that this mode is experimentally accessible. It will then be certainly

[6] One possible way to set up the elliptic mode is to start with a more circular trap and exciting a rotational mode by using rotating lasers using a set up similar to Ref. [208]. If the rotational frequency is small enough, vortices will not be excited and only the normal fluid will rotate like a rigid body. On adiabatically deforming the trap one would then get the elliptic mode because during adiabatic deformations, hydrodynamics is satisfied at each time and we expect that the normal fluid will go smoothly from circular rotation to the elliptic mode.

interesting to explore its properties, especially since this mode in a very direct way measures the resistance to shear in the resulting fluid flow.

Finally we note that all the five conditions which were listed at the end of Sec. 5.2 for observing the suppression of viscosity can be met in the system being analyzed here. Conditions 1 and 2 are met by the two modes discussed above in the unitary Fermi gas. We have ensured that $l < 1$ (Table 5.2) so that the contribution arises from a localized region where the potential is approximately linear, meeting condition 4. As argued above, for the scissors mode the anisotropy can be made large enough while staying within the fluid mechanics approximation ($\alpha_x < \alpha_x^{max}$) thereby meeting conditions 3 and 5. The resulting values for the total energy and the damping time we find lie within the experimentally accessible range.

To summarize, we have seen in this section that for experimentally reasonable values of parameters one can increase the anisotropy of the trapping potential and probe the viscosity tensor by measuring the energy loss and related damping time in the scissor mode. As the anisotropy is increased, its effects could well become quite significant driving some components of the viscosity (spin 1 in our notation) to become very small, and potentially making them even smaller than the KSS bound.

5.3.10 Discussion on $\kappa_{\rm LDA}$

In this subsection, we present a detailed discussion on $\kappa_{\rm LDA}$ given in the last column of Table. 5.2. The results discussed so far assume LDA is valid. LDA rests on the assumption that the trap potential varies slowly on the scale of the local Fermi wavelength $k_F^{-1}(\mathbf{r}) = \left(3\pi^2 n(\mathbf{r})\right)^{\frac{1}{3}}$ ie. at any local point $\mathbf{r}$ along the length of the trap, the following condition holds true -

$$\left|\nabla_{\mathbf{r}}(\mu(\mathbf{r}))\frac{1}{k_F(\mathbf{r})}\right|_{\mathbf{r}} \ll \mu(\mathbf{r})$$

Since we desire $\omega_x, \omega_y \ll \omega_z$, the gradient is strongest in the z direction and hence taking $x,\ y = 0$ and moving along the harmonic trap in the z direction, $\frac{d(\mu(z))}{dz} = -m\omega_z^2 z$, we note that LDA violations will be significant if

$$m\omega_z^2 z \frac{1}{(3\pi^2 n(z))^{\frac{1}{3}}} \sim \mu(z)\ . \tag{5.94}$$

For any trap geometry at the outer edges of the trap when the density becomes small enough, LDA will be violated ($\mu(z) < 0$ for $z > z_{\rm trap}$). These regions typically do not contribute significantly to the trap energy loss. But focusing on the region near z_0, LDA is a good approximation if

$$\kappa_{\mathrm{LDA}} = \frac{\sqrt{\frac{m}{2}}\omega_z^2 z_0}{[\mathcal{F}(\frac{T}{\mu(z_0)})]^{1/3}[\mu(z_0)]^{\frac{3}{2}}} \ll 1 \,, \tag{5.95}$$

Approximating $\mathcal{F}(\frac{T}{\mu(z_0)})]^{1/3} \approx \frac{1}{\sqrt{\xi}}$ [Since $\mathcal{F}(0) = 1/\xi^{3/2}$, and the deviations from $\mathcal{F}(0)$ are small for $T/\mu \lesssim 1$], we find

$$\kappa_{\mathrm{LDA}} = \frac{\sqrt{\frac{m}{2}}\omega_z^2 z_0}{[\mu(z_0)]^{\frac{3}{2}}}\sqrt{\xi} \ll 1 \,, \tag{5.96}$$

Since z_0 scales as $1/\omega_z$ for fixed μ and T, LDA will be violated at z_0 if ω_z is large enough. From Table 5.2 one can see that for $\mu = 10\mu$K and $T = T_c/2$, $\kappa_{\mathrm{LDA}} > 1$ for $\omega_z > 2\pi \times 77000$ rads/s. Alternatively, taking $\omega_z = 2\pi \times 10^4$ rads/s and $T = T_c/2$, κ_{LDA} can become larger than 1 if $\mu < 1.3\ \mu$K.

For $T \to 0$ the corrections to LDA have been previously studied in Refs. [209, 210]. One can write

$$n(\mathbf{r}) = n_{\mathrm{LDA}}\big(1 - \frac{c_\chi}{64}\frac{(\nabla\phi(\mathbf{r}))^2 + 4(\mu - \phi(\mathbf{r}))\nabla^2\phi(\mathbf{r})}{m(\mu - \phi(\mathbf{r}))^3} + \mathcal{O}(\nabla^3\phi(\mathbf{r}))\big) \,, \tag{5.97}$$

where c_χ is related to the response of the density to a periodic fluctuation in the potential. The low energy constant c_χ has not been calculated using *ab-initio* techniques so far. In all model calculations $c_\chi \sim 1$, including in a sophisticated analysis using SLDA (Ref. [210]).

For finite T for an isothermal system, the deviations from LDA are not related to the density response but for $T \lesssim (\mu - \phi(\mathbf{r}))$ we can write corrections to LDA in analogy with Eq. 5.97

$$n(\mathbf{r}) = n_{\mathrm{LDA}}\big(1 - \frac{c_1}{64}\frac{(\nabla\phi(\mathbf{r}))^2}{m(\mu - \phi(\mathbf{r}))^3} - \frac{c_2}{16}\frac{\nabla^2\phi(\mathbf{r})}{m(\mu - \phi(\mathbf{r}))^2} + \mathcal{O}((\nabla V)^3)\big) \,, \tag{5.98}$$

where $c_{1,\,2}$ are functions of (T/μ) and tend to 1 as $T/\mu \to 0$. In particular, for the interesting region the term proportional to c_1 is dominant (the exception is near the center of the trap). Therefore, the corrections to LDA near z_0 can be written as

$$n(z) = n_{\mathrm{LDA}}\big(1 - \frac{c_1}{64}\frac{2}{\xi}\kappa_{\mathrm{LDA}}^2 + \cdot\cdot\big) \,, \tag{5.99}$$

where we have used the low temperature expression

$$m\mu(\mathbf{r}) = \frac{\xi}{2}k_F^2(\mathbf{r}) \,, \tag{5.100}$$

to write the correction in terms of κ_{LDA}.

In the absence of further information about c_1 at finite T it is difficult to make precise statements about the relevance of LDA corrections for the traps with large values of ω_z

that we show in the next Section are needed to make the shear viscosity tensor locally anisotropic. Therefore, we simply use $\kappa_{\mathrm{LDA}} \gtrsim 1$ as a marker for significant LDA violation. However, it is important to keep in mind that if $c_1(\frac{T}{\mu(z_0)}) \sim c_1(0.54) \sim 1$ (since $\frac{T}{\mu(z_0)} \sim 0.54$ for the cases we consider), then the pre-factor of $1/(32\xi)$ implies that the corrections to LDA can be small even for $\kappa_{\mathrm{LDA}} \approx 1$.

5.4 Local anisotropy

Hydrodynamics is an effective theory: The conserved currents are written as a series of terms ordered by the number of derivatives acting on the local fluid velocity. The lowest order terms are simply given by the Galilean (for non-relativistic systems) or Lorentz (for relativistic systems) transforms of the local thermodynamic properties like the density and the pressure, from the local rest frame of the fluid to the laboratory frame. The first order terms are given by the local gradients of the velocity $(\partial_i u_j + \partial_j u_i)/2$ multiplied by proportionality constants given by the transport coefficients — for example viscosities — of the system. We will not consider higher derivative terms in this chapter, instead restricting ourselves to situations (see Eq. 5.52) where the first order correction is smaller than the lowest order terms.

In the presence of external fields, the law of conservation of energy features a source term proportional to the driving force, $\nabla\phi(\mathbf{r})$. If $\nabla\phi(\mathbf{r})$ is "small" (which we shall define in a moment), its effect on the thermodynamics and transport can be neglected, and hydrodynamics describes a locally isotropic fluid (with isotropic thermodynamic functions and isotropic transport coefficients) [7] moving in a space dependent potential. The key realization therefore is that to observe an anisotropy in thermal or transport properties it is not sufficient for $\omega_x, \omega_y \ll \omega_z$. Corrections to isotropy will start becoming significant as we increase ω_z, if ω_z starts becoming comparable to some microscopic scale of the system.

The criterion for the thermodynamic quantities to exhibit the effect of $\nabla\phi(\mathbf{r})$ is clear from the previous section. If the potential varies on length scales comparable to the inter-particle separation — the Thomas-Fermi approximation, or LDA breaks down — the pressure of the fluid in the direction of the gradient will be different from the pressure in the perpendicular directions. In this case, clearly the transport coefficients will also be anisotropic. To explore an analogous system to the one described in Sec. 5.2, this argument prompts us to consider ω_z large enough that LDA is broken (see Table 5.2). For such systems, the estimates for the density Fig. C.1 and viscosities Fig. 5.8 using LDA will be only rough guiding values, but if the analogy with the system in Sec. 5.2 holds true, the viscosity values relevant for the modes described in Sec. 5.3.1 will be lower than the LDA values, and could be lower than $1/(4\pi)$ in suitable quantum units.

[7] This assumes that microscopically the fluid is isotropic. For example it is not a crystal [183] or a fluid phase with an anisotropic order parameter.

To estimate the order of the correction to the shear viscosity due to potential gradients we note that the first order correction to transport due to $\nabla\phi(\mathbf{r})$ simply appear as the source term, and hence assuming that the next order corrections will be analytic in $\nabla\phi(\mathbf{r})$, we expect

$$\eta_{ijkl} = \eta\frac{1}{2}[(\delta_{ik}\delta_{jl}+\delta_{il}\delta_{jk}-\frac{2}{3}\delta_{ij}\delta_{kl})+\big(\frac{\lambda^2(\nabla\phi(\mathbf{r}))(\nabla\phi(\mathbf{r}))}{[\mu(\mathbf{r})]^2}\big)\sum_{\alpha=0}^{4}c_{(\alpha)}M_{\alpha\,ijkl}]+\mathcal{O}(\nabla^2\phi,(\nabla\phi)^4)\;, \tag{5.101}$$

where λ is a microscopic length scale of the system, $c_{(\alpha)}$ are dimensional constants of order 1 which depend on the microscopic details of the system, and M_i are 5 orthonormal projection operators that arise in a system with one special direction (for eg. see Ref. [211]). We have given these projection operators in Appendix. D.2 (Eq. D.23).

λ is a length scale that determines transport behavior. In a system admitting a quasi-particle description we expect λ to be of the order of the mean free path. (We show this explicitly in Appendix. D.2.) The other length scale in the system is the inter-particle separation $1/k_F$. In terms of k_F we can write the corrections as

$$\begin{aligned}\eta_{ijkl} &\approx \eta\frac{1}{2}[(\delta_{ik}\delta_{jl}+\delta_{il}\delta_{jk}-\frac{2}{3}\delta_{ij}\delta_{kl})+(\lambda k_F)^2\big(\frac{(\nabla\phi(\mathbf{r}))(\nabla\phi(\mathbf{r}))}{k_F^2[\mu(\mathbf{r})]^2}\big)\sum_{\alpha=0}^{4}c_{(\alpha)}M_{\alpha\,ijkl}]\\ &= \eta\frac{1}{2}[(\delta_{ik}\delta_{jl}+\delta_{il}\delta_{jk}-\frac{2}{3}\delta_{ij}\delta_{kl})+(\lambda k_F)^2\big(\kappa_{\rm LDA}^2\big)\sum_{\alpha=0}^{4}c_{(\alpha)}M_{\alpha\,ijkl}]\;,\end{aligned} \tag{5.102}$$

For weakly interacting quasi-particles, the $\lambda k_F \gg 1$. But for a strongly interacting system in the absence of more information about λk_F and $c_{(\alpha)}$ it is not possible to make a more concrete statement about the corrections to viscosity. We can only state that the corrections are important if $\kappa_{\rm LDA}\sim 1$ as we did in Eq. 5.78.

As discussed in Sec. 5.2, for the theories considered in Sec. 5.2, there is no quasi-particle description. The only relevant length scale is $1/T$ and the field ϕ changes by order 1 on a length scale $1/\rho$. Using AdS/CFT it has been shown [178] that the corrections to isotropy go as Eq. 5.10.

For the unitary Fermi gas there is no known gravitational dual [212] and we will need to resort to a rough calculation to estimate $c_{(\alpha)}$ and λk_F. We solve the Boltzmann transport equation in the relaxation time approximation. We hope this will give semi-quantitative results. We leave the challenging calculation of the viscosity for temperatures in the strongly coupled regime just above the critical temperature in the presence of a background potential for future work.

As we show in Appendix. D.2, the corrections to η for a weakly interacting, normal (unpaired) Fermi gas at low temperatures ($T < \mu$) are given by (Eq. D.30)

$$\begin{aligned}
\eta_0 &= \eta(0)[1 - \frac{31}{84}(\lambda k_F)^2 \frac{(\nabla\phi)^2}{k_F^2\mu^2} + \mathcal{O}((\tau\nabla\phi)^4)] = \eta(0)[1 - \frac{31}{84}(\lambda k_F)^2 \kappa_{\text{LDA}}^2 + \mathcal{O}((\tau\nabla\phi)^4)] \\
\eta_1 &= \eta(0)[1 - \frac{13}{28}(\lambda k_F)^2 \frac{(\nabla\phi)^2}{k_F^2\mu^2} + \mathcal{O}((\tau\nabla\phi)^4)] = \eta(0)[1 - \frac{13}{28}(\lambda k_F)^2 \kappa_{\text{LDA}}^2 + \mathcal{O}((\tau\nabla\phi)^4)] \\
\eta_2 &= \eta(0)[1 - \frac{11}{28}(\lambda k_F)^2 \frac{(\nabla\phi)^2}{k_F^2\mu^2} + \mathcal{O}((\tau\nabla\phi)^4)] = \eta(0)[1 - \frac{11}{28}(\lambda k_F)^2 \kappa_{\text{LDA}}^2 + \mathcal{O}((\tau\nabla\phi)^4)] \\
\eta_3 &= 0, \;\; \eta_4 = 0 \; ,
\end{aligned} \tag{5.103}$$

where τ is the effective relaxation time.
For the Elliptic mode $\frac{1}{2}(\partial_i u_j + \partial_j u_i) = \frac{1}{2}\alpha_x(1 - \frac{\omega_x^2}{\omega_z^2}) = V_{xz}$ which probes the viscosity contribution to the stress energy tensor

$$\sigma_{2_{\alpha\beta}} = 2 \; \eta_2 \; (V_{\alpha\gamma} b_\beta b_\gamma + b_\alpha V_{\beta\gamma} b_\gamma - 2 b_\alpha b_\beta b_\gamma b_\delta V_{\gamma\delta}) \; , \tag{5.104}$$

where b is a unit vector along the gradient of the potential. For the Scissor mode, $\frac{1}{2}(\partial_i u_j + \partial_j u_i) = \alpha_x = V_{xz}$ which also probes η_2. (η_2 is the coefficient that corresponds to the projection operator M_2 in Eq. D.23.)

In both cases (see Appendix. D.2) , η is reduced from its value in the absence of the potential, $\eta(0)$, for $\frac{\tau^2}{k_F^2}(\nabla\phi)^2 \lesssim 1$. To estimate the value of τ near $z = z_0$, we note that for $z \sim z_0$, $T(z_0) \sim 0.54 \; \mu(z_0)$. At this T, $\eta(0)/n|_{z_0} \sim 1$.

Using the relaxation time approximation and thermodynamic expressions for a weakly interacting Fermi gas to estimate λ near z_0, we obtain (Eq. D.31)

$$\begin{aligned}
\eta(0)(z_0) &= \frac{(2m\mu(z_0))^{\frac{5}{2}}\tau(z_0)}{15\pi^2 m} \\
&= \frac{2}{5} n(z_0)\mu(z_0)\tau(z_0) \; .
\end{aligned} \tag{5.105}$$

Therefore near z_0, $\tau(z_0) \sim \frac{5}{2\mu(z_0)}\frac{\eta(0)}{n}|_{z_0}$, or,

$$\begin{aligned}
\lambda(z_0) &= v_F(z_0)\tau(z_0) \\
&\sim \frac{k_F(z_0)}{m}\frac{5}{2\mu(z_0)}\frac{\eta(0)}{n}|_{z_0} \\
&= \frac{5}{4k_F(z_0)}\frac{\eta(0)}{n}|_{z_0} \; .
\end{aligned} \tag{5.106}$$

(We have just kept the pre-factors of the order of 1 to serve as mnemonics of the derivation of λ. They have no quantitative significance.)

Therefore, (since $\frac{\eta(0)}{n}|_{z_0} \sim 1$ from $\frac{\eta}{n}$ data)

$$\lambda(z_0)k_F(z_0) = \frac{5}{4}\frac{\eta(0)}{n}|_{z_0} \sim 1 \ . \tag{5.107}$$

The fact that $k_F(z_0)\lambda(z_0) \sim 1$ means that the Boltzmann transport calculation shown in Appendix. D.2 is not quantitatively trustworthy near z_0. But we hope that two the main qualitative consequences of Eq. 5.103 survive a more controlled calculation.

1. First, the coefficient of $\kappa^2_{\rm LDA}$ in Eq. 5.103 is of the order of 1.

2. Second, the sign of the correction term is negative

If true, this would imply that the shear viscosity component η_{xzxz} measured using the Elliptic mode or the Scissor mode will reduced by order 1 from its value in isotropic traps, if $\omega_z \gtrsim 2\pi \times 77000$ rads/s (Table. 5.2).

One might be concerned that for $\omega_z \sim 2\pi \times 77000$ rads/s, our conclusions in the previous section about $\delta z/z_0$ will be violated because of the violation of LDA. In the absence of more concrete information on these coefficients we can not assure this will not happen. We simply note that if the coefficient c_1 in Eq. 5.99 is of the order of 1 (which it is at $T \ll \mu$, but may be larger for $T \sim 0.54\ \mu(z_0)$) then there is a regime where the corrections to the thermodynamics due to LDA is small, but the reduction in transport coefficients is substantial.

5.5 Comments and discussions

In this chapter, we presented a concrete realization of a system of ultra-cold Fermi gases at unitarity, in an anisotropic trap, which may show significant reduction in the viscosity compared to its value in isotropic traps. Given that the value of the isotropic viscosity has been measured to be few times the KSS bound in this system, it presents a candidate setup to observe a shear viscosity smaller than the KSS bound when it is subjected to an anisotropic driving force.[8]

The anisotropic force is obtained by placing the system in an anisotropic trap. The trapping potential is harmonic, Eq. 5.14, and characterized by three angular frequencies, $\omega_x, \omega_y, \omega_z$.

[8] The equations of fluid mechanics of an isotropic phase are rotationally invariant. The solutions of these equations however can be anisotropic due to anisotropic initial conditions or boundary conditions etc. For example, in heavy ion collision experiments, the anisotropic viscosity arises due to anisotropic initial conditions resulting in anisotropic fluid flows. In contrast, the system we studied here has no rotational invariance in equilibrium, and the resulting equations of fluid mechanics themselves break rotational invariance regardless of initial or boundary conditions. In our work, thus the anisotropic viscosity arising in the ultracold gases is not a geometric effect but a field theoretic effect since this is happening in the dense part of the trap (where hydrodynamics is valid and the equations of fluid mechanics themselves break rotational symmetry in equilibrium, see Eq.5.20 with $\phi(\mathbf{r})$ given by Eq.5.14.)

We consider an anisotropic situation where $\omega_z \gg \omega_x, \omega_y$, so that the trapping potential is much stronger in the z direction. For simplicity, we also take $\omega_x = \omega_y$ so that the system preserves rotational invariance in the $x - y$ plane. For some of the discussion below we can neglect the effects of the trapping potential in the x, y directions characterized by ω_x, ω_y.

We work in conventions where $k_B = \hbar = 1$. There are three energy scales T, μ, ω_z and two dimensionless ratios T/μ and ω_z/μ which then characterize the system. The Li_6 atoms have a mass m, using this parameter, any of the energy scales can be converted to a length scale, $L = \frac{1}{\sqrt{2mE}}$.

Based on the behavior seen quite generically in gravity systems we identify five criterion (Sec. 5.2) which when met could plausibly lead to a decrease in the value of some components of the viscosity tensor (the spin one components). These are summarized towards the end of Sec. 5.2 . On studying the superfluid equations we identify two modes which are sensitive to these components of the viscosity tensor. One of these is the scissor mode which has already been studied experimentally in some detail. By taking reasonable values for the parameters- T, μ, $\omega_z, \omega_x, \omega_y$, which are in the experimentally accessible range, Ref. [173], we find that all the five criteria can be met. Furthermore, we find that the resulting energy and damping rate of this energy, from which the viscosity can be extracted, lie within the range of values which are measured by experiments currently being done on cold atom systems, in particular on Li_6 unitary Fermi gas systems, Ref. [182]. For example, for $\mu = 10\mu$K, $\omega_z \sim 2\pi \times 77000$ rads/s, and $T = \frac{T_c}{2}$ ($T_c = 0.4\mu$) we find that the anisotropy, as measured by the parameter κ_{LDA} , Eq. 5.80, is of order unity and therefore significant. At these extreme values of anisotropy our theoretical calculation, strictly speaking, do not apply, but a reasonable extrapolation suggests that the maximum total energy is of the order of 10^{-17} joules which corresponds to the angular amplitude of the scissor mode of about 24° which is within the experimental range of [182]. The damping time τ_0 is of the order of 10^{-2} seconds, which is roughly ten times longer than the observed amplitude damping time that has been accurately measured in the experiments on ultracold Fermi gases [182].
While the system is certainly close to being two-dimensional when $\kappa_{LDA} \sim 1$ and $z_{trap} \sim 5.4\ k_F^{-1}$ (this corresponds to $\mu/\omega_z \sim 2.7$) is on the small side, the effect of small viscosity can already set in when κ_{LDA} is somewhat smaller than unity. We illustrate this with concrete quantitative examples below.
For concreteness, let us consider traps where we fix $T/T_c = 1/2$ ($T_c = 0.4\mu$, where μ is the chemical potential at the center of the trap) and change ω_z. Further, for concreteness, we set the overall scale by $\mu = 10\mu$K. Considering first a representative trap geometry where the shear viscosity tensor is locally isotropic to a large accuracy, we take $\omega_z = 0.048\mu$ (corresponding to $\omega_z = 2\pi \times 10^4$Hz which is typical), for which $\kappa = 0.13$. The fractional reduction in the shear viscosity for this value of ω_z, taking c_2 to be its Boltzmann transport value 11/28 is

$$\frac{\Delta\eta}{\eta} \approx -\frac{11}{28}(\kappa)^2 = -0.7\% \ , \tag{5.108}$$

which is a small reduction in the shear viscosity and may not be even measurable above measurement errors. At the other extreme we considered, $\omega_z = \frac{\mu}{2.7}$ (corresponding to $\omega_z = 2\pi \times 77.16$ kHz), for which $\kappa = 1$ and the fractional reduction is

$$\frac{\Delta\eta}{\eta} \approx -\frac{11}{28}(\kappa)^2 = -39\% \ , \tag{5.109}$$

which is very large. However, in this extreme limit ($\omega_z = \frac{\mu}{2.7}$) only the lowest $2-3$ Landau levels are occupied and the dynamics may be approximately two dimensional. Now consider an intermediate value, say $\omega_z = 0.9T = 0.18\mu$ for which $\kappa_{LDA} = 0.48 < 1$. This gives a correction

$$\frac{\Delta\eta}{\eta} \approx -9\% \tag{5.110}$$

which — while not large — is still substantial. More generally, the criterion for confinement in the z direction is

$$\omega_z \gtrsim \max(\Delta, T) \ , \tag{5.111}$$

since both T and pairing allow for excitations between the harmonic oscillator levels. At these extreme values, where the inequality above is met, our approximations do break down, as we have mentioned in the conclusions (shell effects become important as $\omega_z \gtrsim T$, which is another way of saying that confinement in the z direction becomes strong). For $\omega_z = \frac{\mu}{2.7}$, $\omega_z = 1.85\ T$ and indeed confinement in the z direction is too strong. But, as illustrated by the cases above, by taking ω_z a factor of 2 or 3 smaller (say $\omega_z = 0.9\ T$ that was chosen above for illustration) than the extreme limit, one can measure the tendency of the spin one component of the viscosity to decrease from its lowest value observed in ultra-cold Fermi gases. In an optimistic scenario where c_2 is larger in magnitude than the approximate value of $11/28$ in the Boltzmann transport approximation, the reduction will be even more substantial. Let us also point out that comparing with Ref.[213] the typical values of ω_z/E_F in the chapter is about 80 and the value of ω_z/T is 120. In that case, the trap is truly 2 dimensional as opposed to when $\omega_z/T \sim 0.9$.
Thus, for smaller values of anisotropy, the theoretical estimates are more reliable and suggest that the different viscosity tensor components should have a fractional difference given in terms of κ_{LDA} by Eq. 5.103. This tendency of the viscosity to decrease should already be measurable at more moderate values of the anisotropy.

Our proposal is the first proposal to measure parametrically suppressed anisotropic viscosity components in ultra-cold Fermi gases. Our proposal is different from the discussion of anisotropic hydrodynamics in Ref. [190] since we are demanding that hydrodynamics be a good description (in the sense of Eq. 5.52) in the regime which dominantly contributes to the dissipation of the fluid dynamics modes.

Future theoretical work can improve upon our proposal in several ways. First, our estimate of the corrections to the shear viscosity components due to the potential (Eq. 5.103) was based on a relaxation time treatment of the Boltzmann equation. For strongly interacting fermions, this is not a good approximation and a more rigorous calculation of the anisotropy corrections is desirable. This will require calculating transport properties in a strongly coupled theory without a gravitational dual, in the presence of a background potential: a formidable challenge. Second, we have focused on the region that dominantly contributes to the dissipation. In particular we have neglected the contributions from the tail of the cloud. While this is presumably small, it would be nice to establish this by solving the Boltzmann transport equations in this dilute regime.

It is also worth noting that while the cold-atom system proposed here shares many features with those discussed in Chapter 4 (Ref. [178]), it also has some differences. First, in equilibrium the stress energy tensor is not invariant under translations even for a linear potential. Rather the density decreases with increasing z, but the driving force is proportional to the gradient of the potential $\phi(\mathbf{r})$ (see Eq. 5.3) as in Chapter 4 (Ref. [178]). Second, in addition to energy-momentum, the cold-atom system features another conserved quantity: the particle number. Consequently the system is locally characterized by two thermodynamic variables T and μ rather than just T. It would also be interesting to further study the behavior of viscosity in gravitational systems which correspond to anisotropy driven strongly coupled systems with a finite chemical potential. The examples in Chapter 4 (Ref. [178]) did not have a finite chemical potential, for some discussion of anisotropic gravity systems with a chemical potential see Ref. [214, 215]. As a first step, we have analyzed a weakly coupled system with a linear varying potential in Appendix B and find that the viscosity does become anisotropic in this case.

However, the central point of this chapter is that there is already enough motivation, based on the behavior quite generically seen in gravitational systems, to suggest that some components of the viscosity tensor in anisotropic strongly coupled systems might well become small, making η/s for these components potentially even smaller than the KSS bound, $1/4\pi$. Such a decrease in the viscosity might well happen in cold atom systems, for example the unitary fermi gas, which are experimentally well studied. As argued above, the range of values involved for temperature, chemical potential and angular frequencies are well within the experimental regime for such a system, and the scissor mode which is sensitive to the relevant components of the viscosity has already been realised experimentally in them. Further, the resulting values for the energy and the damping time from which the viscosity can be extracted lie in the experimentally accessible range which has already been achieved.

We thus hope our experimental colleagues in the cold atoms community will find our results interesting and relevant.

Chapter 6

Probing Lepton Flavor Violation in Supersymmetry at the LHC

6.1 Introduction

In this chapter, we turn to a somewhat different exploration and thus can be read independent of the preceding chapters.
The experiments dedicated towards the investigation of flavour physics are considered to be one of best indirect ways to establish the existence of new physics (NP). They play an important role in constraining the viability of various new physics scenarios, thereby complementing the direct collider searches. The effects which give rise to large flavour changing neutral currents (FCNC), can also be potentially probed at the colliders. For instance, the possibility of observing a flavour violating Higgs decay at the Large Hadron Collider (LHC) was discussed in [216, 217, 218]. Further, an observation of a 2.5 σ excess in the $H \to \tau\mu$ channel by CMS [219] in the LHC experiment has generated a lot of interest in this sector and has led to a plethora of analysis [220, 221, 222, 223, 224, 225, 226, 227, 228, 229, 230, 231, 232, 233]. The leptonic sector in the Standard Model (SM) is also interesting owing to the absence of FCNC. This can be attributed to the massless nature of neutrinos in the SM. The observation of neutrino oscillations, which consequently led to a confirmation of the massive nature of left handed neutrinos, resulting in a non-zero decay rate for rare processes like $\mu \to e\gamma$. The predicted branching ratio (BR) in the SM, however is negligibly small ($\sim 10^{-40}$) due to the tiny neutrino mass and is beyond the sensitivity of the current flavour experiments. There exist several extensions of the SM which contribute to rare processes such as $\mu \to e\gamma$ via loops, enhancing the BR substantially to $\sim 10^{-13} - 10^{-15}$ and expected to be within the reach of the indirect flavour probes. Needless to say, an observation of such processes is a definitive signal of the presence of physics beyond the SM. Therefore, looking for a signal of lepton flavour violation (LFV) directly or indirectly is a challenging avenue to find NP. Following this argument, we explore the possibility of

observing lepton flavour violation at the LHC.

There are several models in literature which discuss the possibility of flavour violation in the leptonic sector. In the current analysis we focus on the supersymmetric extensions of the SM which can possess soft masses having significant flavour mixing in the mass basis of fermions. This can lead to new contributions to the BR of rare processes. For instance, soft masses with flavour mixing can arise in see-saw extensions of SUSY [234, 235, 236] and also inspired by SUSY GUT [237, 238, 239, 240, 241]. Alternatively, introduction of flavour symmetries [242, 243], models with messenger matter mixing in gauge mediated supersymmetry breaking (GMSB)[244, 245, 246, 247, 248], models with R-symmetric supersymmetry [249, 250], supersymmetric theories in the presence of extra-spatial dimensions [251, 252, 253] *etc.* also lead to flavourful soft masses. Scenarios in which mass splitting lead to flavour violation have been considered in [246, 254, 255]. Such extensions in general lead to flavoured soft masses and depending on the parameters can lead to observable rates for the flavour violating decays in the squark and leptonic sector.

Flavour mixing in the sfermion mass matrices can be probed at the collider by the flavour violating decay of a sparticle of flavour (say i) into a fermion of flavour j where $j \neq i$. Flavour violating decays of sleptons were studied in the context of e^+e^- linear collider [256, 257, 258, 259, 260, 261, 262]. In Ref. [263] the authors studied the possibility of observing CP violation from slepton oscillations at the LHC and NLC. At the LHC, the sleptons can be produced either through Drell-Yan (DY) process or by cascade decays from heavier sparticles. Subsequent flavour violating decays of sleptons produced by DY were studied in [264, 265] while those produced by cascade decays were studied in [266, 267, 268, 269, 270, 271, 272]. Probing LFV through the measurement of splitting in the mass eigenstates of sleptons was considered in [273, 274, 275]. In this chapter we report on our study of flavour violation in the leptonic sector by producing sleptons in cascade decays through pair production of neutralino-chargino at the future LHC experiments.

Starting with MSSM, we write the most general structure for the slepton mass matrix. The constraints on the model from the non-observation of flavour violating processes can be expressed by working in the mass-insertion approximation (MIA) [235, 276] in terms of bounds on the flavour violating parameter δ_{ij}, $i \neq j$ as defined in Eq.6.2 [277]. A non-zero δ_{ij} also opens up the possibility of flavour violating decay as far as collider implications of flavoured slepton masses are concerned.

Our goal is to probe the flavour violating decay in the case of first two generations in the slepton sector in SUSY. In this context strong bounds exist on the flavour violating parameter, coming primarily from the non-observation of $\mu \to e\gamma$ [278]. There exist regions of parameter space where these bounds can be relaxed owing to cancellations between different diagrams contributing to this process, thereby giving access to probe LFV at the colliders.

In this letter we explore this possibility to look for LFV decays considering neutralino-chargino pair production in proton-proton collisions, which eventually leads to three lepton and missing energy final state. The tri-lepton final state is characterized by the presence of two leptons with opposite flavour and opposite sign combination (OFOS). The presence of LFV in the tri-lepton final state is ensured by demanding a combination of same flavour same sign (SFSS) lepton pair along with the OFOS combination. While an imposition of this SFSS criteria along with OFOS has a tendency to decrease the signal, it aids in suppressing the backgrounds due to SM and SUSY significantly.

The chapter is organized as follows: In Section 6.2 we discuss the model set-up introducing the various parameters relevant for the analysis in the framework of a simplified model. Relevant regions of parameter space consistent with the flavour constraints and conducive to be probed at the colliders are identified in this section. In Section 6.3 we explain our choice of OFOS and SFSS combination to extract the signal with a detailed description of the simulation. The results of the simulation for the background and the representative points for the signal events are presented. In Section 6.4 we show regions of the parameter space which can be probed at the LHC Run 2 experiment in the near future. We conclude in Section 6.5.

6.2 Model Parametrization

In this section we introduce the basic model set-up and related parameters necessary to describe LFV. In order to reduce the dependence on many parameters, we consider a simplified SUSY model (SMS) approach with only left handed sleptons, wino and a bino while decoupling the rest of the spectrum. The μ term is assumed to be ~ 1 TeV to make the neutralino/chargino dominantly composed of gauginos with a very small higgsino component. In this case, the mass of χ_2^0, the second lightest neutralino and $\chi_1^\pm$, the lightest chargino, are roughly the same as $\sim M_2$, the mass of the $SU(2)$ gauginos. The lightest neutralino χ_1^0, which is assumed to be the lightest supersymmetric particle (LSP) has mass $\sim M_1$, same as the mass of the $U(1)$ gaugino.

For the slepton sector we focus on the flavour violation in the left handed sector making the right handed sleptons very heavy and set the left-right chiral mixing in the slepton mass matrix to be negligible. For simplicity, we assume only two generations. With these assumptions, the left handed slepton mass matrix in the basis $l_F \equiv (\tilde{e}_F, \tilde{\mu}_F)$ is given as,

$$\tilde{m}^2 = \begin{bmatrix} m^2_{L_{11}} & m^2_{L_{12}} \\ m^2_{L_{12}} & m^2_{L_{22}} \end{bmatrix}, \tag{6.1}$$

where F denotes the flavour basis (SUPER CKM) for the sleptons. In this basis the flavour violating parameter δ_{12} is parametrised as [235, 276],

$$\delta_{12} = \frac{m^2_{L_{12}}}{\sqrt{m^2_{L_{11}} m^2_{L_{22}}}}. \tag{6.2}$$

Naturally, this flavour violating parameter δ_{12} is coupled to the rates corresponding to flavour violating rare decays in the first and second generation lepton sector. Hence an upper bound on this parameter exists due to non-observations of these rare decays like $\mu \to e\gamma$ [278], $\mu - e$ conversion [279] and $\mu \to eee$ [280].

In order to obtain the mass eigenvalues of the sleptons, the matrix in Eq.6.1 can be rotated into a diagonal form by an angle θ given by,

$$\sin 2\theta = \frac{2m^2_{L_{12}}}{m^2_{L_2} - m^2_{L_1}}, \tag{6.3}$$

where $m^2_{L_i}$ are the eigenvalues. It can be related to the flavour violating parameter δ_{12} as,

$$\delta_{12} = \frac{\sin 2\theta (m^2_{L_2} - m^2_{L_1})}{2m^2_L} \tag{6.4}$$

where $m_L = \frac{m_{L_1} + m_{L_2}}{2}$. The structure of the mass matrix, Eq.6.1 allows for the possibility of flavour oscillations similar to neutrino flavour oscillations. The probability $P(\tilde{e}_F \to \mu)$ of a flavour eigenstate $\tilde{e}_F$ decaying into a muon is given by [258],

$$\begin{aligned} P(\tilde{e}_F \to \mu) &= \sin^2 2\theta \frac{(\Delta m^2)^2}{4\bar{m}^2\Gamma^2 + (\Delta m^2)^2} BR(\tilde{\mu} \to \mu), \\ &\sim \sin^2 2\theta \; BR(\tilde{\mu} \to \mu) \text{ for } \Gamma \ll \Delta m^2, \end{aligned} \tag{6.5}$$

with $\Delta m^2 = m^2_{L_2} - m^2_{L_1}$. The above expression can be re-expressed in terms of the parameter δ_{12} from Eq.6.4. Thus the branching ratio for the flavour violating decay, $\chi^0_2 \to e\, \tilde{e} \to e\, \mu\, \chi^0_1$ can be computed as,

$$BR(\chi^0_2 \to e\; \mu\; \chi^0_1) = \mathcal{B}_{LFV}\; BR(\chi^0_2 \to \tilde{e}\; e)\; BR(\tilde{e} \to e\chi^0_1) + e \leftrightarrow \mu \tag{6.6}$$

Here the suppression factor due to flavour violation is given by,

$$\mathcal{B}_{LFV} = \sin^2 2\theta = \left(\frac{m_L\; \delta_{12}}{\Delta m_{12}}\right)^2, \tag{6.7}$$

where $\Delta m_{12} = m_{L_2} - m_{L_1}$.

As mentioned before, bounds on δ_{12} and hence $\mathcal{B}_{LFV}$ can be obtained by taking into account the experimental upper limit on the $BR(\mu \to e\gamma) < 5.7 \times 10^{-13}$ [278]. The higher dimensional operator contributing to this process is parametrized as [281],

$$\mathcal{L}_{FV} = e\frac{m_l}{2}\ \bar{e}\ \sigma_{\alpha\beta}\left(A_L P_L + A_R P_R\right)\ \mu\ F^{\alpha\beta}, \tag{6.8}$$

where the model dependence is captured by the Wilson coefficients $A_{L,R}$. The branching ratio for this process is then given by [281],

$$BR(\mu \to e\gamma) = \frac{48\pi^3}{G_F^2}\left(|A_L|^2 + |A_R|^2\right). \tag{6.9}$$

In our considered model, $A_R \equiv 0$, as the right handed sleptons are assumed to be very heavy. A_L on the other hand receives three contributions due to chargino, neutralino and bino mediated diagrams and is given as [281],

$$A_L = \frac{\delta_{12}}{m_L^2}\left(\frac{\alpha_Y}{4\pi}f_n\left(\frac{M_1^2}{m_L^2}\right) + \frac{\alpha_Y}{4\pi}f_n\left(\frac{M_1^2}{m_L^2}\right) + \frac{\alpha_2}{4\pi}f_c\left(\frac{M_2^2}{m_L^2}\right)\right) \tag{6.10}$$

where $f_{n,c}$ are loop factors defined in [281] with a non-trivial mass dependence of related sparticles and α_Y, α_2 are the $U(1)_Y$ and $SU(2)$ gauge couplings.

The analysis can be simplified again by choosing the following parametrization for the mass M_1 of the (LSP) χ_1^0,

$$M_1 = \frac{M_2}{2}, \tag{6.11}$$

which is the relation at the electroweak scale due to unification of gaugino masses at the GUT scale. For the sleptons we choose,

$$M_2 > m_L > M_1. \tag{6.12}$$

This relation assumes that the intermediate sleptons in χ_2^0 decay are produced on-shell by requiring that they are lighter than the mass of $\chi_2^0 \simeq M_2$. Under these assumptions, we try to find the available range of parameters allowed by existing $\mu \to e\gamma$ constraints as will be discussed later. Fig.6.1 shows the region in the $M_2 - m_L$ plane for which the conditions in Eq.6.11 and 6.12 are satisfied (green region). It depicts the region of parameter space which is of interest as far as collider implications are concerned as discussed in this chapter.

The blue region shows the parameter space for which $BR(\mu \to e\gamma) < 5.7 \times 10^{-13}$ is satisfied for $\delta_{12} = 0.01$ in the left plot and for $\delta_{12} = 0.02$ in the right plot. As expected, due to the smaller value of δ_{12}, the blue region in the left plot has a larger overlap with the green region as compared to the plot in the right, thereby admitting smaller slepton masses. The orange region in both the plots shows the parameter space for which $BR(\mu \to e\gamma) < 5.7 \times 10^{-13}$ is satisfied for $\delta_{12} = 0.1$. We find that there is virtually no overlap with the region which is of interest to us from the view of collider searches.

It would be interesting to estimate the suppression factor $\mathcal{B}_{LFV}$ corresponding to the allowed region in the $M_2 - m_L$ plane for the values of δ_{12} in Fig.6.1. As seen in Eq.6.7, the parameter

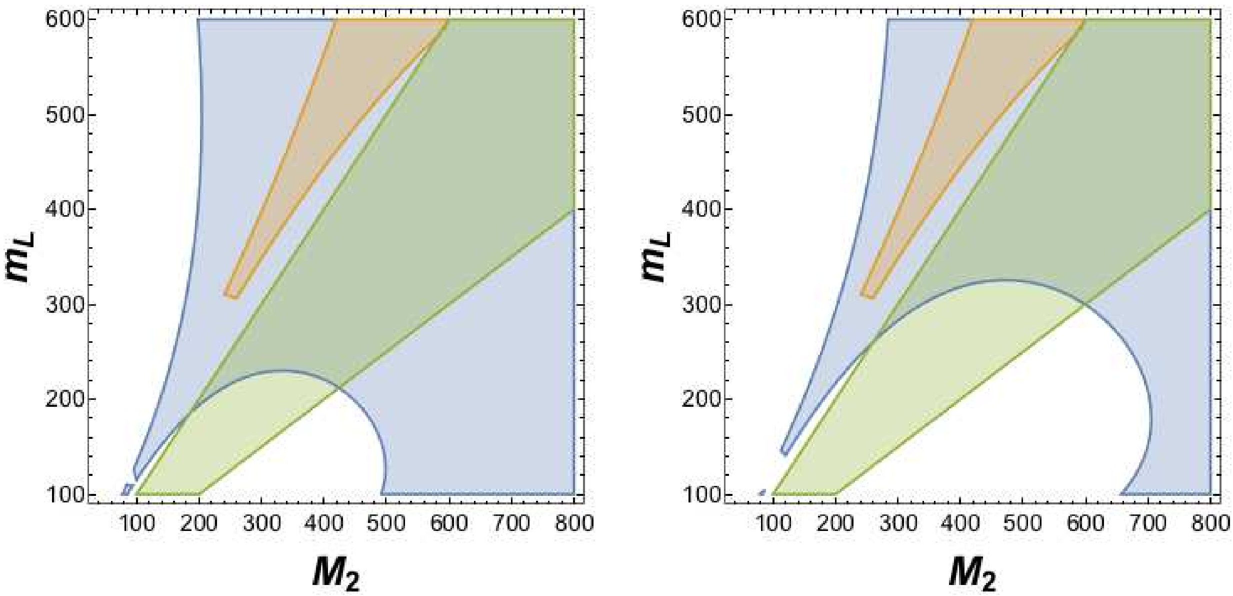

Figure 6.1: Region satisfying Eq.6.11 and 6.12 (green), while the orange regions satisfy the $\mu \to e\gamma$ constraint for $\delta_{12} = 0.1$. The blue regions are allowed by the upper bound on $\mathrm{BR}(\mu \to e\gamma)$ for $\delta_{12} = 0.01$ (left) and $\delta_{12} = 0.02$ (right). Units of mass are in GeV.

$\mathcal{B}_{LFV}$, which determines the rate for LFV, is sensitive to the mass-splitting $\Delta m = m_{L_2} - m_{L_1}$ and m_L. $\mathcal{B}_{LFV}$ increases with δ_{12} which can only be accommodated with a larger m_L. Thus smaller values of δ_{12} are not conducive to generate a large $\mathcal{B}_{LFV}$. $\mathcal{B}_{LFV}$ is also inversely proportional to the mass splitting Δm. However, it cannot increase indefinitely as $\mathcal{B}_{LFV} \leq 1$, leading to a lower bound on Δm. Fig.6.2 demonstrates the contours of constant $\mathcal{B}_{LFV}$ in the $\Delta m - m_L$ plane. We find that for $\delta_{12} = 0.02$, slepton in excess of 250 GeV are required to get $\mathcal{B}_{LFV} \geq 0.1$, while being consistent with the flavour constraints (overlap of blue and green region) in Fig. 6.1.

6.3 Signal and Background simulations

As mentioned in the introduction, we probe the signal of LFV in slepton decay producing it via cascade decays of sparticles which are produced in proton-proton collisions at the LHC. Here we focus on $\chi_1^\pm \chi_2^0$ production which eventually leads to a tri-lepton final state as,

$$pp \to \begin{cases} \chi_2^0 \to l_i^\pm \tilde{l}_i^\mp \to l_i^\pm l_j^\mp \chi_1^0, & i \neq j, \\ \chi_1^\pm \to l_i^\pm \nu \chi_1^0, \end{cases} \tag{6.13}$$

where i, j denote flavour indices (e, μ). The flavour violating vertex causes the decay of a slepton $(\tilde{l}_i)$, coming from χ_2^0 decay, in Eq.6.13, into a lepton of flavour l_j with $i \neq j$. It is clear from the above process that the signature of LFV is the presence of 3 leptons of which 2 leptons are with opposite flavour and opposite sign (OFOS) in addition to missing

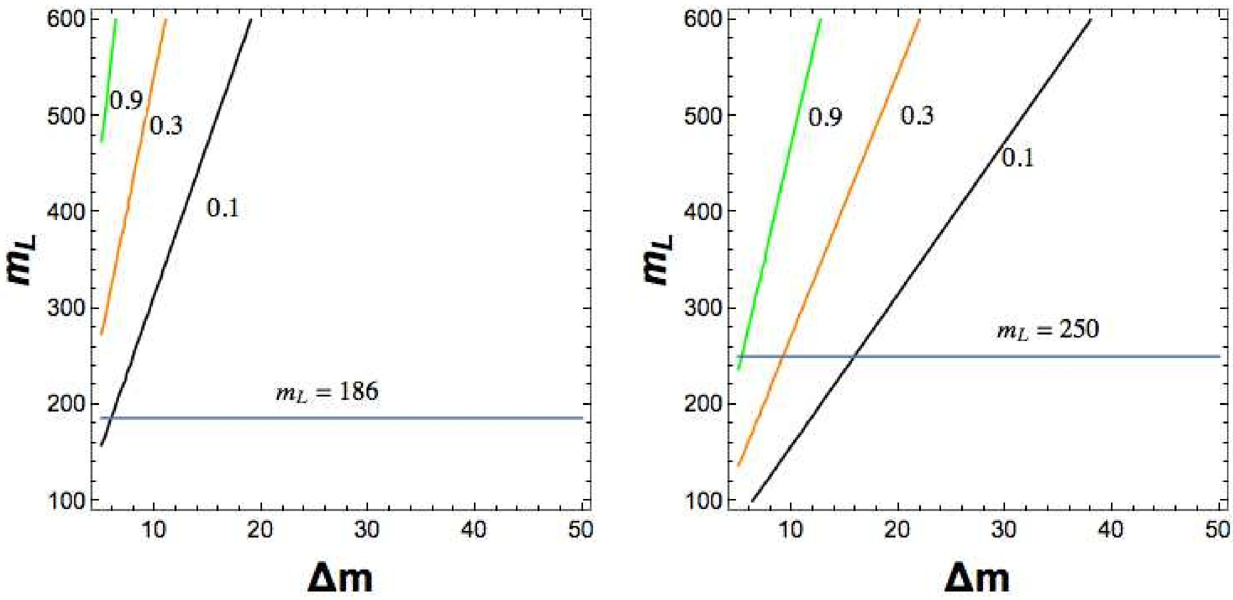

Figure 6.2: Contours of $\mathcal{B}_{LFV}$ for δ_{12}=0.01 (left) and $\delta_{12} = 0.02$ (right). The horizontal blue line is excluded by $BR(\mu \to e\gamma)$ for $\delta_{12} = 0.01$ (left) and $\delta_{12} = 0.02$ (right). The units of mass are in GeV.

energy (E) due to the presence of two LSP and neutrino. The leptons with OFOS originate from χ_2^0 decay while the third lepton comes from the $\chi_1^\pm$ decay. Thus, following this decay scenario, it is possible to have 8 combinations of tri-leptons, each having at least one OFOS lepton pair as,

$$\begin{aligned} &e^+e^+\mu^- \ ; e^-e^-\mu^+ \ ; \mu^-e^+\mu^- \ ; \mu^+e^-\mu^+ \\ &e^+e^-\mu^+ \ ; e^-e^+\mu^- \ ; \mu^+e^+\mu^- \ ; \mu^-e^-\mu^+. \end{aligned} \tag{6.14}$$

On the other hand, the pair production of $\chi_1^\pm\chi_2^0$ will also give rise to tri-lepton final state with a flavour conserving decay of χ_2^0 *i.e.* $\chi_2^0 \to l^+l^-\chi_1^0$. Note that this flavour conserving decay scenario also results in 8 combinations of tri-lepton final state given as

$$\begin{aligned} &e^+\mu^+\mu^- \ ; e^-\mu^+\mu^- \ ; \mu^-e^+e^- \ ; \mu^+e^+e^- \\ &\mu^+\mu^+\mu^- \ ; e^-e^+e^- \ ; e^+e^+e^- \ ; \mu^-\mu^-\mu^+ \end{aligned} \tag{6.15}$$

out of which four combinations of OFOS exist as seen in the first line of Eq.6.15. It is clearly a potential background corresponding to the signal channel in Eq.6.14 and expected to have the same rate as signal. However, a closer look at these two final states in Eq.6.14 and 6.15 reveals a characteristic feature. For example, in the case of signal, out of the 8 combinations of tri-leptons with OFOS combinations, notice that four combinations shown in the first line in Eq.6.14, also possess a pair of leptons with same flavour and same sign (SFSS) which are absent in the background final states, shown in Eq.6.15. The rest of the states with

OFOS combination in Eq.6.14 are identical to the final states given in Eq.6.15. We exploit this characteristic feature to extract the LFV signal events out of all three lepton events including all backgrounds. Thus our signal is composed of three leptons having combinations of both OFOS and SFSS together, which is an unambiguous and robust signature of LFV in SUSY. Note that while choosing a clean signature of LFV decay in SUSY, we pay a price by a factor of half as is clear from Eq.6.14. However, this specific choice of combinations in tri-leptons is very powerful in eliminating much of the dominant SM backgrounds arising from WZ and $t\bar{t}$ following leptonic decays of W/Z and top quarks.

We now discuss our simulation strategy to estimate the signal rates while suppressing the SM and SUSY backgrounds. We performed simulations for both signal and background using `PYTHIA8` [282] at 14 TeV centre of mass energy and applying the following selections:

• **Jet selection:** The jets are reconstructed using `FastJet` [283] and based on anti k_T algorithm [284] setting the jet size parameter $R = 0.5$. The jets passing the cuts on transverse momentum $p_T^j \geq 30$ GeV, pseudo-rapidity $|\eta^j| \leq 3.0$, are accepted.

• **Lepton selection:** Our signal event is composed of three leptons and are selected according to the following requirement on their transverse momenta and the pseudo-rapidity: $p_T^{\ell_{1,2,3}} \geq 20, 20, 10$ GeV; $|\eta^{\ell_{1,2,3}}| \leq 2.5$, where the leptons are p_T ordered with $p_T^{\ell_1}$ being the hardest one. In addition, the leptons are also required to be isolated *i.e.* free from nearby hadronic activities. It is ensured by requiring the total accompanying transverse energy, which is the scalar sum of transverse momenta of jets within a cone of size $\Delta R(l, j) \leq 0.3$ around the lepton, is less than 10% of the transverse momentum of the corresponding lepton.

• **Missing transverse momentum:** We compute the missing transverse momentum by carrying out a vector sum over the momenta of all visible particles and then reverse its sign. Since p_T is hard in signal events, so we apply a cut $p_T \geq 100$ GeV.

• **Z mass veto:** We require that in three lepton events, the invariant mass of two leptons with opposite sign and same flavour should not lie in the mass window $m_{ll} = M_Z \pm 20$ GeV. It helps to get rid of significant amount of WZ background.

• ***b* like jet selection:** The b jets are identified through jet-quark matching *i.e.* those jets which lie with in $\Delta R(b, j) < 0.3$ are assumed to be b like jets.

• **OFOS:** Our signal event is characterised by the requirement that it has at least one lepton pair with opposite flavour and opposite sign.

• **SFSS:** We require the presence of SFSS combination along with OFOS combination in three lepton final state, which is the characteristic of our signal. As stated before, this criteria is very effective in isolating the background due to the same SUSY process but for their subsequent flavour conserving decays, in particular for χ_2^0 decay.

We perform our analysis by choosing various representative points in the SUSY parameter space. The spectrum is generated using `SUSPECT` [285] and the decays of the sparticles are computed using `SUSYHIT` [286]. Table 6.1 presents the six representative points (A-F) for which we discuss the details of our simulation. From A to F, the spectrum is characterized by increasing masses of gauginos, with the slepton mass m_L lying midway between the two,

$m_L = (M_1 + M_2)/2$.

Spectrum Characteristics	A	B	C	D	E	F
$\chi_2^0/\chi_1^\pm$	210	314	417	518	619	718
χ_1^0	95.8	144	193	241	290	339
m_L	156	229	303	377	452	526
$BR(\chi_2^0 \to \tilde{e}_L e)$	0.13	0.15	0.16	0.16	0.16	0.16
$BR(\chi_2^0 \to \tilde{\mu}_L \mu)$	0.13	0.15	0.16	0.16	0.16	0.16

Table 6.1: Representative choices of SUSY parameter space. All masses are in GeV.

In Table 6.2 and 6.3 we present the effects of selection of cuts in simulation for both the signal and backgrounds respectively. In addition to the SM backgrounds which are mainly due to $t\bar{t}$ and WZ, we also simulate the background taking into account the contributions due to flavour conserving decay of χ_2^0 for each of the representative points in Table 6.1. There are other sub-dominant backgrounds like tbW, ZZ if one lepton is missed or WW, if jets fake as leptons. However these backgrounds are expected to be very small and not considered here. We present results for signals corresponding to those representative parameter space as shown in Table 6.2 . In this table, the first column shows the sequence of cuts applied in the simulation, while the second column onwards event yields for the signal are shown. Table 6.3 presents the same for the backgrounds due to SUSY in the second column and the SM in the third column. Notice that lepton isolation requirement and a cut on p_T has considerable impact in reducing $t\bar{t}$ and WZ background. As noted earlier, we find the SFSS criteria to be very effective in isolating the SUSY background due to flavour conserving decay of χ_2^0 for all the representative points in Table 6.1 . Finally, it is possible to have large number of tri-lepton events in background processes, but imposition of specific choices like OFOS and SFSS along with large missing energy cut help in isolating it to a great extent as shown in Table 6.3 . In spite of this suppression of background events, the signal yields are far below than the total background contribution owing to it's huge production cross sections as shown in Table 6.3. Therefore, in order to improve signal sensitivity further, we impose additional requirements by looking into the other characteristics of signal events. For example, signal events are free from any kind of hadronic activities at the parton level i.e. no hard jets are expected in the signal final state, whereas in background process, in particular events from $t\bar{t}$ are accompanied with large number of jets. We exploit this fact to increase signal sensitivity by adding following criteria.

Case a: Jet veto
In this case we reject events if it contain any hard jets. In Table 6.3 we see that while the jet veto criteria reduces the $t\bar{t}$ and WZ background significantly, but it also substantially damage the signal by a factor of 2 or 3 as shown in Table 6.2 . In signal process, jets arise mainly from the hadronic radiation in initial and final states and it is true for all the representative signal points. The reason can be attributed to enhancement of hadronic activities at higher energies. Nevertheless the jet veto seems to be useful to improve signal

	Signal($\chi_2^0\chi_1^\pm$)					
$M_2 \Longrightarrow$	200	300	400	500	600	700
No. of events generated	10000	10000	10000	10000	10000	10000
$p_T^{\ell_{1,2}} > 20, p_T^{\ell_3} > 10, \lvert\eta\rvert < 2.5$	1371	1752	2014	2218	2225	2342
Lepton isolation cut	1330	1669	1883	2055	2036	2112
$p_T > 100$	474	959	1326	1600	1683	1860
OFOS	470	952	1319	1581	1659	1828
Z mass veto	423	849	1218	1485	1574	1752
SFSS	223	462	640	783	804	892
Case a: jet veto	91	205	288	337	346	380
Case b: b-like jet veto	221	458	635	777	798	884
Case c: $n_j \leq 1$ and b-like veto	161	375	479	604	617	687

Table 6.2: Event summary for signal after all selections. All energy units are in GeV.

	SUSY($\chi_2^0\chi_1^\pm$)						SM	
	A	B	C	D	E	F	$t\bar{t}$	WZ
$M_2 \Longrightarrow$	200	300	400	500	600	700	-	-
Cross section (fb) at 14 TeV	1.65×10^3	370.5	118.8	45.6	20.5	9.57	9.3×10^5	4.47×10^4
No. of events generated	10000	10000	10000	10000	10000	10000	10^7	3×10^6
$p_T^{\ell_{1,2}} > 20, p_T^{\ell_3} > 10, \lvert\eta\rvert < 2.5$	1299	1779	2015	2195	2245	2361	164895	23960
Lepton isolation cut	1251	1672	1874	2044	2051	2131	70233	22366
$p_T > 100$	454	967	1311	1624	1722	1872	19241	1669
OFOS	209	482	656	820	855	918	14012	858
Z mass veto	126	346	547	728	768	853	12395	122
SFSS	4	6	11	14	15	25	4598	22
Case a: jet veto	≤ 1	1	1	5	4	4	29	≤ 1
Case b: b-like jet veto	4	5	10	14	13	23	131	13
Case c: $n_j \leq 1$ and b-like veto	1	3	7	9	9	19	48	5

Table 6.3: Event summary for SUSY and SM background. All energy units are in GeV.

to background ratio. However we consider two more alternatives with a goal to increase signal sensitivity further:

Case b: b-like jet veto
Here we eliminate events if there be at least one b like jet. As can be seen Table 6.3, b jet veto is more efficient than the jet veto condition, as the $t\bar{t}$ background is suppressed by a few orders of magnitude without costing the signal too much.

Case c: Apply b-like jet veto and number of jets $n_j \leq 1$
Here we apply the b-like jet veto condition along with the presence of maximum one jet. As seen in Table 6.3 , it is very helpful in reducing the $t\bar{t}$ background significantly but it does not affect the signal as much as the simple jet veto condition ($n_j = 0$) does alone.

Note that we have identified b-like jets by a naive jet-quark matching which is an overestimation from the realistic b-jet tagging[287] which is out of scope of the present analysis. However, for the sake of illustration, we present these results with b-jet veto, (case (b) and (c)), to demonstrate that this criteria might be very useful in suppressing backgrounds, which requires more detector based simulation. In view of this, we focus only on the results obtained by using jet veto, case(a) for further discussion.

We also present the dilepton ($e\mu$) invariant mass distributions for the spectrum A (left) and F (right) in Fig.6.3 normalizing it to unity. It is subject to all primary selection cuts on leptons and jets, including the OFOS and SFSS combination. The $m_{e\mu}$ distribution is expected to have a sharp edge on higher side, which can be derived analytically from kinematical consideration. The position of this edge of $m_{e\mu}$ is given as [268, 288],

$$(m_{e\mu}^{max})^2 = m_{\chi_2^0}^2 \left(1 - \frac{m_L^2}{m_{\chi_2^0}^2}\right)\left(1 - \frac{m_{\chi_1^0}^2}{m_L^2}\right). \tag{6.16}$$

The appearance of an edge in the $m_{e\mu}$ distribution is a clear indication of LFV vertex in the χ_2^0 decay. However, this $m_{e\mu}$ distribution is affected by a combinatorial problem. For each tri-lepton event, two OFOS pairs can be constructed: a) both leptons coming from χ_2^0 decay and b) "imposter" pair with one lepton from χ_2^0 and the other from $\chi_1^\pm$. In Fig.6.3 the red (dotted) curve represents the dilepton invariant mass distribution of the leptons tracked to the χ_2^0 vertex while blue (solid) curve corresponds to dilepton without any prior information about their origin. It (red dotted line) exhibits a very distinct edge as the identity of the lepton pair originating for χ_2^0 is known a-priori. The (solid) blue line is more realistic as it includes both the correct OFOS and SFSS pair as well as the contamination due to the "impostor" pair which is responsible for a tail beyond the edge. As a result it exhibits a more diffused behaviour near the position of the edge. However, we can roughly estimate the position of the edge using the blue (solid) line as ~ 120 GeV for the left panel and ~ 375 GeV for the right panel. We find that these values are in fairly good agreement with the corresponding numbers used in our simulation. It may be noted here that such distributions with a sharp edge are the characteristic feature of these type of decays which can also be

Figure 6.3: OFOS dilepton invariant mass distribution for spectrum A (left) and spectrum F (right). The events are selected at the SFSS level.

Properties	Signal (S)						Background (B)	
	A	B	C	D	E	F	$t\bar{t}$	WZ
Cross section (fb) at 14 TeV	1.65×10^3	370.5	118.8	45.6	20.5	9.57	9.3×10^5	4.47×10^4
Normalized cross sections								
Case a: jet veto	15.01	7.59	3.41	1.51	0.67	0.37	2.69	≤ 1
Case b: b-like veto	36.4	16.9	7.54	3.54	1.63	0.85	12.1	0.19
Case c: $n_j \leq 1$ and b-like veto	26.5	13.9	5.7	2.75	1.26	0.66	4.4	0.07
$\frac{S}{\sqrt{B}}$(@100) fb^{-1}								
Case a: jet veto	91.43	45.93	20.78	9.32	4.31	2.24	-	-
Case b: b-like veto	100.99	47.87	21.34	10.04	4.64	2.43	-	-
Case c: $n_j \leq 1$ and b-like veto	122.4	64.4	26.4	12.8	5.92	3.12	-	-

Table 6.4: Normalized cross-section (fb) and $S/\sqrt{B}$ for signal and background subject to three selection conditions

exploited to suppress backgrounds [268] in order to increase signal to background ratio.

6.4 Results and Discussions

Table 6.4 gives the normalized signal and background cross-sections due to all selection cuts. These are obtained by multiplying the production cross section given in the first row by acceptance efficiencies. The production cross section are estimated by multiplying the leading order (LO) cross section obtained from `PYTHIA8` with the corresponding k factors [1]. Corresponding to these signal and background cross sections, we also present the signal significance by computing $S/\sqrt{\text{B}}$ for integrated luminosity 100 fb^{-1} as shown in the bottom of Table 6.4. Although case(b) corresponding to b-like jet veto results in the largest cross section for all signal parameter space, signal significance does not improve due to comparatively less suppression of SM backgrounds. With the increase of gaugino masses acceptance efficiencies goes up as final state particles become comparatively harder, but $S/\sqrt{B}$ is depleted due to drop in $\chi_2^0\chi_1^\pm$ pair production cross-section. While estimating signal rates and significance, we assume a maximal flavour violation *i.e.* $\mathcal{B}_{LFV} = 1$. Obviously, a further suppression is expected by a factor $\mathcal{B}_{LFV}$ which depletes the BR of χ_2^0, (see Eq.6.6). For a given δ_{12}, $\mathcal{B}_{LFV}$ is a function of the slepton mass as well as the mass splitting Δm as shown in Fig. 6.2. For instance $S/\sqrt{B}$ may suffer by an order of magnitude for $\mathcal{B}_{LFV} = 0.1$. While the lower end of the spectrum can lead to a larger $S/\sqrt{B}$, the corresponding $\mathcal{B}_{LFV}$ decreases as we move further towards the IR part of the

[1]The appropriate k factors for $t\bar{t}$ and WZ processes is 1.6 [289] and 1.7 [290] respectively while for the signal it is 1.5 [291].

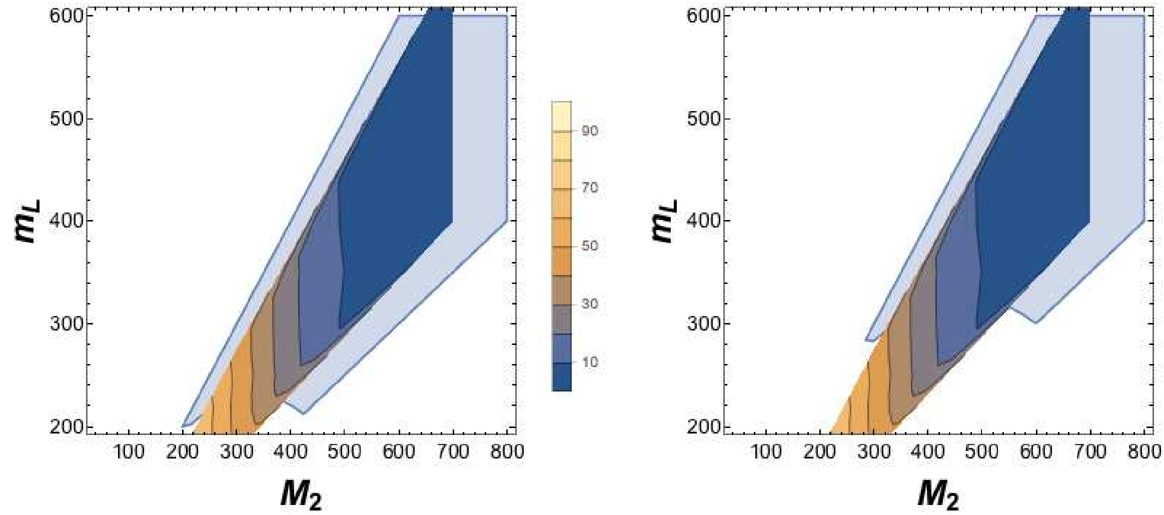

Figure 6.4: Variation of $S/\sqrt{B}$ (using jet veto, case (a) for different regions with two choices of $\delta_{12} = 0.01$ (left) and $\delta_{12} = 0.02$(right). The regions light blue are allowed by BR($\mu \to e\gamma$) constraint. Here we assume $\mathcal{B}_{LFV} = 1$. Masses are in GeV.

slepton spectrum. This can be attributed to stronger bounds on δ_{12} for lower slepton masses. Though the lower mass is not yet ruled out, it is more economical to consider relatively heavier slepton masses as the bounds from current and future experiments will be relatively weaker.

In Fig.6.4, we illustrate this mass sensitivity by presenting $S/\sqrt{B}$ obtained using jet veto condition case (a). Notice that for a given $\chi_1^\pm$ and χ_2^0 masses, signal is not very sensitive to slepton mass as long as it is produced on-shell from χ_2^0 decay and $M_{\chi_2^0} - m_L$ is sufficiently high. The regions in the $M_2 - m_L$ plane correspond to different values of $S/\sqrt{B}$ computed for $\mathcal{L} = 100$ fb^{-1} and by assuming $\mathcal{B}_{LFV} = 1$. The sleptons and gaugino masses follow the parametrisation in Eq.6.11 and 6.12. It is superimposed on the region satisfying $BR(\mu \to e\gamma) < 5.7 \times 10^{-13}$ for $\delta_{12} = 0.01$ (left) and $\delta_{12} = 0.02$ (right). As seen from Table 6.4 and Fig. 6.4, the signal significance is better for lower masses due to larger $\chi_2^0\chi_1^\pm$ pair production cross section. However, it suffers by smaller values of $\mathcal{B}_{LFV}$ corresponding to those slepton masses as shown in Eq.6.7 and Fig.6.2.

Fig.6.5 shows the sensitivity reach of $\mathcal{B}_{LFV}$ in the $M_2 - m_L$ plane using the parametrisation in Eq.6.11 and 6.12. The numbers in boxes for different coloured regions give the minimum values of $\mathcal{B}_{LFV}$ which can be probed, while requiring a 5σ discovery corresponding to those values of M_2 and m_L and are presented for two different options of luminosities: $\mathcal{L} = 100\ fb^{-1}$ (left) and $\mathcal{L} = 1000\ fb^{-1}$ (right). As the constraints from indirect flavour measurements get tighter, larger $\mathcal{B}_{LFV}$ can be attained with heavier slepton masses, while respecting bounds from the rare decays as shown in Fig. 6.1 and 6.2. For example, for lower masses $\chi_2^0 \sim \chi_1^\pm \sim 250$ GeV and $m_L \sim 200$ GeV, the LFV parameter $\mathcal{B}_{LFV} \sim 0.05$ or more can be probed at 5σ level of signal sensitivity for $\mathcal{L} = 100\ fb^{-1}$. As expected, the minimum $\mathcal{B}_{LFV}$ required for a 5σ sensitivity goes up, thereby reducing the sensitivity

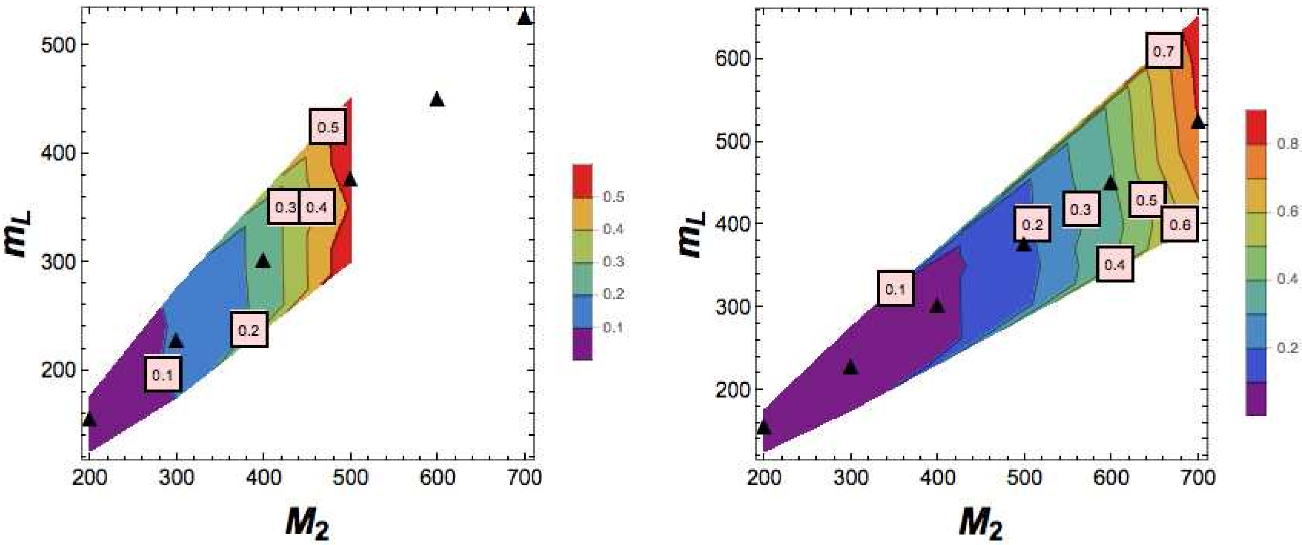

Figure 6.5: Minimum value (in small box) of $\mathcal{B}_{LFV}$ for a $S/\sqrt{B} = 5$ discovery for $\mathcal{L} = 100\ fb^{-1}$ (left) and $\mathcal{L} = 1000\ fb^{-1}$ (right). The $S/\sqrt{B}$ is computed using jet veto condition. The filled triangles correspond to the representative points A-F from left to right. The plot is truncated at the point where $\mathcal{B}_{LFV} > 1$ is required to get a 5 σ sensitivity of signal for that particular luminosity. Masses are in GeV.

of $\mathcal{B}_{LFV}$ measurement with the increase of gaugino and slepton masses and this can be attributed to the drop in cross-sections. The left plot in Fig.6.5 is terminated at the point corresponding to a requirement of $B_{LFV=1}$ for a 5σ discovery. As a result, the representative points E and F corresponding to heavier slepton masses are beyond the sensitivity of LHC at $\mathcal{L} = 100\ fb^{-1}$ as they require $\mathcal{B}_{LFV} > 1$ to achieve a 5σ discovery. However, flavour violating decays with heavier slepton masses as high as 650 GeV can be probed with an integrated luminosity of $\mathcal{L} = 1000\ fb^{-1}$ as shown in the right plot of Fig 6.5.

6.5 Comments and discussions

The observation of flavour violating rare decays would be one of the best indicators of the existence of physics beyond the SM. Measurements of such decays play an important role in constraining several new physics models and hence has received a lot of attention recently. We attempt to explore the flavour violation in the lepton sector in the context of well motivated models of flavourful supersymmetry. We follow an approach based on a simplified model with only the left handed sleptons along with the neutralinos which are gaugino dominated. We consider pair production of $\chi_2^0\chi_1^{\pm}$ and their subsequent leptonic decays which includes the LFV decays of χ_2^0. The final state is composed of three leptons and accompanied by large missing energy. In addition to the presence of a lepton pair with OFOS, we observed that certain tri-lepton combinations are also characterized by a lepton pair with SFSS -which is a unique and robust signature of LFV in SUSY.

The discovery potential of observing this LFV signal is primarily dependent on the masses of sleptons and gauginos. These masses are however constrained by non-observation of FCNC decays such as $\mu \to e\gamma$ and they get stronger as the flavour violating parameter δ_{12} becomes larger. We have identified the allowed range of slepton and gaugino masses relevant for our study. In addition variation of LFV parameter $\mathcal{B}_{LFV}$ with masses of slepton and mass difference between lepton mass eigenstates (Δm) are also presented.

Estimating the various background contributions, we predict the signal sensitivity for a few representative choices of SUSY parameters. The combination of three leptons with OFOS and SFSS is found to be very useful to achieve a reasonable sensitivity. It is found that for gaugino masses $\sim$ 250 GeV and slepton masses $\sim$200 GeV, the LFV parameter $\mathcal{B}_{LFV}$ as low as 0.05 can be probed with 100 fb^{-1} integrated luminosity. For heavier masses $\sim 600 - 700$ GeV, because of reduced $\chi_2^0\chi_1^\pm$ pair production cross section, the measurement of LFV parameter $\mathcal{B}_{LFV}$ requires higher luminosity $\sim$1000 fb^{-1}. Our study clearly establishes the prospects of finding LFV signal in this SUSY channel at the LHC Run 2 experiment with high luminosity options.

Chapter 7

Conclusions

The primary goal of this thesis was to use AdS-CFT tools to understand the shear viscosity of a class of strongly coupled field theories, in the presence of anisotropy. For this purpose, we had to construct and study several anisotropic blackbrane geometries. We found that in all our examples we studied, there was a parametric suppression of some components of shear viscosity in the presence of a constant driving force that broke the rotational symmetry. Motivated by the generality of the result, we also proposed an experiment involving trapped fermions at low temperatures where such an anisotropic shear viscosity tensor may arise. We found that there exist a suitable region of parameter space where the parametric suppression of suitable components of the anisotropic shear viscosity tensor may be measured. In this concluding chapter of the thesis we try to emphasize what we have learned so far. We also discuss some points which we need to investigate further in future.

- In Chapter 2 we performed the interpolation of the Bianchi attractor geometries (which are dual to anisotropic phases in the field theory with generalized translational invariance) in the IR (infrared) to Lifshitz and AdS spacetimes in the UV (ultraviolet). We wish to emphasize that we did not obtain these interpolating metrics as solutions to Einstein gravity coupled to suitable matter. Rather, what we achieved to show is that the matter required to support such geometries obey the weak and null energy conditions. These interpolating metrics do not have any non-normalizable metric deformations turned on near the boundary. This ensures that the dual field theory can indeed reside in flat space as opposed to some background of non-trivial geometry. The lesson we learn from these interpolations is that the symmetries of various Bianchi classes can emerge in the IR, either spontaneously or in response to some suitable source not involving the metric. We believe that these results will be of interest to the condensed matter community, given the fact that many interesting phases of matter are currently showing up in this arena of physics.

- In Chapter 3 we try to realize the near horizon geometries with Bianchi symmetries as solutions in gauged supergravity theories. We find a Bianchi III attractor solution in $\mathcal{N} = 2, D = 5$ gauged supergravity which is stable in the RG sense. We analyze the relevant Killing spinor equations and find that a radial ansatz for the spinor breaks all supersymmetry. This suggests that the above solution we found may be a non-supersymmetric attractor.

- In the second half of the thesis, in Chapter 4 we find a general formula for the shear viscosity in units of the entropy density given by the ratio of appropriate metric components evaluated at the horizon. In a situation with anisotropy, these metric components need not be the same. This can lead to a parametric violation of the bound proposed by Kovtun, Son and Starinets. ($\eta/s \geq \frac{1}{4\pi}$) which we abbreviate as KSS. Using techniques of Kaluza Klein reduction, we give a proof of this general formula for all situations where the force breaking isotropy is spatially constant and there is some residual Lorentz symmetry left in the boundary theory after breaking isotropy.

The general formula can be presented as follows: let z be the field theory direction along which a spatially constant driving force is turned on breaking rotational symmetry and x be a direction along which the boost symmetry is left unbroken, then the viscosity component η_{xz} is given by

$$\frac{\eta_{xz}}{s} = \frac{1}{4\pi}\frac{g_{xx}}{g_{zz}}\Big|_{u=u_h}, \tag{7.1}$$

where $g_{xx}|_{u=u_h}, g_{zz}|_{u=u_h}$ refer to the components of the background metric evaluated at the horizon. This result is true for all the anisotropic situations studied in Chapter 4 (Ref. [178]). This result was first derived in an anisotropic axion-dilaton system considered in [134].
In the isotropic situation, the metric components g_{xx} and g_{zz} are the same and we recover the result $\frac{1}{4\pi}$ of KSS. However in anisotropic situations, these metric components can behave very differently and thus leads to the parametric violations of the KSS bound.
Let us note that the proof of this general formula that was carried out in Chapter 4 relies on the assumption that the force responsible for breaking of rotational symmetry is spatially constant. The proof essentially maps the spin one shear viscosity components to conductivity in a lower dimensional theory using dimensional reduction. Since the fields breaking isotropy were linearly varying (the gradients of those fields were constants), different Kaluza Klein (KK) modes in the extra dimensions do not mix with each other. This can be easily seen from the fact that the equations of motion involve only gradients of these fields which are spatially constant.

- Motivated by these interesting results found in Chapter 4, we try to propose an experiment in Chapter 5 to measure such spin one components of shear viscosity in the unitary fermi gases. This set-up involves trapped, ultracold fermions in the unitary regime of the BEC-BCS crossover. Anisotropy is achieved by implementing a stronger confinement of the gas in one of the directions compared to the other directions. Based on the lessons learnt on the gravity side, we lay down a set of conditions such that the suppression of spin one component of shear viscosity may be measured experimentally in such systems. We present the relevant hydrodynamic modes which solve the equations of superfluid hydrodynamics and the trap parameters where this effect is likely to be seen. To the best of our knowledge, the proposal presented here is the first proposal to probe anisotropic shear viscosity in trapped fermions at low temperatures.

Our proposal involves a unitary Fermi gas in an anisotropic harmonic trap. We find that for the temperature at the center of the trap between 0.2 to 0.4 times the central chemical potential μ, the damping of oscillatory modes is dominated by a region where the background harmonic potential can be approximated as linear. AdS/CFT then suggests a reduction in the spin 1 component of the shear viscosity. For $\mu = 10\mu$K, $T = \frac{T_c}{2}$ ($T_c \approx 0.4\mu$), and $\omega_z \sim 2\pi \times 77000$ rad/s, we find $\kappa \sim 1$. A Boltzmann analysis in this regime also predicts an order unity reduction in spin 1 shear viscosity components.
Two hydrodynamic modes, an elliptic mode and the well known scissor mode, are sensitive to this reduction in viscosity. The angular amplitudes and the decay times are comparable to those measured in [182]. In the extreme situation for where $\kappa \sim 1$, our theoretical estimate for the correction to the viscosity (Eq. 5.101) breaks down. (For example higher order terms in Eq. 5.101 become important. Additionally, for $\kappa \sim 1$, $\mu/\omega_z \sim 2.7$ and shell effects, although somewhat weak in the unitary Fermi gases [210], may also become important.) But by gradually increasing ω_z from $\omega_z \sim 2\pi \times 10^4$rad/s to $\omega_z \sim 2\pi \times 77000$ rad/s one could measure the tendency of η_{xz} to decrease. For example, one can consider $\omega_z = 0.9T = 0.18\mu$ for which $\kappa_{LDA} = 0.48 < 1$. This gives a correction

$$\frac{\Delta\eta}{\eta} \approx -9\% \tag{7.2}$$

which — while not large — is still substantial.
The damping rate for the scissor mode has been measured in the BEC-BCS crossover region for weakly anisotropic traps in [182]. It will be interesting to see how the damping rate changes as ω_z is increased. On the other extreme, damping of the breathing and the radial quadrupole mode (both insensitive to η_{xz}) was measured in the 2D Fermi gas [213]. It will be interesting to study the scissor mode in these traps for smaller ω_z. We hope our experimental colleagues in the cold atoms community

will find our proposal interesting and explore anisotropic viscosities in trapped unitary fermions.

- The final chapter of the thesis is a parallel investigation that is independent of the developments of the earlier chapters and hence can be read independently. Here we considered models of supersymmetry which can incorporate sizeable mixing between different generations of sfermions and performed a detailed collider analysis to devise a signal to probe the lepton flavour violating parameter in such models relevant for the LHC.

We now list a few open and interesting questions that we have left for the future.

- Although we were successful regarding the interpolation of Bianchi Types II, III, VI and IX in Chapter 2, the interpolating metric of Bianchi Type V failed to satisfy the null energy conditions. Our failure in this case may be due to the restricted class of functions we used to construct the interpolating metrics or perhaps it may suggest a more fundamental constraint. Another interesting question is how the anisotropic and homogeneous phases in these field theories, described by the Bianchi attractor regions, can arise in practice? It will be interesting to examine the possibility of a spontaneous breaking of rotational invariance or by turning on sources other than the metric in the field theory.

- An immediate extension of the work on shear viscosity in strongly coupled fluid in presence of anisotropy is to extend our analysis to cases where the breaking of isotropy is spontaneous or when the driving force is not spatially constant. It is also natural to consider string theory embeddings of the anisotropic systems we have studied and examining if they are stable. In principle all transport coefficients which determine the fluid mechanics can be obtained by carrying out a more systematic derivative expansion on the gravity side as discussed in the fluid gravity correspondence described in [292], [293],[294], [295]. It will be great to perform a similar analysis along those lines. Another direction is to consider transport properties in phases corresponding to Bianchi spaces which describe homogeneous but anisotropic phases in general. Some progress in this regard has been made [159] for Bianchi VII. It will be interesting to extend the analysis to all Bianchi types. It will also be interesting to see if these results are relevant for neutron stars with very high magnetic fields (known as magnetars) for breaking rotational invariance [1]. The resulting equilibrium phase could then be highly anisotropic and our results hint that suitable components of the viscosity might become small.

- An important point worth noting is that while the cold-atom system proposed in this thesis shares many features with those discussed in Chapter 4 (Ref. [139, 178]),

[1]A magnetic field of order 10^{16} Tesla or so is needed in order to contribute an energy density comparable to the QCD scale ~ 200 Mev.

it also has some differences. First, in equilibrium the stress energy tensor is not invariant under translations even for a linear potential. Second, in addition to energy-momentum, the cold-atom system features another conserved quantity: the particle number. Consequently the system is locally characterized by two thermodynamic variables T and μ rather than just T. It will be interesting to further study the behavior of viscosity in gravitational systems which correspond to anisotropy driven strongly coupled systems with a finite chemical potential. As a first step, we have analyzed a weakly coupled system with a linearly varying potential and also a system in gravity ie. the RN blackbrane (see [215]). In both situations we find that the anisotropic viscosity does become parametrically small.

Appendix A

Appendices for Chapter 2: *Interpolating from Bianchi Attractors to Lifshitz and AdS spacetimes*

A.1 Three Dimensional Homogeneous spaces

We now discuss the three dimensional homogeneous spaces and their classification. Such spaces have three linearly independent Killing vector fields, ξ_i, $i = 1, 2, 3$. The infinitesimal transformations generated by these Killing vectors can carry any point in this space to another neighbouring point. The real algebra of these Killing vectors is given by

$$[\xi_i, \xi_j] = C^k_{ij}\xi_k. \tag{A.1}$$

There are 9 different such algebras and this is known as the Bianchi classification ([296], [297]).

In each case there are three linearly independent invariant vector fields, X_i, which commute with the three Killing vectors

$[\xi_i, X_j] = 0.$

The X_i's satisfy the algebra

$[\mathrm{X}_i, X_j] = -C^k_{ij}X_k.$

There are also three one-forms, ω^i, which are dual to the above invariant vectors X_i. The Lie derivatives of these one-forms along the ξ_i vanish, thus they are invariant along the ξ directions as well. The ω^i's satisfy the relations

$\mathrm{d}\omega^i = \frac{1}{2}C^i_{jk}\omega^j \wedge \omega^k.$

Below we give a list which contains the structure constants for the 9 Bianchi algebras, in a particular basis of generators. We refer to [297] for more details.

- **Type I**: $C^i_{jk} = 0$

$$\xi_i = X_i = \partial_i,\ \omega^i = dx^i,\ d\omega^i = 0 \tag{A.2}$$

- **Type II**: $C^1_{23} = -C^1_{32} = 1$ and rest $C^i_{j,k} = 0$

$$\begin{array}{cccc} \xi_1 = \partial_2 & X_1 = \partial_2 & \omega^1 = dx^2 - x^1 dx^3 & d\omega^1 = \omega^2 \wedge \omega^3 \\ \xi_2 = \partial_3 & X_2 = x^1\partial_2 + \partial_3 & \omega^2 = dx^3 & d\omega^2 = 0 \\ \xi_3 = \partial_1 + x^3\partial_2 & X_3 = \partial_1 & \omega^3 = dx^1 & d\omega^3 = 0 \end{array}$$

- **Type III**: $C^1_{13} = -C^1_{31} = 1$ and rest $C^i_{j,k} = 0$

$$\begin{array}{cccc} \xi_1 = \partial_2 & X_1 = e^{x^1}\partial_2 & \omega^1 = e^{-x^1}dx^2 & d\omega^1 = \omega^1 \wedge \omega^3 \\ \xi_2 = \partial_3 & X_2 = \partial_3 & \omega^2 = dx^3 & d\omega^2 = 0 \\ \xi_3 = \partial_1 + x^2\partial_2 & X_3 = \partial_1 & \omega^3 = dx^1 & d\omega^3 = 0 \end{array}$$

- **Type V**: $C^1_{13} = -C^1_{31} = 1$, $C^2_{23} = -C^2_{32} = 1$ and rest $C^i_{j,k} = 0$

$$\begin{array}{cccc} \xi_1 = \partial_2 & X_1 = e^{x^1}\partial_2 & \omega^1 = e^{-x^1}dx^2 & d\omega^1 = \omega^1 \wedge \omega^3 \\ \xi_2 = \partial_3 & X_2 = e^{x^1}\partial_3 & \omega^2 = e^{-x^1}dx^3 & d\omega^2 = \omega^2 \wedge \omega^3 \\ \xi_3 = \partial_1 + x^2\partial_2 + x^3\partial_3 & X_3 = \partial_1 & \omega^3 = dx^1 & d\omega^3 = 0 \end{array}$$

- **Type VI**: $C^1_{13} = -C^1_{31} = 1$, $C^2_{23} = -C^2_{32} = h$ with $(h \neq 0, 1)$ and rest $C^i_{j,k} = 0$

$$\begin{array}{cccc} \xi_1 = \partial_2 & X_1 = e^{x^1}\partial_2 & \omega^1 = e^{-x^1}dx^2 & d\omega^1 = \omega^1 \wedge \omega^3 \\ \xi_2 = \partial_3 & X_2 = e^{hx^1}\partial_3 & \omega^2 = e^{-hx^1}dx^3 & d\omega^2 = h\omega^2 \wedge \omega^3 \\ \xi_3 = \partial_1 + x^2\partial_2 + hx^3\partial_3 & X_3 = \partial_1 & \omega^3 = dx^1 & d\omega^3 = 0 \end{array}$$

- **Type VII$_\mathbf{0}$**: $C^1_{23} = -C^1_{32} = -1$, $C^2_{13} = -C^2_{31} = 1$ and

  rest $C^i_{j,k} = 0$.

$$\begin{array}{cc} \xi_1 = \partial_2 & X_1 = \cos(x^1)\partial_2 + \sin(x^1)\partial_3 \\ \xi_2 = \partial_3 & X_2 = -\sin(x^1)\partial_2 + \cos(x^1)\partial_3 \\ \xi_3 = \partial_1 - x^3\partial_2 + x^2\partial_3 & X_3 = \partial_1 \end{array}$$

  And also,

$$\begin{array}{cc} \omega^1 = \cos(x^1)dx^2 + \sin(x^1)dx^3 & d\omega^1 = -\omega^2 \wedge \omega^3 \\ \omega^2 = -\sin(x^1)dx^2 + \cos(x^1)dx^3 & d\omega^2 = \omega^1 \wedge \omega^3 \\ \omega^3 = dx^1 & d\omega^3 = 0 \end{array}$$

- **Type IX**: $C^1_{23} = -C^1_{32} = 1$, $C^2_{31} = -C^2_{13} = 1$, $C^3_{12} = -C^3_{21} = 1$ and rest are zero.

$$\begin{aligned} \xi_1 &= \partial_2 \\ \xi_2 &= \cos(x^2)\partial_1 - \cot(x^1)\sin(x^2)\partial_2 + \tfrac{\sin(x^2)}{\sin(x^1)}\partial_3 \\ \xi_3 &= -\sin(x^2)\partial_1 - \cot(x^1)\cos(x^2)\partial_2 + \tfrac{\cos(x^2)}{\sin(x^1)}\partial_3 \end{aligned}$$

  With

$$\begin{aligned} X_1 &= -\sin(x^3)\partial_1 + \tfrac{\cos(x^3)}{\sin(x^1)}\partial_2 - \cot(x^1)\cos(x^3)\partial_3 \\ X_2 &= \cos(x^3)\partial_1 + \tfrac{\sin(x^3)}{\sin(x^1)}\partial_2 - \cot(x^1)\sin(x^3)\partial_3 \\ X_3 &= \partial_3 \end{aligned}$$

And also,

$$\begin{aligned}
\omega^1 &= -\sin(x^3)dx^1 + \sin(x^1)\cos(x^3)dx^2; \quad & d\omega^1 &= \omega^2 \wedge \omega^3 \\
\omega^2 &= \cos(x^3)dx^1 + \sin(x^1)\sin(x^3)dx^2; \quad & d\omega^2 &= \omega^3 \wedge \omega^1 \\
\omega^3 &= \cos(x^1)dx^2 + dx^3; \quad & d\omega^3 &= \omega^1 \wedge \omega^2
\end{aligned}$$

For Types IV and VIII we give the structure constants only. For more explicit data on these Types, see [297]

- **Type IV**: $C^1_{13} = -C^1_{31} = 1$, $C^1_{23} = -C^1_{32} = 1$, $C^2_{23} = -C^2_{32} = 1$ and rest $C^i_{j,k} = 0$

- **Type $\mathbf{VII_h}$ $(\mathbf{0 < h^2 < 4})$**: $C^2_{13} = -C^2_{31} = 1$, $C^1_{23} = -C^1_{32} = -1$, $C^2_{23} = -C^2_{32} = h$ and rest $C^i_{j,k} = 0$

- **Type VIII**: $C^1_{23} = -C^1_{32} = -1$, $C^2_{31} = -C^2_{13} = 1$, $C^3_{12} = -C^3_{21} = 1$ and rest $C^i_{j,k} = 0$

A.2 The Weak and Null Energy Conditions

We shall now review the weak and null energy conditions in detail. The weak energy condition (WEC) stipulates that the local energy density as observed by a time-like observer is nonnegative. In other words, if u^μ are the components of a time-like vector, we must have $T_{\mu\nu}u^\mu u^\nu \geq 0$ everywhere, with $T_{\mu\nu}$ being the components of the stress tensor. Note that if we raise one of the indices of $T_{\mu\nu}$ to get T^μ_ν, we could interpret the stress tensor as a linear transformation T that acts on the components of a vector u via $(Tu)^\mu = T^\mu_\nu u^\nu$.

The WEC now simply becomes $\langle u, Tu\rangle \geq 0$, where the angle brackets denote the inner product with respect to the metric. Since T is a linear transformation from a vector space to itself, it makes sense to talk of the eigenvalues and eigenvectors of T. In particular, if u is a time-like eigenvector which is normalized so that $\langle u, u\rangle = -1$ and which belongs to some eigenvalue λ (not to be confused with the λ parameter we had introduced in the interpolating metric), then we have

$$\langle u, Tu\rangle = \lambda\langle u, u\rangle = -\lambda. \tag{A.3}$$

Thus, a necessary condition for the WEC to hold is that the eigenvalues corresponding to all time-like eigenvectors of T be non-positive.

Note that this isn't a sufficient condition for the WEC to hold. To go further, let us first note that T is self-adjoint:

$$\langle u, Tv\rangle = T_{\mu\nu}u^\mu v^\nu = \langle Tu, v\rangle.$$

However, it does not follow from this property that T is diagonalizable and that its eigenvalues are necessarily real, since the inner product is indefinite in a Lorentzian metric. For the metrics we are interested, we fortunately do not have to deal with this complication because, it turns out that in all the cases we analyze, T does turn out to be diagonalizable with real eigenvalues. Accordingly, we restrict our discussion to this case below.

It then follows that there exists a vierbein $\{u_0, u_1, u_2, u_3, u_4\}$ consisting of the eigenvectors of T, which is orthonormal in the sense that $\langle u_a, u_b\rangle = \eta_{ab}$. If we let $Tu_a = \lambda_a u_a$, then our claim is that the WEC is equivalent to the following statement: $\lambda_0 \leq 0$ and $|\lambda_0| + \lambda_c \geq 0$ for $c = 1, 2, 3, 4$.

To prove necessity, we note that we have already shown that $\lambda_0 \leq 0$. Now, for an arbitrary time-like vector of the form $v = Au_0 + Bu_c$, where c can be 1, 2, 3 or 4, we have $\langle v, v\rangle = -A^2 + B^2 < 0$. By the WEC we have

$$\langle v, Tv\rangle = |\lambda_0|A^2 + \lambda_c B^2 \geq 0.$$

If we let $\epsilon = A^2 - B^2$, the above can rewritten as

$$(|\lambda_0| + \lambda_c)B^2 + \epsilon|\lambda_0| \geq 0.$$

Since v is arbitrary, ϵ can be an arbitrarily small positive real number. It follows that $|\lambda_0| + \lambda_c \geq 0$ for $c = 1, 2, 3, 4$.

To prove sufficiency, we note that a generic time-like vector v may be given by

$$v = Au_0 + Bu_1 + Cu_2 + Du_3 + Eu_4.$$

where the coefficients are subject to the following

$$A^2 > B^2 + C^2 + D^2 + E^2.$$

The conditions $\lambda_0 \leq 0$ and $|\lambda_0| + \lambda_c \geq 0$ for $c = 1, 2, 3, 4$ hence guarantee that

$$\begin{aligned}
\langle v, Tv\rangle &= |\lambda_0|A^2 + \lambda_1 B^2 + \lambda_2 C^2 + \lambda_3 D^2 + \lambda_4 E^2 \\
&\geq |\lambda_0|(B^2 + C^2 + D^2 + E^2) + \lambda_1 B^2 + \lambda_2 C^2 + \lambda_3 D^2 + \lambda_4 E^2 \\
&= (|\lambda_0| + \lambda_1)B^2 + (|\lambda_0| + \lambda_2)C^2 + (|\lambda_0| + \lambda_3)D^2 + (|\lambda_0| + \lambda_4)E^2 \\
&\geq 0.
\end{aligned}$$

In fact, we can go further and easily show this implies the null energy condition (which states that $\langle n, Tn\rangle \geq 0$ for all null vectors n everywhere) by following the same outline as the proof above. We note that a generic null vector n may be given by

$$n = Au_0 + Bu_1 + Cu_2 + Du_3 + Eu_4,$$

where the coefficients are subject to the following

$$A^2 = B^2 + C^2 + D^2 + E^2.$$

The conditions $\lambda_0 \leq 0$ and $|\lambda_0| + \lambda_c \geq 0$ for $c = 1, 2, 3, 4$ hence guarantee that

$$\begin{aligned}\langle n, Tn\rangle &= |\lambda_0|A^2 + \lambda_1 B^2 + \lambda_2 C^2 + \lambda_3 D^2 + +\lambda_4 E^2 \\ &= \lambda_0|(B^2 + C^2 + D^2 + E^2) + \lambda_1 B^2 + \lambda_2 C^2 + \lambda_3 D^2 + \lambda_4 E^2 \\ &= (|\lambda_0| + \lambda_1)B^2 + (|\lambda_0| + \lambda_2)C^2 + (|\lambda_0| + \lambda_3)D^2 + (|\lambda_0| + \lambda_4)E^2 \\ &\geq 0,\end{aligned}$$

which is the null energy condition (NEC). Thus, in terms of the eigenvalues, the NEC is equivalent to the following statement: $-\lambda_0 + \lambda_c \geq 0$ for $c = 1, 2, 3, 4$ where λ_0 is the eigenvalue corresponding to the time-like eigenvector and λ_c corresponds to any of the space-like eigenvectors.

To summarize the above observations:

1. For the WEC, it suffices to have (i) $\lambda_0 \leq 0$ and (ii) $|\lambda_0| + \lambda_c \geq 0$ for $c = 1, 2, 3, 4$.
2. For the NEC, it suffices to have $-\lambda_0 + \lambda_c \geq 0$ for $c = 1, 2, 3, 4$, where λ_0 is the eigenvalue corresponding to the time-like eigenvector and λ_c corresponds to any of the space-like eigenvectors.

Appendix B

Appendices for Chapter 3: *Bianchi III attractor in Gauged Supergravity*

B.1 Notations and conventions

In this section, we summarize our notations and conventions on tangent space and spinors. We use greek indices for spacetime and roman for tangent space. Our conventions for the flat tangent space metric is $\eta_{ab} = (-, +, +, +, +)$. The tangent space indices are denoted by $a, b = 0, 1, 2, 3, 4$.

The tangent space matrices satisfy the usual Clifford algebra

$\{\ \gamma_a, \gamma_b\} = 2\eta_{ab}$ .Antisymmetrization is done with the following convention,

$\gamma_{a_1 a_2 \ldots a_n} = \gamma_{[a_1 a_2 \ldots a_n]} = \frac{1}{n!} \sum_{\sigma \in P_n} Sign(\sigma) \gamma_{a_{\sigma(1)}} \gamma_{a_{\sigma(2)}} \ldots \gamma_{a_{\sigma(n)}}$ .In $d = 5$ only I, γ_a, γ_{ab} form an independent set, other matrices are related by the general identity for $d = 2k + 3$,

$\gamma^{\mu_1 \mu_2 \ldots \mu_s} = \frac{-i^{-k+s(s-1)}}{(d-s)!} \epsilon^{\mu_1 \mu_2 \ldots \mu_s} \gamma_{\mu_{s+1} \ldots \mu_d}$ .We also recollect that the spinors in five dimensions satisfy the symplectic majorana condition

$^i \equiv (\epsilon_i^*)^t \gamma^0 = (\epsilon^i)^t C$,where C is the charge conjugation matrix which obeys $C^t = C^{-1} = -C$.

Unlike the case in four dimensions, the $SU(2)$ indices are not raised and lowered by complex conjugation. Instead they are raised and lowered by the $SU(2)$ covariant tensor with the conventions $\varepsilon_{12} = \varepsilon^{12} = 1$. Note that the $SU(2)$ indices are always raised or lowered in the NW-SE direction

$\epsilon^i = \varepsilon^{ij} \epsilon_j \ , \quad \epsilon_i = \epsilon^j \varepsilon_{ji}\ .$

The covariant derivative acting on ϵ_i is with respect to the Lorentz covariant spin connection ω_μ^{ab} defined as

$\nabla_\mu(\omega)\epsilon_i = \partial_\mu\epsilon_i + \frac{1}{4}\omega_\mu^{ab}\gamma_{ab}$

B.2 Linearized Einstein equations

In this section, we provide the explicit form of the linearized equations that follow from (3.81). We substitute the expressions for the attractor potential (3.62), the scalar fluctuations (3.73), the terms from the stress energy tensor (3.76), (3.79) and the metric fluctuations (3.82) into the linearized Einstein equation (3.81). We then contract it with the vielbeins e_a^μ to obtain the following equations. The $\hat{t}\hat{t}$ equation is

$$\hat{r}^2\tilde{\gamma}''_{\hat{r}\hat{r}} - \hat{r}^2\tilde{\gamma}''_{\hat{t}\hat{t}} + \hat{r}^2\tilde{\gamma}''_{\hat{x}\hat{x}} + \hat{r}^2\tilde{\gamma}''_{\hat{y}\hat{y}} + \hat{r}^2\tilde{\gamma}''_{\hat{z}\hat{z}} + 12{\beta_t}^2\tilde{\gamma}_{\hat{r}\hat{r}} + 4(3{\beta_t}^2 + 2)\tilde{\gamma}_{\hat{t}\hat{t}} + 4{\beta_t}^2\tilde{\gamma}_{\hat{x}\hat{x}} + 4{\beta_t}^2\tilde{\gamma}_{\hat{y}\hat{y}} \tag{B.1}$$

$$+ 12{\beta_t}^2\tilde{\gamma}_{\hat{z}\hat{z}} + 6\beta_t\hat{r}\tilde{\gamma}'_{\hat{r}\hat{r}} - 6\beta_t\hat{r}\tilde{\gamma}'_{\hat{t}\hat{t}} + 6\beta_t\hat{r}\tilde{\gamma}'_{\hat{x}\hat{x}} + 6\beta_t\hat{r}\tilde{\gamma}'_{\hat{y}\hat{y}} + 6\beta_t\hat{r}\tilde{\gamma}'_{\hat{z}\hat{z}} \tag{B.2}$$

$$+ \hat{r}\tilde{\gamma}'_{\hat{r}\hat{r}} - \hat{r}\tilde{\gamma}'_{\hat{t}\hat{t}} + \hat{r}\tilde{\gamma}'_{\hat{x}\hat{x}} + 4(\tilde{\gamma}_{\hat{x}\hat{x}} + \tilde{\gamma}_{\hat{y}\hat{y}}) + \hat{r}\tilde{\gamma}'_{\hat{y}\hat{y}} + \hat{r}\tilde{\gamma}'_{\hat{z}\hat{z}} = 0\ . \tag{B.3}$$

The $\hat{r}\hat{r}$ equation is

$$\hat{r}^2\tilde{\gamma}''_{\hat{r}\hat{r}} - \hat{r}^2\tilde{\gamma}''_{\hat{t}\hat{t}} - \hat{r}^2\tilde{\gamma}''_{\hat{x}\hat{x}} - \hat{r}^2\tilde{\gamma}''_{\hat{y}\hat{y}} - \hat{r}^2\tilde{\gamma}''_{\hat{z}\hat{z}} - 4(5{\beta_t}^2 + \beta_t + 1)\tilde{\gamma}_{\hat{r}\hat{r}} + 4{\beta_t}^2\tilde{\gamma}_{\hat{x}\hat{x}} + 4{\beta_t}^2\tilde{\gamma}_{\hat{y}\hat{y}} \tag{B.4}$$

$$- 4{\beta_t}^2\tilde{\gamma}_{\hat{z}\hat{z}} + 2\beta_t\hat{r}\tilde{\gamma}'_{\hat{r}\hat{r}} - 2\beta_t\hat{r}\tilde{\gamma}'_{\hat{t}\hat{t}} - 4(\beta_t - 1)\beta_t\tilde{\gamma}_{\hat{t}\hat{t}} - 2\beta_t\hat{r}\tilde{\gamma}'_{\hat{x}\hat{x}} + 4\beta_t\tilde{\gamma}_{\hat{x}\hat{x}} \tag{B.5}$$

$$- 2\beta_t\hat{r}\tilde{\gamma}'_{\hat{y}\hat{y}} + 4\beta_t\tilde{\gamma}_{\hat{y}\hat{y}} - 2\beta_t\hat{r}\tilde{\gamma}'_{\hat{z}\hat{z}} + 4\beta_t\tilde{\gamma}_{\hat{z}\hat{z}} - 3\hat{r}\tilde{\gamma}'_{\hat{r}\hat{r}} + 3\hat{r}\tilde{\gamma}'_{\hat{t}\hat{t}} \tag{B.6}$$

$$- 4(\tilde{\gamma}_{\hat{t}\hat{t}} + 2(\tilde{\gamma}_{\hat{x}\hat{x}} + \tilde{\gamma}_{\hat{y}\hat{y}}) + \tilde{\gamma}_{\hat{z}\hat{z}}) + 3\hat{r}\tilde{\gamma}'_{\hat{x}\hat{x}} + 3\hat{r}\tilde{\gamma}'_{\hat{y}\hat{y}} + 3\hat{r}\tilde{\gamma}'_{\hat{z}\hat{z}} = 0\ . \tag{B.7}$$

The $\hat{x}\hat{x}$ equation is

$$-\frac{(2{\beta_t}^2 - 1)(8C_s\hat{r}^\Delta + \phi_c\tilde{\gamma}_{\hat{y}\hat{y}})}{\phi_c} - 2{\beta_t}^2(\tilde{\gamma}_{\hat{r}\hat{r}} + \tilde{\gamma}_{\hat{t}\hat{t}} + 3\tilde{\gamma}_{\hat{x}\hat{x}} + \tilde{\gamma}_{\hat{z}\hat{z}}) - \frac{1}{2}\hat{r}\big((2\beta_t + 1)\tilde{\gamma}'_{\hat{r}\hat{r}} \tag{B.8}$$

$$+ 2\beta_t(\tilde{\gamma}'_{\hat{t}\hat{t}} - \tilde{\gamma}'_{\hat{x}\hat{x}} + \tilde{\gamma}'_{\hat{y}\hat{y}} + \tilde{\gamma}'_{\hat{z}\hat{z}}) + \hat{r}(\tilde{\gamma}''_{\hat{r}\hat{r}} + \tilde{\gamma}''_{\hat{t}\hat{t}} - \tilde{\gamma}''_{\hat{x}\hat{x}} + \tilde{\gamma}''_{\hat{y}\hat{y}} + \tilde{\gamma}''_{\hat{z}\hat{z}}) \tag{B.9}$$

$$+ \tilde{\gamma}'_{\hat{t}\hat{t}} - \tilde{\gamma}'_{\hat{x}\hat{x}} + \tilde{\gamma}'_{\hat{y}\hat{y}} + \tilde{\gamma}'_{\hat{z}\hat{z}}\big) - 6\tilde{\gamma}_{\hat{x}\hat{x}} - \tilde{\gamma}_{\hat{y}\hat{y}} = 0\ . \tag{B.10}$$

The $\hat{y}\hat{y}$ equation is

$$-\frac{16(2\beta_t{}^2-1)C_s\hat{r}^{\Delta}}{\phi_c}+2(-2\beta_t{}^2(\tilde{\gamma}_{\hat{r}\hat{r}}+\tilde{\gamma}_{\hat{t}\hat{t}}+3\tilde{\gamma}_{\hat{y}\hat{y}}+\tilde{\gamma}_{\hat{z}\hat{z}})-\tilde{\gamma}_{\hat{x}\hat{x}}-3\tilde{\gamma}_{\hat{y}\hat{y}})+2(1-2\beta_t{}^2)\tilde{\gamma}_{\hat{x}\hat{x}} \tag{B.11}$$

$$-\hat{r}\big((2\beta_t+1)\tilde{\gamma}'_{\hat{r}\hat{r}}+2\beta_t(\tilde{\gamma}'_{\hat{t}\hat{t}}+\tilde{\gamma}'_{\hat{x}\hat{x}}-\tilde{\gamma}'_{\hat{y}\hat{y}}+\tilde{\gamma}'_{\hat{z}\hat{z}})+\hat{r}(\tilde{\gamma}''_{\hat{r}\hat{r}}+\tilde{\gamma}''_{\hat{t}\hat{t}}+\tilde{\gamma}''_{\hat{x}\hat{x}} \tag{B.12}$$

$$-\tilde{\gamma}''_{\hat{y}\hat{y}}+\tilde{\gamma}''_{\hat{z}\hat{z}})+\tilde{\gamma}'_{\hat{t}\hat{t}}+\tilde{\gamma}'_{\hat{x}\hat{x}}-\tilde{\gamma}'_{\hat{y}\hat{y}}+\tilde{\gamma}'_{\hat{z}\hat{z}}\big)-6\tilde{\gamma}_{\hat{r}\hat{r}}-6\tilde{\gamma}_{\hat{t}\hat{t}}-6\tilde{\gamma}_{\hat{x}\hat{x}}-6\tilde{\gamma}_{\hat{z}\hat{z}}=0\ . \tag{B.13}$$

The $\hat{z}\hat{z}$ equation is

$$\hat{r}^2(-\tilde{\gamma}''_{\hat{r}\hat{r}})-\hat{r}^2\tilde{\gamma}''_{\hat{t}\hat{t}}-\hat{r}^2\tilde{\gamma}''_{\hat{x}\hat{x}}-\hat{r}^2\tilde{\gamma}''_{\hat{y}\hat{y}}+\hat{r}^2\tilde{\gamma}''_{\hat{z}\hat{z}}-12\beta_t{}^2\tilde{\gamma}_{\hat{r}\hat{r}}-12\beta_t{}^2\tilde{\gamma}_{\hat{t}\hat{t}}-4\beta_t{}^2\tilde{\gamma}_{\hat{x}\hat{x}}-4\beta_t{}^2\tilde{\gamma}_{\hat{y}\hat{y}} \tag{B.14}$$

$$-12\beta_t{}^2\tilde{\gamma}_{\hat{z}\hat{z}}-6\beta_t\hat{r}\tilde{\gamma}'_{\hat{r}\hat{r}}-6\beta_t\hat{r}\tilde{\gamma}'_{\hat{t}\hat{t}}-6\beta_t\hat{r}\tilde{\gamma}'_{\hat{x}\hat{x}}-6\beta_t\hat{r}\tilde{\gamma}'_{\hat{y}\hat{y}}+6\beta_t\hat{r}\tilde{\gamma}'_{\hat{z}\hat{z}}-\hat{r}\tilde{\gamma}'_{\hat{r}\hat{r}} \tag{B.15}$$

$$-\hat{r}\tilde{\gamma}'_{\hat{t}\hat{t}}-\hat{r}\tilde{\gamma}'_{\hat{x}\hat{x}}-4(\tilde{\gamma}_{\hat{x}\hat{x}}+\tilde{\gamma}_{\hat{y}\hat{y}}+2\tilde{\gamma}_{\hat{z}\hat{z}})-\hat{r}\tilde{\gamma}'_{\hat{y}\hat{y}}+\hat{r}\tilde{\gamma}'_{\hat{z}\hat{z}}=0\ . \tag{B.16}$$

In the above equations, the prime indicates derivative with respect to $\hat{r}$. We see that all the double derivatives are multiplied by $\hat{r}^2$, while the single derivatives are multiplied by $\hat{r}$. Now, the $\hat{x}\hat{x}$ and $\hat{y}\hat{y}$ equations contain the source term which goes like $\hat{r}^{\Delta}$. It is then clear that the metric fluctuations $\tilde{\gamma}_{\mu\nu}$ all go like $\hat{r}^{\Delta}$.

B.3 Coefficients of the linearized fluctuations

The various functions that appear in the coefficients (3.85) are

$$F_0(\beta_t)=-64(\beta_t{}^2+4)(2\beta_t{}^2-1)\frac{N^1_{\hat{t}}(\beta_t)+N^2_{\hat{t}}(\beta_t)}{D_1(\beta_t)+D_2(\beta_t)+D_3(\beta_t)+D_4(\beta_t)}\ , \tag{B.17}$$

$$F_1(\beta_t)=64(\beta_t{}^2+4)(2\beta_t{}^2-1)\frac{N^1_{\hat{r}}(\beta_t)+N^2_{\hat{r}}(\beta_t)}{D_1(\beta_t)+D_2(\beta_t)+D_3(\beta_t)+D_4(\beta_t)}\ , \tag{B.18}$$

$$F_2(\beta_t)=8(2\beta_t{}^2-1)\frac{N^1_{\hat{x}}(\beta_t)+N^2_{\hat{x}}(\beta_t)+N^3_{\hat{x}}(\beta_t)}{D_1(\beta_t)+D_2(\beta_t)+D_3(\beta_t)+D_4(\beta_t)}\ , \tag{B.19}$$

$$F_3(\beta_t)=8(2\beta_t{}^2-1)\frac{N^1_{\hat{y}}(\beta_t)+N^2_{\hat{y}}(\beta_t)+N^3_{\hat{y}}(\beta_t)}{D_1(\beta_t)+D_2(\beta_t)+D_3(\beta_t)+D_4(\beta_t)}\ , \tag{B.20}$$

$$F_4(\beta_t)=-64(\beta_t{}^2+4)(2\beta_t{}^2-1)\frac{N^1_{\hat{z}}(\beta_t)+N^1_{\hat{z}}(\beta_t)}{D_1(\beta_t)+D_2(\beta_t)+D_3(\beta_t)+D_4(\beta_t)}\ , \tag{B.21}$$

where,

$$N^1_{\hat{t}}(\beta_t) = 272{\beta_t}^4 + 80(f(\beta_t) - 1){\beta_t}^2 + 4(f(\beta_t) - 84)\beta_t \ , \tag{B.22}$$

$$N^2_{\hat{t}}(\beta_t) = -4f(\beta_t) + 16(7f(\beta_t) + 33){\beta_t}^3 + 107 \ , \tag{B.23}$$

$$N^1_{\hat{r}}(\beta_t) = 304{\beta_t}^4 + 8(14f(\beta_t) - 53){\beta_t}^2 + 4(5f(\beta_t) + 84)\beta_t \ , \tag{B.24}$$

$$N^2_{\hat{r}}(\beta_t) = 28f(\beta_t) + 16(5f(\beta_t) - 33){\beta_t}^3 - 179 \ , \tag{B.25}$$

$$N^1_{\hat{x}}(\beta_t) = 4928{\beta_t}^6 + 4(1000f(\beta_t) + 4821){\beta_t}^2 - 4(53f(\beta_t) - 924)\beta_t \ , \tag{B.26}$$

$$N^2_{\hat{x}}(\beta_t) = 644f(\beta_t) - 64(5f(\beta_t) - 33){\beta_t}^5 + 16(68f(\beta_t) + 1419){\beta_t}^4 \ , \tag{B.27}$$

$$N^3_{\hat{x}}(\beta_t) = -16(166f(\beta_t) + 447){\beta_t}^3 + 671 \ , \tag{B.28}$$

$$N^1_{\hat{y}}(\beta_t) = 4928{\beta_t}^6 + 4(1216f(\beta_t) + 6009){\beta_t}^2 - 4(107f(\beta_t) + 3612)\beta_t \ , \tag{B.29}$$

$$N^2_{\hat{y}}(\beta_t) = -4f(\beta_t) - 64(5f(\beta_t) - 33){\beta_t}^5 + 16(68f(\beta_t) + 1689){\beta_t}^4 \ , \tag{B.30}$$

$$N^3_{\hat{y}}(\beta_t) = (21360 - 64f(\beta_t)){\beta_t}^3 + 7745 \ , \tag{B.31}$$

$$N^1_{\hat{z}}(\beta_t) = (272{\beta_t}^4 + 80(f(\beta_t) - 1){\beta_t}^2 + 4(f(\beta_t) - 84)\beta_t \ , \tag{B.32}$$

$$N^2_{\hat{z}}(\beta_t) = -4f(\beta_t) + 16(7f(\beta_t) + 33){\beta_t}^3 + 107) \ , \tag{B.33}$$

$$D_1(\beta_t) = -33024{\beta_t}^8 - 8(3910f(\beta_t) + 13839){\beta_t}^2 + 4(367f(\beta_t) - 1428)\beta_t \ , \tag{B.34}$$

$$D_2(\beta_t) = -3276f(\beta_t) + 256(25f(\beta_t) + 99){\beta_t}^7 - 128(58f(\beta_t) + 1525){\beta_t}^6 \ , \tag{B.35}$$

$$D_3(\beta_t) = 192(147f(\beta_t) + 400){\beta_t}^5 - 32(1178f(\beta_t) + 8565){\beta_t}^4 \ , \tag{B.36}$$

$$D_4(\beta_t) = 48(309f(\beta_t) - 1045){\beta_t}^3 - 10445 \ , \tag{B.37}$$

$$f(\beta_t) = \sqrt{-21 + 33\beta_t^2} \ . \tag{B.38}$$

Appendix C

Appendices for Chapter 4: *The Shear Viscosity in Anisotropic Phases*

C.1 Numerical interpolation from the near horizon $AdS_3 \times R \times R$ to asymptotic AdS_5,

Our action consists of gravity, a massless dilaton ϕ and a cosmological constant Λ, in 5 space time dimensions,

$S_{bulk} = \frac{1}{2\kappa^2}\int d^5x\sqrt{-g}\,\left(R + 12\Lambda - \frac{1}{2}(\partial\phi)^2\right)$.Here $2\kappa^2 = 16\pi G$ is the gravitational coupling (G is the Newton's Constant in 5 dimensions) and we set Λ=1.

It is easy to show that this system admits an AdS_5 solution with metric given by

$ds^2 = \left[- u^2dt^2 + \frac{du^2}{u^2} + u^2(dx^2 + dy^2 + dz^2)\right]$,and the dilaton is kept constant.

We now show that starting with the near horizon geometry given by eq.(4.30), one can add a suitable perturbation which grows in the UV such that the solution matches asymptotically to AdS_5 metric as provided in eq.(C.1).

This perturbation is given as follows-

$$\begin{aligned}
g_{tt}(u) &= 2u^2\left(1 + \delta A(u)\right), \\
g_{uu}(u) &= \frac{1}{2u^2\left(1 + \delta A(u)\right)} \\
g_{xx}(u) &= 2u^2\left(1 + \delta A(u)\right), \\
g_{yy}(u) &= \frac{\rho_1^2}{8}\left(1 + \delta C(u)\right) \\
g_{zz}(u) &= \frac{\rho_2^2}{8}\left(1 + \delta D(u)\right)
\end{aligned} \tag{C.1}$$

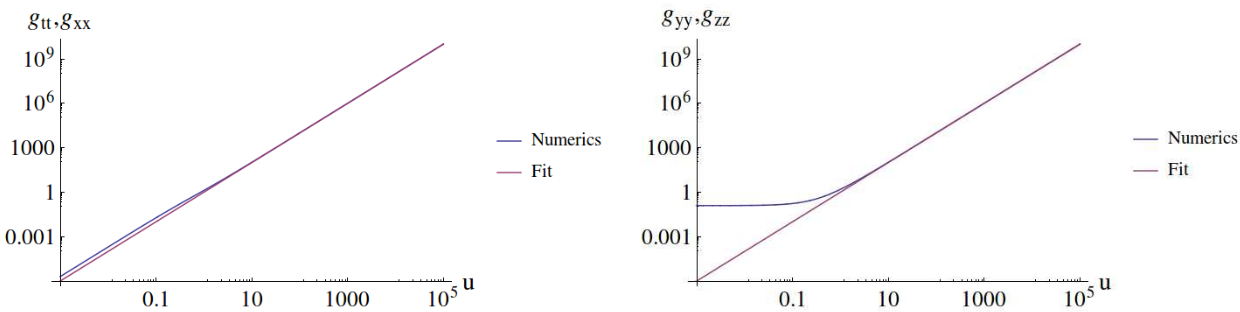

Figure C.1: Log-log plot showing the numerical interpolation of near horizon $AdS_3 \times R \times R$ to asymptotic AdS_5 , with $\rho_1 = 1$, $\rho_2 = 1$.

with

$$\delta A(u) = a_1\ u^{\nu},\ \ \delta C(u) = c_2\ u^{\nu},\ \ \delta D(u) = c_3\ u^{\nu} \tag{C.2}$$

$$a_1 = \frac{1}{5}(-5 + 2\sqrt{5})(c_2 + c_3),\ \ \nu = \sqrt{5} - 1. \tag{C.3}$$

The numerical analysis is carried out using NDSolve in mathematica. For the case $\rho_1 = 1$, $\rho_2 = 1$ the suitably chosen values for c_2 and c_3 are as follows

$c_2 = 85,\ \ c_3 = 85.$

By adjusting the coefficients c_2, c_3 to the above values one can ensure that the asymptotic behaviour of the metric eq.(C.1) agrees with eq.(C.1) at large u, say u=100000 ;

The plots in Fig (C.1) show the metric components as a function of u. These plots were obtained by numerical interpolation for the case $\rho_1 = 1$, $\rho_2 = 1$ and $c_2 = 85, c_3 = 85$.

C.2 Ratio of normalizable over non-normalizable mode near boundary

Here we check that asymptotically the canonical momentum Π goes to a constant independent of u . To see this , we consider the action

$S_{bulk} = \frac{1}{2\hat{\kappa}^2}\int d^5x\sqrt{-\hat{g}}\ \left(\hat{R} + 12\Lambda\right)$ .we get the following solution for AdS_5 (setting Λ=1).

$ds^2 = \left(-u^2dt^2 + \frac{du^2}{u^2} + u^2dx^2 + u^2dy^2 + u^2dz^2\right)$ .The metric perturbations go like $u^2(1+\frac{C_1}{u^4})$ where C_1 is constant.
Hence, using eq.(4.92) and eq.(4.90) we find that

$\Pi(u) = -\frac{1}{2\kappa^2}N(u)Z' = -\frac{1}{2\kappa^2}\sqrt{-g}\frac{1}{g_{\rm eff}^2}g^{xx}g^{uu}\partial_u(\frac{C_1}{u^4}) = -\frac{1}{2\kappa^2}\sqrt{-g}\ e^{3\psi}g^{xx}g^{uu}\partial_u(\frac{C_1}{u^4})$.Plugging in the higher dimensional metric components from (C.2)we get $\Pi(u) = \frac{2}{\kappa^2}C_1$ which is independent of u. Thus asymptotically, the ratio of the normalizable to the non - normalizable mode behaves like $\frac{2}{\kappa^2}C_1$.

C.3 Conductivity formula in terms of horizon quantities

In this appendix , we show the derivation of (4.96) following [147]. The electrical conductivity is defined in (4.93) as

$$\sigma(u,\omega) = \frac{\Pi(u,\omega)}{i\omega Z(u,w)}|_{u\to\infty,\omega\to 0}. \tag{C.4}$$

The real part can be written as

$$\begin{aligned}\mathrm{Re}\,(\sigma) &= \mathrm{Re}\left(\frac{\Pi(u,\omega)}{i\omega Z(u,\omega)}\right)|_{u\to\infty,\omega\to 0} = \mathrm{Re}\left(\frac{\Pi(u,\omega)Z(u,-\omega)}{i\omega Z(u,\omega)Z(u,-\omega)}\right)|_{u\to\infty,\omega\to 0}\\ &= \mathrm{Im}\left(\frac{\Pi(u,\omega)Z(u,-\omega)}{\omega Z^2(u)}\right)|_{u\to\infty,\omega\to 0} = \frac{\mathrm{Im}\left(\Pi(u,\omega)Z(u,-\omega)\right)}{\omega Z^2(u)}|_{u\to\infty,\omega\to 0}.\end{aligned} \tag{C.5}$$

Here we used the fact that $Z(u,\omega) \sim Z(u)$ is real to leading order when $\omega \to 0$.
We now proceed to show that[1]

$$\frac{d}{du}\mathrm{Im}\,[\Pi(u,\omega)Z(u,-\omega)] = 0, \tag{C.6}$$

This can be seen as follows

$$\begin{aligned}\frac{d}{du}\mathrm{Im}\left(N(u)\frac{d}{du}Z(u,\omega)Z(u,-\omega)\right) = \mathrm{Im}\Big[\frac{d}{du}\left(N(u)\frac{d}{du}Z(u,\omega)\right)Z(u,-\omega)\\ +N(u)\frac{d}{du}Z(u,\omega)\frac{d}{du}Z(u,-\omega)\Big].\end{aligned} \tag{C.7}$$

Using (4.89), r.h.s of above equation reduces to

$$\mathrm{Im}\Big[-M(u)Z(u,\omega)Z(u,-\omega) + N(u)\frac{d}{du}Z(u,\omega)\frac{d}{du}Z(u,-\omega)\Big], \tag{C.8}$$

which is equal to zero since the quantity in the bracket is real. Thus $\mathrm{Im}\,[\Pi(u,\omega)Z(u-\omega)]$ can be evaluated at the horizon i.e. at $u = u_h$.

Demanding regularity at the future horizon , we can approximate the behaviour of $Z(u,\omega)$ as follows

Z $\sim e^{-i\omega(t+r_*)}$,where r_* is the tortoise coordinate,

r$_* = \int\sqrt{\frac{g_{uu}}{g_{tt}}}\,du$.

[1] $\Pi(u,\omega) = \frac{\delta S}{\delta Z'(u,-\omega)} = -\frac{1}{2\kappa^2}N(u)\frac{d}{du}Z(u,\omega)$, hence $\mathrm{Im}\,[\Pi(u,\omega)Z(u,-\omega)]$ behaves like a current .

Using eq.(4.92) and

$$\lim_{u\to u_h}\frac{d}{du}Z(u,\omega)=-i\omega\lim_{u\to u_h}\sqrt{\frac{g_{uu}}{g_{tt}}}Z(u)+\mathcal{O}(\omega^2). \tag{C.9}$$

we get (in the limit $\omega\to 0$)

$$\begin{aligned}\mathrm{Re}\,(\sigma) &= \frac{1}{2\kappa^2}\left(\sqrt{\frac{g_{uu}}{g_{tt}}}N(u)\right)_{u=u_h}\left(\frac{Z(u_h)}{Z(u\to\infty)}\right)^2\\ &= \frac{1}{2\kappa^2}\left(\sqrt{\frac{g_{uu}}{g_{tt}}}\;\sqrt{-g}\frac{1}{g_{\text{eff}}^2}g^{xx}g^{uu}\right)_{u=u_h}\left(\frac{Z(u_h)}{Z(u\to\infty)}\right)^2\\ &= \sigma_H\;\left(\frac{Z(u_h)}{Z(u\to\infty)}\right)^2,\end{aligned} \tag{C.10}$$

where σ_H is the conductivity evaluated at the horizon and its expression is given by,

$$\sigma_H=\frac{1}{2\kappa^2 g_{\text{eff}}^2}\Big|_{u=u_h}. \tag{C.11}$$

where we used isotropy along the spatial directions in the lower dimensional theory.

Appendix D

Appendices for Chapter 6: *The Shear Viscosity in an Anisotropic Unitary Fermi Gas*

D.1 Ideal hydrodynamic modes

In this section we contrast the modes discussed in Sec. 5.3.1 with the breathing modes discussed in Ref. [172] in normal fluids.

We start with the linearized continuity and Euler equations for a fluid with a polytropic equation of state, which can be used to derive the following equation valid for ideal fluid dynamics for the normal component [172],

$$m\frac{\partial^2 \mathbf{v}}{\partial t^2} = -\gamma\left(\nabla\cdot\mathbf{v}\right)\left(\nabla\phi(\mathbf{r})\right) - \nabla\left(\mathbf{v}\cdot\nabla\phi(\mathbf{r})\right) \ . \tag{D.1}$$

As shown in Ref. [172] breathing modes can be obtained by considering a scaling ansatz $v_i = a_i x_i \exp(i\omega t)$ (no sum over i). Substituting in Eq. D.1 one obtains an eigenequation

$$\left(2\omega_j^2 - \omega^2\right) a_j + \gamma\omega_j^2 \sum_k a_k = 0. \tag{D.2}$$

This is a simple linear equation of the form $Ma = 0$. Non-trivial solutions correspond to $\det(M) = 0$.

In the case of a trapping potential with axial symmetry, $\omega_1 = \omega_2 = \omega_0$, $\omega_3 = \lambda\omega_0$, we get

$\omega^2 = 2\omega_0^2$ and [184, 200, 298]

$$
\begin{aligned}
\omega^2 =& \omega_0^2 \left\{ \gamma + 1 + \frac{\gamma+2}{2}\lambda^2 \right. \\
& \left. \pm \sqrt{\frac{(\gamma+2)^2}{4}\lambda^4 + (\gamma^2 - 3\gamma - 2)\lambda^2 + (\gamma+1)^2} \right\} .
\end{aligned}
\tag{D.3}
$$

In the unitarity limit ($\gamma = 2/3$) and for a very asymmetric trap, $\lambda \to 0$, the eigen-frequencies are $\omega^2 = 2\omega_0^2$ and $\omega^2 = (10/3)\omega_0^2$. The mode $\omega^2 = (10/3)\omega_0^2$ is a radial breathing mode with $\mathbf{a} = (a, a, 0)$ and the mode $\omega^2 = 2\omega_0^2$ corresponds to a radial quadrupole $\mathbf{a} = (a, -a, 0)$.

Here we consider a different class of modes, with the scaling form Eq. D.4 (since x and z are exchanged, they are "twisted"). The eigen-equations are now given by Eq. D.5. It has two solutions, $\omega = 0$ and $\omega = \sqrt{\omega_x^2 + \omega_y^2}$. Hydrodynamic modes can be obtained by considering an ansatz of the form

$$
v = e^{i\omega t}(\alpha_x \; z \; \hat{x} + \alpha_z \; x \; \hat{z}) \; . \tag{D.4}
$$

Substituting Eq. D.4 in Eq. D.1 gives the simultaneous equations

$$
\begin{aligned}
\omega^2 \alpha_z &= \alpha_x \; \omega_x^2 + \alpha_z \; \omega_z^2 \\
\omega^2 \alpha_x &= \alpha_x \; \omega_x^2 + \alpha_z \; \omega_z^2 \; .
\end{aligned}
\tag{D.5}
$$

One mode of interest for us is the $\omega = 0$ mode since it has a velocity profile similar to that we studied in Chapter 4. This is what we call the Elliptic mode. If $\omega_x = \omega_z$, the mode looks like a rigid body rotation and can not exhibit viscous damping. For $\omega_x \neq \omega_z$ however we get a non-zero energy dissipation due to viscosity given by Eq. 5.47. The second mode of interest for us is what we call the Scissor mode which is well known in literature.

D.2 Anisotropic viscosities in the relaxation time approximation

In this section, we compute the anisotropic shear viscosities associated with the motion of a weakly interacting Fermi gas in the presence of an external potential in the relaxation time approximation [177]. For this section we explicitly keep $\hbar$ and c in the expressions to ease comparisons with existing literature.

The Boltzmann equation in the relaxation time approximation is

$$
\frac{\partial f(x,p)}{\partial x^\alpha} V_\alpha + \frac{\partial f(x,p)}{\partial p^\alpha}(-\nabla_\alpha \phi) = -\frac{\delta f}{\tau} \tag{D.6}
$$

where f is the distribution function, and τ is the effective relaxation time.

In equilibrium, the distribution function of occupied states for a weakly interacting gas is given by the Fermi-Dirac distribution function $f_0(x,p) = 1/\{\exp[(\epsilon(p) - p \cdot V(x) - \mu)/T(x)] + 1\}$, where ϵ, p represent electron energy and momentum respectively. If a slowly varying local fluid velocity V_α ($\alpha = 1, 2, 3$) is set up in the system, the electron distribution function is modified. To the lowest order in the derivatives of V_α, we can write

$$f(p) = f_0(\epsilon) + \delta f(p), \tag{D.7}$$

where the non-equilibrium correction $\delta f(p)$ is of the form where

$$\delta f(p) = -\left(\frac{\partial f_0}{\partial \mu}\right) v_\alpha p_\beta C_{\alpha\beta\gamma\delta}(\epsilon) V_{\gamma\delta} \tag{D.8}$$

where $C_{\alpha\beta\gamma\delta}$ is a 4-rank tensor, μ represents the electron chemical potential, $v_\alpha = d\epsilon/dp_\alpha$ denotes the electron velocity, and $V_{\alpha\beta}$ is proportional to the derivative of the macroscopic fluid velocity defined as follows

$$V_{\alpha\beta} = \frac{1}{2}\left(\frac{\partial V_\alpha}{\partial x_\beta} + \frac{\partial V_\beta}{\partial x_\alpha}\right), \tag{D.9}$$

Similarly, in the presence of a slowly varying external potential ϕ, Eq. D.7 holds with

$$\delta f(p) = -\left(\frac{\partial f_0}{\partial \mu}\right) v_\alpha D_{\alpha\gamma}(\epsilon) \partial_\gamma \phi \ . \tag{D.10}$$

Here we consider both $\partial_\alpha \phi$ and $V_{\alpha\beta}$ non-zero, and hence δf is the sum of Eq. D.8 and Eq. D.10. After canceling out the terms proportional to D (which are related to conductivity) the linearized Boltzmann equation within the relaxation time approximation of the collision integral takes the form

$$\left(\frac{\partial f_0}{\partial \mu}\right)\left(v_\alpha p_\beta \frac{\partial V_\alpha}{\partial x_\beta} - \frac{1}{3} v_\alpha p_\alpha \nabla \cdot V\right) = -\frac{\delta f}{\tau} + (\nabla \phi) \cdot \frac{\partial \delta f}{\partial p} \ , \tag{D.11}$$

in analogy with Eq. 2 of [177] for the magnetic field case,

$$\left(\frac{\partial f_0}{\partial \mu}\right)\left(v_\alpha p_\beta \frac{\partial V_\alpha}{\partial x_\beta} - \frac{1}{3} v_\alpha p_\alpha \nabla \cdot V\right) = -\frac{\delta f}{\tau} + \frac{e}{c}(v \times B) \cdot \frac{\partial \delta f}{\partial p} \ . \tag{D.12}$$

For ease of calculation, let us decompose the $\nabla \phi$ term on the R.H.S of Boltzmann equation as

$$\nabla \phi = \hat{p}(\hat{p}.\nabla \phi) + (\nabla \phi - \hat{p}(\hat{p}.\nabla \phi)) = \hat{p}(\hat{p}.\nabla \phi) + \hat{p} \times (\nabla \phi \times \hat{p}) \tag{D.13}$$

In what follows, it is useful to define a basis ξ' for the 8 dimensional non-commutative algebra for the 4-rank tensor $C_{\gamma\delta\mu\nu}$ built out of the Kroenecker delta, Levi-civita and the components of the unit vector along the direction $\nabla \phi \times \hat{p}$ denoted by $\hat{b}$.

The basis $\xi'_1 - \xi'_8$ is defined as

$$\begin{aligned}
\xi'_{1_{\alpha\beta\gamma\delta}} &= \delta_{\alpha\gamma}\delta_{\beta\delta} + \delta_{\alpha\delta}\delta_{\beta\gamma} \\
\xi'_{2_{\alpha\beta\gamma\delta}} &= \delta_{\alpha\beta}\delta_{\gamma\delta} \\
\xi'_{3_{\alpha\beta\gamma\delta}} &= \hat{b}_\alpha\hat{b}_\delta\delta_{\beta\gamma} + \hat{b}_\alpha\hat{b}_\gamma\delta_{\beta\delta} + \delta_{\alpha\gamma}\hat{b}_\beta\hat{b}_\delta + \delta_{\alpha\delta}\hat{b}_\beta\hat{b}_\gamma \\
\xi'_{4_{\alpha\beta\gamma\delta}} &= \delta_{\alpha\beta}\hat{b}_\gamma\hat{b}_\delta \\
\xi'_{5_{\alpha\beta\gamma\delta}} &= \hat{b}_\beta\hat{b}_\delta\delta_{\gamma\delta} \\
\xi'_{6_{\alpha\beta\gamma\delta}} &= \hat{b}_\alpha\hat{b}_\beta\hat{b}_\gamma\hat{b}_\delta \\
\xi'_{7_{\alpha\beta\gamma\delta}} &= \delta_{\alpha\gamma}\hat{b}_{\beta\delta} + \hat{b}_{\alpha\gamma}\delta_{\beta\delta} + \delta_{\alpha\delta}\hat{b}_{\beta\gamma} + \hat{b}_{\alpha\delta}\delta_{\beta\gamma} \\
\xi'_{8_{\alpha\beta\gamma\delta}} &= \hat{b}_\alpha\hat{b}_{\beta\gamma}\hat{b}_\delta + \hat{b}_\alpha\hat{b}_{\beta\delta}\hat{b}_\gamma + \hat{b}_{\alpha\gamma}\hat{b}_\beta\hat{b}_\delta + \hat{b}_{\alpha\delta}\hat{b}_\beta\hat{b}_\gamma
\end{aligned} \tag{D.14}$$

Let us now simplify the L.H.S of Eq. D.11

$$\begin{aligned}
&\left(\frac{\partial f_0}{\partial\mu}\right)\left(v_\alpha p_\beta\frac{\partial V_\alpha}{\partial x_\beta} - \frac{1}{3}v_\alpha p_\alpha\nabla\cdot V\right) \\
&= \left(\frac{\partial f_0}{\partial\mu}\right)v_\alpha p_\beta V_{\mu\nu}\frac{1}{2}\left(\xi'_{1_{\alpha\beta\mu\nu}} - \frac{2}{3}\xi'_{2_{\alpha\beta\mu\nu}}\right)
\end{aligned} \tag{D.15}$$

Similarly the R.H.S of Eq. D.11 can be simplified as follows-

$$\begin{aligned}
\text{R.H.S} = -\frac{\delta f}{\tau} + (\nabla\phi)_\alpha\frac{\partial\delta f}{\partial(m)p_\alpha} &= -\frac{\delta f}{\tau} + (\hat{p}(\hat{p}.\nabla\phi) + \hat{p}\times(\nabla\phi\times\hat{p}))_\alpha\frac{\partial\delta f}{\partial(m)p_\alpha} \\
= -\delta f\left(\frac{1}{\tau} - \left(\frac{\hat{p}.\nabla\phi}{p}\right)\right) &- (\hat{p}\times(\nabla\phi\times\hat{p}))_\alpha\, v_a C_{a\alpha\gamma\delta}V_{\gamma\delta}\left(\frac{\partial f_0}{\partial\mu}\right)
\end{aligned} \tag{D.16}$$

Taking τ to the L.H.S we get

$$\begin{aligned}
\tau\text{L.H.S} &= -\delta f\left(1 - \tau\left(\frac{\hat{p}.\nabla\phi}{p}\right)\right) - \tau\left(\hat{p}\times(\nabla\phi\times\hat{p})\right)_\alpha v_a C_{a\alpha\gamma\delta}V_{\gamma\delta}\left(\frac{\partial f_0}{\partial\mu}\right) \\
&= v_\alpha p_\beta V_{rs}\left(\frac{\partial f_0}{\partial\mu}\right)\left(C_{\alpha\beta rs}\left(1 - \tau\frac{\hat{p}.\nabla\phi}{p}\right) - \frac{\tau b}{p}\epsilon_{\theta\beta\gamma}\hat{b}_\gamma C_{\alpha\theta rs}\right)
\end{aligned} \tag{D.17}$$

where b denotes the magnitude of the vector $\nabla\phi\times\hat{p}$.

Let $a = \left(1 - \tau\frac{\hat{p}.\nabla\phi}{p}\right)$ and $x = \frac{\tau b}{p}$. If we denote the angle between $\nabla\phi$ and $\hat{p}$ as θ, then $a = 1 - \frac{\nabla\phi\tau}{p}\cos\theta$ and $x = \frac{\tau\nabla\phi}{p}\sin\theta$.

Hence we get

$$\tau\text{L.H.S} = v_\alpha p_\beta V_{rs}\left(\frac{\partial f_0}{\partial\mu}\right)\left(aC_{\alpha\beta rs} - x\epsilon_{\theta\beta\gamma}\hat{b}_\gamma C_{\alpha\theta rs}\right) \tag{D.18}$$

Symmetrizing in α and β, we get

$$\begin{aligned}
\tau \text{L.H.S} &= v_\alpha p_\beta V_{rs} \left(\frac{\partial f_0}{\partial \mu}\right) \left(a \frac{C_{\alpha\beta rs} + C_{\beta\alpha rs}}{2} - x \frac{\epsilon_{\theta\beta\gamma} \hat{b}_\gamma C_{\alpha\theta rs} + \epsilon_{\theta\alpha\gamma} \hat{b}_\gamma C_{\beta\theta rs}}{2} \right) \\
&= v_\alpha p_\beta V_{rs} \frac{1}{2} C_{\gamma\delta rs} \left(\frac{\partial f_0}{\partial \mu}\right) \left(a\delta_{\alpha\gamma}\delta_{\beta\delta} + a\delta_{\beta\gamma}\delta_{\alpha\delta} + x(b_{\beta\delta}\delta_{\gamma\alpha} + b_{\alpha\delta}\delta_{\gamma\beta}) \right)
\end{aligned} \tag{D.19}$$

Subtracting the trace in $\alpha\beta$, we get

$$\begin{aligned}
\tau \text{L.H.S} &= v_\alpha p_\beta V_{rs} \frac{1}{2} C_{\gamma\delta rs} \left(\frac{\partial f_0}{\partial \mu}\right) \left(a\delta_{\alpha\gamma}\delta_{\beta\delta} + a\delta_{\beta\gamma}\delta_{\alpha\delta} - \frac{2}{3} a\delta_{\gamma\delta}\delta_{\alpha\beta} + x(b_{\beta\delta}\delta_{\gamma\alpha} + b_{\alpha\delta}\delta_{\gamma\beta} + b_{\alpha\gamma}\delta_{\beta\delta} + b_{\beta\gamma}\delta_{\alpha\delta} \right. \\
&= v_\alpha p_\beta V_{rs} \frac{1}{2} C_{\gamma\delta rs} \left(\frac{\partial f_0}{\partial \mu}\right) \left(a\xi'_1 - \frac{2}{3} a\xi'_2 + x\xi'_7 \right)_{\alpha\beta\gamma\delta}
\end{aligned}$$

Now combining L.H.S and R.H.S we finally get

$$\begin{aligned}
&\tau \left(\frac{\partial f_0}{\partial \mu}\right) v_\alpha p_\beta V_{\mu\nu} \frac{1}{2} \left(\xi'_{1_{\alpha\beta\mu\nu}} - \frac{2}{3} \xi'_{2_{\alpha\beta\mu\nu}} \right) = v_\alpha p_\beta V_{rs} \frac{1}{2} C_{\gamma\delta rs} \left(\frac{\partial f_0}{\partial \mu}\right) \left(a\xi'_1 - \frac{2}{3} a\xi'_2 + x\xi'_7 \right)_{\alpha\beta\gamma\delta} \\
&\Rightarrow \tau \left(\xi'_{1_{\alpha\beta\mu\nu}} - \frac{2}{3} \xi'_{2_{\alpha\beta\mu\nu}} \right) = \left(a\xi'_1 - \frac{2}{3} a\xi'_2 + x\xi'_7 \right)_{\alpha\beta\gamma\delta} C_{\gamma\delta\mu\nu}
\end{aligned}$$

Writing $C_{\gamma\delta\mu\nu} = \left(\sum_{i=1}^{8} c_i \xi'_{i\,\gamma\delta\mu\nu} \right)$ we can now solve for the coefficients

$$\begin{aligned}
&c_1 = \frac{a\tau}{2(a^2 + 4x^2)},\ c_2 = -\frac{\tau(a^2 - 2x^2)}{3a(a^2 + 4x^2)},\ c_3 = \frac{3a\tau x^2}{2(a^2 + x^2)(a^2 + 4x^2)}, c_4 = c_5 = -\frac{2\tau x^2}{a(a^2 + 4x^2)}, \\
&c_6 = \frac{6\tau x^4}{a(a^2 + x^2)(a^2 + 4x^2)},\ c_7 = -\frac{\tau x}{2(a^2 + 4x^2)},\ c_8 = -\frac{3\tau x^3}{2(a^2 + x^2)(a^2 + 4x^2)}
\end{aligned} \tag{D.20}$$

The viscosity tensor is given as

$$\eta_{\alpha\beta ab} = -\frac{2}{(2\pi\hbar)^3} \int \mathrm{d}^3(m)p \left(\frac{\partial f_0}{\partial \mu}\right) v_\alpha p_\beta v_\gamma p_\delta \left(\sum_{i=1}^{8} c_i \xi'_{i\,\gamma\delta ab} \right). \tag{D.21}$$

It is convenient to decompose the tensor $\eta_{\alpha\beta ab}$ in to 5 irreducible components corresponding to 5 tensors $M_{i\,\alpha\beta ab}$ $(i = 0, \cdot\cdot 4)$ in a system with a special direction $\hat{E} = \nabla\phi/|\nabla\phi|$ and reflection symmetry.

$$\eta_{\alpha\beta\gamma\delta} = \sum_{i=0}^{4} \eta_i M_{i\,\alpha\beta\gamma\delta}\ . \tag{D.22}$$

The tensors M_i are

$$
\begin{aligned}
M_0 &= 3\xi_6 - \xi_4 - \xi_5 + \frac{\xi_2}{3} \\
M_1 &= \xi_1 - \xi_2 - \xi_3 + \xi_4 + \xi_5 + \xi_6 \\
M_2 &= \xi_3 - 4\xi_6 \\
M_3 &= -\frac{1}{2}(\xi_7 - \xi_8) \\
M_4 &= -\xi_8
\end{aligned}
\tag{D.23}
$$

where the basis $\xi_1 - \xi_8$ is defined as

$$
\begin{aligned}
\xi_{1_{\alpha\beta\gamma\delta}} &= \delta_{\alpha\gamma}\delta_{\beta\delta} + \delta_{\alpha\delta}\delta_{\beta\gamma} \\
\xi_{2_{\alpha\beta\gamma\delta}} &= \delta_{\alpha\beta}\delta_{\gamma\delta} \\
\xi_{3_{\alpha\beta\gamma\delta}} &= \hat{E}_\alpha\hat{E}_\delta\delta_{\beta\gamma} + \hat{E}_\alpha\hat{E}_\gamma\delta_{\beta\delta} + \delta_{\alpha\gamma}\hat{E}_\beta\hat{E}_\delta + \delta_{\alpha\delta}\hat{E}_\beta\hat{E}_\gamma \\
\xi_{4_{\alpha\beta\gamma\delta}} &= \delta_{\alpha\beta}\hat{E}_\gamma\hat{E}_\delta \\
\xi_{5_{\alpha\beta\gamma\delta}} &= \hat{E}_\beta\hat{E}_\delta\delta_{\gamma\delta} \\
\xi_{6_{\alpha\beta\gamma\delta}} &= \hat{E}_\alpha\hat{E}_\beta\hat{E}_\gamma\hat{E}_\delta \\
\xi_{7_{\alpha\beta\gamma\delta}} &= \delta_{\alpha\gamma}\hat{E}_{\beta\delta} + \hat{E}_{\alpha\gamma}\delta_{\beta\delta} + \delta_{\alpha\delta}\hat{E}_{\beta\gamma} + \hat{E}_{\alpha\delta}\delta_{\beta\gamma} \\
\xi_{8_{\alpha\beta\gamma\delta}} &= \hat{E}_\alpha\hat{E}_{\beta\gamma}\hat{E}_\delta + \hat{E}_\alpha\hat{E}_{\beta\delta}\hat{E}_\gamma + \hat{E}_{\alpha\gamma}\hat{E}_\beta\hat{E}_\delta + \hat{E}_{\alpha\delta}\hat{E}_\beta\hat{E}_\gamma \ ,
\end{aligned}
\tag{D.24}
$$

where $\hat{E}$ is the unit vector along the gradient of the potential.

The components η_i can be extracted by projecting onto M_i and performing the three dimensional momentum integral in Eq. D.21. For arbitrarily large $\frac{|\tau\nabla\phi|}{k_F}$ the momentum integrals can not be performed analytically in general. However, we are interested in $\frac{|\tau\nabla\phi|}{k_F} \lesssim 1$, where the corrections to isotropy just start to become important. Then one can expand in $|\tau\nabla\phi|$ and perform the angular integrals to obtain,

$$
\begin{aligned}
\eta_0 &= \eta(0)[1 - \frac{31}{21}\tau^2(\nabla\phi)^2\frac{I_2}{I_1} + \mathcal{O}((\tau\nabla\phi)^4)] \\
\eta_1 &= \eta(0)[1 - \frac{13}{7}\tau^2(\nabla\phi)^2\frac{I_2}{I_1} + \mathcal{O}((\tau\nabla\phi)^4)] \\
\eta_2 &= \eta(0)[1 - \frac{11}{7}\tau^2(\nabla\phi)^2\frac{I_2}{I_1} + \mathcal{O}((\tau\nabla\phi)^4)] \\
\eta_3 &= 0, \ \ \eta_4 = 0 \ ,
\end{aligned}
\tag{D.25}
$$

where

$$
\eta(0) = \int p^6 dp \, \frac{\tau}{15\pi^2 m^2 \hbar^3}\left(\frac{\partial f_0}{\partial\mu}\right) \tag{D.26}
$$

is the shear viscosity in the absence of $\nabla\phi$, and I_1 and I_2 are.

$$
I_1 \ = \int p^6 dp \left(\frac{\partial f_0}{\partial\mu}\right), I_2 \ = \int p^4 dp \left(\frac{\partial f_0}{\partial\mu}\right) \tag{D.27}
$$

In particular, in the degenerate limit ($T \ll \mu$)

$$\left(\frac{\partial f_0}{\partial \mu}\right) \approx \delta(\frac{p^2}{2m} - \mu) \; , \tag{D.28}$$

and $\frac{I_1}{I_2} \approx \frac{1}{k_F^2}$ where $k_F = (3\pi^2 n)^{1/3}$ as before.

We can write Eq. D.25 in the form Eq. 5.101 by relating the relaxation time τ to the mean free path λ

$$\frac{\tau}{k_F} = \frac{\tau}{k_F}\frac{E_F}{E_F} = \frac{\lambda}{2E_F} \tag{D.29}$$

where we have used $E_F/k_F = v_F/2$, and $\tau v_F = \lambda$ is the mean free path.

This gives,

$$\begin{aligned}
\eta_0 &= \eta(0)[1 - \frac{31}{84}\frac{\lambda^2(\nabla\phi)^2}{\mu^2} + \mathcal{O}((\tau\nabla\phi)^4)] \\
\eta_1 &= \eta(0)[1 - \frac{13}{28}\frac{\lambda^2(\nabla\phi)^2}{\mu^2} + \mathcal{O}((\tau\nabla\phi)^4)] \\
\eta_2 &= \eta(0)[1 - \frac{11}{28}\frac{\lambda^2(\nabla\phi)^2}{\mu^2} + \mathcal{O}((\tau\nabla\phi)^4)] \\
\eta_3 &= 0, \;\; \eta_4 = 0 \; ,
\end{aligned} \tag{D.30}$$

where

$$\eta(0) = \frac{(2m\mu)^{\frac{5}{2}}\tau}{15\pi^2\hbar^3 m} \; , \tag{D.31}$$

in the degenerate limit.

Eq. D.30 gives an explicit result of the calculation in the relaxation time approximation which shows that the correction to the viscosity has the form Eq. 5.101. Hearteningly, the sign of $c_{(i)}$ is negative, meaning that the viscosity is reduced due to the external potential, a feature found is strongly coupled theories where a quasi-particle description is not possible and hence the Boltzmann transport equation can not be used to calculate the viscosity.

Interestingly, in the degenerate limit it is possible to do the momentum integrals analytically for general $\nabla\phi$. Using $\left(\frac{\partial f_0}{\partial \mu}\right) = \delta(\frac{p^2}{2m} - \mu)$, we get (here $x = \frac{\nabla\phi\tau}{\sqrt{2m\mu}}$)

$$\begin{aligned}
\eta_0 =& \frac{(2m\mu)^{\frac{5}{2}}\tau}{96 m\hbar^3\pi^2 x^5\sqrt{3\,x^2+1}}\Bigg[- 8\sqrt{3(x^2+1}\left(5x^4+18x^2+9\right)\tanh^{-1}(x) \\
& - 24\,x\sqrt{3x^2+1}\left(5x^2+3\right) - 6\left(8x^4+11x^2+3\right) \\
& \log\left(\frac{x\left(7x-4\sqrt{3x^2+1}\right)+1}{x\left(4\sqrt{3x^2+1}+7x\right)+1}\right)\Bigg]
\end{aligned} \tag{D.32}$$

$$\eta_1 = \frac{(2m\mu)^{\frac{5}{2}}\tau}{96m\hbar^3\pi^2x^5\sqrt{3\ x^2+1}}\Bigg[-4x\left(x^2+3\right)\sqrt{3x^2+1} + 4\sqrt{3x^2+1}\left(x^4-6x^2-3\right)\tanh^{-1}(x) - (3+4x^4+9x^2) \log\left(\frac{x\left(7x-4\sqrt{3x^2+1}\right)+1}{x\left(4\sqrt{3x^2+1}+7x\right)+1}\right)\Bigg] \tag{D.33}$$

$$\eta_2 = \frac{(2m\mu)^{\frac{5}{2}}\tau}{48m\hbar^3\pi^2x^5\sqrt{3\ x^2+1}}\Bigg[8x\sqrt{3x^2+1}\left(4x^2+3\right) + 4\sqrt{3x^2+1}\left(x^4+6x^2+3\right)\tanh^{-1}\left(\frac{2x}{x^2+1}\right) + (6+13x^4+21x^2) \log\left(\frac{x\left(7x-4\sqrt{3x^2+1}\right)+1}{x\left(4\sqrt{3x^2+1}+7x\right)+1}\right)\Bigg] \tag{D.34}$$

$$\eta_3 = 0$$
$$\eta_4 = 0$$

Expanding in small x we obtain,

$$\eta_0 = \frac{(2m\mu)^{\frac{5}{2}}\tau}{15\pi^2\hbar^3 m}\left(1-\frac{31\tau^2\nabla\phi^2}{42m\mu}+\mathcal{O}[(\frac{\tau\nabla\phi}{\sqrt{2m\mu}})^4]\right), \quad \eta_1 = \frac{(2m\mu)^{\frac{5}{2}}\tau}{15\pi^2\hbar^3 m}\left(1-\frac{13\tau^2\nabla\phi^2}{14m\mu}+\mathcal{O}[(\frac{\tau\nabla\phi}{\sqrt{2m\mu}})^4]\right),$$
$$\eta_2 = \frac{(2m\mu)^{\frac{5}{2}}\tau}{15\pi^2\hbar^3 m}\left(1-\frac{11\tau^2\nabla\phi^2}{14m\mu}+\mathcal{O}[(\frac{\tau\nabla\phi}{\sqrt{2m\mu}})^4]\right),$$
$$\eta_3 = 0, \qquad \eta_4 = 0.$$

Bibliography

[1] N. Iizuka, S. Kachru, N. Kundu, P. Narayan, N. Sircar, and S. P. Trivedi, "Bianchi attractors: a classification of extremal black brane geometries.", *Journal of High Energy Physics*, **7**, (July, 2012), 193, [arXiv:1201.4861]. 1, 84

[2] N. Iizuka, S. Kachru, N. Kundu, P. Narayan, N. Sircar, et al., "Extremal Horizons with Reduced Symmetry: Hyperscaling Violation, Stripes, and a Classification for the Homogeneous Case.", *JHEP*, **1303**, (2013), 126, [arXiv:1212.1948]. 1, 39, 84

[3] O. Aharony, S. S. Gubser, J. M. Maldacena, H. Ooguri, and Y. Oz, "Large N field theories, string theory and gravity.", *Phys.Rept.*, **323**, (2000), 183–386, [hep-th/9905111]. 2

[4] S. A. Hartnoll, "Lectures on holographic methods for condensed matter physics.", *Class.Quant.Grav.*, **26**, (2009), 224002, [arXiv:0903.3246]. 3

[5] C. P. Herzog, "Lectures on Holographic Superfluidity and Superconductivity.", *J. Phys.*, **A42**, (2009), 343001, [arXiv:0904.1975]. 3, 5

[6] J. McGreevy, "Holographic duality with a view toward many-body physics.", *Adv. High Energy Phys.*, **2010**, (2010), 723105, [arXiv:0909.0518]. 3, 5

[7] S. Sachdev, "What can gauge-gravity duality teach us about condensed matter physics?.", *Ann. Rev. Condensed Matter Phys.*, **3**, (2012), 9–33, [arXiv:1108.1197]. 3, 5

[8] J. Casalderrey-Solana, H. Liu, D. Mateos, K. Rajagopal, and U. A. Wiedemann, "Gauge/String Duality, Hot QCD and Heavy Ion Collisions.", arXiv:1101.0618, [arXiv:1101.0618]. 3

[9] S. A. Hartnoll, "Lectures on holographic methods for condensed matter physics.", *Class. Quant. Grav.*, **26**, (2009), 224002, [arXiv:0903.3246]. 5

[10] S. S. Gubser, "Breaking an Abelian gauge symmetry near a black hole horizon.", *Phys. Rev.*, **D78**, (2008), 065034, [arXiv:0801.2977]. 5

[11] S. A. Hartnoll, C. P. Herzog, and G. T. Horowitz, "Building a Holographic Superconductor.", *Phys. Rev. Lett.*, **101**, (2008), 031601, [arXiv:0803.3295]. 5

[12] S. A. Hartnoll, C. P. Herzog, and G. T. Horowitz, “Holographic Superconductors.”, *JHEP*, **12**, (2008), 015, [arXiv:0810.1563]. 5

[13] G. T. Horowitz, “Introduction to Holographic Superconductors.”, *Lect. Notes Phys.*, **828**, (2011), 313–347, [arXiv:1002.1722]. 5

[14] S. Kachru, X. Liu, and M. Mulligan, “Gravity duals of Lifshitz-like fixed points.”, *Phys. Rev.*, **D78**, (2008), 106005, [arXiv:0808.1725]. 5

[15] M. Taylor, “Non-relativistic holography.”, arXiv:0812.0530, [arXiv:0812.0530]. 5

[16] K. Goldstein, S. Kachru, S. Prakash, and S. P. Trivedi, “Holography of Charged Dilaton Black Holes.”, *JHEP*, **08**, (2010), 078, [arXiv:0911.3586]. 5, 7

[17] C. Charmousis, B. Gouteraux, B. S. Kim, E. Kiritsis, and R. Meyer, “Effective Holographic Theories for low-temperature condensed matter systems.”, *JHEP*, **11**, (2010), 151, [arXiv:1005.4690]. 5

[18] N. Iizuka, N. Kundu, P. Narayan, and S. P. Trivedi, “Holographic Fermi and Non-Fermi Liquids with Transitions in Dilaton Gravity.”, *JHEP*, **01**, (2012), 094, [arXiv:1105.1162]. 5

[19] N. Ogawa, T. Takayanagi, and T. Ugajin, “Holographic Fermi Surfaces and Entanglement Entropy.”, *JHEP*, **01**, (2012), 125, [arXiv:1111.1023]. 5

[20] L. Huijse, S. Sachdev, and B. Swingle, “Hidden Fermi surfaces in compressible states of gauge-gravity duality.”, *Phys. Rev.*, **B85**, (2012), 035121, [arXiv:1112.0573]. 5

[21] E. Shaghoulian, “Holographic Entanglement Entropy and Fermi Surfaces.”, *JHEP*, **05**, (2012), 065, [arXiv:1112.2702]. 5

[22] X. Dong, S. Harrison, S. Kachru, G. Torroba, and H. Wang, “Aspects of holography for theories with hyperscaling violation.”, *JHEP*, **06**, (2012), 041, [arXiv:1201.1905]. 5

[23] E. Perlmutter, “Hyperscaling violation from supergravity.”, *JHEP*, **06**, (2012), 165, [arXiv:1205.0242]. 5

[24] K. Balasubramanian and K. Narayan, “Lifshitz spacetimes from AdS null and cosmological solutions.”, *JHEP*, **08**, (2010), 014, [arXiv:1005.3291]. 5

[25] A. Donos and J. P. Gauntlett, “Lifshitz Solutions of D=10 and D=11 supergravity.”, *JHEP*, **12**, (2010), 002, [arXiv:1008.2062]. 5

[26] R. Gregory and R. Laflamme, “Black strings and p-branes are unstable.”, *Phys. Rev. Lett.* **70**, *2837 (1993)*. 5

[27] K. Narayan, "On Lifshitz scaling and hyperscaling violation in string theory.", *Phys. Rev.*, **D85**, (2012), 106006, [arXiv:1202.5935]. 5, 7

[28] H. Singh, "Lifshitz/Schródinger Dp-branes and dynamical exponents.", *JHEP*, **07**, (2012), 082, [arXiv:1202.6533]. 5

[29] P. Dey and S. Roy, "Lifshitz-like space-time from intersecting branes in string/M theory.", *JHEP*, **06**, (2012), 129, [arXiv:1203.5381]. 5, 7

[30] P. Dey and S. Roy, "Intersecting D-branes and Lifshitz-like space-time.", *Phys. Rev.*, **D86**, (2012), 066009, [arXiv:1204.4858]. 5, 7

[31] [arXiv:1204.4858]. 5

[32] H. Ooguri and C.-S. Park, "Holographic End-Point of Spatially Modulated Phase Transition.", *Phys. Rev.*, **D82**, (2010), 126001, [arXiv:1007.3737]. 5

[33] A. Donos, J. P. Gauntlett, and C. Pantelidou, "Spatially modulated instabilities of magnetic black branes.", *JHEP*, **01**, (2012), 061, [arXiv:1109.0471]. 5, 33

[34] N. Iizuka, S. Kachru, N. Kundu, P. Narayan, N. Sircar, and S. P. Trivedi, "Bianchi Attractors: A Classification of Extremal Black Brane Geometries.", *JHEP*, **07**, (2012), 193, [arXiv:1201.4861]. 5, 6, 9, 11, 18, 20, 26, 33

[35] N. Iizuka, S. Kachru, N. Kundu, P. Narayan, N. Sircar, S. P. Trivedi, and H. Wang, "Extremal Horizons with Reduced Symmetry: Hyperscaling Violation, Stripes, and a Classification for the Homogeneous Case.", *JHEP*, **03**, (2013), 126, [arXiv:1212.1948]. 5, 6

[36] N. Iizuka and K. Maeda, "Stripe Instabilities of Geometries with Hyperscaling Violation.", *Phys. Rev.*, **D87**, (2013), no. 12, 126006, [arXiv:1301.5677]. 5

[37] G. T. Horowitz, J. E. Santos, and D. Tong, "Optical Conductivity with Holographic Lattices.", *JHEP*, **07**, (2012), 168, [arXiv:1204.0519]. 5

[38] Y.-Y. Bu, J. Erdmenger, J. P. Shock, and M. Strydom, "Magnetic field induced lattice ground states from holography.", *JHEP*, **03**, (2013), 165, [arXiv:1210.6669]. 5

[39] M. Rozali, D. Smyth, E. Sorkin, and J. B. Stang, "Holographic Stripes.", *Phys. Rev. Lett.*, **110**, (2013), no. 20, 201603, [arXiv:1211.5600]. 5

[40] A. Donos and S. A. Hartnoll, "Interaction-driven localization in holography.", *Nature Phys.*, **9**, (2013), 649–655, [arXiv:1212.2998]. 5

[41] S. Cremonini and A. Sinkovics, "Spatially Modulated Instabilities of Geometries with Hyperscaling Violation.", *JHEP*, **01**, (2014), 099, [arXiv:1212.4172]. 5

[42] D. Vegh, “Holography without translational symmetry.”, arXiv:1301.0537, [arXiv:1301.0537]. 5

[43] N. Bao, S. Harrison, S. Kachru, and S. Sachdev, “Vortex Lattices and Crystalline Geometries.”, *Phys. Rev.*, **D88**, (2013), no. 2, 026002, [arXiv:1303.4390]. 5

[44] A. Donos, “Striped phases from holography.”, *JHEP*, **05**, (2013), 059, [arXiv:1303.7211]. 5

[45] N. Bao and S. Harrison, “Crystalline Scaling Geometries from Vortex Lattices.”, *Phys. Rev.*, **D88**, (2013), 046009, [arXiv:1306.1532]. 5

[46] S. Harrison, “Landau Levels, Anisotropy and Holography.”, arXiv:1306.3224, [arXiv:1306.3224]. 5, 9

[47] P. Chesler, A. Lucas, and S. Sachdev, “Conformal field theories in a periodic potential: results from holography and field theory.”, *Phys. Rev.*, **D89**, (2014), no. 2, 026005, [arXiv:1308.0329]. 5

[48] S. Ferrara, R. Kallosh, and A. Strominger, “N=2 extremal black holes.”, *Phys. Rev.*, **D52**, (1995), R5412–R5416, [hep-th/9508072]. 5

[49] S. Bellucci, S. Ferrara, R. Kallosh, and A. Marrani, “Extremal Black Hole and Flux Vacua Attractors.”, *Lect. Notes Phys.*, **755**, (2008), 115–191, [arXiv:0711.4547]. 5

[50] S. Ferrara, G. W. Gibbons, and R. Kallosh, “Black holes and critical points in moduli space.”, *Nucl. Phys.*, **B500**, (1997), 75–93, [hep-th/9702103]. 6

[51] G. W. Gibbons, R. Kallosh, and B. Kol, “Moduli, scalar charges, and the first law of black hole thermodynamics.”, *Phys. Rev. Lett.*, **77**, (1996), 4992–4995, [hep-th/9607108]. 6

[52] A. Sen, “Black hole entropy function and the attractor mechanism in higher derivative gravity.”, *JHEP*, **09**, (2005), 038, [hep-th/0506177]. 6

[53] K. Goldstein, N. Iizuka, R. P. Jena, and S. P. Trivedi, “Non-supersymmetric attractors.”, *Phys. Rev.*, **D72**, (2005), 124021, [hep-th/0507096]. 6

[54] R. Kallosh, N. Sivanandam, and M. Soroush, “The Non-BPS black hole attractor equation.”, *JHEP*, **03**, (2006), 060, [hep-th/0602005]. 6

[55] S. Kachru, R. Kallosh, and M. Shmakova, “Generalized Attractor Points in Gauged Supergravity.”, *Phys. Rev.*, **D84**, (2011), 046003, [arXiv:1104.2884]. 6

[56] H. Braviner, R. Gregory, and S. F. Ross, “Flows involving Lifshitz solutions.”, *Class. Quant. Grav.*, **28**, (2011), 225028, [arXiv:1108.3067]. 7

[57] Y. Korovin, K. Skenderis, and M. Taylor, "Lifshitz as a deformation of Anti-de Sitter.", *JHEP*, **08**, (2013), 026, [arXiv:1304.7776]. 7

[58] S. P. Kumar, "Heavy quark density in N=4 SYM: from hedgehog to Lifshitz spacetimes.", *JHEP*, **08**, (2012), 155, [arXiv:1206.5140]. 7

[59] H. Singh, "Lifshitz to AdS flow with interpolating p-brane solutions.", *JHEP*, **08**, (2013), 097, [arXiv:1305.3784]. 7

[60] A. F. Faedo, B. Fraser, and S. P. Kumar, "Supersymmetric Lifshitz-like backgrounds from $\mathcal{N} = 4$ SYM with heavy quark density.", *JHEP*, **02**, (2014), 066, [arXiv:1310.0206]. 7

[61] E. Poisson, "A Relativist's Toolkit: The Mathematics of Black-Hole Mechanics.", *Cambridge University Press*. 8

[62] M. M. C. H. H. Stephani, D. Kramer and E. Herlt, "The Large Scale Structure of Space-Time.", *Cambridge Monographs on Mathematical Physics*. 8

[63] M. M. C. H. H. Stephani, D. Kramer and E. Herlt, "Exact Solutions of Einstein's Field Equations.", *Cambridge Monographs on Mathematical Physics*. 9

[64] L. D. Landau and E. M. Lifshitz, "The Classical Theory of Fields.", *Princeton Series in Physic*. 10

[65] M. P. Ryan and L. C. Shepley, "Homogeneous Relativistic Cosmologies.", *Princeton Series in Physics*. 10, 18

[66] J. T. Liu and Z. Zhao, "Holographic Lifshitz flows and the null energy condition.", arXiv:1206.1047, [arXiv:1206.1047]. 30

[67] R. M. Wald, "General Relativity.", *University Of Chicago Press*. 30

[68] *University Of Chicago Press*. 30

[69] *University Of Chicago Press*. 30

[70] E. T. Akhmedov, "A Remark on the AdS / CFT correspondence and the renormalization group flow.", *Phys. Lett.*, **B442**, (1998), 152–158, [hep-th/9806217]. 30

[71] E. Alvarez and C. Gomez, "Geometric holography, the renormalization group and the c theorem.", *Nucl. Phys.*, **B541**, (1999), 441–460, [hep-th/9807226]. 30

[72] A. Gorsky, "Integrability of the RG flows and the bulk / boundary correspondence.", hep-th/9812250, [hep-th/9812250]. 30

[73] M. Porrati and A. Starinets, "RG fixed points in supergravity duals of 4-D field theory and asymptotically AdS spaces.", *Phys. Lett.*, **B454**, (1999), 77–83, [hep-th/9903085]. 30

[74] V. Balasubramanian and P. Kraus, “Space-time and the holographic renormalization group.”, *Phys. Rev. Lett.*, **83**, (1999), 3605–3608, [hep-th/9903190]. 30

[75] D. Z. Freedman, S. S. Gubser, K. Pilch, and N. P. Warner, “Renormalization group flows from holography supersymmetry and a c theorem.”, *Adv. Theor. Math. Phys.*, **3**, (1999), 363–417, [hep-th/9904017]. 30

[76] L. Girardello, M. Petrini, M. Porrati, and A. Zaffaroni, “Novel local CFT and exact results on perturbations of N=4 superYang Mills from AdS dynamics.”, *JHEP*, **12**, (1998), 022, [hep-th/9810126]. 30

[77] S. Kachru, N. Kundu, A. Saha, R. Samanta, and S. P. Trivedi, “Interpolating from Bianchi Attractors to Lifshitz and AdS Spacetimes.”, *JHEP*, **1403**, (2014), 074, [arXiv:1310.5740]. 35, 49, 55

[78] S. Ferrara, R. Kallosh, and A. Strominger, “N=2 extremal black holes.”, *Phys.Rev.*, **D52**, (1995), 5412–5416, [hep-th/9508072]. 35, 48

[79] A. Strominger, “Macroscopic entropy of N=2 extremal black holes.”, *Phys.Lett.*, **B383**, (1996), 39–43, [hep-th/9602111]. 35, 48

[80] S. Bellucci, S. Ferrara, R. Kallosh, and A. Marrani, “Extremal Black Hole and Flux Vacua Attractors.”, *Lect.Notes Phys.*, **755**, (2008), 115–191, [arXiv:0711.4547]. 35

[81] S. Ferrara, K. Hayakawa, and A. Marrani, “Lectures on Attractors and Black Holes.”, *Fortsch.Phys.*, **56**, (2008), 993–1046, [arXiv:0805.2498]. 35

[82] S. Ferrara, G. W. Gibbons, and R. Kallosh, “Black holes and critical points in moduli space.”, *Nucl.Phys.*, **B500**, (1997), 75–93, [hep-th/9702103]. 35

[83] A. Sen, “Black Hole Entropy Function, Attractors and Precision Counting of Microstates.”, *Gen.Rel.Grav.*, **40**, (2008), 2249–2431, [arXiv:0708.1270]. 35

[84] K. Goldstein, N. Iizuka, R. P. Jena, and S. P. Trivedi, “Non-supersymmetric attractors.”, *Phys.Rev.*, **D72**, (2005), 124021, [hep-th/0507096]. 35, 36, 44, 55

[85] N. Halmagyi, “BPS Black Hole Horizons in N=2 Gauged Supergravity.”, arXiv:1308.1439, [arXiv:1308.1439]. 35

[86] S. Barisch-Dick, G. Lopes Cardoso, M. Haack, and S. Nampuri, “Extremal black brane solutions in five-dimensional gauged supergravity.”, *JHEP*, **1302**, (2013), 103, [arXiv:1211.0832]. 35

[87] D. Klemm and O. Vaughan, “Nonextremal black holes in gauged supergravity and the real formulation of special geometry.”, *JHEP*, **1301**, (2013), 053, [arXiv:1207.2679]. 35

[88] S. Barisch, G. Lopes Cardoso, M. Haack, S. Nampuri, and N. A. Obers, "Nernst branes in gauged supergravity.", *JHEP*, **1111**, (2011), 090, [arXiv:1108.0296]. 35

[89] S. Kachru, R. Kallosh, and M. Shmakova, "Generalized Attractor Points in Gauged Supergravity.", *Phys.Rev.*, **D84**, (2011), 046003, [arXiv:1104.2884]. 35, 43

[90] G. Dall'Agata and A. Gnecchi, "Flow equations and attractors for black holes in N = 2 U(1) gauged supergravity.", *JHEP*, **1103**, (2011), 037, [arXiv:1012.3756]. 35

[91] K. Hristov, H. Looyestijn, and S. Vandoren, "BPS black holes in N=2 D=4 gauged supergravities.", *JHEP*, **1008**, (2010), 103, [arXiv:1005.3650]. 35

[92] A. Ceresole, G. Dall'Agata, R. Kallosh, and A. Van Proeyen, "Hypermultiplets, domain walls and supersymmetric attractors.", *Phys.Rev.*, **D64**, (2001), 104006, [hep-th/0104056]. 35

[93] S. L. Cacciatori and D. Klemm, "Supersymmetric AdS(4) black holes and attractors.", *JHEP*, **1001**, (2010), 085, [arXiv:0911.4926]. 35

[94] K. Inbasekar and P. K. Tripathy, "Stability of Bianchi attractors in Gauged Supergravity.", *JHEP*, **1310**, (2013), 163, [arXiv:1307.1314]. 35, 36, 44, 47, 48, 49, 54

[95] K. Inbasekar and P. K. Tripathy, "Generalized Attractors in Five-Dimensional Gauged Supergravity.", *JHEP*, **1209**, (2012), 003, [arXiv:1206.3887]. 35, 36, 43, 44, 45

[96] D. Cassani and A. F. Faedo, "Constructing Lifshitz solutions from AdS.", *JHEP*, **1105**, (2011), 013, [arXiv:1102.5344]. 35, 37, 53

[97] N. Halmagyi, M. Petrini, and A. Zaffaroni, "Non-Relativistic Solutions of N=2 Gauged Supergravity.", *JHEP*, **1108**, (2011), 041, [arXiv:1102.5740]. 35, 37, 53

[98] P. Breitenlohner and D. Z. Freedman, "Stability in Gauged Extended Supergravity.", *Annals Phys.*, **144**, (1982), 249. 36

[99] P. Breitenlohner and D. Z. Freedman, "Positive Energy in anti-De Sitter Backgrounds and Gauged Extended Supergravity.", *Phys.Lett.*, **B115**, (1982), 197. 36

[100] H. Lu, C. Pope, and P. Townsend, "Domain walls from anti-de Sitter space-time.", *Phys.Lett.*, **B391**, (1997), 39–46, [hep-th/9607164]. 37, 53

[101] H. Lu, C. Pope, and J. Rahmfeld, "A Construction of Killing spinors on S**n.", *J.Math.Phys.*, **40**, (1999), 4518–4526, [hep-th/9805151]. 37, 53

[102] S. L. Cacciatori, D. Klemm, and W. A. Sabra, "Supersymmetric domain walls and strings in D = 5 gauged supergravity coupled to vector multiplets.", *JHEP*, **03**, (2003), 023, [hep-th/0302218]. 37

[103] D. Klemm and W. A. Sabra, “Supersymmetry of black strings in D = 5 gauged supergravities.”, *Phys. Rev.*, **D62**, (2000), 024003, [hep-th/0001131]. 37

[104] A. Almuhairi and J. Polchinski, “Magnetic AdS x R2: Supersymmetry and stability.”, arXiv:1108.1213, [arXiv:1108.1213]. 37, 53

[105] M. Ryan and L. Shepley. *Homogeneous Relativistic Cosmologies*. Princeton Series in Physics. Princeton University Press, (1975). 38, 45

[106] L. Landau and . Lifshitz. *The classical theory of fields*. Teoreticheskaia fizika (Izd. 4-e) (Landau, L. D, 1908-1968). Pergamon Press, (1975). 38, 39, 45

[107] N. Iizuka, S. Kachru, N. Kundu, P. Narayan, N. Sircar, et al., “Bianchi Attractors: A Classification of Extremal Black Brane Geometries.”, *JHEP*, **1207**, (2012), 193, [arXiv:1201.4861]. 39

[108] A. Ceresole and G. Dall’Agata, “General matter coupled N=2, D = 5 gauged supergravity.”, *Nucl.Phys.*, **B585**, (2000), 143–170, [hep-th/0004111]. 40

[109] M. Gunaydin, G. Sierra, and P. Townsend, “Gauging the d = 5 maxwell/einstein supergravity theories: More on jordan algebras.”, *Nuclear Physics B*, **253**, (1985), no. 0, 573 – 608. 40, 41

[110] M. Gunaydin, G. Sierra, and P. Townsend, “The geometry of n = 2 maxwell-einstein supergravity and jordan algebras.”, *Nuclear Physics B*, **242**, (1984), no. 1, 244 – 268. 40, 41

[111] M. Gunaydin and M. Zagermann, “The Gauging of five-dimensional, N=2 Maxwell-Einstein supergravity theories coupled to tensor multiplets.”, *Nucl.Phys.*, **B572**, (2000), 131–150, [hep-th/9912027]. 40, 53

[112] M. Gunaydin and M. Zagermann, “The Vacua of 5-D, N=2 gauged Yang-Mills/Einstein tensor supergravity: Abelian case.”, *Phys.Rev.*, **D62**, (2000), 044028, [hep-th/0002228]. 40, 42

[113] B. de Wit and A. Van Proeyen, “Special geometry, cubic polynomials and homogeneous quaternionic spaces.”, *Commun.Math.Phys.*, **149**, (1992), 307–334, [hep-th/9112027]. 40

[114] G. Policastro, D. T. Son, and A. O. Starinets, “The Shear viscosity of strongly coupled N=4 supersymmetric Yang-Mills plasma.”, *Phys.Rev.Lett.*, **87**, (2001), 081601, [hep-th/0104066]. 57

[115] P. Kovtun, D. T. Son, and A. O. Starinets, “Holography and hydrodynamics: Diffusion on stretched horizons.”, *JHEP*, **0310**, (2003), 064, [hep-th/0309213]. 57, 72

[116] P. K. Kovtun, D. T. Son, and A. O. Starinets, “Viscosity in strongly interacting quantum field theories from black hole physics.”, *Phys. Rev. Lett.*, **94**, (Mar, 2005), 111601. 57

[117] Y. Kats and P. Petrov, “Effect of curvature squared corrections in AdS on the viscosity of the dual gauge theory.”, *JHEP*, **0901**, (2009), 044, [arXiv:0712.0743]. 57

[118] A. Buchel, R. C. Myers, and A. Sinha, “Beyond eta/s = 1/4 pi.”, *JHEP*, **0903**, (2009), 084, [arXiv:0812.2521]. 57

[119] A. Sinha and R. C. Myers, “The Viscosity bound in string theory.”, *Nucl.Phys.*, **A830**, (2009), 295C–298C, [arXiv:0907.4798]. 57

[120] S. Cremonini, “The Shear Viscosity to Entropy Ratio: A Status Report.”, *Mod.Phys.Lett.*, **B25**, (2011), 1867–1888, [arXiv:1108.0677]. 57

[121] P. Basu and J.-H. Oh, “Analytic Approaches to Anisotropic Holographic Superfluids.”, *JHEP*, **1207**, (2012), 106, [arXiv:1109.4592]. 57, 58

[122] A. Bhattacharyya and D. Roychowdhury, “Viscosity bound for anisotropic superfluids in higher derivative gravity.”, *JHEP*, **03**, (2015), 063, [arXiv:1410.3222]. 57

[123] M. Brigante, H. Liu, R. C. Myers, S. Shenker, and S. Yaida, “Viscosity Bound Violation in Higher Derivative Gravity.”, *Phys.Rev.*, **D77**, (2008), 126006, [arXiv:0712.0805]. 57

[124] M. Brigante, H. Liu, R. C. Myers, S. Shenker, and S. Yaida, “The Viscosity Bound and Causality Violation.”, *Phys.Rev.Lett.*, **100**, (2008), 191601, [arXiv:0802.3318]. 57

[125] T. D. Cohen, “Is there a ’most perfect fluid’ consistent with quantum field theory?.”, *Phys. Rev. Lett.*, **99**, (2007), 021602, [hep-th/0702136]. 58

[126] A. Buchel and S. Cremonini, “Viscosity Bound and Causality in Superfluid Plasma.”, *JHEP*, **10**, (2010), 026, [arXiv:1007.2963]. 58

[127] K. Landsteiner and J. Mas, “The Shear viscosity of the non-commutative plasma.”, *JHEP*, **0707**, (2007), 088, [arXiv:0706.0411]. 58

[128] T. Azeyanagi, W. Li, and T. Takayanagi, “On String Theory Duals of Lifshitz-like Fixed Points.”, *JHEP*, **0906**, (2009), 084, [arXiv:0905.0688]. 58, 68, 83

[129] M. Natsuume and M. Ohta, “The Shear viscosity of holographic superfluids.”, *Prog.Theor.Phys.*, **124**, (2010), 931–951, [arXiv:1008.4142]. 58

[130] J. Erdmenger, P. Kerner, and H. Zeller, “Non-universal shear viscosity from Einstein gravity.”, *Phys.Lett.*, **B699**, (2011), 301–304, [arXiv:1011.5912]. 58

[131] J. Erdmenger, P. Kerner, and H. Zeller, "Transport in Anisotropic Superfluids: A Holographic Description.", *JHEP*, **1201**, (2012), 059, [arXiv:1110.0007]. 58

[132] D. Mateos and D. Trancanelli, "The anisotropic N=4 super Yang-Mills plasma and its instabilities.", *Phys.Rev.Lett.*, **107**, (2011), 101601, [arXiv:1105.3472]. 58

[133] D. Mateos and D. Trancanelli, "Thermodynamics and Instabilities of a Strongly Coupled Anisotropic Plasma.", *JHEP*, **1107**, (2011), 054, [arXiv:1106.1637]. 58

[134] A. Rebhan and D. Steineder, "Violation of the Holographic Viscosity Bound in a Strongly Coupled Anisotropic Plasma.", *Phys.Rev.Lett.*, **108**, (2012), 021601, [arXiv:1110.6825]. 58, 59, 67, 72, 144

[135] J. Polchinski and E. Silverstein, "Large-density field theory, viscosity, and '$2k_F$' singularities from string duals.", *Class.Quant.Grav.*, **29**, (2012), 194008, [arXiv:1203.1015]. 58, 84

[136] D. Giataganas, "Probing strongly coupled anisotropic plasma.", *JHEP*, **07**, (2012), 031, [arXiv:1202.4436]. 58

[137] N. Iizuka and K. Maeda, "Study of Anisotropic Black Branes in Asymptotically anti-de Sitter.", *JHEP*, **1207**, (2012), 129, [arXiv:1204.3008]. 58

[138] K. A. Mamo, "Holographic RG flow of the shear viscosity to entropy density ratio in strongly coupled anisotropic plasma.", *JHEP*, **1210**, (2012), 070, [arXiv:1205.1797]. 58, 72

[139] S. Jain, N. Kundu, K. Sen, A. Sinha, and S. P. Trivedi, "A Strongly Coupled Anisotropic Fluid From Dilaton Driven Holography.", *JHEP*, **01**, (2015), 005, [arXiv:1406.4874]. 58, 59, 60, 61, 65, 71, 83, 86, 88, 89, 90, 91, 146

[140] R. Critelli, S. Finazzo, M. Zaniboni, and J. Noronha, "Anisotropic shear viscosity of a strongly coupled non-Abelian plasma from magnetic branes.", *Phys.Rev.*, **D90**, (2014), no. 6, 066006, [arXiv:1406.6019]. 58, 66, 67, 81, 82

[141] X.-H. Ge, Y. Ling, C. Niu, and S.-J. Sin, "Thermoelectric conductivities, shear viscosity, and stability in an anisotropic linear axion model.", *Phys. Rev.*, **D92**, (2015), no. 10, 106005, [arXiv:1412.8346]. 58

[142] E. Witten, "Anti-de Sitter space, thermal phase transition, and confinement in gauge theories.", *Adv.Theor.Math.Phys.*, **2**, (1998), 505–532, [hep-th/9803131]. 60

[143] I. R. Klebanov and M. J. Strassler, "Supergravity and a confining gauge theory: Duality cascades and chi SB resolution of naked singularities.", *JHEP*, **0008**, (2000), 052, [hep-th/0007191]. 60

[144] N. Iqbal and H. Liu, “Universality of the hydrodynamic limit in AdS/CFT and the membrane paradigm.”, *Phys.Rev.*, **D79**, (2009), 025023, [arXiv:0809.3808]. 62, 72

[145] E. D’Hoker and P. Kraus, “Magnetic Brane Solutions in AdS.”, *JHEP*, **0910**, (2009), 088, [arXiv:0908.3875]. 66

[146] R. C. Myers, M. F. Paulos, and A. Sinha, “Holographic Hydrodynamics with a Chemical Potential.”, *JHEP*, **0906**, (2009), 006, [arXiv:0903.2834]. 74

[147] S. K. Chakrabarti, S. Chakrabortty, and S. Jain, “Proof of universality of electrical conductivity at finite chemical potential.”, *JHEP*, **1102**, (2011), 073, [arXiv:1011.3499]. 74, 161

[148] J. Maharana and J. H. Schwarz, “Noncompact symmetries in string theory.”, *Nucl.Phys.*, **B390**, (1993), 3–32, [hep-th/9207016]. 78, 79

[149] L. D. Landau and E. M. Lifshitz, “*Fluid Mechanics, Second Edition: Volume 6 (Course of Theoretical Physics)*.”, *Butterworth-Heinemann, 2 ed.*, (January, 1987). 82, 86

[150] F. Reif, “*Fundamentals of Statistical and Thermal Physics*.”, *McGraw Hill, Tokyo*, (1965). 82

[151] M. Bocquet, S. Bonazzola, E. Gourgoulhon, and J. Novak, “Rotating neutron star models with magnetic field.”, *Astron.Astrophys.*, **301**, (1995), 757, [gr-qc/9503044]. 82

[152] A. K. Harding and D. Lai, “Physics of Strongly Magnetized Neutron Stars.”, *Rept.Prog.Phys.*, **69**, (2006), 2631, [astro-ph/0606674]. 82

[153] G. Endrdi, “Magnetic structure of isospin-asymmetric QCD matter in neutron stars.”, *Phys.Rev.*, **D90**, (2014), no. 9, 094501, [arXiv:1407.1216]. 82

[154] D. E. Kharzeev, L. D. McLerran, and H. J. Warringa, “The Effects of topological charge change in heavy ion collisions: ’Event by event P and CP violation’.”, *Nucl.Phys.*, **A803**, (2008), 227–253, [arXiv:0711.0950]. 82

[155] K. Fukushima, D. E. Kharzeev, and H. J. Warringa, “The Chiral Magnetic Effect.”, *Phys.Rev.*, **D78**, (2008), 074033, [arXiv:0808.3382]. 82

[156] V. Skokov, A. Y. Illarionov, and V. Toneev, “Estimate of the magnetic field strength in heavy-ion collisions.”, *Int.J.Mod.Phys.*, **A24**, (2009), 5925–5932, [arXiv:0907.1396]. 82

[157] A. B. Bardon, S. Beattie, C. Luciuk, W. Cairncross, D. Fine, N. S. Cheng, G. J. A. Edge, E. Taylor, S. Zhang, S. Trotzky, and J. H. Thywissen, “Transverse Demagnetization Dynamics of a Unitary Fermi Gas.”, *Science*, **344**, (May, 2014), 722–724, [arXiv:1310.5140]. 83

[158] M. Koschorreck, D. Pertot, E. Vogt, and M. Köhl, "Universal spin dynamics in two-dimensional Fermi gases.", *Nature Physics*, **9**, (July, 2013), 405–409, [arXiv:1304.4980]. 83

[159] O. Ovdat and A. Yarom, "A modulated shear to entropy ratio.", *JHEP*, **1411**, (2014), 019, [arXiv:1407.6372]. 84, 146

[160] A. Adams, L. D. Carr, T. Schäfer, P. Steinberg, and J. E. Thomas, "Strongly Correlated Quantum Fluids: Ultracold Quantum Gases, Quantum Chromodynamic Plasmas, and Holographic Duality.", *New J. Phys.*, **14**, (2012), 115009, [arXiv:1205.5180]. 85

[161] A. Bulgac, M. M. Forbes, and P. Magierski, "The Unitary Fermi Gas: From Monte Carlo to Density Functionals.", *Lect. Notes Phys.*, **836**, (2012), 305–373, [arXiv:1008.3933]. 85

[162] R. S. Bhalerao, "Transport properties of the fluid produced at RHIC.", *Pramana*, **75**, (2010), 247–258, [arXiv:1003.3293]. 85

[163] D. Page and S. Reddy, "Dense Matter in Compact Stars: Theoretical Developments and Observational Constraints.", *Ann. Rev. Nucl. Part. Sci.*, **56**, (2006), 327–374, [astro-ph/0608360]. 85

[164] M. G. Alford, H. Nishimura, and A. Sedrakian, "Transport coefficients of two-flavor superconducting quark matter.", *Phys. Rev.*, **C90**, (2014), no. 5, 055205, [arXiv:1408.4999]. 85

[165] A. Gezerlis and J. Carlson, "Strongly paired fermions: Cold atoms and neutron matter.", *Phys. Rev.*, **C77**, (2008), 032801, [arXiv:0711.3006]. 85, 106

[166] R. V. Gavai, S. Gupta, and S. Mukherjee, "A New method for computation of QCD thermodynamics: EOS, specific heat and speed of sound.", *PoS*, **LAT2005**, (2006), 173, [hep-lat/0509127]. 85

[167] G. Wlazlowski, P. Magierski, and J. E. Drut, "Shear Viscosity of a Unitary Fermi Gas.", *Phys. Rev. Lett.*, **109**, (2012), 020406, [arXiv:1204.0270]. 85, 105

[168] G. Wlazowski, W. Quan, and A. Bulgac, "Perfect-fluid behavior of a dilute Fermi gas near unitary.", *Phys. Rev.*, **A92**, (2015), no. 6, 063628, [arXiv:1504.0256]. 85, 105

[169] H. B. Meyer, "Transport properties of the quark-gluon plasma from lattice qcd.", *Nuclear Physics A*, **830**, (2009), no. 1, 641c–648c. 85

[170] J. Maldacena, "The large-n limit of superconformal field theories and supergravity.", *International journal of theoretical physics*, **38**, (1999), no. 4, 1113–1133. 85, 90

[171] U. Heinz and R. Snellings, "Collective flow and viscosity in relativistic heavy-ion collisions.", *Ann. Rev. Nucl. Part. Sci.*, **63**, (2013), 123–151, [arXiv:1301.2826]. 85

[172] T. Schäfer, "The Shear Viscosity to Entropy Density Ratio of Trapped Fermions in the Unitarity Limit.", *Phys. Rev.*, **A76**, (2007), 063618, [cond-mat/0701251]. 85, 92, 105, 106, 163

[173] C. Cao, E. Elliott, J. Joseph, H. Wu, J. Petricka, T. Schäfer, and J. E. Thomas, "Universal quantum viscosity in a unitary fermi gas.", *Science*, **331**, (2011), no. 6013, 58–61, [http://science.sciencemag.org/content/331/6013/58.full.pdf]. 85, 92, 101, 105, 109, 116, 124

[174] J. A. Joseph, E. Elliott, and J. E. Thomas, "Shear viscosity of a unitary fermi gas near the superfluid phase transition.", *Phys. Rev. Lett.*, **115**, (Jul, 2015), 020401. 85, 92, 101, 102, 105, 107, 109, 110

[175] M. Martinez, R. Ryblewski, and M. Strickland, "Boost-Invariant (2+1)-dimensional Anisotropic Hydrodynamics.", *Phys. Rev.*, **C85**, (2012), 064913, [arXiv:1204.1473]. 86

[176] K. Tuchin, "On viscous flow and azimuthal anisotropy of quark-gluon plasma in strong magnetic field.", *J. Phys.*, **G39**, (2012), 025010, [arXiv:1108.4394]. 86

[177] D. D. Ofengeim and D. G. Yakovlev, "Shear viscosity in magnetized neutron star crust.", *Europhys. Lett.*, **112**, (2015), no. 5, 59001, [arXiv:1512.0391]. 86, 164, 165

[178] S. Jain, R. Samanta, and S. P. Trivedi, "The Shear Viscosity in Anisotropic Phases.", *JHEP*, **10**, (2015), 028, [arXiv:1506.0189]. 86, 87, 88, 89, 90, 91, 121, 126, 144, 146

[179] W. Ketterle and M. W. Zwierlein, "Making, probing and understanding ultracold fermi gases.", *arXiv preprint arXiv:0801.2500*, (2008). 86, 92

[180] D. Guéry-Odelin and S. Stringari, "Scissors mode and superfluidity of a trapped bose-einstein condensed gas.", *Phys. Rev. Lett.*, **83**, (Nov, 1999), 4452–4455. 86, 95

[181] O. M. Maragò, S. A. Hopkins, J. Arlt, E. Hodby, G. Hechenblaikner, and C. J. Foot, "Observation of the scissors mode and evidence for superfluidity of a trapped bose-einstein condensed gas.", *Phys. Rev. Lett.*, **84**, (Mar, 2000), 2056–2059. 86, 95, 116

[182] M. J. Wright, S. Riedl, A. Altmeyer, C. Kohstall, E. R. S. Guajardo, J. H. Denschlag, and R. Grimm, "Finite-temperature collective dynamics of a fermi gas in the bec-bcs crossover.", *Phys. Rev. Lett.*, **99**, (Oct, 2007), 150403. 86, 95, 103, 116, 124, 145

[183] L. D. Landau and E. M. Lifshitz, "*Fluid Mechanics, First Edition: Volume 10 (Course of Theoretical Physics).*", *Pergamon Press*, (1981). 89, 100, 120

[184] S. Giorgini, L. P. Pitaevskii, and S. Stringari, "Theory of ultracold atomic fermi gases.", *Rev. Mod. Phys.*, **80**, (Oct, 2008), 1215–1274. 92, 164

[185] D. T. Son, "Vanishing bulk viscosities and conformal invariance of the unitary fermi gas.", *Phys. Rev. Lett.*, **98**, (Jan, 2007), 020604. 92

[186] E. Taylor and M. Randeria, "Viscosity of strongly interacting quantum fluids: Spectral functions and sum rules.", *Phys. Rev. A*, **81**, (May, 2010), 053610. 92

[187] M. Randeria, W. Zwerger, and M. Zwierlein. "The bcsbec crossover and the unitary fermi gas.". In *The BCS-BEC Crossover and the Unitary Fermi Gas,* W. Zwerger, editor, volume 836 of *Lecture Notes in Physics*, 1–32. Springer Berlin Heidelberg (2012). 100

[188] G. M. Bruun and H. Smith, "Viscosity and thermal relaxation for a resonantly interacting Fermi gas.", *Phys. Rev.*, **A72**, (2005), 043605, [cond-mat/0504734]. 100, 105

[189] G. M. Bruun and H. Smith, "Shear viscosity and damping for a Fermi gas in the unitarity limit.", *Phys. Rev.*, **A75**, (2007), 043612, [cond-mat/0612460]. 100, 105, 111

[190] M. Bluhm and T. Schäfer, "Dissipative fluid dynamics for the dilute Fermi gas at unitarity: Anisotropic fluid dynamics.", *Phys. Rev.*, **A92**, (2015), no. 4, 043602, [arXiv:1505.0084]. 100, 101, 105, 125

[191] G. M. Bruun and H. Smith, "Viscosity and thermal relaxation for a resonantly interacting fermi gas.", *Phys. Rev. A*, **72**, (Oct, 2005), 043605. 101

[192] G. M. Bruun and H. Smith, "Frequency and damping of the scissors mode of a fermi gas.", *Phys. Rev. A*, **76**, (Oct, 2007), 045602. 101

[193] T. Schäfer, "Generalized theory of diffusion based on kinetic theory.", *Phys. Rev. A*, **94**, (Oct, 2016), 043644. 101

[194] S. Riedl, E. R. Sánchez Guajardo, C. Kohstall, A. Altmeyer, M. J. Wright, J. H. Denschlag, R. Grimm, G. M. Bruun, and H. Smith, "Collective oscillations of a fermi gas in the unitarity limit: Temperature effects and the role of pair correlations.", *Phys. Rev. A*, **78**, (Nov, 2008), 053609. 101

[195] M. Bluhm and T. Schäfer, "Model-independent determination of the shear viscosity of a trapped unitary fermi gas: Application to high-temperature data.", *Phys. Rev. Lett.*, **116**, (Mar, 2016), 115301. 101

[196] M. J. H. Ku, A. T. Sommer, L. W. Cheuk, and M. W. Zwierlein, "Revealing the superfluid lambda transition in the universal thermodynamics of a unitary fermi gas.", *Science*, **335**, (2012), no. 6068, 563–567,

[http://science.sciencemag.org/content/335/6068/563.full.pdf]. 104, 106, 107, 110

[197] G. Rupak and T. Schäfer, "Shear viscosity of a superfluid fermi gas in the unitarity limit.", *Phys. Rev. A*, **76**, (Nov, 2007), 053607. 105, 114

[198] H. Guo, D. Wulin, C.-C. Chien, and K. Levin, "Microscopic Approach to Shear Viscosities in Superfluid Gases: From BCS to BEC.", *Phys. Rev. Lett.*, **107**, (2011), 020403, [arXiv:1008.0423]. 105

[199] T. Enss, R. Haussmann, and W. Zwerger, "Viscosity and scale invariance in the unitary Fermi gas.", *Annals Phys.*, **326**, (2011), 770–796, [arXiv:1008.0007]. 105

[200] A. Bulgac, J. E. Drut, and P. Magierski, "Thermodynamics of a trapped unitary fermi gas.", *Phys. Rev. Lett.*, **99**, (Sep, 2007), 120401. 106, 164

[201] M. M. Forbes, S. Gandolfi, and A. Gezerlis, "Resonantly Interacting Fermions In a Box.", *Phys. Rev. Lett.*, **106**, (2011), 235303, [arXiv:1011.2197]. 106

[202] R. Haussmann, "Properties of a fermi liquid at the superfluid transition in the crossover region between bcs superconductivity and bose-einstein condensation.", *Phys. Rev. B*, **49**, (May, 1994), 12975–12983. 106

[203] O. Goulko and M. Wingate, "Numerical study of the unitary fermi gas across the superfluid transition.", *Phys. Rev. A*, **93**, (May, 2016), 053604. 106

[204] E. Burovski, N. Prokof'ev, B. Svistunov, and M. Troyer, "Critical temperature and thermodynamics of attractive fermions at unitarity.", *Phys. Rev. Lett.*, **96**, (Apr, 2006), 160402. 106

[205] A. Bulgac, J. E. Drut, and P. Magierski, "Spin 1/2 fermions in the unitary regime: A superfluid of a new type.", *Phys. Rev. Lett.*, **96**, (Mar, 2006), 090404. 106

[206] R. Haussmann, W. Rantner, S. Cerrito, and W. Zwerger, "Thermodynamics of the bcs-bec crossover.", *Phys. Rev. A*, **75**, (Feb, 2007), 023610. 107

[207] C. Cao, "Section 6.2 of phd thesis - universal quantum viscosity in a unitary fermi gas.". 109

[208] M. W. Zwierlein, J. R. Abo-Shaeer, A. Schirotzek, C. H. Schunck, and W. Ketterle, "Vortices and superfluidity in a strongly interacting Fermi gas.", , **435**, (June, 2005), 1047–1051, [cond-mat/0505635]. 117

[209] D. T. Son and M. Wingate, "General coordinate invariance and conformal invariance in nonrelativistic physics: Unitary Fermi gas.", *Annals Phys.*, **321**, (2006), 197–224, [cond-mat/0509786]. 119

[210] M. M. Forbes, "The Unitary Fermi Gas in a Harmonic Trap and its Static Response.", arXiv:1211.3779, [arXiv:1211.3779]. 119, 145

[211] M. Goossens, R. Erdélyi, and M. S. Ruderman, "Resonant mhd waves in the solar atmosphere.", *Space Science Reviews*, **158**, (2010), no. 2, 289–338. 121

[212] X. Bekaert, E. Meunier, and S. Moroz, "Towards a gravity dual of the unitary Fermi gas.", *Phys. Rev.*, **D85**, (2012), 106001, [arXiv:1111.1082]. 121

[213] E. Vogt, M. Feld, B. Fröhlich, D. Pertot, M. Koschorreck, and M. Köhl, "Scale invariance and viscosity of a two-dimensional fermi gas.", *Phys. Rev. Lett.*, **108**, (Feb, 2012), 070404. 125, 145

[214] X.-H. Ge, Y. Ling, C. Niu, and S.-J. Sin, "Thermoelectric conductivities, shear viscosity, and stability in an anisotropic linear axion model.", *Phys. Rev. D*, **92**, (Nov, 2015), 106005. 126

[215] S. Chakraborty and R. Samanta, "Viscosity for anisotropic reissner-nordström black branes.", *Phys. Rev. D*, **95**, (May, 2017), 106012. 126, 147

[216] J. L. Diaz-Cruz and J. Toscano, "Lepton flavor violating decays of Higgs bosons beyond the standard model.", *Phys.Rev.*, **D62**, (2000), 116005, [hep-ph/9910233]. 127

[217] G. Blankenburg, J. Ellis, and G. Isidori, "Flavour-Changing Decays of a 125 GeV Higgs-like Particle.", *Phys.Lett.*, **B712**, (2012), 386–390, [arXiv:1202.5704]. 127

[218] R. Harnik, J. Kopp, and J. Zupan, "Flavor Violating Higgs Decays.", *JHEP*, **1303**, (2013), 026, [arXiv:1209.1397]. 127

[219] C. Collaboration, "Search for Lepton Flavour Violating Decays of the Higgs Boson.". 127

[220] A. Pilaftsis, "Lepton flavor nonconservation in H0 decays.", *Phys.Lett.*, **B285**, (1992), 68–74. 127

[221] A. Brignole and A. Rossi, "Lepton flavor violating decays of supersymmetric Higgs bosons.", *Phys.Lett.*, **B566**, (2003), 217–225, [hep-ph/0304081]. 127

[222] E. Arganda, A. M. Curiel, M. J. Herrero, and D. Temes, "Lepton flavor violating Higgs boson decays from massive seesaw neutrinos.", *Phys.Rev.*, **D71**, (2005), 035011, [hep-ph/0407302]. 127

[223] A. Azatov, M. Toharia, and L. Zhu, "Higgs Mediated FCNC's in Warped Extra Dimensions.", *Phys.Rev.*, **D80**, (2009), 035016, [arXiv:0906.1990]. 127

[224] A. Arhrib, Y. Cheng, and O. C. Kong, "Higgs to mu+tau Decay in Supersymmetry without R-parity.", *Europhys.Lett.*, **101**, (2013), 31003, [arXiv:1208.4669]. 127

[225] A. Falkowski, D. M. Straub, and A. Vicente, "Vector-like leptons: Higgs decays and collider phenomenology.", *JHEP*, **1405**, (2014), 092, [arXiv:1312.5329]. 127

[226] M. Arana-Catania, E. Arganda, and M. Herrero, "Non-decoupling SUSY in LFV Higgs decays: a window to new physics at the LHC.", *JHEP*, **1309**, (2013), 160, [arXiv:1304.3371]. 127

[227] M. Arroyo, J. L. Diaz-Cruz, E. Diaz, and J. A. Orduz-Ducuara, "Flavor Violating Higgs signals in the Texturized Two-Higgs Doublet Model (2HDM-Tx).", arXiv:1306.2343, [arXiv:1306.2343]. 127

[228] E. Arganda, M. Herrero, X. Marcano, and C. Weiland, "Imprints of massive inverse seesaw model neutrinos in lepton flavor violating Higgs boson decays.", *Phys.Rev.*, **D91**, (2015), no. 1, 015001, [arXiv:1405.4300]. 127

[229] D. Aristizabal Sierra and A. Vicente, "Explaining the CMS Higgs flavor violating decay excess.", *Phys.Rev.*, **D90**, (2014), no. 11, 115004, [arXiv:1409.7690]. 127

[230] J. Heeck, M. Holthausen, W. Rodejohann, and Y. Shimizu, "Higgs $\to \mu\tau$ in Abelian and Non-Abelian Flavor Symmetry Models.", arXiv:1412.3671, [arXiv:1412.3671]. 127

[231] C.-J. Lee and J. Tandean, "Lepton-Flavored Scalar Dark Matter with Minimal Flavor Violation.", *JHEP*, **1504**, (2015), 174, [arXiv:1410.6803]. 127

[232] A. Crivellin, G. DAmbrosio, and J. Heeck, "Explaining $h \to \mu^{\pm}\tau^{\mp}$, $B \to K^*\mu^+\mu^-$ and $B \to K\mu^+\mu^-/B \to Ke^+e^-$ in a two-Higgs-doublet model with gauged $L_\mu - L_\tau$.", *Phys.Rev.Lett.*, **114**, (2015), 151801, [arXiv:1501.0099]. 127

[233] L. de Lima, C. S. Machado, R. D. Matheus, and L. A. F. do Prado, "Higgs Flavor Violation as a Signal to Discriminate Models.", arXiv:1501.0692, [arXiv:1501.0692]. 127

[234] F. Borzumati and A. Masiero, "Large Muon and electron Number Violations in Supergravity Theories.", *Phys.Rev.Lett.*, **57**, (1986), 961. 128

[235] L. J. Hall, V. A. Kostelecky, and S. Raby, "New Flavor Violations in Supergravity Models.", *Nucl.Phys.*, **B267**, (1986), 415. 128, 130

[236] A. Masiero, S. K. Vempati, and O. Vives, "Massive neutrinos and flavor violation.", *New J.Phys.*, **6**, (2004), 202, [hep-ph/0407325]. 128

[237] A. Masiero, S. K. Vempati, and O. Vives, "Seesaw and lepton flavor violation in SUSY SO(10).", *Nucl.Phys.*, **B649**, (2003), 189–204, [hep-ph/0209303]. 128

[238] A. Masiero, S. Vempati, and O. Vives, "Flavour physics and grand unification.", arXiv:0711.2903, [arXiv:0711.2903]. 128

[239] L. Calibbi, A. Faccia, A. Masiero, and S. Vempati, “Lepton flavour violation from SUSY-GUTs: Where do we stand for MEG, PRISM/PRIME and a super flavour factory.”, *Phys.Rev.*, **D74**, (2006), 116002, [hep-ph/0605139]. 128

[240] M. Hirsch, F. Joaquim, and A. Vicente, “Constrained SUSY seesaws with a 125 GeV Higgs.”, *JHEP*, **1211**, (2012), 105, [arXiv:1207.6635]. 128

[241] L. Calibbi, D. Chowdhury, A. Masiero, K. Patel, and S. Vempati, “Status of supersymmetric type-I seesaw in SO(10) inspired models.”, *JHEP*, **1211**, (2012), 040, [arXiv:1207.7227]. 128

[242] J. L. Feng, C. G. Lester, Y. Nir, and Y. Shadmi, “The Standard Model and Supersymmetric Flavor Puzzles at the Large Hadron Collider.”, *Phys.Rev.*, **D77**, (2008), 076002, [arXiv:0712.0674]. 128

[243] J. L. Feng, S. T. French, I. Galon, C. G. Lester, Y. Nir, et al., “Measuring Slepton Masses and Mixings at the LHC.”, *JHEP*, **1001**, (2010), 047, [arXiv:0910.1618]. 128

[244] B. Fuks, B. Herrmann, and M. Klasen, “Flavour Violation in Gauge-Mediated Supersymmetry Breaking Models: Experimental Constraints and Phenomenology at the LHC.”, *Nucl.Phys.*, **B810**, (2009), 266–299, [arXiv:0808.1104]. 128

[245] Y. Shadmi and P. Z. Szabo, “Flavored Gauge-Mediation.”, *JHEP*, **1206**, (2012), 124, [arXiv:1103.0292]. 128

[246] M. Abdullah, I. Galon, Y. Shadmi, and Y. Shirman, “Flavored Gauge Mediation, A Heavy Higgs, and Supersymmetric Alignment.”, *JHEP*, **1306**, (2013), 057, [arXiv:1209.4904]. 128

[247] L. Calibbi, P. Paradisi, and R. Ziegler, “Gauge Mediation beyond Minimal Flavor Violation.”, *JHEP*, **1306**, (2013), 052, [arXiv:1304.1453]. 128

[248] L. Calibbi, P. Paradisi, and R. Ziegler, “Lepton Flavor Violation in Flavored Gauge Mediation.”, *Eur.Phys.J.*, **C74**, (2014), no. 12, 3211, [arXiv:1408.0754]. 128

[249] G. D. Kribs, E. Poppitz, and N. Weiner, “Flavor in supersymmetry with an extended R-symmetry.”, *Phys.Rev.*, **D78**, (2008), 055010, [arXiv:0712.2039]. 128

[250] G. D. Kribs, A. Martin, and T. S. Roy, “Squark Flavor Violation at the LHC.”, *JHEP*, **0906**, (2009), 042, [arXiv:0901.4105]. 128

[251] Y. Nomura, M. Papucci, and D. Stolarski, “Flavorful supersymmetry.”, *Phys.Rev.*, **D77**, (2008), 075006, [arXiv:0712.2074]. 128

[252] Y. Nomura and D. Stolarski, “Naturally Flavorful Supersymmetry at the LHC.”, *Phys.Rev.*, **D78**, (2008), 095011, [arXiv:0808.1380]. 128

[253] Y. Nomura, M. Papucci, and D. Stolarski, "Flavorful Supersymmetry from Higher Dimensions.", *JHEP*, **0807**, (2008), 055, [arXiv:0802.2582]. 128

[254] I. Galon, G. Perez, and Y. Shadmi, "Non-Degenerate Squarks from Flavored Gauge Mediation.", *JHEP*, **1309**, (2013), 117, [arXiv:1306.6631]. 128

[255] L. Calibbi, A. Mariotti, C. Petersson, and D. Redigolo, "Selectron NLSP in Gauge Mediation.", *JHEP*, **1409**, (2014), 133, [arXiv:1405.4859]. 128

[256] N. Krasnikov, "Flavor lepton number violation at LEP-2.", *Mod.Phys.Lett.*, **A9**, (1994), 791–794. 128

[257] N. Krasnikov, "Search for flavor lepton number violation in slepton decays at LEP-2 and NLC.", *Phys.Lett.*, **B388**, (1996), 783–787, [hep-ph/9511464]. 128

[258] N. Arkani-Hamed, H.-C. Cheng, J. L. Feng, and L. J. Hall, "Probing lepton flavor violation at future colliders.", *Phys.Rev.Lett.*, **77**, (1996), 1937–1940, [hep-ph/9603431]. 128, 130

[259] J. Hisano, M. M. Nojiri, Y. Shimizu, and M. Tanaka, "Lepton flavor violation in the left-handed slepton production at future lepton colliders.", *Phys.Rev.*, **D60**, (1999), 055008, [hep-ph/9808410]. 128

[260] M. Guchait, J. Kalinowski, and P. Roy, "Supersymmetric lepton flavor violation in a linear collider: The Role of charginos.", *Eur.Phys.J.*, **C21**, (2001), 163–169, [hep-ph/0103161]. 128

[261] E. Carquin, J. Ellis, M. Gomez, and S. Lolab, "Searches for Lepton Flavour Violation at a Linear Collider.", *JHEP*, **1111**, (2011), 050, [arXiv:1106.4903]. 128

[262] A. Abada, A. Figueiredo, J. Romao, and A. Teixeira, "Lepton flavour violation: physics potential of a Linear Collider.", *JHEP*, **1208**, (2012), 138, [arXiv:1206.2306]. 128

[263] N. Arkani-Hamed, J. L. Feng, L. J. Hall, and H.-C. Cheng, "CP violation from slepton oscillations at the LHC and NLC.", *Nucl.Phys.*, **B505**, (1997), 3–39, [hep-ph/9704205]. 128

[264] S. Bityukov and N. Krasnikov, "The Search for sleptons and flavor lepton number violation at LHC (CMS).", *Phys.Atom.Nucl.*, **62**, (1999), 1213–1225, [hep-ph/9712358]. 128

[265] N. Krasnikov, "Search for flavor lepton number violation in slepton decays at LHC.", *JETP Lett.*, **65**, (1997), 148–153, [hep-ph/9611282]. 128

[266] K. Agashe and M. Graesser, "Signals of supersymmetric lepton flavor violation at the CERN LHC.", *Phys.Rev.*, **D61**, (2000), 075008, [hep-ph/9904422]. 128

[267] I. Hinchliffe and F. Paige, “Lepton flavor violation at the CERN LHC.”, *Phys.Rev.*, **D63**, (2001), 115006, [hep-ph/0010086]. 128

[268] J. Hisano, R. Kitano, and M. M. Nojiri, “Slepton oscillation at large hadron collider.”, *Phys.Rev.*, **D65**, (2002), 116002, [hep-ph/0202129]. 128, 137, 138

[269] R. Kitano, “A Clean Slepton Mixing Signal at the LHC.”, *JHEP*, **0803**, (2008), 023, [arXiv:0801.3486]. 128

[270] S. Kaneko, J. Sato, T. Shimomura, O. Vives, and M. Yamanaka, “Measuring Lepton Flavour Violation at LHC with Long-Lived Slepton in the Coannihilation Region.”, *Phys.Rev.*, **D87**, (2013), no. 3, 039904, [arXiv:0811.0703]. 128

[271] Y. Andreev, S. Bityukov, N. Krasnikov, and A. Toropin, “Using the e+- mu-+ + E**miss(T) signature in the search for supersymmetry and lepton flavour violation in neutralino decays.”, *Phys.Atom.Nucl.*, **70**, (2007), 1717–1724, [hep-ph/0608176]. 128

[272] F. Deppisch, “Lepton Flavor Violation at the LHC.”, arXiv:0710.2525, [arXiv:0710.2525]. 128

[273] B. Allanach, J. Conlon, and C. Lester, “Measuring Smuon-Selectron Mass Splitting at the CERN LHC and Patterns of Supersymmetry Breaking.”, *Phys.Rev.*, **D77**, (2008), 076006, [arXiv:0801.3666]. 128

[274] A. J. Buras, L. Calibbi, and P. Paradisi, “Slepton mass-splittings as a signal of LFV at the LHC.”, *JHEP*, **1006**, (2010), 042, [arXiv:0912.1309]. 128

[275] I. Galon and Y. Shadmi, “Kinematic Edges with Flavor Splitting and Mixing.”, *Phys.Rev.*, **D85**, (2012), 015010, [arXiv:1108.2220]. 128

[276] F. Gabbiani and A. Masiero, “FCNC in Generalized Supersymmetric Theories.”, *Nucl.Phys.*, **B322**, (1989), 235. 128, 130

[277] F. Gabbiani, E. Gabrielli, A. Masiero, and L. Silvestrini, “A Complete analysis of FCNC and CP constraints in general SUSY extensions of the standard model.”, *Nucl.Phys.*, **B477**, (1996), 321–352, [hep-ph/9604387]. 128

[278] J. Adam et al., “New constraint on the existence of the $\mu^+ \to e^+\gamma$ decay.”, *Phys.Rev.Lett.*, **110**, (2013), 201801, [arXiv:1303.0754]. 128, 130

[279] P. Wintz et al., “Test of LFC in mu —¿ e conversion on titanium.”. 130

[280] M. De Gerone, “mu to e gamma and mu to eee Status and perspectives.”, arXiv:1108.2670, [arXiv:1108.2670]. 130

[281] L. Calibbi, I. Galon, A. Masiero, P. Paradisi, and Y. Shadmi, "Charged Slepton Flavor post the 8 TeV LHC: A Simplified Model Analysis of Low-Energy Constraints and LHC SUSY Searches.", arXiv:1502.0775, [arXiv:1502.0775]. 131

[282] T. Sjostrand, S. Mrenna, and P. Z. Skands, "A Brief Introduction to PYTHIA 8.1.", *Comput.Phys.Commun.*, **178**, (2008), 852–867, [arXiv:0710.3820]. 134

[283] M. Cacciari, G. P. Salam, and G. Soyez, "FastJet User Manual.", *Eur.Phys.J.*, **C72**, (2012), 1896, [arXiv:1111.6097]. 134

[284] M. Cacciari, G. P. Salam, and G. Soyez, "The Anti-k(t) jet clustering algorithm.", *JHEP*, **0804**, (2008), 063, [arXiv:0802.1189]. 134

[285] A. Djouadi, J.-L. Kneur, and G. Moultaka, "SuSpect: A Fortran code for the supersymmetric and Higgs particle spectrum in the MSSM.", *Comput.Phys.Commun.*, **176**, (2007), 426–455, [hep-ph/0211331]. 134

[286] A. Djouadi, M. Muhlleitner, and M. Spira, "Decays of supersymmetric particles: The Program SUSY-HIT (SUspect-SdecaY-Hdecay-InTerface).", *Acta Phys.Polon.*, **B38**, (2007), 635–644, [hep-ph/0609292]. 134

[287] S. Chatrchyan et al., "Identification of b-quark jets with the CMS experiment.", *JINST*, **8**, (2013), P04013, [arXiv:1211.4462]. 137

[288] B. Gjelsten, D. Miller, and P. Osland, "Measurement of SUSY masses via cascade decays for SPS 1a.", *JHEP*, **0412**, (2004), 003, [hep-ph/0410303]. 137

[289] N. Kidonakis, "Top Quark Theoretical Cross Sections and pT and Rapidity Distributions.", arXiv:1109.3231, [arXiv:1109.3231]. 138

[290] J. M. Campbell, R. K. Ellis, and C. Williams, "Vector boson pair production at the LHC.", *JHEP*, **1107**, (2011), 018, [arXiv:1105.0020]. 138

[291] W. Beenakker, M. Klasen, M. Kramer, T. Plehn, M. Spira, et al., "The Production of charginos / neutralinos and sleptons at hadron colliders.", *Phys.Rev.Lett.*, **83**, (1999), 3780–3783, [hep-ph/9906298]. 138

[292] S. Bhattacharyya, V. E. Hubeny, S. Minwalla, and M. Rangamani, "Nonlinear Fluid Dynamics from Gravity.", *JHEP*, **0802**, (2008), 045, [arXiv:0712.2456]. 146

[293] S. Bhattacharyya, V. E. Hubeny, R. Loganayagam, G. Mandal, S. Minwalla, et al., "Local Fluid Dynamical Entropy from Gravity.", *JHEP*, **0806**, (2008), 055, [arXiv:0803.2526]. 146

[294] J. Bhattacharya, S. Bhattacharyya, S. Minwalla, and A. Yarom, "A Theory of first order dissipative superfluid dynamics.", *JHEP*, **1405**, (2014), 147, [arXiv:1105.3733]. 146

[295] V. E. Hubeny, S. Minwalla, and M. Rangamani, "The fluid/gravity correspondence.", arXiv:1107.5780, [arXiv:1107.5780]. 146

[296] L. D. Landau and E. M. Lifshitz. *The Classical Theory of Fields*. Butterworth-Heinemann, 4 edition, January (1980). 149

[297] M. P. Ryan and L. C. Shepley. *Homogeneous relativistic cosmologies*. Princeton, N.J. : Princeton University Press, (1975). 149, 151

[298] H. Heiselberg, "Collective Modes of Trapped Gases at the BEC-BCS Crossover.", *Phys. Rev. Lett.*, **93**, (2004), 040402. 164